

Bacterial multidrug efflux pumps: Structure, function, and regulation

by

Jani Reddy Bolla

A dissertation submitted to the graduate faculty
in partial fulfillment of the requirements for the degree of

DOCTOR OF PHILOSOPHY

Major: Chemistry

Program of Study Committee:
Edward W. Yu, Major Professor
Robert S. Houk
Keith L. Woo
Young Jin Lee
Drena L. Dobbs

Iowa State University

Ames, Iowa

2014

Copyright © Jani Reddy Bolla, 2014. All rights reserved.

TABLE OF CONTENTS

	Page
ABSTRACT.....	iii
LIST OF ABBREVIATIONS.....	iv
CHAPTER 1 GENERAL INTRODUCTION.....	1
CHAPTER 2 STRUCTURAL AND FUNCTIONAL ANALYSIS OF THE TRANSCRIPTIONAL REGULATOR RV3066 OF <i>MYCOBACTERIUM TUBERCULOSIS</i>	14
CHAPTER 3 BIOMOLECULAR MEMBRANE PROTEIN CRYSTALLIZATION.....	68
CHAPTER 4 CRYSTAL STRUCTURE OF THE <i>NEISSERIA GONORRHOEAE</i> MTRD INNER MEMBRANE MULTIDRUG EFFLUX PUMP.....	92
CHAPTER 5 STRUCTURE AND FUNCTION OF <i>NEISSERIA GONORRHOEAE</i> MTRF ILLUMINATES A NOVEL CLASS OF ANTIMETABOLITE EFFLUX PUMPS.....	114
CHAPTER 6 YDAH IS AN EFFLUX PUMP THAT MEDIATES RESISTANCE TO SULFONAMIDE ANTIMETABOLITES.....	154
CHAPTER 7 GENERAL CONCLUSIONS AND FUTURE DIRECTIONS.....	194
ACKNOWLEDGEMENTS.....	199
VITA.....	201

ABSTRACT

The emergence and spread of multidrug resistance among human pathogenic bacteria is an increasing worldwide problem. A comprehensive understanding of the molecular basis of resistance mechanisms of bacteria will be vital for the future development of new and more effective antibiotics and for novel therapeutic treatment strategies. One of the common resistance mechanisms is the active efflux of toxic compounds from the cell by bacterial multidrug efflux systems, which are polyspecific and able to accommodate a variety of structurally and functionally unrelated compounds. Moreover, it is well recognized that the expression of these multidrug efflux transporters is tightly controlled by transcriptional regulators with the same multidrug recognition properties. Elucidation of structural and functional relationships of these multidrug efflux transporters and transcriptional regulators is the major concern of this dissertation. In order to understand the role of Rv3066 in regulating the expression level of the multidrug efflux pump Mmr in *M. tuberculosis*, we have determined the crystal structure of Rv3066, both in the absence and presence of ethidium bromide. With the aid of other experimental data, induction mechanism of Rv3066 is studied in detail. Currently available various methodologies to crystallize membrane proteins have also been outlined in this dissertation. Towards understanding the molecular mechanism of MtrCDE efflux pump of *N. gonorrhoeae*, which mediates the export of several structurally diverse toxic chemicals, we have determined the crystal structure of MtrD. In addition, the Mtr efflux system includes another inner membrane protein MtrF, which belongs to the AbgT family of transporters. To date, approximately 13,000 putative transporters of this family have been identified. However, no structural information has been made available and even functional data are fairly minimal. To understand how members of the AbgT family function, we have determined the crystal structure of MtrF and combination of functional studies suggests that MtrF acts as an antibiotic efflux pump. In addition, we have exploited our knowledge on AbgT transporter family, by determining the crystal structure of another member YdaH, of this family. Based on our observations, we believe that many members of the AbgT family transporters may serve as antimetabolite efflux pumps to protect cells against these noxious agents.

LIST OF ABBREVIATIONS

Abbreviation	Description
ABC	ATP binding cassette
<i>A. borkumensis</i>	<i>Alcanivorax borkumensis</i>
BSA	Bovine serum albumin
CCCP	Carbonyl cyanide <i>m</i> -chlorophenylhydrazone
CHAPS	3-[(3-Cholamidopropyl)dimethylammonio]-1-propanesulfonate
CHAPSO	3-[(3-Cholamidopropyl)dimethylammonio]-2-hydroxy-1-propanesulfonate
CMC	Critical micelle concentration
Cymal-6	6-Cyclohexyl-1-pentyl- β -D-maltoside
DDM	<i>n</i> -Dodecyl- β -D-maltopyranoside
<i>E. coli</i>	<i>Escherichia coli</i>
EDTA	Ethylenediaminetetraacetic acid
EMSA	Electrophoretic mobility shift assay
HAE-RND	Hydrophobic and amphiphilic efflux RND
HME-RND	Heavy-metal efflux RND
HP	Hairpin
HTH	Helix-turn-helix
IPTG	Isopropyl- β -D-thiogalactopyranoside
IR	Inverted repeat
LB	Luria broth
LDAO	<i>n</i> -Dodecyl- <i>N,N</i> - dimethylamine- <i>N</i> -oxide

MATE	Multidrug and toxic compound extrusion
MDR	Multidrug-resistant
MFS	Major facilitator superfamily
MIC	Minimum growth inhibitory concentration
MO	1-Mono-olein- <i>rac</i> -glycerol
mP	Millipolarization
MPD	2- Methyl-2,4-pentanediol
MR	Molecular replacement
MRSA	Methicillin-resistant <i>staphylococcus aureus</i>
Mtr	Multiple transferable resistance
<i>M. tuberculosis</i>	<i>Mycobacterium tuberculosis</i>
<i>M. smegmatis</i>	<i>Mycobacterium smegmatis</i>
<i>N. gonorrhoeae</i>	<i>Neisseria gonorrhoeae</i>
OD	Optical density
OG	<i>n</i> -Octyl- β -D-glucopyranoside
PABA	<i>p</i> -Aminobenzoic acid
<i>P. aeruginosa</i>	<i>Pseudomonas aeruginosa</i>
PEG	Polyethylene glycol
PMF	Proton motive force
PMSF	Phenylmethanesulfonyl fluoride
RND	Resistance nodulation cell division
SAD	Single-wavelength anomalous dispersion
SIRAS	Single isomorphous replacement with anomalous scattering

SMR	Small multidrug resistance
TB	Tuberculosis
TDR	Totally drug-resistant
TM	Transmembrane
TX-100	Triton X-100
VRE	Vancomycin- resistant <i>Enterococci</i>
WHO	World Health Organization
XDR	Extensive-drug resistant

CHAPTER 1

GENERAL INTRODUCTION

The introduction of antibiotics for the treatment of infectious diseases in the 20th century is considered to be one of the major advances of modern medicine. Development of a wide range of antibiotics enabled successful treatment of the previously life-threatening diseases and radically improved global health and extended average life expectancy [1,2]. Not only did antibiotics save many millions of lives, but they also created wealth, and their discovery was a turning point in human history. Unfortunately, the use of these wonder drugs has been hampered by the rapid emergence of resistance strains. Today, drug resistance is common among all the major pathogens and all classes of antibiotics. Many of the bacterial pathogens associated with clinical infection have evolved in multidrug-resistant (MDR-resistant to one or more drugs) and extensive-drug resistant (XDR- only one or two classes of drugs left) forms. MDR/XDR has appeared in *Acinetobacter baumannii*, *Campylobacter jejuni*, *Neisseria gonorrhoeae*, Group B streptococcus, *Klebsiella pneumoniae*, MRSA, *Escherichia coli*, *Neisseria meningitidis*, *Salmonella* (non-typhoidal serotypes), *Shigella*, *Streptococcus pneumoniae*, Vancomycin-resistant *Enterococci* (VRE), Vancomycin-Intermediate/Resistant *Staphylococcus aureus* (VISA/VRSA), *Mycobacterium tuberculosis*. Infections caused by these MDR/XDR bacteria are associated with substantial extra costs of treatments due to reduced options and the major risk to both the hospital and the community [3]. The World Health Organization (WHO) even warns of a post-antibiotic era, in which common infections and minor injuries can once again become deadly threats, if no efficient countermeasures are taken within the next few years [4]. Thus,

there is a pressing need for new antibiotics or for new therapeutic approaches to treat infectious diseases.

A common and major antibiotic resistance mechanism is the active efflux of drugs from cells by membrane bound transporters. These transporter proteins are found in all organisms. In bacteria, genes encoding this class of proteins can be located on chromosomes or plasmids [5,6]. Although some of these efflux systems transport specific substrates, many are transporters of multiple substrates, designated multidrug resistance efflux pumps. These efflux pumps are prominent in terms of both their broad substrate specificities and high efficiency of drug extrusion.

According to their sequence similarity, number of transmembrane spanning regions, energy sources and substrates, bacterial multidrug efflux transporters can be classified into five families: major facilitator superfamily (MFS)[7-9], resistance nodulation cell division (RND) [10] family, small multidrug resistance (SMR) family [11], ATP binding cassette (ABC) family [12], multidrug and toxic compound extrusion (MATE) family [13,14]. The transporters of MFS, RND, SMR and MATE families use proton motive force to drive the extrusion of their substrates by an antiport H^+ : drug mechanism, with the exception of the MATE family, which can also use sodium ion gradient as the energy source. On the other hand, transporters of ABC superfamily use ATP hydrolysis to drive the extrusion of their substrates [15].

The RND family transporters are responsible for a large portion of intrinsic and acquired multidrug resistance to clinically significant antibiotics in Gram-negative bacteria [16]. The RND family can be further divided into two sub-families, the hydrophobic and amphiphilic efflux RND (HAE-RND) and heavy-metal efflux (HME-RND) subfamilies. The efflux systems of the RND family are organized as tripartite protein complex: composed of an inner membrane

component (RND protein), an adapter protein (membrane fusion protein) and an outer membrane protein. These three components form a continuous channel that traverse both the inner and outer membranes ensuring that the substrates, captured from the outer leaflet of the inner membrane bilayer, are effluxed directly across the periplasm and the outer membrane into the external medium using the proton-gradient as an energy source.

At present, two crystal structures of HAE-RND type efflux pumps are available. These efflux pumps are the *E. coli* AcrB [17-25] and *Pseudomonas aeruginosa* MexB [26] multidrug transporters, both of which are involved in export of organic substances such as various antibiotics, bile salts, and other hydrophobic substances. Structural data suggested that both AcrB and MexB function as a trimer. Each monomer has a transmembrane domain composed of 12 membrane-spanning helices and a large periplasmic domain. Their structures suggest that both AcrB and MexB span the entire width of the inner membrane and protrude approximately 70 Å into the periplasm. Crystal structures of AcrB with its substrates reveal at least three alternative binding sites [19,22,23] and all are located in the periplasmic domain of AcrB. Drug export by RND transporters is proton-motive force dependent. Three amino acid residues, Asp 407, Asp 408, and Lys 940, found on the fourth and tenth transmembrane domains, are crucial for proton translocation pathway [19,27]. The transmembrane domains of AcrB and MexB are particularly well conserved with almost all residues being identical, including the residues involved in proton translocation, suggesting that the mechanism may be common to all RND systems [26]. Along with the models of these two HAE-RND transporters, the crystal structures of other components of these tripartite complex systems have also been determined. These include the outer membrane channels *E. coli* TolC [28] and *P. aeruginosa* OprM [29], as well as the periplasmic membrane fusion proteins *E. coli* AcrA [30] and *P. aeruginosa* MexA [31,32].

In addition, crystal structures of two HME-RND transporters, CusA of *E. coli* and ZneA of *Cupriavidus metallidurans* CH34, have been solved recently [33,34]. Although HAE-RND proteins typically have broad substrate specificity, HME-RND proteins are highly substrate-specific and are able to differentiate between monovalent and divalent ions. Crystal structures of their membrane fusion partner structures, CusB of *E. coli* and ZneB of *C. metallidurans*, have also been reported [35,36]. More recently, the crystal structure of CusC (outer membrane channel) of *E. coli* completed the structural analysis of components of the complex [37,38]. The first efflux complex of RND transporter with its adaptor, CusBA of *E. coli*, has been reported recently [39]. This structure was critical in elucidating specific interactions between the pump and adaptor proteins and provided the backbone to develop models of tripartite efflux complexes [40]. Based on the cocrystal structure, functional studies on other RND efflux systems and cryo-electron microscopy model of AcrAB-TolC, it is believed that a trimeric RND pump in the inner membrane is coupled by a hexameric periplasmic membrane fusion protein, to a pore formed by a trimeric outer membrane channel, forming a continuous channel that spans both inner and outer membranes [41-43].

N. gonorrhoeae is a Gram-negative obligate human pathogen and is the causative agent of the sexually transmitted infection gonorrhea. The best characterized and most clinically important efflux system in *N. gonorrhoeae* is the MtrCDE tripartite multidrug efflux system (for multiple transferable resistance) [44-47]. The complex is formed by interactions between the inner membrane transporter MtrD (of the HAE-RND family), the periplasmic membrane fusion protein MtrC, and the outer membrane channel MtrE [48-52]. This powerful efflux complex provides resistance to a broad spectrum of antimicrobial agents, including bile salts, fatty acids, dyes, antibiotics, and spermicides [45,46,48]. The Mtr multidrug efflux system is also

responsible for resistance to host-derived cationic antimicrobial peptides, which are important mediators of the innate host defense [47]. Given that gonococci commonly infect mucosal sites bathed in fluids containing such peptides, the Mtr system indeed underscores the pathogenesis of gonococcal disease and its contribution to virulence. In addition, it has been shown that the MtrCDE tripartite efflux pump is capable of enhancing long-term colonization of the mouse vaginal mucosal layer and that gonococci lacking this efflux pump were highly attenuated [53].

In addition, the Mtr efflux system includes another inner membrane protein MtrF [54,55], which belongs to the AbgT family of transporters (for *p*-aminobenzoyl-glutamate transporter) [56]. It has been proposed that MtrF cooperates with the MtrCDE complex to export certain antimicrobials by a yet unknown mechanism [54]. To date, approximately 13,000 putative transporters of the AbgT family have been identified. AbgT-type proteins are commonly found in Gram-negative bacteria such as *S. enterica*, Gram-positive bacteria such as *S. aureus*, as well as yeasts such as *Saccharomyces arboricola*. Surprisingly, among proteins in this diverse AbgT family, only *E. coli* AbgT and *N. gonorrhoeae* MtrF [54-58] have been partially characterized.

However, recent work demonstrated that *E. coli* AbgT is capable of catalyzing the uptake of the catabolite *p*-aminobenzoyl-glutamate for *de novo* folic acid synthesis [58]. Because of this finding, it is hypothesized that AbgT-family transporters contribute to the bacterial folate synthesis pathway by importing *p*-aminobenzoyl-glutamate for producing this essential vitamin. On the other hand, it has been observed that *N. gonorrhoeae* MtrF, also belonging to the AbgT family, functions as an antimicrobial resistant protein. It is needed for the high-level resistance of gonococci to hydrophobic antimicrobials including erythromycin and TX-100 [54,55]. In addition, in some bacteria such as *Alcanivorax borkumensis*, AbgT family proteins exist, as a single transporter. In other words, the gene *ydaH*, which codes for YdaH transporter is preceded

neither by *abgA*, *abgB* genes nor by *mtrC*, *mtrD*, *mtrE* genes. Thus far, there is no structural information available for this family of membrane proteins, obscuring the details of their function and mechanism.

Expression of the majority of efflux systems is subject to tight control by various transcriptional regulators, underlying their roles in facilitating the adaptation of bacteria to environmental changes. These regulatory proteins usually bind to many of the structurally unrelated toxic compounds that are effluxed by the transporters that they regulate. Although the function and composition of MDR efflux pumps are relatively conserved in different species but their regulatory mechanisms vary significantly. Among the >20 classes of regulatory families, members of the TetR family of regulators are best known for their roles as regulators of antibiotic efflux pumps and tolerance to toxic chemical compounds [59,60]. TetR family members consist of an N-terminal helix-turn-helix (HTH) DNA-binding domain, and a larger C-terminal ligand-binding domain. While amino acid sequences of DNA-binding domain share high similarity among the family members, those of ligand-binding domain are diverse. TetR family proteins usually bind to their operators composed of ~10-30-bp palindromic sequences, to repress the target genes, and derepression occurs due to the conformational change within the dimer when cognate ligands bind to the regulators [61]. Understanding the structures and mechanisms of these efflux transporters and their transcriptional regulators will aid in the design and development of novel drugs to combat the multidrug resistant bacteria.

Thesis organization

Chapter 1 is the general introduction that provides the background information of the RND efflux systems, AbgT transporter family and TetR family regulatory proteins.

Chapter 2 is a manuscript published in *Nucleic Acid Research*, which describes the role of Rv3066 in regulating the expression level of the multidrug efflux pump Mmr in *M. tuberculosis*. The crystal structures of Rv3066 regulator both in the absence and presence of bound ethidium, together with the functional data provide new insight into the mechanisms of ligand binding and Rv3066 regulation.

Chapter 3 is a review published in *Philosophical Magazine*, summarizing a variety of methodologies for use in crystallizing integral membrane proteins. Since 50% of currently administrative pharmaceutical agents are designed for targeting them, understanding the structure and function of these membrane proteins is hampered by difficulties in crystallizing these membrane proteins.

Chapter 4 is a manuscript published in *PLoS One*, describing the crystal structure of the *N. gonorrhoeae* MtrD inner membrane multidrug efflux pump. The findings reveal a novel structural feature that is not found in other known RND efflux pumps.

Chapter 5 is a manuscript submitted to *Cell Reports*, presenting the crystal structure of *N. gonorrhoeae* MtrF transporter, which belongs to AbgT family of transporters. The findings from the structure reveal a dimeric molecule with a fold very distinct from all other families of transporters. Functional analysis suggests that MtrF is an antibiotic efflux pump, mediating bacterial resistance to sulfonamide antimetabolite drugs.

Chapter 6 is a manuscript submitted to *Nature Communications*, describing the crystal structure of the *A. borkumensis* YdaH transporter, which is also another member of AbgT family.

A combination of three-dimensional structure and functional analysis suggest a novel mechanism for sulfonamide antimetabolite resistance in bacteria.

Chapter 7 outlines conclusions and future directions. In this chapter, all the findings are summarized and organized by theme of understanding bacterial multidrug efflux pumps.

References

1. Walsh C. 2003 *Antibiotics: actions, origins, resistance*. Washington, DC: ASM Press.
2. Jones DS, Podolsky SH, Greene JA. 2012. The burden of disease and the changing task of medicine. *N Engl J Med* 366, 2333–2338.
3. Livermore DM. 2009. Has the era of untreatable infections arrived? *J Antimicrob Chemother* 64: i29-36.
4. World Health Organization. 2014. *Antimicrobial resistance: global report on surveillance*. WHO Press, Geneva, Switzerland.
5. Poole K. 2007. Efflux pumps as antimicrobial resistance mechanisms. *Ann Med* 39:162–176.
6. Piddock LJ. 2006. Multidrug-resistance efflux pumps? Not just for resistance. *Nat Rev Microbiol* 4:629–636.
7. Griffith JK, Baker ME, Rouch DA, Page MG, Skurray RA, Paulsen IT, Chater KF, Baldwin SA, Henderson PJ. 1992. Membrane transport proteins: Implications of sequence comparisons. *Curr Opin Cell Biol* 4:684-695.
8. Marger MD, Saier MH Jr. 1993. A major superfamily of transmembrane facilitators that catalyze uniporter, symporter and antiporter. *Trends Biochem Sci* 18:13-20.
9. Pao SS, Paulsen IT, Saier MH Jr. 1998. Major facilitator superfamily. *Microbiol Mol Biol Rev* 62:1-34.
10. Tseng TT, Gratwick KS, Kollman J, Park D, Nies DH, Goffeau A, Saier MH Jr. 1999. The RND permease superfamily: an ancient, ubiquitous and diverse family that includes human disease and development proteins. *J Mol Microbiol Biotechnol* 1:107-125.
11. Paulsen IT, Skurray RA, Tam R, Saier MH Jr, Turner RJ, Weiner JH, Goldberg EB, Grinius LL. 1996. The SMR family: a novel family of multidrug efflux proteins involved with the efflux of lipophilic drugs. *Mol Microbiol* 19:1167-1175.

12. Higgins CF. 1992. ABC transporters: from microorganisms to man. *Annu. Rev. Cell Biol* 8:67-113.
13. Brown MH, Paulsen IT, Skurray RA. 1999. The multidrug efflux protein NorM is a prototype of a new family of transporters. *Mol Microbiol* 31:394-395.
14. Morita Y, Kodama K, Shiota S, Mine T, Kataoka A, Mizushima T, Tsuchiya T. 1998. NorM, a putative multidrug efflux protein, of *Vibrio parahaemolyticus* and its homolog in *Escherichia coli*. *Antimicrob Agents Chemother* 42:1778-1782.
15. Piddock LJ. 2006. Clinically relevant chromosomally encoded multidrug resistance efflux pumps in bacteria. *Clin Microbiol Rev* 19 382–402.
16. Kumar A, Schweizer HP. 2005. Bacterial resistance to antibiotics: active efflux and reduced uptake. *Adv Drug Deliv Rev* 57:1486-1513.
17. Murakami S, Nakashima R, Yamashita E, Yamaguchi A. 2002. Crystal structure of bacterial multidrug efflux transporter AcrB. *Nature* 419: 587–593.
18. Yu EW, McDermott G, Zgurskaya HI, Nikaido H, Koshland DE Jr. 2003. Structural basis of multiple drug binding capacity of the AcrB multidrug efflux pump. *Science* 300: 976–980.
19. Murakami S, Nakashima R, Yamashita E, Matsumoto T, Yamaguchi A. 2006. Crystal structures of a multidrug transporter reveal a functionally rotating mechanism. *Nature* 443: 173–179.
20. Seeger MA, Schiefner A, Eicher T, Verrey F, Dietrichs K, Pos KM. 2006. Structural asymmetry of AcrB trimer suggests a peristaltic pump mechanism. *Science* 313: 1295–1298.
21. Sennhauser G, Amstutz P, Briand C, Storchenegger O, Grueter MG. 2007. Drug export pathway of multidrug exporter AcrB revealed by DARPin inhibitors. *PLoS Biol* 5: e7.
22. Yu EW, Aires JR, McDermott G, Nikaido H. 2005. A periplasmic-drug binding site of the AcrB multidrug efflux pump: a crystallographic and site-directed mutagenesis study. *J Bacteriol* 187: 6804–6815.
23. Nakashima R, Sakurai K, Yamasaki S, Nishino K, Yamaguchi A. 2011. Structures of the multidrug exporter AcrB reveal a proximal multisite drug-binding pocket. *Nature* 480: 565–569.
24. Nakashima R, Sakurai K, Yamasaki S, Hayashi K, Nagata C, Hoshino K, Onodera Y, Nishino K, Yamaguchi A. 2013. Structural basis for the inhibition of bacterial multidrug exporters. *Nature* 500: 102–106.

25. Eicher T, Cha H, Seeger MA, Brandstaetter L, El-Delik J, Bohnert JA, Kern WV, Verrey F, Gruetter MG, Diederichs K, Pos KM. 2012. Transport of drugs by the multidrug transporter AcrB involves an access and a deep binding pocket that are separated by a switch-loop. *Proc Natl Acad Sci USA* 109: 5687–5692.
26. Sennhauser G, Bukowska MA, Briand C, Gruetter MG. 2009. Crystal structure of the multidrug exporter MexB from *Pseudomonas aeruginosa*. *J Mol Biol* 389: 134–145.
27. Seeger MA, von Ballmoos C, Verrey F, Pos KM. 2009. Crucial role of Asp408 in the proton translocation pathway of multidrug transporter AcrB: evidence from site-directed mutagenesis and carbodiimide labeling. *Biochemistry* 48: 5801–5812.
28. Koronakis V, Sharff A, Koronakis E, Luisi B, Hughes C. 2000. Crystal structure of the bacterial membrane protein TolC central to multidrug efflux and protein export. *Nature* 405: 914–919.
29. Akama H, Kanemaki M, Yoshimura M, Tsukihara T, Kashiwaga T, Yoneyama H, Narita S, Nakagawa A, Nakae T. 2004. Crystal structure of the drug discharge outer membrane protein, OprM, of *Pseudomonas aeruginosa*. *J Biol Chem* 279: 52816–52819.
30. Mikolosko J, Bobyk K, Zgurskaya HI, Ghosh P. 2006. Conformational flexibility in the multidrug efflux system protein AcrA. *Structure* 14: 577–587.
31. Higgins MK, Bokma E, Koronakis E, Hughes C, Koronakis V. 2004. Structure of the periplasmic component of a bacterial drug efflux pump. *Proc Natl Acad Sci USA* 101: 9994–9999.
32. Akama H, Matsuura T, Kashiwaga S, Yoneyama H, Narita S, Tsukihara T, Nakagawa A, Nakae T. 2004. Crystal structure of the membrane fusion protein, MexA, of the multidrug transporter in *Pseudomonas aeruginosa*. *J Biol Chem* 279: 25939–25942.
33. Long F, Su CC, Zimmermann MT, Boyken SE, Rajashankar KR, Jernigan RL, Yu EW. 2010. Crystal structures of the CusA heavy-metal efflux pump suggest methionine-mediated metal transport mechanism. *Nature* 467: 484–488.
34. Pak JE, Ekende EN, Kifle EG, O'Connell JD, De Angelis F, Tessema MB, Derfoufi KM, Robles-Colmenares Y, Robbins RA, Goormaghtigh E, Vandenbussche G, Stroud RM. 2013. Structures of intermediate transport states of ZneA, a Zn(II)/proton antiporter. *Proc Natl Acad Sci USA* 110, 18484–18489.
35. Su CC, Yang F, Long F, Reyon D, Routh MD, Kuo DW, Mokhtari AK, Van Ornam JD, Rabe KL, Hoy JA, Lee YJ, Rajashankar KR, Yu EW. 2009. Crystal structure of the membrane fusion protein CusB from *Escherichia coli*. *J Mol Biol* 393: 342–355.
36. De Angelis F, Lee JK, O'Connell JD 3rd, Miercke LJ, Verschuere KH, Srinivasan V, Bauvois C, Govaerts C, Robbins RA, Ruyschaert JM, Stroud RM, Vandenbussche G. 2010. Metal-induced conformational changes in ZneB suggest an active role of

- membrane fusion proteins in efflux resistance systems. *Proc Natl Acad Sci USA* 107:11038–11043.
37. Kulathila R, Kulathila R, Indic M, van den Berg B. 2011. Crystal structure of *Escherichia coli* CusC, the outer membrane component of a heavy-metal efflux pump. *PLoS One* 6: e15610.
 38. Lei HT, Bolla JR, Bishop NR, Su CC, Yu EW. 2014. Crystal structures of CusC reveal conformational changes accompanying folding and transmembrane channel formation. *J Mol Biol* 426: 403–411.
 39. Su CC, Long F, Zimmermann MT, Rajashankar KR, Jernigan RL, Yu EW. 2011. Crystal Structure of the CusBA Heavy-Metal Efflux Complex of *Escherichia coli*. *Nature* 470: 558–562
 40. Delmar JA, Su CC, Yu EW. 2014. Bacterial multidrug efflux transporters. *Annu Rev Biophys* 43: 93-117
 41. Kim EH, Nies DH, McEvoy MM, Rensing C. 2011. Switch or funnel: how RND-type transport systems control periplasmic metal homeostasis. *J Bacteriol* 193, 2381–2387
 42. Janganan, TK, Bavro VN, Zhang L, Matak-Vinkovic D, Barrera NP, Venien-Bryan C, Robinson CV, Borges-Walmsley MI, Walmsley AR. 2011. Evidence for the assembly of a bacterial tripartite multidrug pump with a stoichiometry of 3:6:3. *J Biol Chem* 286: 26900–26912.
 43. Du D, Wang Z, James NR, Voss JE, Klimont E, Ohene-Agyei T, Venter H, Chiu W, Luisi BF. 2014. Structure of the AcrAB-TolC multidrug efflux pump. *Nature* 509: 512–516.
 44. Warner DM, Shafer WM, Jerse AE. 2008. Clinically relevant mutations that cause derepression of the *Neisseria gonorrhoeae* MtrC-MtrD-MtrE efflux pump system confer different levels of antimicrobial resistance and in vivo fitness. *Mol Microbiol* 70: 462–478.
 45. Hagman KE, Lucas CE, Balthazar JT, Snyder LA, Nilles M, Judd RC, Shafer WM. 1997. The MtrD protein of *Neisseria gonorrhoeae* is a member of resistance/nodulation/ division protein family constituting part of an efflux system. *Microbiology* 143: 2117–2125.
 46. Lucas CE, Hagman KE, Levin JC, Stein DC, Shafer WM. 1995. Importance of lipooligosaccharide structure in determining gonococcal resistance to hydrophobic antimicrobial agents resulting from the mtr efflux system. *Mol Microbiol* 16: 1001–1009.
 47. Shafer WM, Qu XD, Waring AJ, Lehrer RI. 1998. Modulation of *Neisseria gonorrhoeae* susceptibility to vertebrate antibacterial peptides due to a member of the resistance/nodulation/division efflux pump family. *Proc Natl Acad Sci USA* 95: 1829–1833.

48. Delahay RM, Robertson BD, Balthazar JT, Ison CA. 1997. Involvement of the gonococcal MtrE protein in the resistance of *Neisseria gonorrhoeae* to toxic hydrophobic agents. *Microbiology* 143, 2127-2133
49. Veal WL, Nicholas RA, Shafer WM. 2002. Overexpression of the MtrC-MtrD-MtrE efflux pump due to an *mtrR* mutation is required for chromosomally mediated penicillin resistance in *Neisseria gonorrhoeae*. *J Bacteriol* 184, 5619-24.
50. Janganan TK, Zhang L, Bavro VN, Matak-Vinkovic D, Barrera NP, Burton MF, Steel PG, Robinson CV, Borges-Walmsley MI, Walmsley AR. 2011. Opening of the outer membrane protein channel in tripartite efflux pumps is induced by interaction with the membrane fusion partner. *J Biol Chem* 286, 5484-5493.
51. Janganan TK, Bavro VN, Zhang L, Borges-Walmsley MI, Walmsley AR. 2013. Tripartite efflux pumps: energy is required for dissociation, but not assembly or opening of the outer membrane channel of the pump. *Mol Microbiol* 88, 590-602.
52. Lei HT, Chou TH, Su CC, Bolla JR, Kumar N, Radhakrishnan A, Long F, Delmar JA, Do SV, Rajashankar KR, Shafer WM, Yu EW. 2014. Crystal structure of the open state of the *Neisseria gonorrhoeae* MtrE outer membrane channel. *PLoS One* 9, e97475.
53. Jerse AE, Sharma ND, Simms AN, Crow ET, Snyder LA, Shafer WM. 2003. A gonococcal efflux pump system enhances bacterial survival in a female mouse model of genital tract infection. *Infection and Immunity* 71: 5576–5582.
54. Veal WL, Shafer WM. 2003. Identification of a cell envelope protein (MtrF) involved in hydrophobic antimicrobial resistance in *Neisseria gonorrhoeae*. *J Antimicrob Chemother* 51, 27-37.
55. Folster JP, Shafer WM. 2005. Regulation of *mtrF* expression in *Neisseria gonorrhoeae* and its role in high-level antimicrobial resistance. *J Bacteriol* 187, 3713-3720.
56. Prakash S, Cooper G, Singhi S, Saier MH Jr. 2003. The ion transporter superfamily. *Biochim Biophys Acta* 1618, 79-92.
57. Hussein MJ, Green JM, Nichols BP. 1998. Characterization of mutations that allow *p*-aminobenzoyl-glutamate utilization by *Escherichia coli*. *J Bacteriol* 180, 6260-6268.
58. Carter EL, Jager L, Gardner L, Hall CC, Willis S, Green JM. 2007. *Escherichia coli* *abg* genes enable uptake and cleavage of the folate catabolite *p*-aminobenzoyl-glutamate. *J Bacteriol* 189, 3329-3334.
59. Ramos JL, Martínez-Bueno M, Molina-Henares AJ, Terán W, Watanabe K, Zhang X, Gallegos MT, Brennan R, Tobes R. 2005. The TetR family of transcriptional repressors. *Microbiol Mol Biol Rev* 69:326–356.

60. Cuthbertson L, Nodwell JR. 2013. The TetR family of regulators. *Microbiol Mol Biol Rev* 77: 440–475
61. Yu Z, Reichheld SE, Savchenko A, Parkinson J, Davidson AR. 2010. A comprehensive analysis of structural and sequence conservation in the TetR family transcriptional regulators. *J Mol Biol* 400: 847-64

CHAPTER 2

**STRUCTURAL AND FUNCTIONAL ANALYSIS OF THE TRANSCRIPTIONAL
REGULATOR RV3066 OF *MYCOBACTERIUM TUBERCULOSIS***

Modified from a paper published in *Nucleic Acids Res*, 2012, 40:9340-9355

**Jani Reddy Bolla^{1,‡}, Sylvia V. Do^{2,‡}, Feng Long¹, Lei Dai³, Chih-Chia Su¹, Hsiang-Ting Lei¹,
Xiao Chen¹, Jillian E. Gerkey¹, Daniel C. Murphy¹, Kanagalaghatta R. Rajashankar⁴,
Qijing Zhang³ and Edward W. Yu^{1,2,5*}**

¹Department of Chemistry, Iowa State University, Ames, IA 50011, USA

²Bioinformatics and Computational Biology Interdepartmental Graduate Program, Iowa State
University, Ames, IA 50011, USA

³Department of Veterinary Microbiology, College of Veterinary Medicine, Iowa State
University, Ames, IA 50011, USA

⁴NE-CAT and Department of Chemistry and Chemical Biology, Cornell University, Bldg. 436E,
Argonne National Laboratory, 9700 S. Cass Avenue, Argonne, IL 60439, USA

⁵Department of Physics and Astronomy, Iowa State University, Ames, IA 50011, USA

[‡]J.R.B. and S.V.D. contributed equally to this work.

* To whom correspondence should be addressed. E-mail: ewyu@iastate.edu

Abstract

The Mmr multidrug efflux pump recognizes and actively extrudes a broad range of antimicrobial agents, and promotes the intrinsic resistance to these antimicrobials in *Mycobacterium tuberculosis*. The expression of Mmr is controlled by the TetR-like transcriptional regulator Rv3066, whose open reading frame is located downstream of the *mmr* operon. To understand the structural basis of Rv3066 regulation, we have determined the crystal structures of Rv3066, both in the absence and presence of bound ethidium bromide, revealing an asymmetric homodimeric two-domain molecule with an entirely helical architecture. The structures underscore the flexibility and plasticity of the regulator essential for multidrug recognition. Comparison of the apo-Rv3066 and Rv3066-ethidium bromide crystal structures suggests that the conformational changes leading to drug mediated derepression is primarily due to a rigid body rotational motion within the dimer interface of the regulator. The Rv3066 regulator creates a multidrug-binding pocket, which contains five aromatic residues. The bound ethidium is found buried within the multidrug-binding site, where extensive aromatic stacking interactions seemingly govern the binding. *In vitro* studies reveal that the dimeric Rv3066 regulator binds to a 14-bp palindromic inverted repeat sequence in the nanomolar range. These findings provide new insight into the mechanisms of ligand binding and Rv3066 regulation.

Introduction

Tuberculosis (TB) is one of the most deadly diseases and was responsible for the death of 1.7 million people in 2009 (1). This disease is caused by the bacterium *Mycobacterium tuberculosis*, which infects an estimated nine million people each year. TB is very difficult to

treat, requiring at least six months of a combination of medications. The treatment must continue even long after the symptoms disappear. However, *M. tuberculosis* has developed resistance to commonly used anti-TB agents, such as isoniazid and rifampicin. The development of these drug resistant strains is mainly due to the mismatch between treatment and symptoms, such as the irregular intake of drugs throughout the course of treatment and inappropriate prescription of medications (2). TB caused by multi-drug resistant (MDR) (3, 4), extensively drug-resistant (XDR) (2, 5), and most recently totally drug-resistant (TDR) (6) strains of *M. tuberculosis* have emerged and spread globally. Based on our current knowledge, TDR-TB is untreatable. The World Health Organization has predicted that there will be two million MDR or XDR cases worldwide by 2012. It is obvious that the emergence of these drug-resistant TB strains has evolved into a major threat and challenges our global prospects for TB control. Thus, knowledge of the molecular mechanisms underlying drug resistance in *M. tuberculosis* is essential for the development of new strategies to combat this disease.

Recent evidence suggests that MDR strains of *M. tuberculosis* are associated with constitutive or inducible expression of multidrug efflux pumps (7). These pumps have been classified into five different families: the ATP-binding cassette (ABC), resistance-nodulation-division (RND), multidrug and toxic compound extrusion (MATE), major facilitator (MF), and small multidrug resistance (SMR) families (8). It has been found that the genome of *M. tuberculosis* contains genes encoding efflux pumps from all these families (9, 10). In addition, several of these MDR efflux pumps have been identified and characterized (9).

One such pump is the Mmr (Rv3065) multidrug efflux pump, which belongs to the SMR family (11). Mmr has been shown to mediate resistance to several toxic compounds, including

acriflavine, ethidium bromide, erythromycin, pyronin Y, safranin O, tetraphenylphosphonium, and thioridazine (11, 12).

Elucidating the regulatory systems of multidrug efflux pumps in *M. tuberculosis* should allow us to understand how this bacterium contributes to multidrug resistance and how it adapts to environmental changes. At present, little is known about the regulatory mechanisms modulating the expression of *mmr* in *M. tuberculosis*. Here, we report the crystal structures of the Rv3066 efflux regulator both in the absence and presence of bound ethidium, suggesting that ethidium binding triggers a rotational motion of the regulator. This motion results in inducing the expression of the Mmr efflux pump by releasing the Rv3066 regulator from its cognate DNA at the promoter region. The *rv3066* gene is located immediately downstream of *mmr* and encodes a 202 amino-acid protein that shares sequence homology to members of the TetR family of regulators (13, 14). Our data indicate that Rv3066 is a TetR-family regulator, which represses the transcription of *mmr* by directly binding to the inverted repeat (IR) of the promoter.

Material and methods

Cloning of *rv3066*

The *rv3066* ORF from genomic DNA of *M. tuberculosis* strain H37Rv was amplified by PCR using the primers 5'-CCATGGCAACCGCAGGCTCCGACC-3' and 5'-GGATCCTCAATGGTGATGATGATGATGGTCGGGGGTTCGTCCCGCAT-3' to generate a product that encodes a Rv3066 recombinant protein with a 6xHis tag at the C-terminus. The corresponding PCR product was digested with *Nco*I and *Bam*HI, extracted from the agarose gel, and inserted into pET15b as described by the manufacturer (Merck KGaA, Darmstadt, Germany). The recombinant plasmid (pET15b Ω *rv3066*) was transformed into DH5 α cells and

the transformants were selected on LB agar plates containing 100 µg/ml ampicillin. The presence of the correct *rv3066* sequence in the plasmid construct was verified by DNA sequencing.

Expression and purification of Rv3066

Briefly, the full-length Rv3066 protein containing a 6xHis tag at the C-terminus was overproduced in *E. coli* BL21(DE3) cells possessing pET15bΩ*rv3066*. Cells were grown in 4 L of Luria Broth (LB) medium with 100 µg/ml ampicillin at 37°C. When the OD₆₀₀ reached 0.5, the culture was treated with 1 mM isopropyl-β-D-thiogalactopyranoside (IPTG) to induce Rv3066 expression, and cells were harvested within 3 h. The collected bacterial cells were suspended in 100 ml ice-cold buffer containing 20 mM Na-HEPES (pH 7.2) and 200 mM NaCl, 10 mM MgCl₂ and 0.2 mg DNase I (Sigma-Aldrich). The cells were then lysed with a French pressure cell. Cell debris was removed by centrifugation for 45 min at 4°C and 20,000 rev/min. The crude lysate was filtered through a 0.2 µm membrane and was loaded onto a 5 ml Hi-Trap Ni²⁺-chelating column (GE Healthcare Biosciences, Pittsburgh, PA) pre-equilibrated with 20 mM Na-HEPES (pH 7.2) and 200 mM NaCl. To remove unbound proteins and impurities, the column was first washed with six column volumes of buffer containing 50 mM imidazole, 250 mM NaCl, and 20 mM Na-HEPES (pH 7.2). The Rv3066 protein was then eluted with four column volume of buffer containing 300 mM imidazole, 250 mM NaCl, and 20 mM Na-HEPES (pH 7.2). The purity of the protein was judged using 12.5% SDS-PAGE stained with Coomassie Brilliant Blue. The purified protein was extensively dialyzed against buffer containing 100 mM imidazole, 250 mM NaCl, and 20 mM Na-HEPES (pH 7.5), and concentrated to 20 mg/ml.

For 6xHis selenomethionyl-substituted (SeMet)-Rv3066 protein expression, a 2 ml LB broth overnight culture containing *E. coli* BL21(DE3)/pET15b Ω r ν 3066 cells was transferred into 40 ml of LB broth containing 100 μ g/ml ampicillin and grown at 37°C. When the OD₆₀₀ value reached 1.2, cells were harvested by centrifugation at 6000 rev/min for 10 min, and then washed two times with 20 ml of M9 minimal salts solution. The cells were re-suspended in 40 ml of M9 media and then transferred into a 4 L pre-warmed M9 solution containing 100 μ g/ml ampicillin. The cell culture was incubated at 37°C with shaking. When the OD₆₀₀ reached 0.4, 100 mg/l of lysine, phenylalanine and threonine, 50 mg/l isoleucine, leucine and valine, and 60 mg/l of L-selenomethionine were added. The protein expression was induced with 1 mM IPTG after 15 min. Cells were then harvested within 3 h after induction. The procedures for purifying the 6xHis SeMet-Rv3066 were identical to those of the native protein.

Crystallization of Rv3066

All crystals of the 6xHis Rv3066 regulator were obtained using hanging-drop vapor diffusion. The form I SeMet-Rv3066 crystals were grown at room temperature in 24-well plates with the following procedures. A 2 μ l protein solution containing 20 mg/ml SeMet-Rv3066 protein in 20 mM Na-HEPES (pH 7.5), 250 mM NaCl and 100 mM imidazole was mixed with a 2 μ l of reservoir solution containing 24% PEG 4000, 0.1 M Na-acetate (pH 5.0) and 0.2 M MgCl₂. The resultant mixture was equilibrated against 500 μ l of the reservoir solution. Crystals of form I grew to a full size in the drops within two weeks. Typically, the dimensions of the crystals were 0.2 mm x 0.05 mm x 0.05 mm. Cryoprotection was achieved by raising the PEG 4000 concentration stepwise to 30% with a 3% increment in each step.

The form II crystals of Rv3066 were prepared using similar procedures. The reservoir solution for the form II crystals consists of 24% PEG 4000, 0.1 M Na-HEPES (pH 8.0) and 0.2 M MgCl₂. Crystals of this form grew to a full size in the drops within two weeks. The dimensions of the mature crystals were 0.1 mm x 0.1 mm x 0.1 mm. Cryoprotection was achieved by raising the PEG 4000 concentration stepwise to 30% with a 3% increment in each step.

The Rv3066-ethidium complex crystals were prepared by incubating the form II crystals of apo-Rv3066 in solution containing 24% PEG 4000, 0.1 M Na-HEPES (pH 8.0), 0.2 M MgCl₂ and 0.5 mM ethidium bromide for 48 h at 25°C. Cryoprotection was achieved by raising the PEG 4000 concentration stepwise to 30% with a 3% increment in each step.

Data collection, structural determination and refinement

All diffraction data were collected at 100K at beamline 24ID-E located at the Advanced Photon Source, using an ADSC Quantum 315 CCD-based detector. Diffraction data were processed using DENZO and scaled using SCALEPACK (16). The crystals of form I belong to space group $P2_12_12$ (Table 1). Based on the molecular weight of Rv3066 (22.78 kDa), a single dimer per asymmetric unit with a solvent content of 36.1% is expected. Two selenium sites were identified using SHELXC and SHELXD (17) as implemented in the HKL2MAP package (18). Single-wavelength anomalous dispersion (SAD) phasing using the program PHASER (19) was employed to obtain experimental phases in addition to phases from the structural model of the EbrR regulator (residues 83-176) (PDB code: 3hta). The resulting phases were then subjected to density modification and NCS averaging using the program PARROT (20). The phases were of excellent quality and allowed for tracing of most of the molecule in PHENIX AutoBuild (22),

which led to an initial model containing 72% amino acid residues and 54% of which contained side-chains. The remaining part of the model was manually constructed using the program Coot (21). Then, the model was refined using TLS refinement techniques adopting a single TLS body as implemented in PHENIX (22) leaving 5% of reflections in Free-R set. Iterations of refinement using PHENIX (22) and CNS (23) and model building in Coot (21) lead to the current model, which consists of 173 residues (residues 12-184) with excellent geometrical characteristics (Table 1).

The form II and Rv3066-ethidium crystals took the space groups $P2_12_12$ and $P3_121$, respectively. These two structures were phased using the molecular replacement (MR) program PHASER (19) by using the form I structure as the search model. Structural refinements were then performed using PHENIX (22) and CNS (23) (Table 1).

Electrophoretic mobility shift assay

To determine the binding of Rv3066 to the operator region of *mmr*, electrophoretic mobility shift assay (EMSA) was performed according to the procedure described by Alekshun et al. (24). The 30-bp oligonucleotide, 5'-CGAGCCTCCTTTGTGTACATTTGTACATGT-3', containing the hypothetical operator site IR1 was labeled at the 3' end with digoxigenin-11-ddUTP (DIG-11-ddUTP) using the DIG Gel Shift Kit (Roche Applied Science, Indianapolis, IN). A random 30-bp internal *rv3066* fragment was used as the control DNA for the gel shift assay. This control DNA fragment was also labeled with DIG-11-ddUTP. The DIG-11-ddUTP-labeled DNA fragments (0.02 μ M) were incubated with the purified Rv3066 protein at concentrations ranging from 0.04 μ M to 0.64 μ M in binding buffer composed of 20 mM HEPES, pH 7.6, 1 mM EDTA, 10 mM $(\text{NH}_4)_2\text{SO}_4$, 5 mM dithiothreitol, 0.2% Tween 20 (w/v), 30 mM KCl, and 0.5 μ g

of Poly [d(I-C)] as a nonspecific competitor. The reaction mixtures were incubated at room temperature for 30 min and then subjected to electrophoresis on a 7.5% (w/v) nondenaturing polyacrylamide gel at 150 V for 30 min. The DNA complexes in the gel were transferred to a nylon membrane with a vacuum blotter. The DIG-labeled DNA was detected and visualized using antidigoxigenin-antibody and the chemiluminescent substrate CDP-star (Roche Applied Science). For the competition experiments, different amounts (5 and 125-fold molar excesses) of either unlabeled 30-bp DNA or unlabeled internal random DNA were added as competitors during the binding step. The ligand binding assays were done by incubating different concentrations of ethidium bromide (6.4, 64, 320, 640, 1,280 μ M) with the purified Rv3066 protein for 30 min before adding the labeled ds-DNA fragments for the experiments.

Dye primer based DNase I footprint assay

The DNase I footprint assay was performed as described by Zianni et al. (25). A 226-bp fragment that encompasses bases -153 to +87, including IR1 (with the sequence of IR2 removed), of the promoter region of *mmr* was generated by PCR and cloned into the pGEM-Teasy vector. The fluorescently labeled probe was amplified using the primers 6FAM-Mmr-F (5'-/6FAM/TCGAGATCTTTCACCATG-3') and HEX-Mmr-R (5'-/HEX/CAACCGAGTGAACCCTTC-3'). 0.6 pmol of the gel purified fluorescently labeled probe was incubated with various amounts of the dimeric Rv3066 protein (0, 1.5 and 3.0 pmol) for 30 minutes at room temperature in a binding buffer containing 20 mM HEPES, pH 7.6, 10 mM (NH₄)₂SO₄, 5 mM dithiothreitol, 0.2% Tween 20 (w/v), 30 mM KCl, and 0.5 μ g of Poly [d(I-C)]. Bovine serum albumin (BSA) was used for the control experiment. After incubation, 10 mM MgCl₂ and 5 mM CaCl₂ was added to the reaction mixture to a final volume of 50 μ l.

Then, 0.0025 U of DNase I (Worthington Biochemicals, Lakewood, NJ) was added and incubated for 5 min at room temperature. The reaction was stopped by adding 0.25 M EDTA and extracted with phenol-chloroform-isoamylalcohol (25:24:1). Control digestions with the probe were performed in the absence of Rv3066. The digested DNA fragments were purified with the QIAquick PCR Purification kit (Qiagen, Valencia, CA) and eluted in 20 µl distilled water. After, 4 µl of the purified DNA was mixed with 5.98 µl HiDi formamide (Applied Biosystems, Foster City, CA) and 0.02 µl GeneScan-500 LIZ size standards (Applied Biosystems). The samples were analyzed with the 3730 DNA analyzer coupled by G5 dye set, using an altered default genotyping module that increased the injection time to 30 sec and the injection voltage to 3 kV.

The 226-bp fragment was sequenced with the primers 6FAM-Mmr-F and HEX-Mmr-R, respectively, using the Thermo Sequenase Dye Primer Manual Cycle Sequencing Kit (USB, Inc., Cleveland, OH) according to the manufacturer's instructions. Each reaction was diluted fivefold in water, and 4 µl was added to 5.98 µl HiDi formamide and 0.02 µl GeneScan-500LIZ size standard. The samples were analyzed using the 3730 DNA analyzer as described above. Electropherograms were analyzed and aligned using the GENEMAPPER software (version 4.0, Applied Biosystems).

Cloning of the *Mycobacterium tuberculosis mmr-3066* operon into *Mycobacterium smegmatis*

Primer pairs (FP: CGCGGATCCATCTTTCACCATGACACGAC, RP: CCCAAGCTTAGGACTGGTATTCGGCGGTT) with added *Bam*HI and *Hind*III sites were used to amplify the complete *mmr-rv3066* operon (including the promoter region) from *M. tuberculosis* H37Rv genomic DNA. The amplified fragment was digested and ligated into *E.*

coli-Mycobacterium shuttle vector pMV261 (kindly provided by Susan T. Howard, The University of Texas Health Science Center) to construct pMMR. pMV261 is a shuttle plasmid commonly used for cloning and expression of genes in mycobacteria. The cloned *mmr-rv3066* operon carried its own promoter sequence. Although there should be constitutive base-level expression from the vector, *mmr* is inducible due to the binding of drug by the regulator. The constructed pMMR in *E. coli* DH5 α was then purified and electroporated into *M. smegmatis* mc²155 (ATCC700084) (26).

Real-time quantitative RT-PCR (qRT-PCR) analysis of *mmr* induction

M. smegmatis mc²155 strain containing pMMR was inoculated into 30 ml of antibiotic-free 7H9 broth. The culture was incubated for overnight to the mid logarithmic phase ($OD_{600} \approx 0.6$) at 37 °C. The culture was divided into three aliquots. One aliquot was used as the non-treated control, while the other three were added with thioridazine (80 μ g/ml), erythromycin (128 μ g/ml) and ethidium bromide (10 μ g/ml), respectively. The cultures were further incubated for 1 h at 37°C. Total bacteria RNA was isolated from the three individual cultures by the Trizol method (27). RNA was further purified by Qiagen RNeasy Column (Qiagen, Valencia, CA) and treated with the Turbo DNA-free Kit (Life Technologies, Grand Island, NY) to eliminate DNA contamination in each preparation. Before being used for qRT-PCR, each RNA template and each primer set were tested with a conventional one-step RT-PCR kit and a regular PCR kit (Life Technologies) to ensure specific amplification from the target mRNA and no detectable DNA contamination in the RNA preparation. Primer pairs 3065F (5'-CCTATACCTCTTGTGCGCGAT-3') and 3065R (5'-CGAAAGCGATGCCATAACCC-3'), specific for the *mmr* gene were designed for qRT-PCR analyses, which were conducted using the

iScript one-step RT-PCR kit with SYBR green (Bio-Rad, Hercules, CA) along with the MyiQ iCycler real-time PCR detection system (Bio-Rad). Triplicate reactions in a volume of 15 μ l were performed for each dilution of the RNA template. Thermal cycling conditions were as follows: 10 min at 50°C, 5 min at 60°C followed by 5 min at 95°C, and then 40 cycles of 10 s at 95°C and 30 s at 56°C. Melt-curve analysis was performed immediately following each amplification. Samples between treatments were normalized using the *aph* gene which was located on the pMV261 vector as an internal standard. Cycle threshold values were determined with the MyiQ software (Bio-Rad). The relative changes (n-fold) in *mmr* transcription between the antibiotic treated and nontreated samples were calculated using $2^{-\Delta\Delta CT}$ method as described by Livak and Schmittgen (28).

Site-directed mutagenesis

Site-directed point mutations on residues that are expected to be critical for the binding of drugs were performed to generate single point mutants, W80A, Y101A, N112A, Y115A, W131A and D156A, and a double-point mutant W80A-W131A. The primers used for these mutations are listed in Table 2. All oligonucleotides were purchased from (Integrated DNA Technologies, Inc., Coralville, IA) in a salt-free grade.

Fluorescence polarization assay for the DNA binding affinity

Fluorescence polarization assays were used to determine the DNA binding affinity of the Rv3066 regulator. Both the 30-bp oligodeoxynucleotide and fluorescein labeled oligodeoxynucleotide were purchased from Integrated DNA Technologies, Inc. (Coralville, IA). These oligodeoxynucleotides contain the predicted 14-bp IR1 site for Rv3066 binding. Their

sequences were 5'-CGAGCCTCCTTTGTGTACATTTGTACATGT-3' and 5'-F-ACATGTACAAATGTACACAAAGGAGGCTCG-3', where F denotes the fluorescein which was covalently attached to the 5' end of the oligodeoxynucleotide by a hexamethylene linker. The 30-bp fluoresceinated ds-DNA was prepared by annealing these two oligodeoxynucleotides together. Fluorescence polarization experiment was done using a DNA binding solution containing 10 mM Na-phosphate (pH 7.2), 100 mM NaCl, 1 nM fluoresceinated DNA, and 1 μ g of poly(dI-dC) as non-specific DNA. The protein solution containing 500 nM dimeric Rv3066 and 1 nM fluoresceinated DNA was titrated into the DNA binding solution until the millipolarization (mP) become unchanged. All measurements were performed at 25°C using a PerkinElmer LS55 spectrofluorometer equipped with a Hamamatsu R928 photomultiplier. The excitation wavelength was 490 nm, and the fluorescence polarization signal (in ΔP) was measured at 520 nm. Each titration point recorded was an average of 15 measurements. Data were analyzed using the equation, $P = \{(P_{\text{bound}} - P_{\text{free}})[\text{protein}]/(K_D + [\text{protein}])\} + P_{\text{free}}$, where P is the polarization measured at a given total protein concentration, P_{free} is the initial polarization of free fluorescein-labeled DNA, P_{bound} is the maximum polarization of specifically bound DNA, and [protein] is the protein concentration. The titration experiments were repeated for three times to obtained the average K_D value. Curve fitting was accomplished using the program ORIGIN (OriginLab Corporation, Northampton, MA).

To study if the binding affinity between Rv3066 and DNA affects by ethidium, fluorescence polarization experiment was carried out in the presence of 1 μ M ethidium. All experimental procedures are the same as above, except that the protein and DNA binding solutions also contain 1 μ M ethidium.

Fluorescence polarization assay for ligand binding affinity

Fluorescence polarization was used to determine ethidium binding affinities of Rv3066 and its mutants. This approach was also employed to study the interaction between the Rv3066 regulator and the anti-TB drug thioridazine. The experiment was done using a ligand binding solution containing 10 mM Na-phosphate (pH 7.2), 100 mM NaCl and 1 μ M ethidium bromide. The protein solution consisting of Rv3066 or Rv3066 mutant in 10 mM Na-phosphate (pH 7.2), 100 mM NaCl and 1 μ M ethidium bromide was titrated into the ligand binding solution until the polarization (P) was unchanged. As this is a steady-state approach, fluorescence polarization measurement was taken after a 5 min incubation for each corresponding concentration of the protein and bile acid to ensure that the binding has reached equilibrium. All measurements were performed at 25°C using a PerkinElmer LS55 spectrofluorometer equipped with a Hamamatsu R928 photomultiplier. The excitation and emission wavelengths were 483 and 620 nm for ethidium binding, whereas these wavelengths were 320 and 430 nm for thioridazine measurement. Fluorescence polarization signal (in ΔP) was measured at the emission wavelength. Each titration point recorded was an average of 15 measurements. Data were analyzed using the equation, $P = \{(P_{\text{bound}} - P_{\text{free}})[\text{protein}]/(K_D + [\text{protein}])\} + P_{\text{free}}$, where P is the polarization measured at a given total protein concentration, P_{free} is the initial polarization of free ligand, P_{bound} is the maximum polarization of specifically bound ligand, and [protein] is the protein concentration. The titration experiments were repeated for three times to obtain the average K_D value. Curve fitting was accomplished using the program ORIGIN (OriginLab Corporation, Northampton, MA).

Gel filtration

A protein liquid chromatography Superdex 200 16/60 column (GE Healthcare Biosciences, Pittsburgh, PA) with a mobile phase containing 20 mM Tris-HCl (pH 8.5) and 300 mM NaCl was used in the gel filtration experiments. Blue dextran (Sigma-Aldrich, St. Louis, MO) was used to determine the column void volume, and proteins for use as gel filtration molecular weight standards were cytochrome C (M_r 12,400), carbonic anhydrase (M_r 29,000), albumin bovine serum (M_r 66,000), alcohol dehydrogenase (M_r 150,000), and β -Amylase (M_r 200,000). All these standards were purchased from Sigma-Aldrich. The molecular weights of the experimental samples were determined following the protocols supplied by the manufacturers.

Results

Overall structure of Rv3066

In the absence of inducer molecule, the Rv3066 regulator was crystallized in two different forms, I and II (Fig. S1). The form I (SeMet) crystal structure was determined to a resolution of 2.3 Å (Table 1 and Fig. 1a). The asymmetric unit contains a single homodimer, suggesting that this regulator is dimeric in nature. Similar to LfrR (30), the left and right subunits of Rv3066 are asymmetrical. The dimeric form I structure of Rv3066, indicating an all-helical protein, is shown in Fig. 1b. Superimposition of both subunits of Rv3066 gives rise to an overall rms deviation of 1.3 Å calculated over the $C\alpha$ atoms.

The crystal structure of form II was refined to a resolution of 1.8 Å (Table 1). Like form I, the structure of form II indicates that this protein is an asymmetric homodimer. Superimposition of the $C\alpha$ atoms of the two subunits of form II results in an rms deviation of 1.8

Å. Surprisingly, the conformations of the structures of forms I and II are quite distinct from each other, suggesting that these two structures probably represent two different transient states of the regulators. Superimposition of the entire dimer of these two apo-Rv3066 structures (forms I and II) provides an rms deviation of 3.0 Å (Fig. 2). Overall, the architecture of these two Rv3066 structures are in good agreement with those of the homolog proteins TetR (31, 32), QacR (33, 34), CprB (35), EthR (36, 37), CmeR (38), AcrR (39), SmeT (40) and LfrR (30). Each subunit of Rv3066 is composed of nine α helices ($\alpha 1$ - $\alpha 9$ and $\alpha 1'$ - $\alpha 9'$, respectively) (Figs. 1b and 2) and can be divided into two motifs: an N-terminal DNA-binding domain and a C-terminal ligand-binding domain. The helices of Rv3066 are designated numerically from the N-terminus as $\alpha 1$ (15-30), $\alpha 2$ (37-44), $\alpha 3$ (48-54), $\alpha 4$ (58-86), $\alpha 5$ (90-103), $\alpha 6$ (105-120), $\alpha 7$ (122-143), $\alpha 8$ (145-165), and $\alpha 9$ (171-182). In this arrangement, the smaller N-terminal domain includes helices $\alpha 1$ through $\alpha 3$ and the N-terminal end of $\alpha 4$ (residues 58-68), with $\alpha 2$ and $\alpha 3$ forming a typical helix-turn-helix motif. However, the larger C-terminal domain comprises the C-terminal end of helices $\alpha 4$ (residues 69-86) through $\alpha 9$, and helices $\alpha 6$, $\alpha 8$ and $\alpha 9$ are involved in the dimerization of the regulator. The smaller N-terminal domain shares considerably high sequence and structural similarities with the TetR-family regulators, suggesting that Rv3066 belongs to the TetR family. For example, residues 13-68 possess 20% amino acid identity and 68% homology to that of TetR (31). This N-terminal region also shows identities of 29% and 25%, and similarities of 62% and 63% to those of the *M. smegmatis* LfrR (30) and *M. tuberculosis* EthR repressors (37), respectively. Protein sequence alignment of Rv3066 with the TetR-family members of other *Mycobacterium* species is shown in Fig. S2. The alignment suggests that Rv3066 is a typical TetR-family regulator.

Conformational flexibility of the Rv3066 regulator

Two distinct conformations of apo-Rv3066 were captured using crystallography, suggesting that this regulatory protein is quite flexible in nature. A comparison of the N-terminal DNA-binding domains of the dimeric structures of forms I and II indicates that these two structures may depict two different transient states of the regulator. Apparently, these two conformations are related in which an 8° rotational motion of the right subunit (helices $\alpha 1'-\alpha 9'$) with respect to the left protomer (helices $\alpha 1-\alpha 9$) is attributed to the difference (Fig. S3). Indeed, we can easily generate the form II conformation using the form I structure as a starting point and then following the rigid-body rotational trajectory based on the TLS (translation/Libration/Screw) parameters. The resulting final B-factors and overall R-factor/R-free of this form II dimeric Rv3066 structure are 24.0 Å²/22.9 Å² (left/right subunits) and 21.4%/25.5%, respectively. Thus, there is a chance that ligand binding triggers a rotational motion within the dimer of the regulator. Presumably, this movement prohibits the binding of the dimeric regulator at its cognate DNA, which in turn releases the regulator from the promoter region and allows for the expression of the Mmr efflux pump.

The C-terminal domain of the form II structure forms a large cavity, presumably creating a ligand-binding pocket of the regulator (Fig. S4). This cavity cannot be found in the form I structure. Thus, it is likely that the form II crystal structure mimics the ligand-bound form of Rv3066. The pocket, predominately formed by helices 5-8, opens horizontally from the side of each protomer. The total volume of these two binding pocket is about 540 Å³ (230 Å³ for the left subunit and 310 Å³ for the right subunit).

Helices $\alpha 4$ - $\alpha 6$ of each subunit of form II make the entrance of the binding pocket, with residues V100, D104 and Y108 participating to form this entrance.

Structure of the Rv3066-ethidium complex

The crystal structure of the Rv3066-ethidium complex (Figs. 3 and S5) was refined to a resolution of 2.3 Å (Table 1), revealing that ethidium indeed binds within the ligand-binding pocket formed by the C-terminal domain. Helices 5-8 contribute to form this pocket, and each subunit of Rv3066 is found to bind an ethidium molecule within the binding pocket. Superimposition of the dimeric Rv3066-ethidium structure to those of forms I and II apo-Rv3066 result in overall rms deviations of 3.4 and 1.9 Å, respectively.

Although the conformations of the two subunits within the dimer are not identical, their ethidium binding modes are quite similar. Both ethidium sites utilize the same set of amino acids to accommodate the binding, with a slight difference in the interaction distances. The $F_o - F_c$ electron density maps of the two bound ethidiums within the dimer are illustrated in Fig. 4a. Interestingly, the total volume of the two ligand-binding pocket has expanded to 929 Å³ (443 Å³ for the left subunit and 486 Å³ for the right subunit) in the ethidium bound structure.

Each bound ethidium molecule is completely buried in the Rv3066 binding pocket. The ligand binding pocket is found to be hydrophobic in nature. Five aromatic residues, W80, Y101, Y115, W131 and F155, participate to make aromatic stacking interactions and hydrophobic contacts with the bound ethidium (Figs. 4b, 4c and S6). In addition, L76, T98, L111 and T159 are involved to secure the binding through hydrophobic interaction. Further, the N1 and N2 amino group nitrogen of the phenanthridinium system of ethidium is hydrogen bonded to the side chain oxygen of T159 and S73 respectively (Table 3). Additional hydrogen bonds have also

been found between the N1 and N2 amino group nitrogens of the bound ethidium and the backbone oxygens of F155 and S73 to secure the binding (Table 3). In addition, a negatively charged residue D156 participates to form the ligand binding site, and this residue is ~ 3.3 Å away from the phenyl groups of the bound ethidium in each subunit of the dimer (Figs. 4b and S6).

Electrophoretic mobility shift assay

Bacterial multidrug efflux regulators usually bind to the palindromic IR sequences at the promoter regions to control the expression of the multidrug efflux pumps. In the *mmr-rv3066* operon, it appears that there are two 14-bp palindromic IR sequences located upstream of *mmr*. These two IRs (IR1 and IR2) are located right next to one another, where their sequences are complementary to each other (Fig. S7). The sequences of IR1 and IR2 are 5'-**TGTACATTTGTACA-3'** and 5'-**TGTACAAATGTACA-3'**, respectively. The presence of these IRs suggests potential binding sites for the Rv3066 regulator. Thus, EMSA was performed using a 30-bp double-stranded DNA containing the IR1 sequence and purified Rv3066 protein to detect if the regulator specifically binds IR1. As shown in Fig. 5a and b, the shift of the labeled DNA band was dependent upon the protein concentration as well as the addition of the unlabeled specific 30-bp double-stranded DNA. The data indicate that the IR1 sequence potentially forms the specific binding site for Rv3066.

EMSA was further performed with the purified Rv3066 protein and 30-bp DNA fragment containing the IR1 site in the presence of ethidium, which is a substrate of the Mmr efflux pump and is found to be bound in the ligand binding site of the Rv3066 regulator. As shown in Fig. 5c, the addition of ethidium to the Rv3066-DNA complex resulted in the loss of the retarded band,

indicating the separation of the protein and DNA components. The result suggests that ethidium is a substrate of Rv3066 and that the binding of ethidium triggers significant conformational change to the regulator, which in turn renders it unable to bind its cognate operator DNA.

Dye primer based DNase I footprint assay

To further confirm the binding site of Rv3066 in the *mmr-rv3066* promoter region, DNase I footprint assay was performed using the method of dye primer sequencing (25). In comparison with different electropherograms at various concentrations of the dimeric Rv3066 protein, we were able to uncover the specific DNA sequence, TTGTGTACATTTGTACACAAAGG, which was protected by the regulator (Figs. 6 and S8). Interestingly, the IR1 sequence (TGTACATTTGTACA) was found within this protected region, suggesting that Rv3066 is likely to specifically bind IR1.

Impact of drugs on *mmr* transcription in *Mycobacterium smegmatis*

We cloned the *mmr-rv3066* operon into *M. smegmatis* to assess its function and induction by antimicrobials. It has been reported that the anti-TB drug thioridazine was used to cure 10 XDR-TB patients (41). Thus, this drug was chosen to investigate its effect on the expression of the Mmr multi-drug efflux pump using qRT-PCR. We also studied the effect of ethidium and erythromycin on *mmr* transcription using the same approach. After 1 h induction with thioridazine, the *mmr* gene was up-regulated by 2.70 ± 0.09 fold (p value = 0.0001). No obvious induction of the *mmr* gene was observed in the presence of ethidium or erythromycin at the same time-point.

Fluorescence polarization assay

Presumably, Rv3066 suppresses the expression of the Mmr multidrug efflux pump by directly binding to its target DNA. Fluorescence polarization-based assay was carried out to study the interaction between Rv3066 and the 30-bp DNA containing the IR1 sequence. Fig. 7a illustrates the binding isotherm of Rv3066 in the presence of 1 nM fluoresceinated DNA. The titration experiment indicated that this regulator binds the 30-bp IR1 operator with a dissociation constant, K_D , of 4.4 ± 0.3 nM. This value is similar to that of the QacR regulator where it binds DNA with the K_D of 5.7 nM (42). The binding data also indicate that Rv3066 binds its cognate DNA with a stoichiometry of one Rv3066 dimer per IR1.

To investigate whether the presence of ethidium affects the binding of Rv3066 with IR1, fluorescence polarization was also carried out to study the interaction between Rv3066 and IR1 in the presence of this drug. The experimental results suggest that the K_D of Rv3066-IR1 becomes 10.7 ± 0.9 nM in the presence of 1 μ M ethidium (Fig. S9), indicating that ethidium significantly weakens the binding affinity between Rv3066 and IR1 by 2.4 times.

In addition, fluorescence polarization was used to determine the binding affinity of ethidium and the anti-TB drug thioridazine by Rv3066. The measurements indicate that the K_D values of the Rv3066-ethidium and Rv3066-thioridazine complexes are 2.9 ± 0.2 and 211.8 ± 34.2 μ M, respectively (Fig. 7b and c). These binding data suggest that the protein employs a simple binding stoichiometry with a 1:1 monomeric Rv3066-to-drug molar ratio. This molar ratio is indeed in good agreement with the crystal structure where each monomer of Rv3066 binds one ethidium molecule.

The structure of Rv3066-ethidium indicates that residues W80, Y101, N112, Y115, W131 and D156 are involved in ligand binding. These residues were mutated into alanines

(W80A, Y101A, N112A, Y115A, W131A and D156A). The corresponding mutant regulators were then expressed and purified. The ability of these mutant regulators to bind ethidium was tested using fluorescence polarization assay (Table 4). The results demonstrate that several of these point mutants show a significant decrease in the binding affinity for ethidium when compared with the wild-type Rv3066 regulator. Particularly, mutant D156A increases the dissociation constant, K_D , of ethidium binding by 20-fold, suggesting that D156 is a critical residue in the multidrug binding site of Rv3066. Moreover, mutants W80A, N112A and W131A decrease the affinity for ethidium binding by 3-4 times. A double-point mutant W80A-W131A was then produced to investigate how these tryptophans affect the binding of ethidium. Similar to the D156A mutant, the W80A-W131A double mutant indicates a significantly weaker binding affinity (20-fold decrease) when compared with that of the wild-type Rv3066, suggesting these two tryptophans, W80 and W131, are important residues for drug recognition.

Gel filtration

To confirm the stoichiometry of one Rv3066 dimer bound to one IR1 operator site, gel filtration experiment was performed using the purified Rv3066 protein pre-incubated with the purified, complementary, annealed 30-bp oligonucleotides containing the IR1 sequence. The result suggests an average molecular weight of 67.3 ± 3.8 kDa for the Rv3066-DNA complex (Fig. 8). This value is in good agreement with the theoretical value of 66.0 kDa for two Rv3066 molecules bound to the 30-bp DNA. Thus, the stoichiometry of the Rv3066-IR1 complex is 1:1 dimeric Rv3066-to-DNA molar ratio.

Discussion

With the rising incidences of multidrug resistant strains of TB, it has become increasingly important to understand how individual proteins function to recognize and confer resistance to multiple antibiotics in this pathogen. The crystal structures of Rv3066 both in the absence and presence of the bound ethidium provide direct information about how this regulator controls the expression of the Mmr multidrug efflux pump, which mediates the resistance of several antimicrobial agents. It appears that ethidium binding triggers a series of cooperativity motions of the C-terminal helices, including the horizontal shifts of helices $\alpha 5$, $\alpha 6$ and $\alpha 7$ toward the dimer interface, and an upward movement of helix $\alpha 8$ within one subunit of the regulator. These conformational changes initiate a rotational motion of the second subunit of Rv3066 with respect to the horizontal axis passing through the two ligand-binding pockets of the dimer (Figs. 3b, 5a and 5b), presumably making the relative orientation of the two N-terminal DNA-binding domains no longer compatible with the two consecutive major grooves of the operator B-DNA. The net result is that this dimeric regulator is released from the promoter, initiating the expression of the Mmr multidrug efflux pump.

By comparing with the apo-Rv3066, Rv3066-ethidium structures, it appears that the induction mechanism of Rv3066 seems to be attributed to the rigid body rotational motion of the two subunits triggered by ethidium binding (Fig. 5c). As mentioned above, this motion changes the relative orientation of the two DNA-binding domains of Rv3066, which makes the dimer incompatible with the two successive major grooves of the IR and results in disallowing the regulator to bind the DNA duplex. This induction mechanism is quite distinct from those of QacR (33, 34) and TetR (31, 32). However, a similar induction mechanism, which is triggered

by the movement as rigid bodies, can be found in the SimR regulator (43), where rigid body rotation within subunits of the dimer in relation to one another contributes to the induction.

In comparison with the form I and ethidium bound structures, the shift in position of helices $\alpha 5$, $\alpha 6$ and $\alpha 7$ toward the dimer interface results in the formation of four new hydrogen bonds. These hydrogen bonds are found within the dimer interface between H120 and R109', and between R121 and Q113'. In addition, the backbone oxygens of R129 and T165 also contribute to the dimer interface. These backbone oxygens interact with I164' and R129' to form two hydrogen bonds. The formation of these new hydrogen bonds is presumed to stabilize the tertiary structure of the ligand bound form of the Rv3066 dimer.

Coupled with the movements of these C-terminal helices, residues located at the binding site are also found to readjust their positions to accommodate for the binding of ethidium. Noticeably, Y115 shifts upward by 2.4 Å presumed to make an interaction with the phenyl group of the bound ethidium, whereas F155 is found to swing upward by 90° to enlarge the volume of the binding site. In addition, W131 adjusts its position to shift upward by 2.3 Å and makes an aromatic stacking interaction with the three-ring system of the phenanthridinium group of ethidium. W80 and Y101 also slightly switch in location by 1.1 and 2.0 Å to contribute aromatic π - π and stacking interactions with the bound ligand (Fig. 4c). One common characteristic of multi-drug binding proteins is their flexibility to accommodate for different ligands in a single ligand-binding pocket. This plasticity and flexibility can easily be seen in the Rv3066 regulator in which many of these residues lining the binding site are found to participate and relocate their side chain positions upon ethidium binding.

A distinguishing feature of multidrug binding proteins that bind cationic drugs is the presence of buried acidic glutamates or aspartates in the ligand binding pockets. This was

clearly demonstrated by the structures of the QacR-ligand complexes (33). Indeed, a completely buried negatively charged aspartate, which is essential for cationic ligand recognition, has also been found in the ligand-binding pocket of the AcrR multidrug efflux regulator (39). A similar characteristic for the TetR-family regulators that recognize negatively charged antimicrobials has also been observed through x-ray crystallography (38, 44). In this case, positively charged histidines or lysines within the ligand-binding pockets are critical for interacting with the negatively charged drugs. For Rv3066, it is found that there is one negatively charged residue (D156) inside the multidrug binding pocket. D156 is critical for ethidium binding as shown using fluorescence polarization and mutagenesis studies, although this residue does not seem to contribute a significant electrostatic interaction to the cationic ligand. A mutation of D156 with an alanine drastically decreases the Rv3066-ethidium binding affinity by 20-fold. Instead of contributing hydrogen-bonded interaction to neutralize the formal positive charge of the bound ethidium, the D156 residue, together with N112, is responsible for forming hydrogen bonds with the aromatic residues, Y101, Y115 and W131 (Fig. 4b). These three residues, in addition to W80, form an aromatic cage-like binding pocket to position the bound ethidium (Fig. S6), suggesting that D156 is important for the organization of the ligand binding site. The importance of the cage-like arrangement of these aromatic residues to bind ethidium is further demonstrated using mutagenesis and fluorescence polarization studies, in which the W80-W131 double mutant has been found to bind ethidium 20 times weaker than the wild-type Rv3066.

It is found that the Rv3066 dimer binds two drug molecules, with each subunit of the regulator contributing to bind one drug. Gel filtration experiment confirmed that the Rv3066-IR1 complex should be in the form of 1:1 dimeric Rv3066-to-DNA molar ratio. Real-time quantitative RT-PCR analysis suggested that the *mmr* gene was significantly up-regulated by

thioridazine induction. This result is indeed in good agreement with a recent finding that the treatment of thioridazine on *M. tuberculosis* causes a profound increase in the expression of the Mmr multidrug efflux pump (12). The structures of the Rv3066 regulator both in the absence and presence of bound ethidium, together with the experimental data from electrophoretic mobility shift, footprinting analysis, qRT-PCR, mutagenesis, gel filtration and fluorescence polarization, support the role of Rv3066 in regulating the expression level of the multidrug efflux pump Mmr in *M. tuberculosis*.

Protein data bank accession codes

Coordinates and structural factors for the structures of Rv3066 have been deposited at the RCSB Protein Data Bank with accession codes 3T6N (form I, apo-Rv3066), 3V6G (form II, apo-Rv3066), and 3V78 (Rv3066-ethidium).

Acknowledgments

We are grateful to Susan T. Howard at the University of Texas Health Science Center (Tyler) for providing the pMV261 plasmid used in this study. This work is based upon research conducted at the Northeastern Collaborative Access Team beamlines of the Advanced Photon Source, supported by award RR-15301 from the National Center for Research Resources at the National Institutes of Health. Use of the Advanced Photon Source is supported by the U.S. Department of Energy, Office of Basic Energy Sciences, under Contract No. DE-AC02-06CH11357. J.E.G. and D.C.M. were supported through the Community College Institute of Science Internship (CCI) and Science Undergraduate Laboratory Internship (SULI) from the DOE.

Funding

National Institutes of Health (NIH) [DK063008 to Q.Z. and GM086431 to E.W.Y.]; Use of the Advanced Photon Source is supported by the U.S. Department of Energy, Office of Basic Energy Sciences [DE-AC02-06CH11357]; Community College Institute of Science Internship (CCI) and Science Undergraduate Laboratory Internship (SULI) from the DOE (to J.E.G. and D.C.M.). Funding for open access charge: NIH [GM086431].

References

1. World Health Organization. (2010) Fact sheet no. 104: tuberculosis. Available at <http://www.who.int/mediacentre/factsheets/fs104/en/index.html>.
2. Goldman, R.C., Plumley, K.V. and Laughon, B.E. (2007) The evolution of extensively drug resistant tuberculosis (XDR-TB): history, status and issues for global control. *Infect. Disord. Drug Targets*, 7, 73-91.
3. Iseman, M.D. (1993) Treatment of multidrug-resistant tuberculosis. *N. Engl. J. Med.*, 329, 784–791.
4. Frieden, T.R., Sterling T., Pablos-Mendez, A. et al. (1993) The emergence of drug-resistant tuberculosis in New York City. *N. Engl. J. Med.*, 328, 521–56.
5. Pillay, M. and Sturm, A.W. (2007) Evolution of the extensively drug-resistant F15/LAM4/KZN strain of *Mycobacterium tuberculosis* in KwaZulu-Natal, South Africa. *Clin. Infect. Dis.*, 45, 1409–1414.
6. Udhwadia, Z.F., Amale, R.A. and Rodrigues, C. (2012) Totally drug-resistant tuberculosis in India. *Clin. Infect. Dis.*, 54, 579–581.
7. Nikaido, H. (2001) Preventing drug access to targets: cell surface permeability barriers and active efflux in bacteria. *Semin. Cell. Dev. Biol.*, 12, 215-223.
8. Li, X.Z. and Nikaido, H. (2004) Efflux-mediated drug resistance in bacteria. *Drugs*, 64, 159-204.
9. De Rossi, E., Ainsa, J.A. and Riccardi, G. (2006) Role of mycobacterial efflux transporters in drug resistance: an unresolved question. *FEMS Microbiol. Rev.*, 30, 36-52.

10. Danilchanka, O., Mailaender, C. and Niederweis, M. (2008) Identification of a novel multidrug efflux pump of mycobacterium tuberculosis. *Antimicrob. Agents Chemother.* 52, 2503-2511.
11. De Rossi, E., Branzoni, M., Cantoni, R., Milano, A., Riccardi, G. and Ciferri, O. (1998) *mmr*, a Mycobacterium tuberculosis gene conferring resistance to small cationic dyes and inhibitors. *J. Bacteriol.* 180, 6068-6071.
12. Dutta, N.K., Mehra, S. and Kaushal, D. (2010) A *Mycobacterium tuberculosis* sigma factor network responds to cell-envelope damage by the promising anti-mycobacterial thioridazine. *PLoS ONE* 5, e10069.
13. Grkovic, S., Brown, M.H. and Skurray, R.A. (2002) Regulation of bacterial drug export systems. *Microbiol. Mol. Biol. Rev.*, 66, 671-701.
14. Ramos, J.L., Martinez-Bueno, M., Molina-Henares, A.J., Teran, W., Watanabe, K., Zhang, X.D., Gallegos, M.T., Brennan, R. and Tobes, R. (2005) The TetR family of transcriptional repressors. *Microbiol. Mol. Biol. Rev.*, 69, 326-356.
15. Yu, Z., Reichheld, S.E., Savchenko, A., Parkinson, J. and Davidson, A. R. (2010) A comprehensive analysis of structural and sequence conservation in the TetR family transcriptional regulators. *J. Mol. Biol.*, 400, 847-864.
16. Otwinowski, Z. and Minor, M. (1997) Processing of X-ray diffraction data collected in oscillation mode. *Methods Enzymol.*, 276, 307-326.
17. Schneider, T.R. and Sheldrick, G.M. (2002) Substructure solution with SHELXD. *Acta Crystallogr.*, D58, 1772-1779.
18. Pape, T. and Schneider, T.R. (2004) HKL2MAP: a graphical user interface for macromolecular phasing with SHELX programs. *J. Appl. Crystallogr.*, 37, 843-844.
19. McCoy, A.J., Grosse-Kunstleve, R.W., Adams, P.D., Winn, M.D., Storoni, L.C. and Read, R.J. (2007) Phaser crystallographic software. *J. Appl. Crystallogr.*, 40, 658-674.
20. Cowtan, K. (2010) Recent developments in classical density modification. *Acta Crystallogr.*, D66, 470-478.
21. Emsley, P. and Cowtan, K. (2004) Coot: model-building tools for molecular graphics. *Acta Crystallogr.*, D60, 2126.
22. Adams, P.D., Grosse-Kunstleve, R.W., Hung, L.W., Ioerger, T.R., McCroy, A.J., Moriarty, N.W. et al. (2002) PHENIX: building new software for automated crystallographic structure determination. *Acta Crystallogr.*, 58, 1948-1954.
23. Brünger, A.T., Adams, P.D., Clore, G.M., DeLano, W.L., Gros, P., Grosse-Kunstleve, R.W., Jiang, J.S., Kuszewski, J., Nilges, M., Pannu, N.S., Read, R.J., Rice, L.M.,

- Simonson, T. and Warren, G.L. (1998) Crystallography & NMR system: A new software suite for macromolecular structure determination. *Acta Crystallogr.*, D54, 905-921.
24. Alekshun, M.N., Kim, Y.S. and Levy, S.B. (2000) Mutational analysis of MarR, the negative regulator of *marRAB* expression in *Escherichia coli*, suggests the presence of two regions required for DNA binding. *Mol. Microbiol.*, 35, 1394-1404.
 25. Zianni, M., Tessanne, K., Merighi, M., Laguna, R. and Tabita, F.R. (2006) Identification of the DNA bases of a DNase I footprint by the use of dye primer sequencing on an automated capillary DNA analysis instrument. *J. Biomolecular Techniques*, 17, 103-113.
 26. Jacobs, W.R., Jr., G. V. Kalpana, G.V., Cirillo, J.D., Pascopella, L., Snapper, S.B., Udani, R.A., Jones, W.D., Jr., Barletta, R.G. and Bloom, B.R. (1991). Genetic systems for mycobacteria. *Methods Enzymol.* 204, 537-555.
 27. Li, X.Z., Zhang, L. and Nikaido, H. (2004). Efflux pump-mediated intrinsic drug resistance in *Mycobacterium smegmatis*. *Antimicrob. Agents Chemother.* 48, 2415-2423.
 28. Livak, K.J. and Schmittgen, T.D. (2001). Analysis of relative gene expression data using real-time quantitative PCR and the 2⁻($\Delta\Delta C(T)$) Method. *Methods*, 25, 402-408.
 29. Trott, O. and Olson, A.J. (2010). AutoDock Vina: Improving the speed and accuracy of docking with a new scoring function, efficient optimization, and multithreading. *J. Comp. Chem.* 31, 455-461.
 30. Bellinzoni, M., Buroni, S., Schaeffer, F., Riccardi, G., De Rossi, E. and Alzari, P.M. (2009) Structural plasticity and distinct drug-binding modes of LfrR, a mycobacterial efflux pump regulator. *J. Bacteriol.*, 191, 7531-7537.
 31. Hinrichs, W., Kisker, C., Duvel, M., Muller, A., Tovar, K., Hillen, W. and Saenger, W. (1994) Structure of the Tet repressor-tetracycline complex and regulation of antibiotic resistance. *Science*, 264, 418-420.
 32. Orth, P., Schnappinger, D., Hillen, W., Saenger, W. and Hinrichs, W. (2000) Structural basis of gene regulation by the tetracycline inducible Tet repressor-operator system. *Nat. Struct. Biol.*, 7, 215-219.
 33. Schumacher, M.A., Miller, M.C., Grkovic, S., Brown, M.H., Skurray, R.A. and Brennan, R.G. (2001) Structural mechanisms of QacR induction and multidrug recognition. *Science*, 294, 2158-2163.
 34. Schumacher, M.A., Miller, M.C., Grkovic, S., Brown, M.H., Skurray, R. A. and Brennan, R.G. (2002) Structural basis for cooperative DNA binding by two dimers of the multidrug-binding protein QacR. *EMBO J.*, 21, 1210-1218.

35. Natsume, R., Ohnishi, Y., Senda, T. and Horinouchi, S. (2003) Crystal structure of a γ -butyrolactone autoregulator receptor protein in *Streptomyces coelicolor* A3(2). *J. Mol. Biol.*, 336, 409-419.
36. Dover L.G., Corsino, P.E., Daniels, I.R., Cocklin, S.L., Tatituri, V., Besra, G.S. and Futterer, K. (2004) Crystal structure of the TetR/CamR family repressor *Mycobacterium tuberculosis* EthR implicated in ethionamide resistance. *J. Mol. Biol.*, 340, 1095-1105.
37. Frenois F, Engohang-Ndong, J., Locht, C., Baulard, A. R. and Villeret, V. (2004) Structure of EthR in a ligand bound conformation reveals therapeutic perspectives against tuberculosis. *Mol. Cell*, 16, 301-307.
38. Gu, R., Su, C.-C., Shi, F., Li, M., McDermott, G., Zhang, Q. and Yu, E.W. (2007) Crystal Structure of the transcriptional regulator CmeR from *Campylobacter jejuni*. *J. Mol. Biol.*, 372, 583-593.
39. Li, M., Gu, R., Su, C.-C., Routh, M.D., Harris, K.C., Jewell, E.S., McDermott, G., Yu, E.W. (2007) Crystal structure of the transcriptional regulator AcrR from *Escherichia coli*. *J. Mol. Biol.*, 374, 591-603.
40. Hernández, A., Maté, M.J., Sánchez-Díaz, P.C., Romero, A., Rojo, F. and Martínez, J.L. (2009) Structural and functional analysis of SmeT, the repressor of the *Stenotrophomonas maltophilia* multidrug efflux pump SmeDEF. *J. Biol. Chem.*, 284, 14428-14438.
41. Amaral, L., Boeree, M.J., Gillespie, S.H., Udawadia, Z.F. and van Soolingen, D. (2010) Thioridazine cures extensively drug-resistant tuberculosis (XDR-TB) and the need for global trials is now! *Int. J. Antimicrob. Agents*, 35, 524-526.
42. Hoffmann, K.M., Williams, D., Shafer, W.M. and Brennan, R.G. (2005) Characterization of the multiple transferable resistance repressor, MtrR, from *Neisseria gonorrhoeae*. *J. Bacteriol.*, 187, 5008-5012.
43. Le, T.B.K., Schumacher, M.A., Lawson, D.M., Brennan, R.G. and Buttner, M.J. (2011) The crystal structure of the TetR family transcriptional repressor SimR bound to DNA and the role of a flexible N-terminal extension in minor groove binding. *Nucleic Acids Res.*, 39, 9443-9447.
44. Alguel, Y., Meng, C., Terán, W., Krell, T., Ramos, J.L., Gallegos, M.-T. and Zhang, X. (2007) Crystal structures of multidrug binding protein TtgR in complex with antibiotics and plant antimicrobials. *J. Mol. Biol.*, 369, 829-840.

Table and figure legends

Table 1. Data collection, phasing and structural refinement statistics.

	Form I	Form II	Rv3066-ethidium
Data Collection			
Wavelength (Å)	0.978	0.978	0.978
Space group	$P2_12_12$	$P2_12_12$	$P3_121$
Cell constants (Å)	a=78.7, b=118.9, c=42.1	a=91.4, b=119.9, c=30.9	a=99.1, b=99.1, c=66.5
Resolution (Å)	2.32 (40.00-2.32)	1.83 (40.00-1.83)	2.30 (40.0-2.30)
Completeness (%)	99.9 (99.9)	96.0 (98.4)	100.0 (99.6)
Total no. of reflections	556,100	524,555	670,642
No. of unique reflections	17,973	31,246	17,079
Redundancy	2.4 (2.5)	2.7 (2.9)	3.1 (3.2)
R_{merge} (%)	36.4 (7.7)	39.8 (4.9)	36.4 (5.7)
($I/\sigma(I)$)	2.17 (11.65)	2.08 (23.47)	2.94 (26.33)
Phasing			
Selenium atom sites	2		
Resolution range of data used (Å)	40.00-2.32		
Figure of merit (acentric/centric)	56.1/42.4		
Refinement			
R_{work} (%)	20.28	20.40	20.59
R_{free} (%)	27.06	24.71	26.16
B-factors			
Overall (Å ²)	38.5	24.6	48.0
Protein chain A/B (Å ²)	39.0/36.9	25.8/23.3	45.8/50.3
Ligand chain A/B (Å ²)	-	-	37.0/36.6
Water (Å ²)	39.2	29.3	41.1
No. of atoms in protein chain A/B	1,329/1,329	1,321/1,321	1,322/1,329
No. of ligands	0	0	2
No. of waters	77	67	64
Rms deviations			
Bond angles (°)	1.1	0.9	1.0
Bond length (Å)	0.008	0.007	0.008
Ramachandran analysis			
Most favored regions (%)	94.9	94.3	94.2
Allowed regions (%)	5.1	5.7	5.8
Generously allowed regions (%)	0.0	0.0	0.0
Disallowed regions (%)	0.0	0.0	0.0

Table 2. Primers for site-directed mutagenesis.

W131A-forward	5'-GTCTGGCTCGTCTGGCGCCGGATGGTCTGC-3'
W131A-reverse	5'-GCAGACCATCCGGCGCCAGACGAGCCAGAC-3'
S73A-forward	5'-CATGCCGCAAATGCAGCCGCAGAT-3'
S73A-reverse	5'-ATCTGCGGCTGCATTTGCGGCATG-3'
T159A-forward	5'-GTTTTTCGACGGCGCCGCGCTGCACGCACTG-3'
T159A-reverse	5'-CAGTGCGTGCAGCGCGGCGCCGTCGAAAAAC-3'
Y101A-forward	5'-CGTCTGACCACGGTCGCACTGGCAGATCAGGAC-3'
Y101A-reverse	5'-GTCCTGATCTGCCAGTGCGACCGTGGTCAGACG-3'
Y115A-forward	5'-CACCCCTGAACGAACTGGCAATGGCGGCCGCACATC-3'
Y115A-reverse	5'-GATGTGCGGCCGCCATTGCCAGTTCGTTTCAGGGTG-3'
W80A-forward	5'-CTGCTGGCCCAGGCGCGTTCTGATCTG-3'
W80A-reverse	5'-CAGATCAGAACGCGCCTGGGCCAGCAG-3'
D156A-forward	5'-GTCACCGTGTTTTTCGCAGGCGCCACGCTGCAC-3'
D156A-reverse	5'-GTGCAGCGTGGCGCCTGCGAAAAACACGGTGAC-3'
N112A-forward	5'-CGTTACCGCACCCCTGGCAGAACTGTATATGGC-3'
N112A-reverse	5'-GCCATATACAGTTCTGCCAGGGTGCGGTAACG-3'

Table 3. Rv3066-ethidium contacts. Contacts within 4.8 Å of the bound ethidiums are listed.

Residue-ligand contacts	Distance (Å)	
	A chain	B chain
S73	2.7 ^a	2.7 ^a
S73 (backbone oxygen)	2.9 ^a	2.9 ^a
L76	3.1	3.6
W80	3.6	3.7
T98	3.5	3.5
Y101	3.4	3.5
L111	4.6	4.3
N112	3.5	3.2
Y115	3.3	3.4
W131	3.0	3.0
F155	3.9	3.8
F155 (backbone oxygen)	2.9 ^a	2.7 ^a
D156	3.3	3.3
T159	2.9 ^a	2.7 ^a

Table 4. Dissociation constants for ethidium binding.

	K_D (μM)
Wild-type Rv3066	2.9 ± 0.2
W80A	8.5 ± 0.6
Y101A	2.1 ± 0.2
N112A	10.3 ± 0.7
Y115A	6.1 ± 0.6
W131A	12.9 ± 1.0
D156A	41.0 ± 5.9
W80A-W131A	43.2 ± 5.2

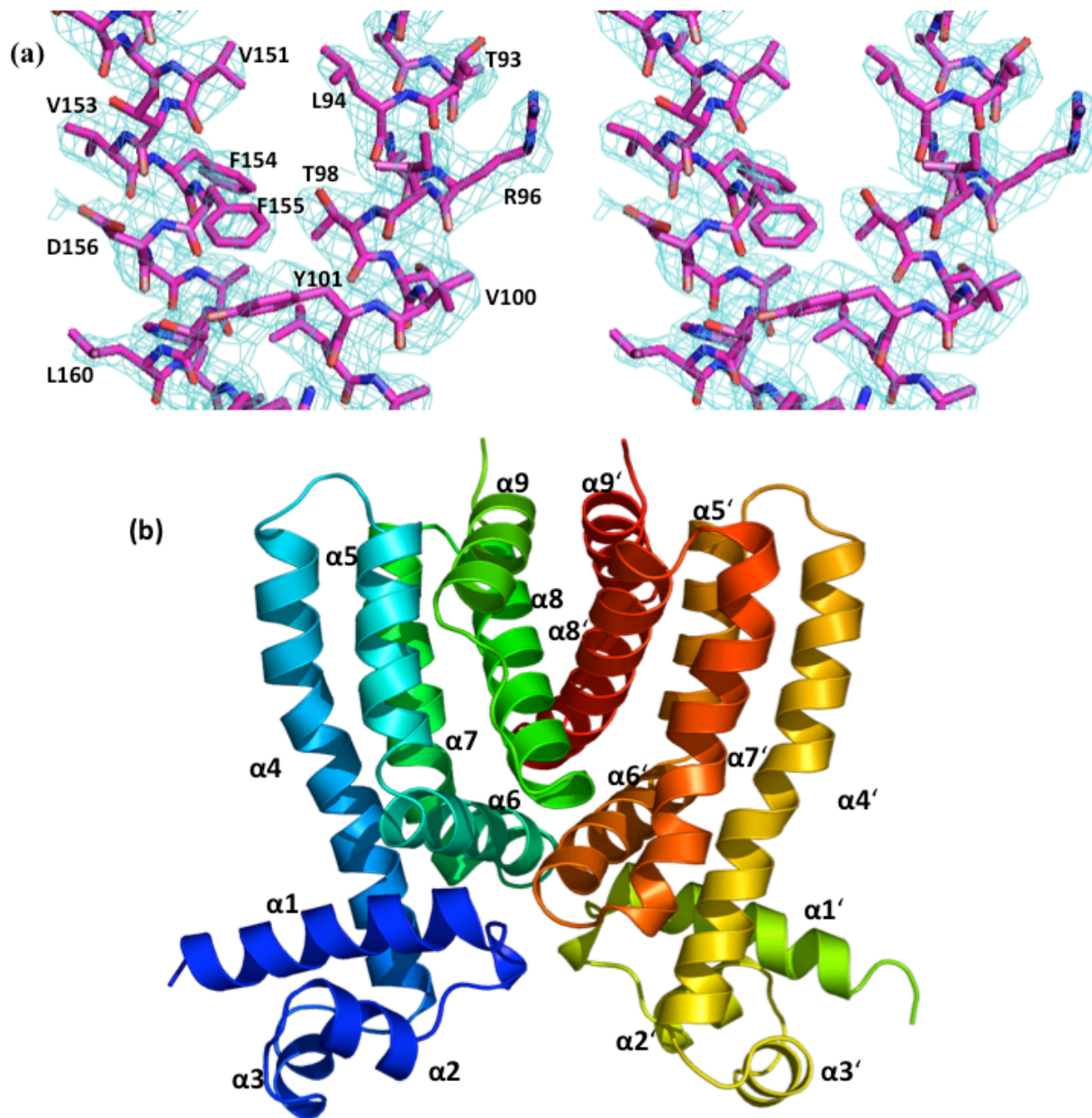


Figure 1. Stereo view of the experimental density map and ribbon diagram of the crystal structure of Rv3066. (a) Representative section of electron density in the vicinity of helices $\alpha 5$ and $\alpha 8$. The solvent-flattened electron density (40-2.3 Å) is contoured at 1σ and superimposed

with the final refined model (magenta, carbon; red, oxygen; blue nitrogen). (b) Ribbon diagram of the Rv3066 dimer. Helices $\alpha 1$ - $\alpha 9$ (left subunit) and $\alpha 1'$ - $\alpha 9'$ (right subunit) are labeled. The Figure was prepared using PyMOL (<http://www.pymol.sourceforge.net>).

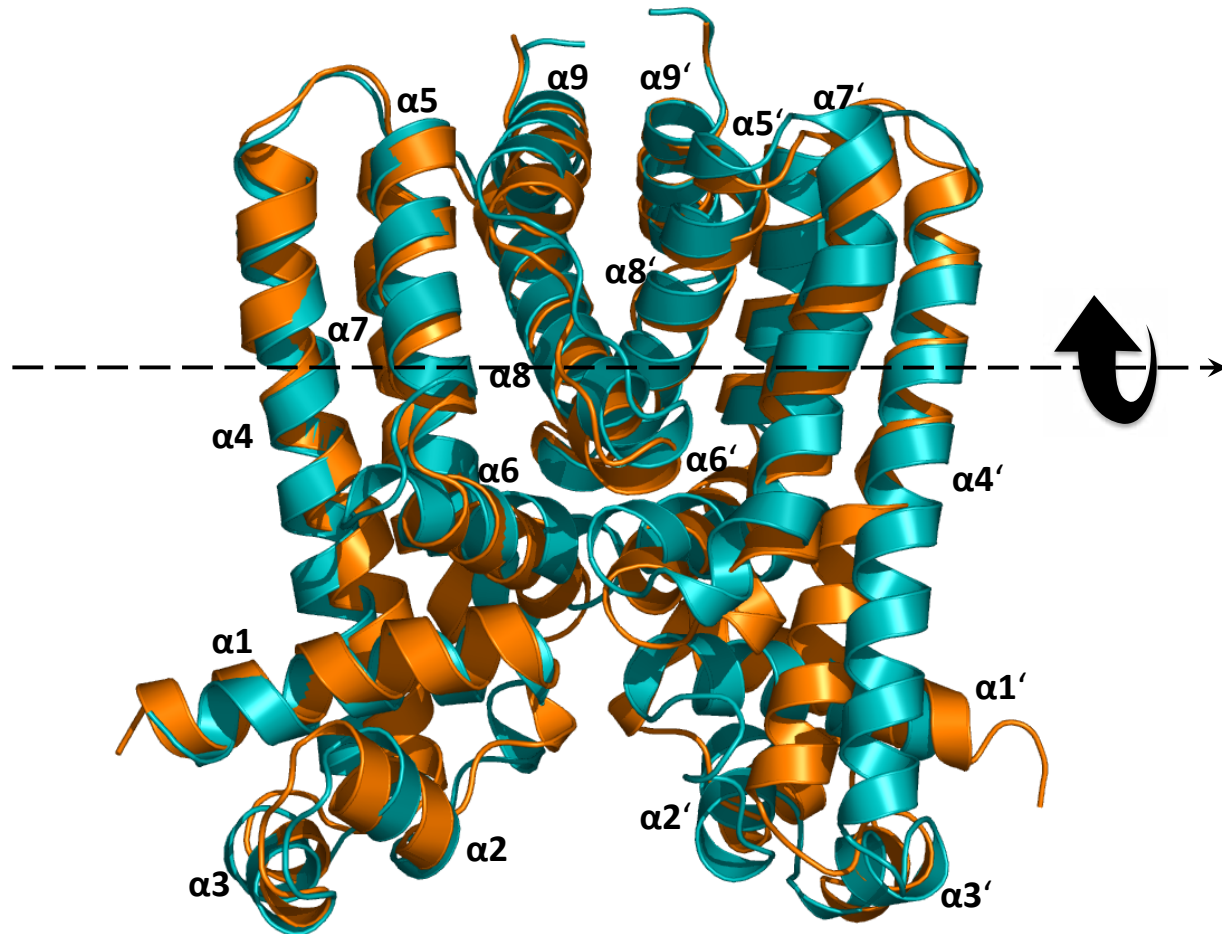


Figure 2. Structural comparison of forms I and II of the Rv3066 regulator. This is a superimposition of the dimeric structures of forms I and II (orange, form I; blue, form II). Helices $\alpha 1$ - $\alpha 9$ (left subunit) and $\alpha 1'$ - $\alpha 9'$ (right subunit) are labeled. The arrow indicates a change in orientation of the right subunit of form II when compared with the structure of form I.

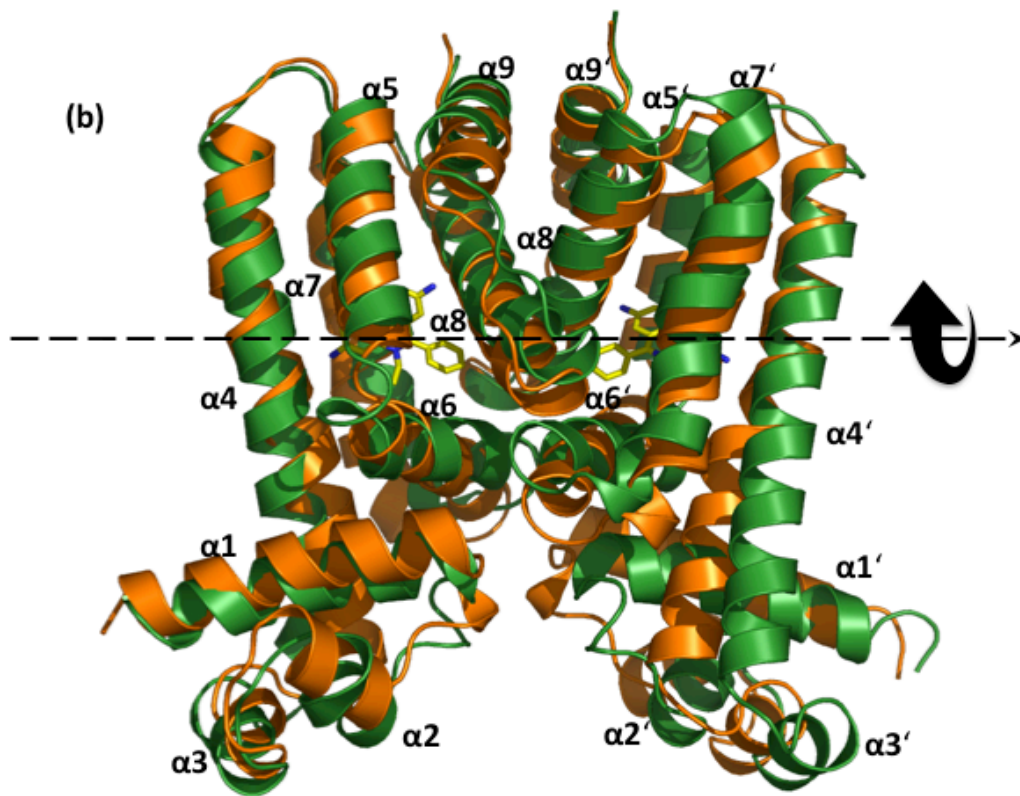
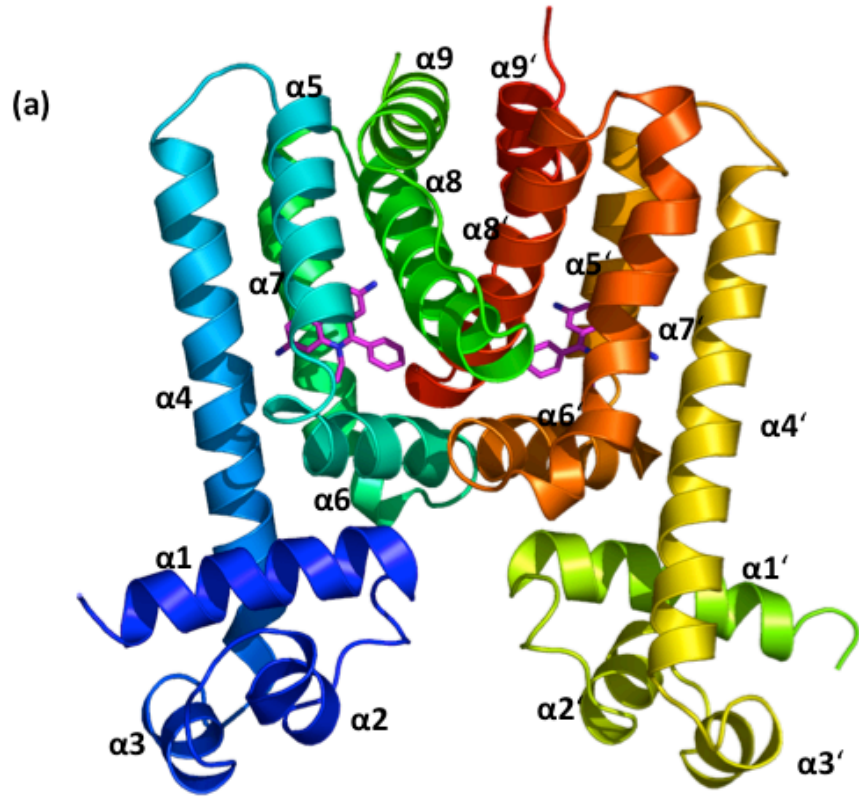


Figure 3. Crystal structure of the Rv3066-ethidium complex. (a) Ribbon diagram of the Rv3066-ethidium complex. The bound ethidiums are shown as sticks (magenta, carbon; blue, nitrogen). (b) Structural comparison of form I and Rv3066-ethidium. This is a superimposition of the dimeric structures of form I (orange) and Rv3066-ethidium (green). The bound ethidiums are in yellow sticks. Helices $\alpha 1$ - $\alpha 9$ (left subunit) and $\alpha 1'$ - $\alpha 9'$ (right subunit) are labeled. The arrow indicates a change in orientation of the right subunit of dimeric Rv3066-ethidium when compared with the form I structure. This conformational change can be interpreted as a rotational motion of the right subunit of Rv3066 with respect to the horizontal axis passing through the two ligand-binding pockets of the dimer upon ethidium binding.

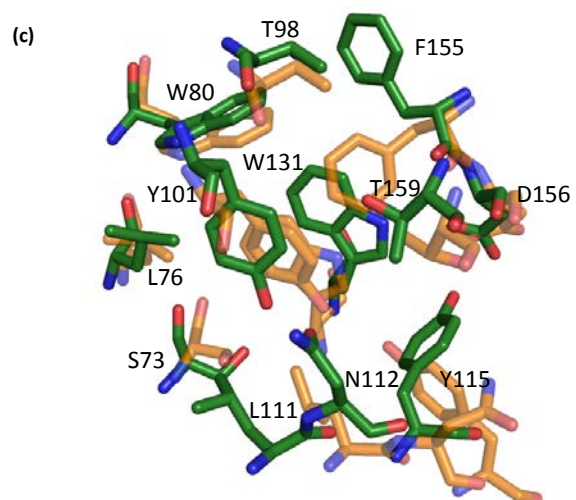
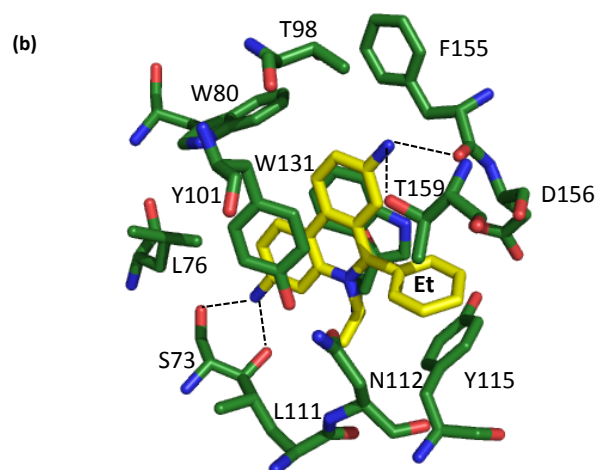
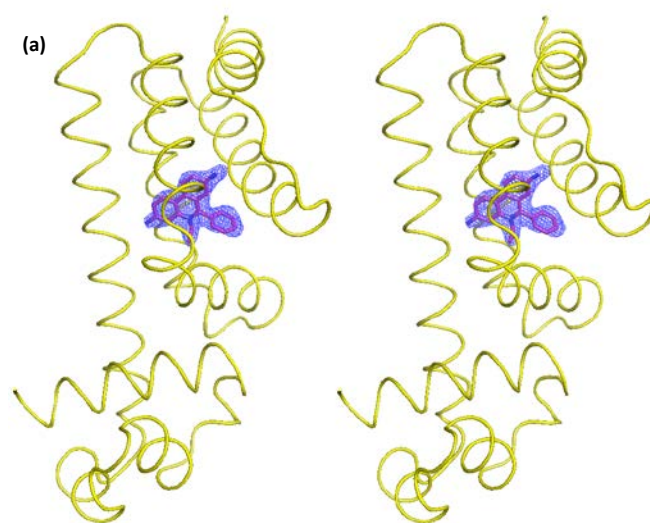


Figure 4. Electron density maps and the ethidium binding site. (a) Stereo view of the $F_o - F_c$ electron density map of the bound ethidium in the left subunit of dimeric Rv3066 (the orientation corresponds to Fig. 3a). The bound ethidium is shown as a stick model (magenta, carbon; blue, nitrogen). The $F_o - F_c$ map is contoured at 3.0σ (blue mesh). The surrounding secondary structural elements are shown as yellow ribbons. (b) The ethidium-binding site of the left subunit of the dimeric Rv3066-ethidium complex. Residues involved in ethidium binding are in green sticks. The bound ethidium is shown as yellow sticks. Dotted lines depict the hydrogen bonds. (c) Superimposition of the ligand-binding pocket before and after ethidium binding. Residues involved in ethidium binding are shown as sticks (orange, form I; green, Rv3066-ethidium).

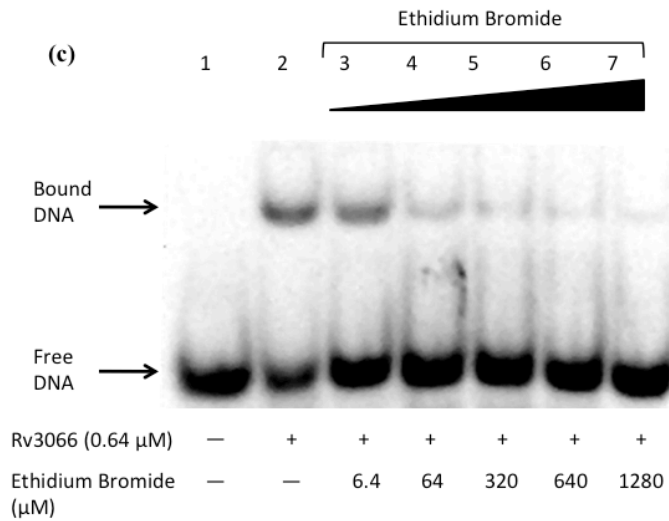
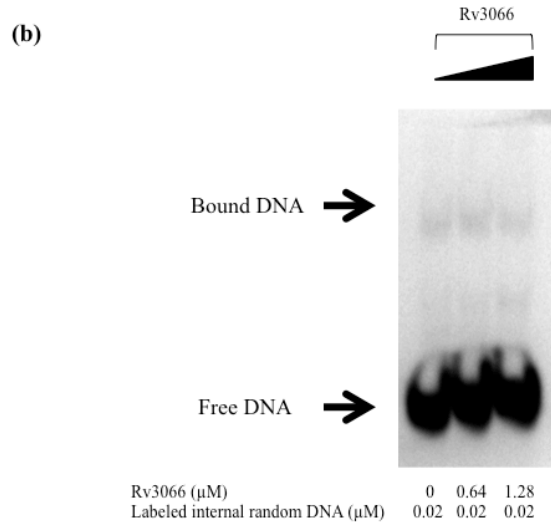
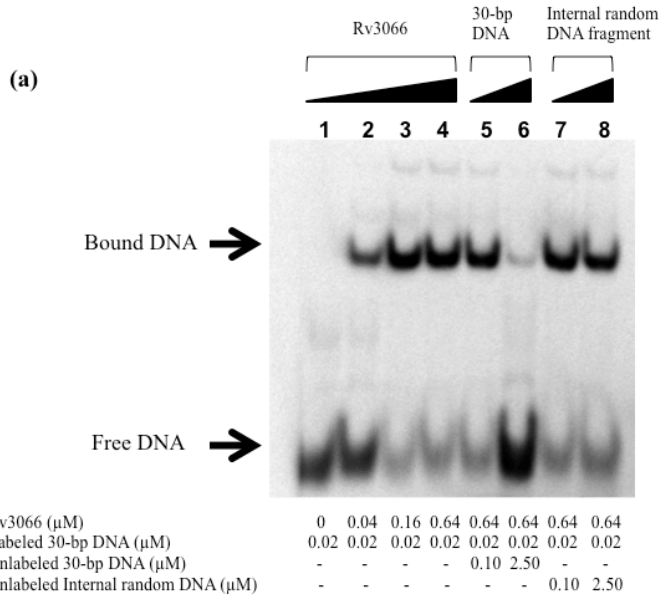


Figure 5. Electrophoretic mobility shift assay for Rv3066 and IR1 binding. (a) The DIG-11-dUTP-labeled DNA (0.02 μM) was incubated with increasing concentrations (0, 0.04, 0.16 and 0.64 μM) of the purified Rv3066 protein (lanes 1-4, respectively). With Rv3066 at 0.64 μM , the binding was competed by the unlabeled 30-bp DNA (0.10 and 2.50 μM , lanes 5 and 6, respectively), and unlabeled internal random DNA fragment (0.10 and 2.50 μM , lanes 7 and 8, respectively). (b) Control experiment of EMSA. The control experiments were performed using 0.02 μM labeled internal random DNA with different concentrations of the Rv3066 regulator (0, 0.64 and 1.28 μM , lanes 1, 2 and 3, respectively). (c) Ethidium bromide dissociates the Rv3066-IR1 complex. Different concentrations (0, 6.4, 64, 320 and 1,280 μM) of ethidium bromide were incubated with 0.64 μM of purified Rv3066 (lanes 2-7, respectively) for 30 min before adding the DIG-11-dUTP-labeled 30-bp DNA (0.02 μM) for the assays. Lane 1 indicates the signal of the free DIG-11-dUTP-labeled DNA.

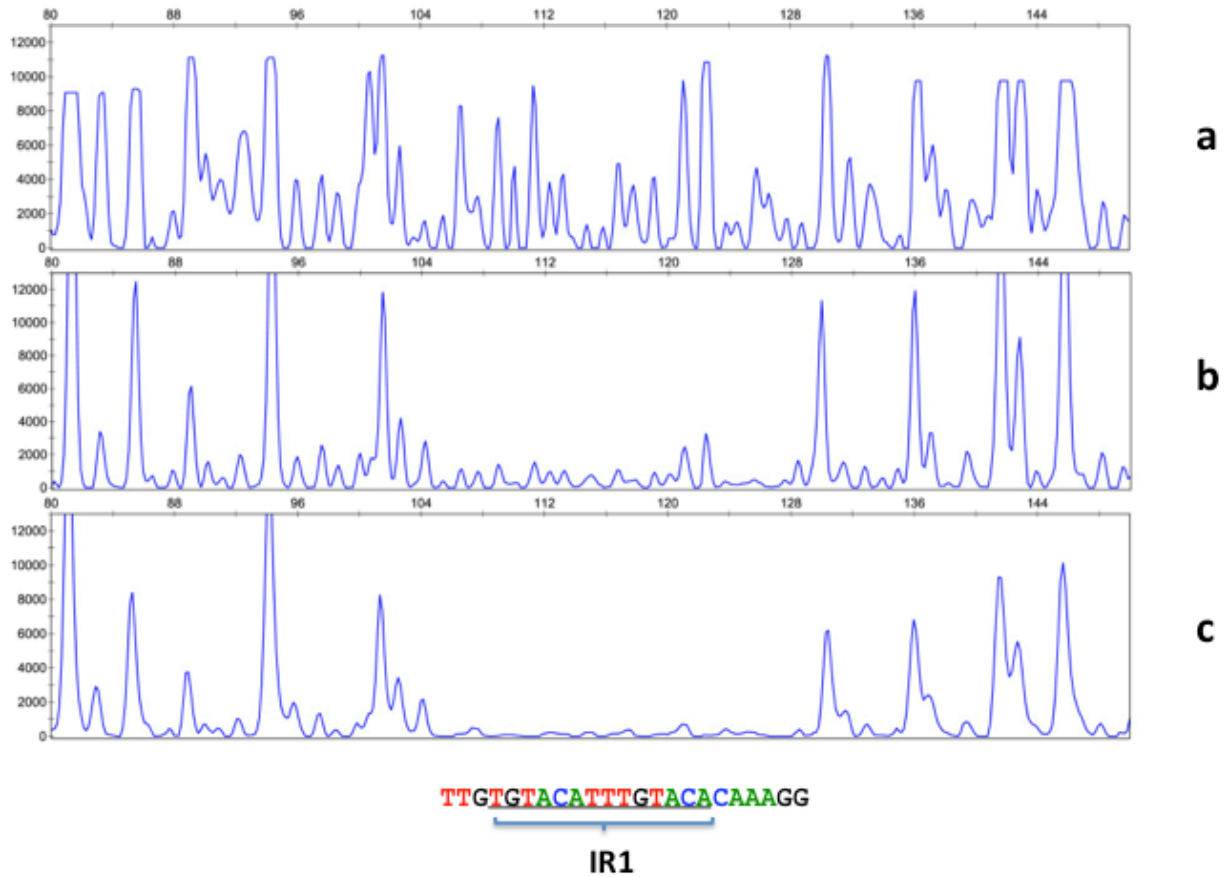


Figure 6. Direct binding of Rv3066 to the *mmr-rv3066* promoter by dye primer based DNase I footprint assay. Electropherograms indicating the protection pattern of the *mmr-rv3066* promoter after digestion with DNase I following incubation with (a) 0, (b) 1.5 pmol, and (c) 3.0 pmol of dimeric Rv3066 are shown. The protected DNA sequence TTGTGTACATTGTACACAAAGG containing IR1 is also shown.

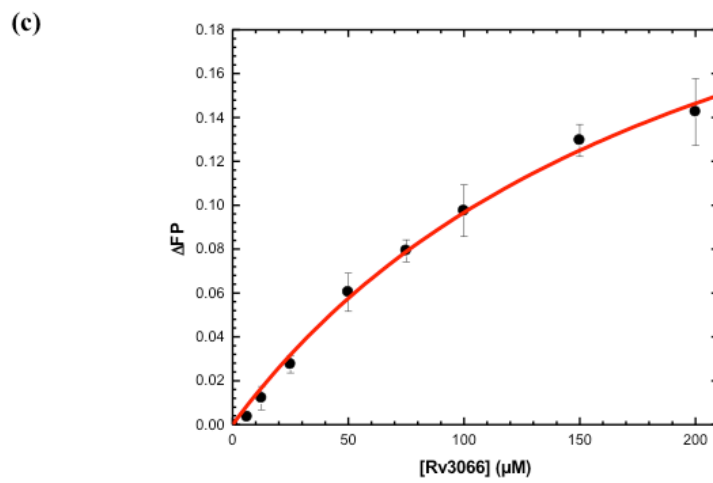
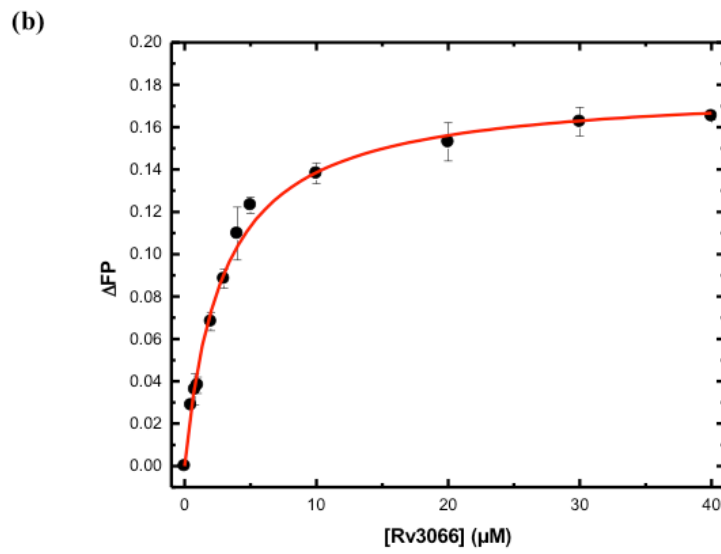
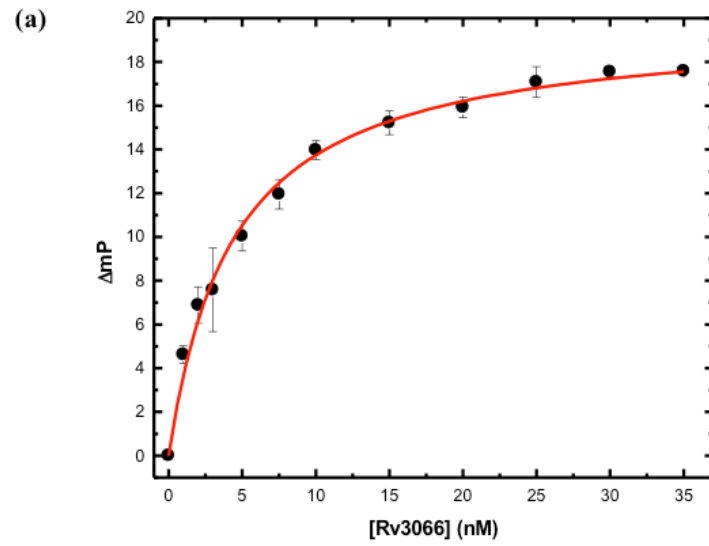


Figure 7. Representative fluorescence polarization of Rv3066. (a) The binding isotherm of Rv3066 with the 30-bp DNA containing the IR1 sequence, showing a K_D of 4.4 ± 0.3 nM. (b) The binding isotherm of Rv3066 with ethidium, showing a K_D of 2.9 ± 0.2 μ M. (c) The binding isotherm of Rv3066 with thioridazine, showing a K_D of 211.8 ± 34.2 μ M. Fluorescence polarization is defined by the equation, $FP = (V - H) / (V + H)$, where FP equals polarization, V equals the vertical component of the emitted light, and H equals the horizontal component of the emitted light of a fluorophore when excited by vertical plane polarized light. FP is a dimensionless entity and is not dependent on the intensity of the emitted light or on the concentration of the fluorophore. mP is related to FP, where 1 mP equals one thousandth of a FP.

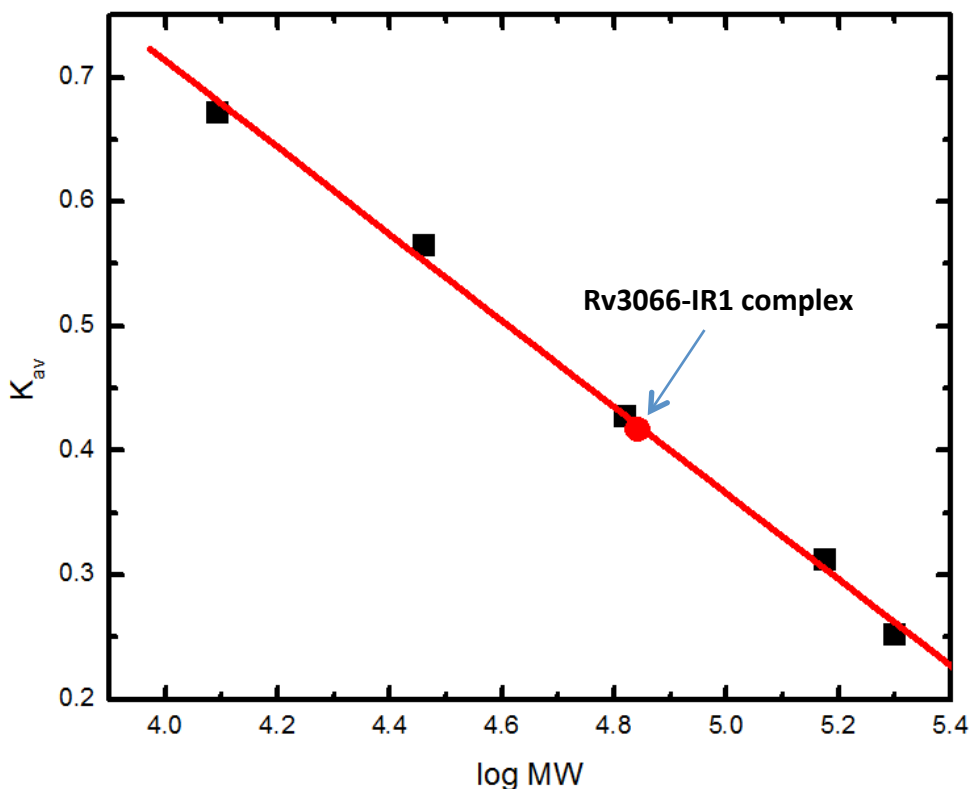


Figure 8. Representative gel filtration experiment. The experiment demonstrated that two Rv3066 molecules are bound to one 30-bp DNA containing the IR1 operator. The y -axis values were defined as: $K_{av} = (V_e - V_0)/(V_T - V_0)$, where V_T , V_e , and V_0 are the total column volume, elution volume, and void volume of the column, respectively. Standards used were: A, cytochrome C (M_r 12,400); B, carbonic anhydrase (M_r 29,000); C, albumin bovine serum (M_r 66,000); D, alcohol dehydrogenase (M_r 150,000); and E, β -Amylase (M_r 200,000). The void volume was measured using blue dextran (M_r 2,000,000).

Supplementary data

Supplementary Figures

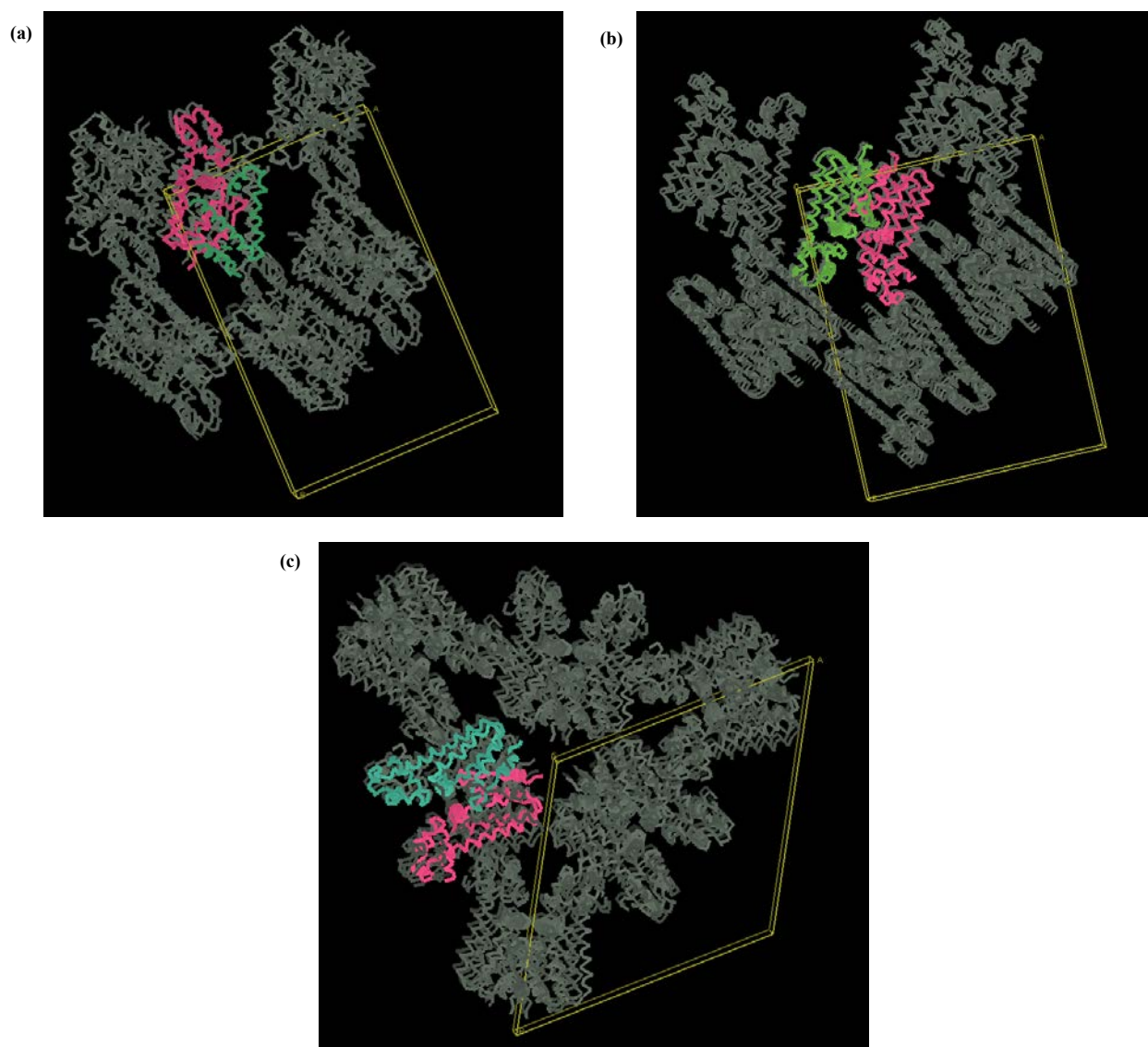


Fig. S1. Packing diagrams of the Rv3066 crystals. (a) Packing diagram of the form I crystal viewed along the c axis. The two subunits of one of the dimeric Rv3066 are colored green and magenta. The rest of the other dimers are colored gray. (b) Packing diagram of the form I crystal viewed along the c axis. The two subunits of one of the dimeric Rv3066 are colored green and magenta. The rest of the other dimers are colored gray. (c) Packing diagram of the

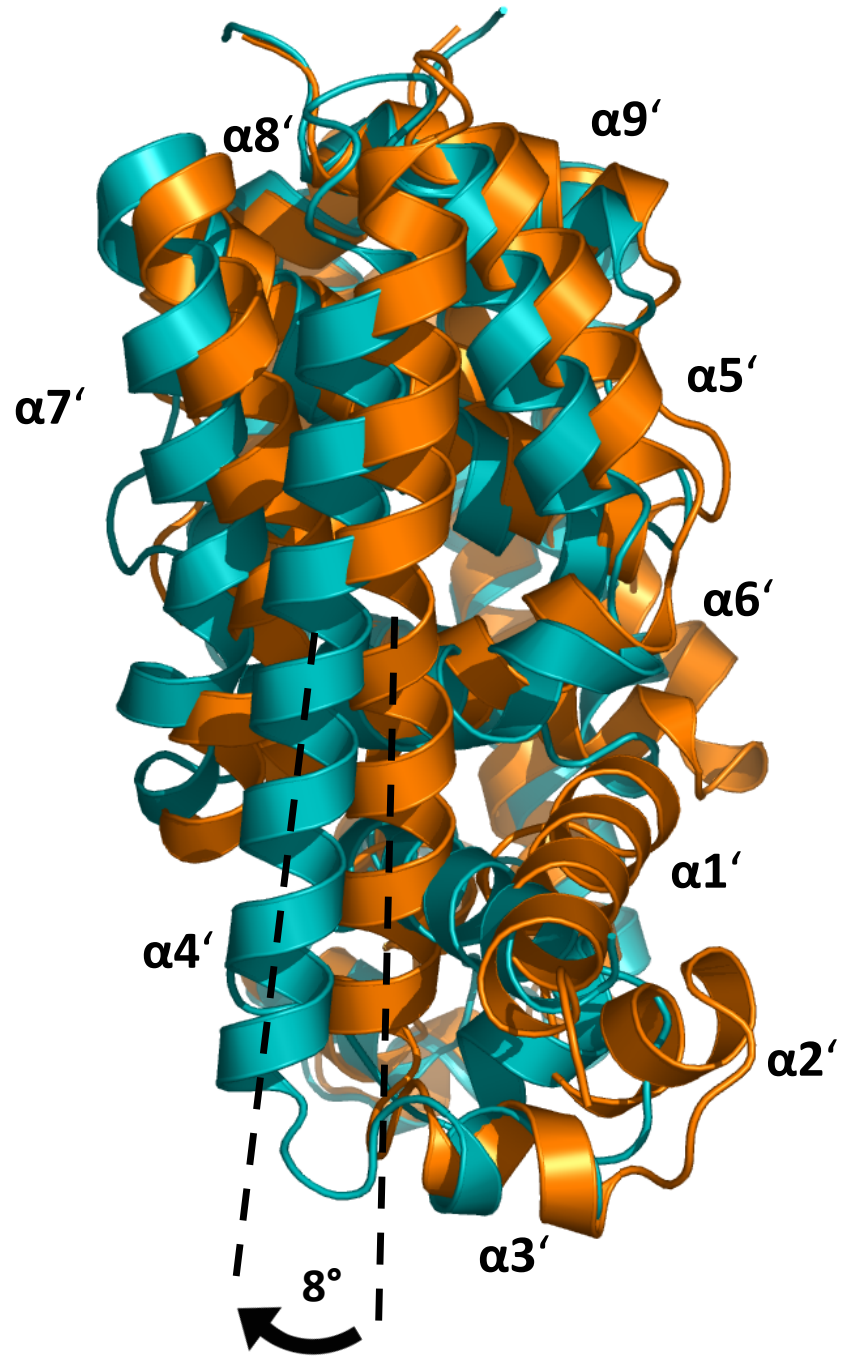


Fig. S3. Side view of the superimposition of the dimeric structures of forms I and II (orange, form I; blue, form II). This view depicts an 8° rigid body rotation of the right subunit ($\alpha 1'$ - $\alpha 9'$) of form II with respect to that of form I.

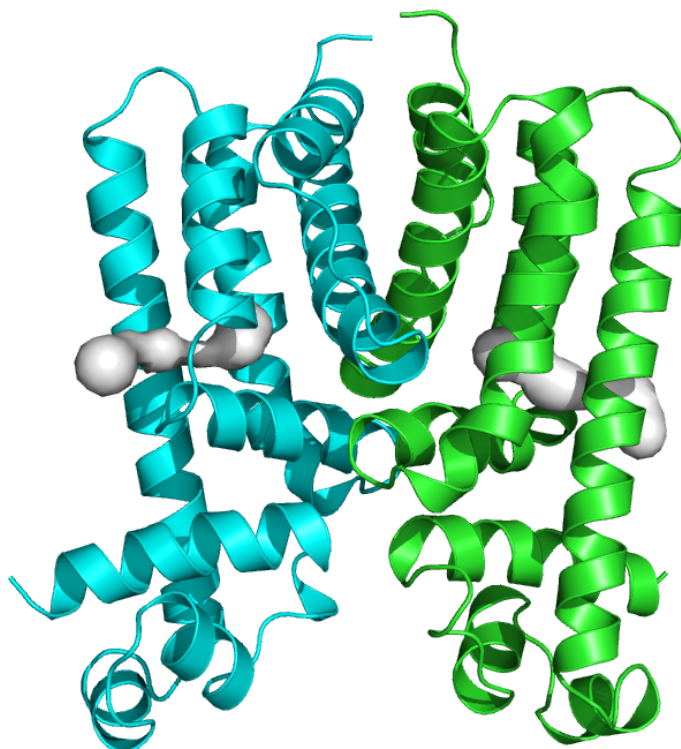


Fig. S4. The hydrophobic binding pocket of form II of apo-Rv3066. This pocket was calculated using the program CAVER (<http://loschmidt.chemi.muni.cz/caver>). The binding tunnel on each subunit of Rv3066 is colored gray.

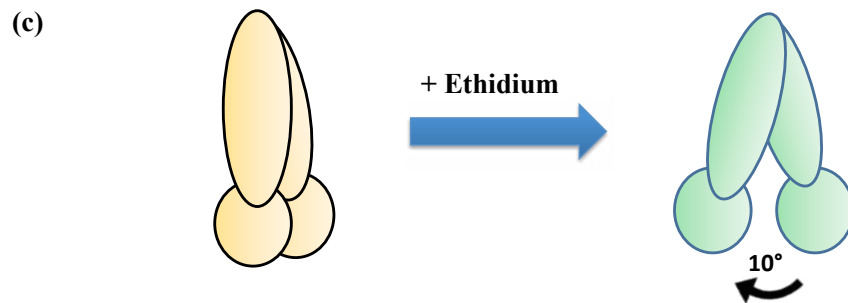
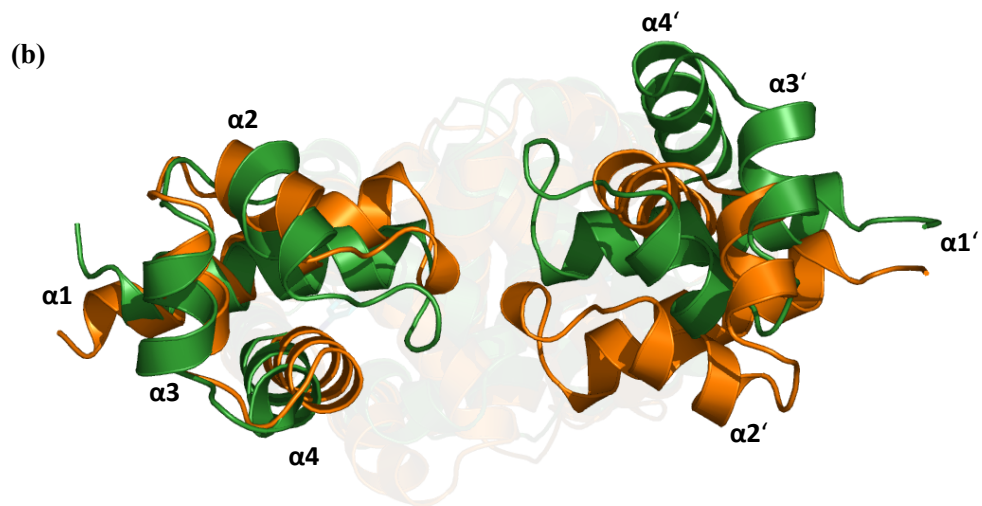
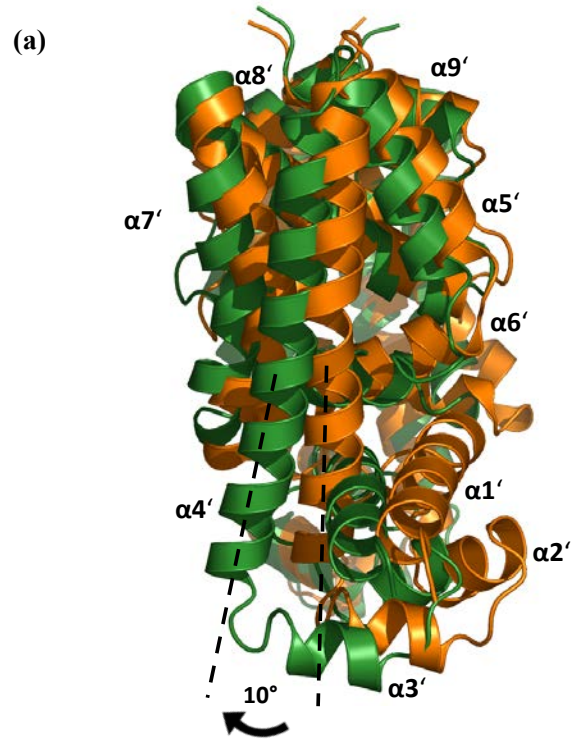


Fig. S5. Structural comparison of form I and Rv3066-ethidium. (a) Side view of the superimposition of the dimeric structures of form I and Rv3066-ethidium (orange, form I; green, ethidium bound). This view depicts a 10° rigid body rotation of the right subunit ($\alpha 1'$ - $\alpha 9'$) of Rv3066-ethidium with respect to that of form I. (b) Superimposition of the N-terminal domains of form I and Rv3066-ethidium. The secondary structural elements are shown as ribbons (orange, form I; green, Rv3066-ethidium). (c) A schematic representation illustrating the rigid-body rotation of the subunits relative to one another. This side view demonstrates a 10° rotation of the right subunit of Rv3066 with respect to the left one after ethidium binding.

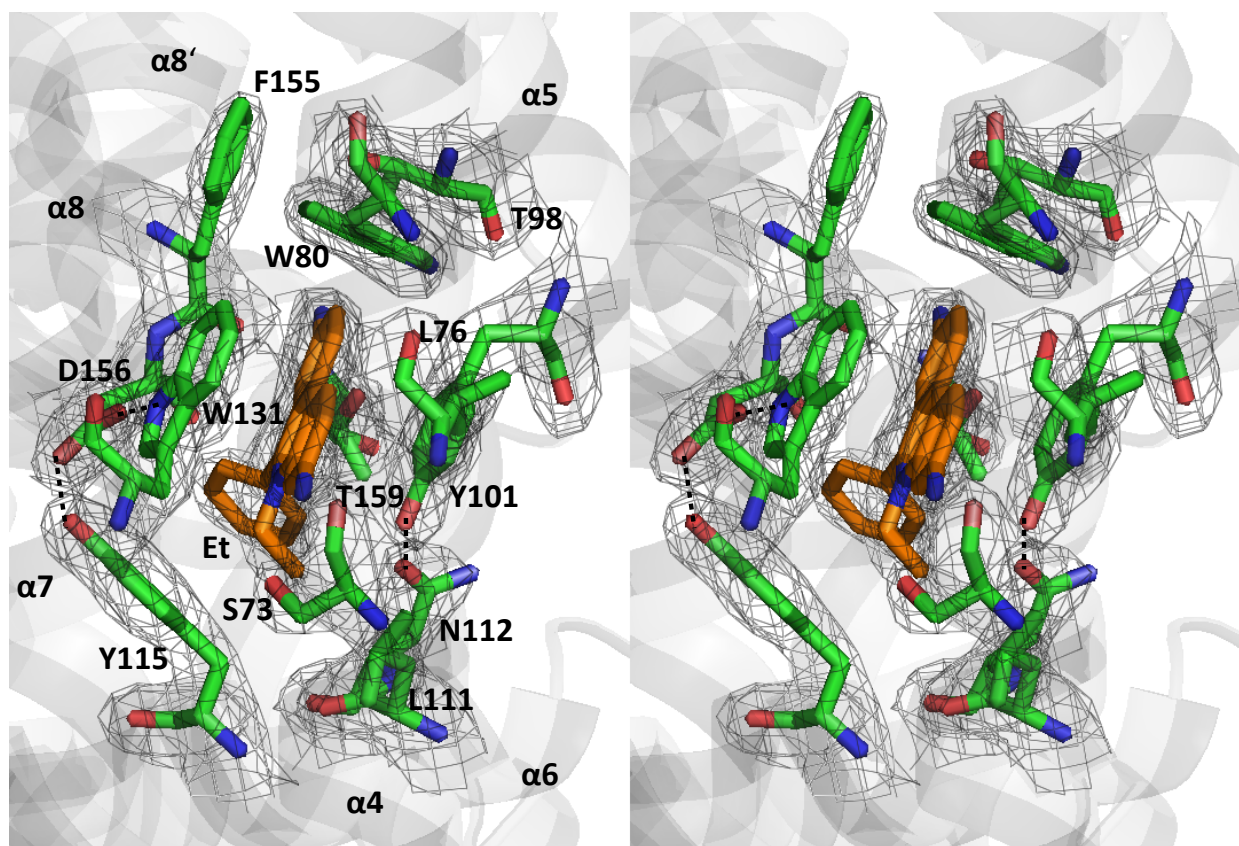


Fig. S6. The ethidium binding pocket and electron density map of the right subunit of dimeric Rv3066. This $2F_o - F_c$ electron density map is contoured at 1.5σ (gray mesh). The figure indicates that the aromatic residues W80, Y101, Y115 and W131 (green) form a cage-like

binding site to house the bound ethidium (orange), suggesting aromatic stacking interactions govern drug recognition of the regulator. The hydrogen bond distances between D156 and Y115, D156 and W131, and N112 and Y101 are 2.7, 2.7, and 2.7 Å, respectively.

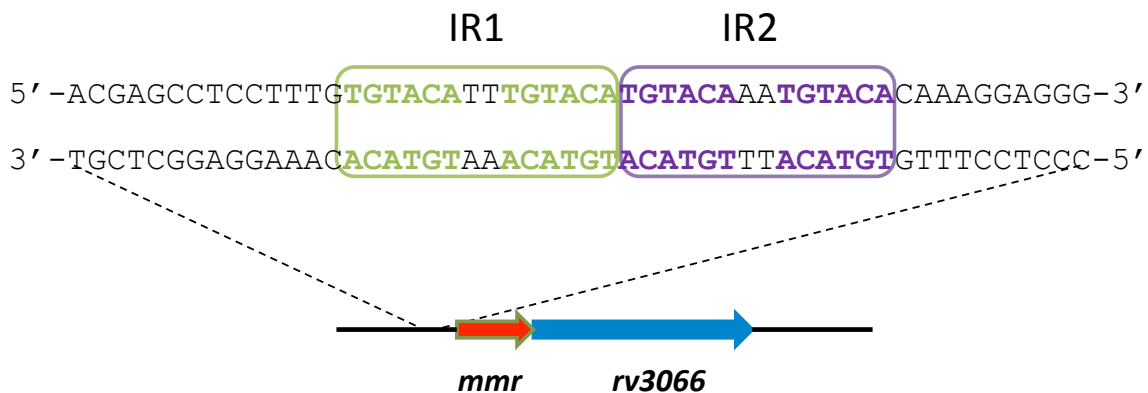


Fig. S7. The palindromic inverted repeat at the promoter region of the *mmr-rv3066* operon. Operons of *mmr* and *rv3066* (red, *mmr*; blue, *rv3066*). The IR1 and IR2 sequences are in green and purple, respectively.

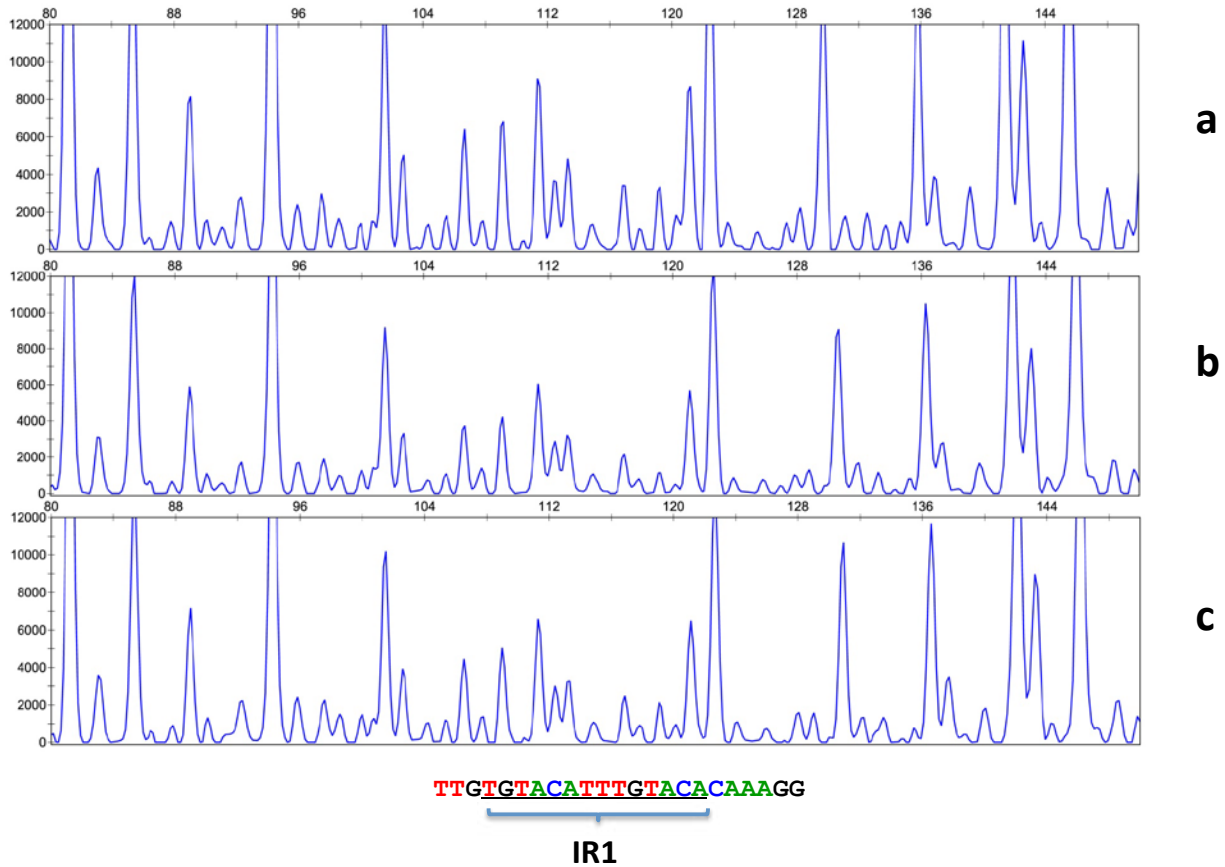


Fig. S8. Binding of BSA to the *mmr-rv3066* promoter by dye primer based DNase I footprint assay. Electropherograms indicating that no protection pattern of the *mmr-rv3066* promoter has been found after digestion with DNase I following incubation with (a) 0, (b) 3.0 pmol, and (c) 6.0 pmol of BSA. The protected DNA sequence TTGTGTACATTTGTACACAAAGG containing IR1 by Rv3066 is also shown.

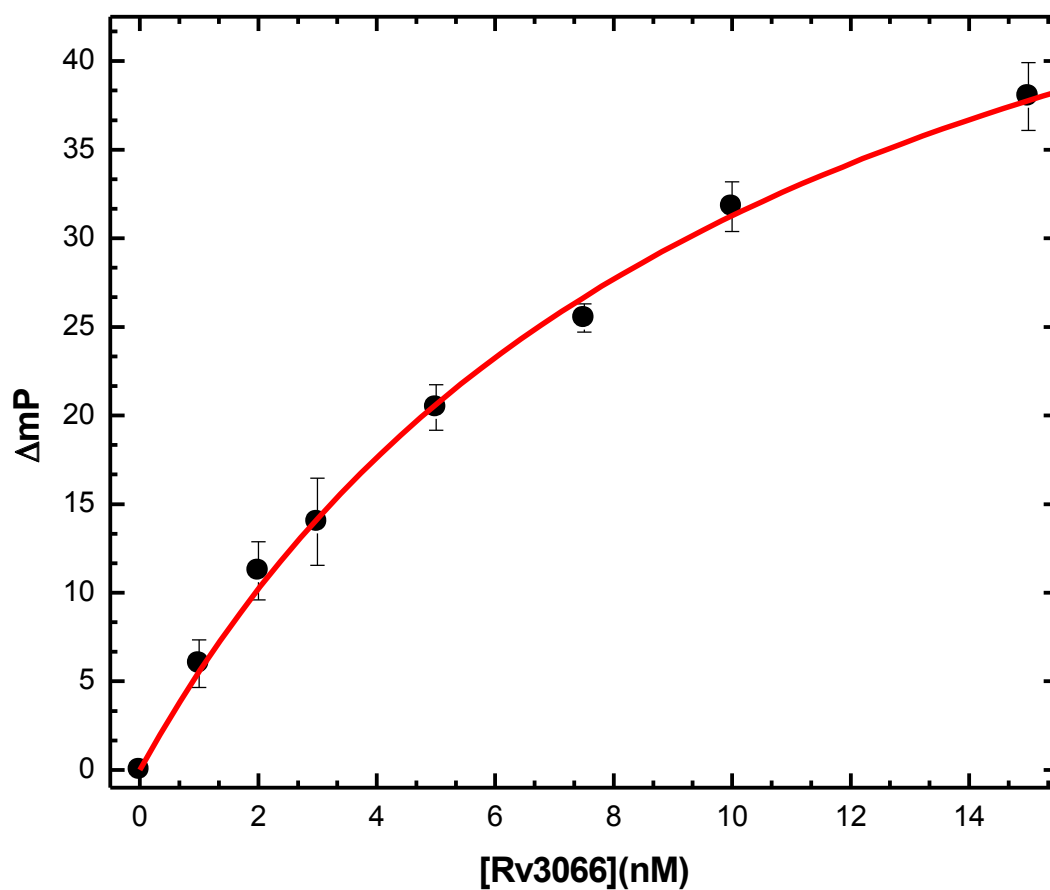


Fig. S9. The binding isotherm of Rv3066 with the 30-bp IR1 in the presence of 1 μM of ethidium. The binding isotherm indicates a K_D of 10.7 ± 0.9 nM.

CHAPTER 3**BIOMOLECULAR MEMBRANE PROTEIN CRYSTALLIZATION**

A review published in Philosophical Magazine, 2012, 92:2648-2661

Jani Reddy Bolla,¹ Chih-Chia Su¹ and Edward W. Yu^{1,2*}

¹Department of Chemistry, Iowa State University, Ames, IA 50011, USA

²Department of Physics and Astronomy, Iowa State University, Ames, IA 50011, USA

* To whom correspondence should be addressed. E-mail: ewyu@iastate.edu

Abstract

Integral membrane proteins comprise approximately 30% of the sequenced genomes, and there is an immediate need for their high-resolution structural information. Currently, the most reliable approach to obtain these structures is x-ray crystallography. However, obtaining crystals of membrane proteins that diffract to high resolution appears to be quite challenging, and remains a major obstacle in structural determination. This brief review summarizes a variety of methodologies for use in crystallizing these membrane proteins. Hopefully, by introducing the available methods, techniques, and providing a general understanding of membrane proteins, a rational decision can be made about how to crystallize these complex materials.

1. Introduction

High-resolution crystal structures of membrane proteins are in great demand, as these structures often provide an immediate insight into the mechanisms on how these protein machines work. Membrane proteins play a vital role in numerous cellular functions. They act as receptors, transporters, channels, and are involved in cell adhesion, signaling, as well as a variety of metabolic pathways. About 30% of the mammalian genome encodes these integral membrane proteins [1], and more than 50% of currently administrative pharmaceutical agents are designed for targeting them [2]. Unfortunately, the understanding of the structure and function of these membrane proteins is hampered by the difficulties associated with expressing and handling them. Membrane proteins are not soluble in aqueous buffer because of their intrinsic characteristics. These proteins possess large hydrophobic surfaces, thus detergents are required to extract them from cell membranes and to maintain them in a soluble form in aqueous solution (Fig. 1). Mild detergents are widely used in handling membrane proteins, however, many of these proteins tend to aggregate or denature when solubilized by these amphiphilic chemicals. Because of the complications related to the stability and solubility of membrane proteins, it is often difficult to study these proteins using common biophysical techniques such as x-ray scattering, magnetic and optical spectroscopies.

Like many chemical compounds, proteins can be crystallized as they become supersaturated in aqueous solution. The crystallization process is often initiated by the addition of various precipitating agents, including salts like NaCl, $(\text{NH}_4)_2\text{SO}_4$ etc., polymers like polyethylene glycols (PEGs), and/or a variety of organic molecules like ethanol, isopropanol, 2-methyl-2,4-pentandiol (MPD), etc. These precipitating agents reduce the solubility of protein molecules and eventually supersaturate them in solution.

As the pH and temperature also affect the solubility of protein samples, the process of protein crystallization is often found to be pH and temperature dependent.

Different from other chemical crystals, protein crystals possess high solvent content. The solvent content of protein crystals was first studied by Matthews [3] in 1968. The study was based on the known soluble protein crystal structures at that time. It was found that the crystal volume occupied by solvent ranged from 27 to 65%, with the most common solvent content at 43%. Although the high solvent content often results in a poorer crystal quality, it provides an environment that is close to the native cellular environment for these protein molecules. Thus this high crystal solvent content indeed offers an opportunity for the protein molecule to better mimic its native structure in the cellular environment. In the case of membrane proteins, this solvent content is even higher (between 65 and 80%) because of the presence of detergent and/or amphiphilic molecules. As a result, membrane protein crystals are often found to diffract x-ray poorly, and many of these crystals can only provide low to medium resolution structural information.

Vapor diffusion is the most popular method that allows the protein samples to reach supersaturation [4]. This method is achieved by increasing the protein concentration gradually through a relatively slow dehydration process. Typically, a drop composed of a mixture of protein sample and precipitating agents is placed in vapor equilibrium with a hygroscopic reservoir solution containing two times higher in concentration of these precipitating agents (Fig. 2). As water leaves the drop, the protein concentration undergoes an increase in relative supersaturation, which eventually initiates nucleation of protein bearing crystals. Although the idea is simple, many proteins simply refuse to form crystals. Thus, protein crystallization is often found to be labor intensive and time consuming.

The principle of membrane protein crystallization is very similar to that of water-soluble proteins except that the presence of detergent, which adds another layer of difficulty, is required to solubilize the membrane protein molecules in aqueous solution. This review provides a brief overview of different approaches in the crystallization of these membrane proteins. To date, a great deal of useful information in the field can be found in internet-based resources. For example, the web sites of “membrane proteins of known structure” (<http://blanco.biomol.uci.edu/mpstruc/>) and “membrane protein data bank” (<http://www.mpdb.ul.ie/>) [5] frequently update the lists of all known membrane protein structures, as well as their crystal growth methods and conditions.

2. Detergent-based methods

Membrane proteins can be crystallized for use in macromolecular structural determination by a variety of methodologies. The detergent-based methods (Fig. 3) employ detergent-solubilized, purified membrane protein samples directly in crystallization trials [6]. To obtain a stable protein sample suitable for crystallization, one needs to get through many obstacles, including finding an effective system for protein expression and choosing the right detergent for protein solubilization and purification. In many successful cases, the membrane proteins were produced in *Escherichia coli* cells. However, *Pichia pastoris* yeasts [7, 8], *Saccharomyces cerevisiae* yeasts [9] as well as Sf9 insect cells [10] have also been commonly used to express the proteins of interest for crystallization. After obtaining the expressed membrane proteins, the proteins have to be extracted from lipid membranes with mild detergents and then purified to stable, homogeneous samples that are essential for crystallization. Table 1 and Figure 4 summarize some of the most frequently used detergents for membrane protein

purification and crystallization. The detergent-based crystallization methods include vapor diffusion [11], micro-batch [12, 13], dialysis [11, 14] and counter-diffusion [15, 16] and microfluidics [17]. A schematic for the detergent-based crystallization approach is shown in Figure 3. At present, the step of crystallizing purified, detergent-solubilized membrane proteins remains the major bottleneck. Nevertheless, the rate of progress is accelerating, especially in the past decade.

Among the detergent-based methods, it appears that vapor diffusion (both of the hanging-drop and sitting-drop types [11]) is the most common approach (Fig. 2). The primary advantage of this approach is that the crystallization setup is rather straightforward and relatively easy to handle. Membrane protein molecules surrounded by belt-like detergent micelles can be treated as ordinary soluble protein molecules (Fig. 1b), and thus standard vapor diffusion crystallization procedures can be used to obtain the crystals. The major drawback, however, is that the protein molecules have to withstand the harsh environment in detergent micelles. Nonetheless, vapor diffusion, which is the first to have been applied to membrane proteins, has been proven to be the most successful approach in crystallizing membrane proteins. The first crystal structure of membrane protein obtained in 1985 is photosynthetic reaction center [18]. This structure was determined using the method of vapor diffusion. To date, over 80% of membrane protein structures in the Protein Data Bank (<http://www.rcsb.org/>) were solved based on crystals grown with this method. A general protocol for the crystallization of membrane proteins using this approach can be found in an article published by Newby et al. [19].

If crystallization of particular membrane proteins does not work, one may want to try to co-crystallize the proteins with antibodies. This approach is especially useful when the membrane protein molecules contain relatively small hydrophilic domains [20]. Antibody

fragments, including Fab and Fv, that recognize native protein conformations have been shown to facilitate crystallization of membrane proteins by increasing the polar surface area for protein-protein contacts. In addition, these antibody fragments can be used to stabilize specific conformations of the proteins by restricting the flexibility of mobile domains, in turn aiding the success of crystallization attempts [20]. The approach of co-crystallizing monoclonal antibody fragments with integral membrane proteins using vapor diffusion has been successfully led to several important crystal structures, including cytochrome *c* oxidase [21], KcsA potassium channel [22], ClC chloride channel [23], and most recently the human β_2 adrenergic receptor [24]. To date, more than 50 membrane protein structures have been reported in the Protein Data Bank using this approach.

Membrane protein molecules tend to be more stable in the presence of lipid. Indeed, it has been revealed that there is a direct link between the presence of lipid environment and the structure and function of integral membrane proteins [25]. Thus, one should be aware of the importance of bound lipid molecules in membrane protein crystallization. It has been shown that the addition of lipid molecules can significantly improve the quality of the membrane protein crystals and allow them to diffract x-rays at high-resolution [26, 27]. If the crystallization trials do not result in high quality membrane protein crystals, one may want to conduct crystallization by adding lipid and changing the protein:lipid molar ratio in the vapor diffusion trials. This approach has been proven to be successful in obtaining high quality crystals of the cytochrome *b₆f* complex [26, 27].

3. Crystallization of the CusBA adaptor-transporter efflux system

The approach of vapor diffusion has allowed researchers in our laboratory to determine the crystal structures of different components, either alone or in a complex form, of the CusBA heavy-metal efflux complex (Figs. 5 and 6) [28-30]. The raw proteins of the CusA transporter and CusB adaptor were individually produced in *E. coli* cells. Then, the CusA protein was extracted and purified with a detergent 6-cyclohexyl-1-hexyl- β -D-maltoside (CYMAL-6) [28]. As CusB is a soluble protein, the presence of detergent was not required for protein extraction and purification. However, it was found that the addition of a detergent *n*-dodecyl- β -D-maltoside (DDM) was helpful to produce a more homogeneous sample and avoid protein aggregation during purification procedures [29].

Crystals of the CusA transporter were grown at 298K using vapor diffusion in the presence of CYMAL-6 with PEG 3350 as precipitant and ammonium sulfate as salt [28]. Crystals of the CusB adaptor were grown using the same approach in the presence of the detergent DDM with PEG 1000 and sodium citrate as precipitant and salt [29]. For the crystallization of the CusBA adaptor-transporter complex, the crystals were produced using vapor diffusion at room temperature in the presence of CYMAL-6. The precipitant and salt for crystallizing the CusBA complex were PEG 6000 and ammonium acetate [30]. Crystals of CusA, CusB and CusBA grew to a full size in the drops within a month (Fig. 5).

For x-ray data collections, a single crystal of CusA or CusBA was flash-cooled in cryoprotectant solutions containing 30% glycerol at 100K. As for CusB, a single crystal was cryoprotected in solution containing 30% PEG 1000 before freezing at 100K. All diffraction data were collected at 100K at beamline 24ID-C located at the Advanced Photon Source, using an ADSC Quantum 315 CCD-based detector.

Crystals of the CusA transporter were found to be trigonal with space group $R32$ ($a = b = 178.4 \text{ \AA}$, $c = 285.8 \text{ \AA}$). In the asymmetric unit, only one CusA protomer was found. The crystal structure of the CusA transporter was then determined at a resolution of 3.5 \AA [28]. For the CusB adaptor, the crystals belonged to orthorhombic space group $I222$, with $a = 85.2 \text{ \AA}$, $b = 113.3 \text{ \AA}$, $c = 258.5 \text{ \AA}$. The asymmetric unit consists of two CusB protomers. The structure of CusB was then resolved to a resolution of 3.4 \AA [29].

The co-crystals of the CusBA adaptor-transporter complex took a trigonal space group $R32$ with unit cell parameters $a = b = 160.2 \text{ \AA}$, $c = 682.7 \text{ \AA}$. The asymmetric unit contains one CusA and two CusB molecules. The final structure of the CusBA adaptor-transporter complex was determined to 2.9 \AA resolution [30] (Fig. 6).

4. Lipid-based methods

As the presence of phospholipids tends to stabilize membrane protein molecules, and in some cases the presence of these lipid molecules is a prerequisite for the protein activity, there is a strong rationale to crystallize membrane proteins in the presence of phospholipids. The lipid-based methods utilize biomolecular lipid bilayers to facilitate membrane protein crystallization [31]. These include the bicelle [32, 33], vesicle [34, 35], and lipidic cubic phase [36, 37] methods. In contrast to the detergent-based methods, these approaches promote the use of lipid bilayers, which mimic the native environment of membrane proteins, as an embedded system to stabilize the protein molecules. A schematic of the lipid-based crystallization is illustrated in Figure 7. The bicelle and vesicle methods are still new and have not been extensively evaluated. However, the lipidic cubic phase approach has been found to be very successful. All these

methods offer an advantage that the protein molecules are removed from the harsh detergent environment and placed into a more hospitable surrounding during the process of crystallization.

Crystallization of membrane proteins in lipidic cubic phases has only been developed in the past 15 years. Nonetheless, this method has already been proven to be effective and essential for crystallizing a certain membrane proteins. The first crystal structure determined using this crystallization method is bacteriorhodopsin [38, 39]. To date, about one in ten integral membrane protein structures in the Protein Data Bank have been solved using crystals grown by this technique. Recent successes with this technique include the crystal structures of β_2 -adrenergic [40] and adenosine A_{2A} [41] G protein-coupled receptors.

In the cubic phase method, the crystallization process takes place in and from a semi-solid bicontinuous lipid matrix (Fig. 8). Thus, this technique involves making a highly ordered artificial lipid bilayer, namely cubic phase, before crystallization trials. The protein of interest is then incorporated into the highly ordered cubic phase. This bicontinuous lipidic cubic phase contains extended water channels, which promote the detergent-solubilized membrane protein molecules to return to the lipid bilayer environment. After, precipitating agents are added to initiate protein crystallization.

1-mono-olein-*rac*-glycerol (MO) is the most commonly used lipid for forming these highly ordered cubic phases. The difficulty of this method is that it is a time consuming process in obtaining the initial cubic phase. As mentioned earlier, cubic phase is a semi-solid lipid matrix. It is also hard to work with because it is extremely viscous and sticky, making it difficult to handle and to dispense accurately in small volumes for setting up protein crystallization trials. A detailed protocol for crystallizing membrane proteins using the technique of lipidic mesophases is described in a review article by Caffrey and Cherezov [37].

Another closely related lipid-based approach is the lipidic spongy phase method [42]. A liquid lipid bilayer in the form of spongy phase can be obtained by adding an additional solvent such as PEGs, MPD, or jeffamine M600 to the MO:water system. The aqueous pores in the spongy phase can be up to three times as large as those in the cubic phase. Thus, the spongy phase method may be more useful in crystallizing membrane proteins with large extracellular domains.

One major advantage of employing lipidic spongy phase for membrane protein crystallization is that it is liquid in form at room temperature, thus it is easy to handle during the course of setting up crystallization trials. This liquid property also makes it suitable for conventional hanging-drop and sitting-drop vapor diffusion experiments. A nice summary of the lipidic spongy phase approach can be found in a literature by Wöhri *et al.* [42].

Both cubic and spongy phases form three-dimensional continuous lipid bilayers and interconnected water channels. This architecture promotes the lateral diffusion of protein molecules in the matrices. Presumably, the membrane protein molecules are first reconstituted in the lipid phase and then diffuse laterally to concentrate and assemble at the nucleation point to form small protein crystals at some point.

Recently, the bicelle method [32, 33] has been gaining popularity in the field after a few successes in crystallizing membrane proteins, including the mouse VADC₁ channel [43] and human β_2 adrenergic receptor [44], by using this approach. Bicelles, formed in a lipid-detergent mixture, have small disc-like features constituting of a planar lipid-bilayer (Fig. 9). The procedures for the bicelle approach are rather simple. First, the protein is mixed with bicelle components containing a mixture of lipid and detergent. Crystallization is then achieved using the method of vapor diffusion. Thus, the bicelle method can be considered as a compromise

between the user-friendly vapor diffusion approach and the more protein-friendly lipidic mesophase technique.

The vesicle method, which makes use of successive fusion of vesicular assemblies, is a lipid bilayer approach initially developed by Takeda et al. [34] to crystallize bacteriorhodopsin. First, the vesicles are formed from the purple membrane fragments in the presence of detergent and precipitating agents. These spherical vesicles can be fused successively to form stacks of planar membranes by altering temperature as well as increasing the concentration of precipitating agents. Similar method has been used to crystallize the light-harvesting complex of photosystem II by reconstituting the purified membrane protein into liposomes [35]. In this case, the purified membrane protein molecules were first reconstituted in liposomes to form two-dimensional arrays. These proteoliposomes containing the two-dimensional arrays of protein molecules were then crystallized to form lattice. This approach may be useful for crystallizing membrane proteins that are unstable in a detergent environment. Yet, it remains to be seen if this remarkable approach can be applied generally in crystallizing other membrane proteins.

5. Detergents

Choosing the right detergent has been the key success for membrane protein crystallization. It is one of the most important factors for obtaining high quality membrane protein crystals suitable for x-ray diffraction. Thus, the rule of thumb is that more efforts should be made in screening a variety of mild detergents than in optimizing other parameters when crystallizing a new membrane protein. Nonionic and zwitterionic detergents are usually used for crystallization of membrane proteins (Table 1 and Fig. 2). The most successfully used detergents are nonionic alkyl sugars with C8-C12 alkyl chains. Thus far, the most common detergent for

use in crystallizing α -helical type membrane proteins is *n*-dodecyl- β -D-maltopyranoside, which contains 12 carbons in the main alkyl chain. The second most popular detergent in membrane protein crystallization is *n*-octyl- β -D-glucopyranoside, which is a C8-alkyl chained detergent.

During the past several years, the development of new detergents has been emerged as a new tool for handling these membrane proteins. Low molecular weight agents, such as hemifluorinated surfactants [45, 46] and cholate acid-based amphiphiles [47], have been proven to be promising in aiding the study of membrane proteins in aqueous solution. In addition, a new family of detergents, designated as maltose-neopentyl glycol amphiphiles [48], is of particular attractive in the field. The new generation of amphiphiles may have a wide application in solubilization, stabilization and crystallization of membrane proteins, and eventually yielding high-quality crystals for diffraction analysis.

6. Concluding remarks

This review is an attempt to outline different methods for use in three-dimensional membrane-protein crystallization. Crystallization of membrane proteins can be a rather difficult and discouraging process. It is hope that this brief summary will provide with a useful guide for researchers to tackle this problem. Particularly, the authors hope that this review will encourage more physicists to undertake research projects in this exciting field.

References

1. E. Wallin and G. von Heijne, *Protein Sci.* 7 (1998) p.1029.
2. J. Liu and B. Rost, *Protein Sci.* 10 (2001) p.1970.
3. B.W. Matthews, *J. Mol. Biol.* 33 (1968) p.491.
4. A. Ducruix and R. Giege, *Crystallization of Nucleic Acids and Proteins: A Practical Approach*. IRL Press, New York, 1992.
5. P. Raman, V. Cherezov and M. Caffrey, *Cellular and Molecular Life Sciences* 63 (2006) p.36.
6. M.C. Wiener, *Methods* 34 (2004) p.364.
7. J.M. Cregg, J.L. Cereghino, J. Shi and D.R. Higgins, *Mol. Biotechnol.* 16 (2000) p.23.
8. J.L. Cereghino and J.M. Cregg, *FEMS Microbiol. Rev.* 24 (2000) p.45.
9. M. Jidenko, et al. *Proc. Natl. Acad. Sci. USA* 102 (2005) p.11687.
10. J. Jasti, H. Furukawa, E.B. Gonzales and E. Gouaux, *Nature* 449 (2007) p.316.
11. B.J.Sutton and M.K. Sohi, *Methods Mol. Biol.* 27(1994) p.1.
12. P.J. Loll, A. Tretiakova and E. Soderblom, *Acta Crystallogr. D Biol. Crystallogr.* 59 (2003) p.1114.
13. N.E. Chayen, *Crystallization of Membrane Proteins in Oils*. In *Methods and Results in Crystallization of Membrane Proteins*, S. Iwata, ed., International University Line, San Diego, 2003, p.131.
14. P. Fromme, *Crystallization of Photosystem I*. In *Methods and Results in Crystallization of Membrane Proteins*, S. Iwata, ed., International University Line, San Diego, 2003, p.145.
15. J.D. Ng, R.C. Stevens and P. Kuhn, *Methods Mol. Biol.* 426 (2008) p.363.
16. J.D. Ng, J.A. Gavira and J.M. Garcia-Ruiz, *J. Struct. Biol.* 142 (2003) p.218.
17. J. Leng and J.-B. Salmon, *Lab Chip* 9 (2009) p.24.
18. J. Deisenhofer, O. Epp, K. Miki, R. Huber and H. Michel, *Nature* 318 (1985) p.618.
19. Z.E.R. Newby, et al., *Nature Protocols* 4 (2009) p.619.
20. C. Hunte and H. Michel, *Curr. Opin. Struct. Biol.* 12 (2002) p.503.

21. S. Iwata, C. Ostermeier, B. Ludwig and H. Michel, *Nature* 376 (1995) p.660.
22. Y. Zhou, J. H. Morais-Cabral, A. Kaufman and R. MacKinnon, *Nature* 414 (2001) p.43.
23. R. Dutzler, E. B. Campbell and R. MacKinnon, *Science* 300 (2003) p.108.
24. S. G. F. Rasmussen, et al., *Nature* 450 (2007) p.383.
25. R. Phillips, T. Ursell, P. Wiggins and P. Sens, *Nature* 459 (2009) p.379.
26. H. Zhang, G. Kurisu, J.L. Smith, and W.A. Cramer, *Proc. Natl. Acad. Sci. USA* 100 (2003) p.5160.
27. G. Kurisu, H. Zhang, J.L. Smith, and W.A. Cramer, *Science*. 302 (2003) p.1009.
28. F. Long, C.-C. Su, M.T. Zimmermann, S.E. Boyken, K.R. Rajashankar, R.L. Jernigan and E.W. Yu, *Nature* 467 (2010) p.484.
29. C.-C. Su, et al., *J. Mol. Biol.* 393 (2009) p.342.
30. C.-C. Su, F. Long, M.T. Zimmermann, K.R. Rajashankar, R.L. Jernigan and E.W. Yu, *Nature* 470 (2011) p.558.
31. M. Caffrey, *J. Struct. Biol.* 142 (2003) p.108.
32. S. Faham and J.U. Bowie, *J. Mol. Biol.* 316 (2002) p.1.
33. S. Faham, G.L. Boulting, E.A. Massey, S. Yohannan, D. Yang and J.U. Bowie, *Protein Sci.* 14 (2005) p.836.
34. K. Takeda, et al., *J. Mol. Biol.* 283 (1998) p.463.
35. Z. Liu, et al., *Nature* 428 (2004) p.287.
36. M. Caffrey, *Annu. Rev. Biophys.* 38 (2009) p.29.
37. M. Caffrey and V. Cherezov, *Nature Protocols* 4 (2009) p.706.
38. E.M. Landau and J.P. Rosenbusch, *Proc. Natl. Acad. Sci. USA* 93 (1996) p.14532.
39. E. Pebay-Peyroula, G. Rummel, J.P. Rosenbusch and E.M. Landau, *Science* 277 (1997) p.1676.
40. V. Cherezov, et al., *Science* 318 (2007) p.1258.
41. V.P. Jaakola, et al., *Science* 322 (2008) p.1211.
42. A.B. Wöhri, et al., *Structure* 16 (2008) p.1003.

43. R. Ujwal, et al. *Proc. Natl. Acad. Sci. USA* 105 (2007) p.17742.
44. S.G.F. Rasmussen, et al. *Nature* 450 (2007) p.383.
45. J.-L. Popot, *Annu. Rev. Biochem.* 79 (2010) p.737.
46. C. Breyton, et al., *Biophys. J.* 97 (2009) p.1077.
47. Q. Zhang, et al., *Angew. Chem. Int. Edn.* 119 (2007) p.7153.
48. P.S. Chae, et al. *Nature Methods* 7 (2010) p.1003.

Legends of figures

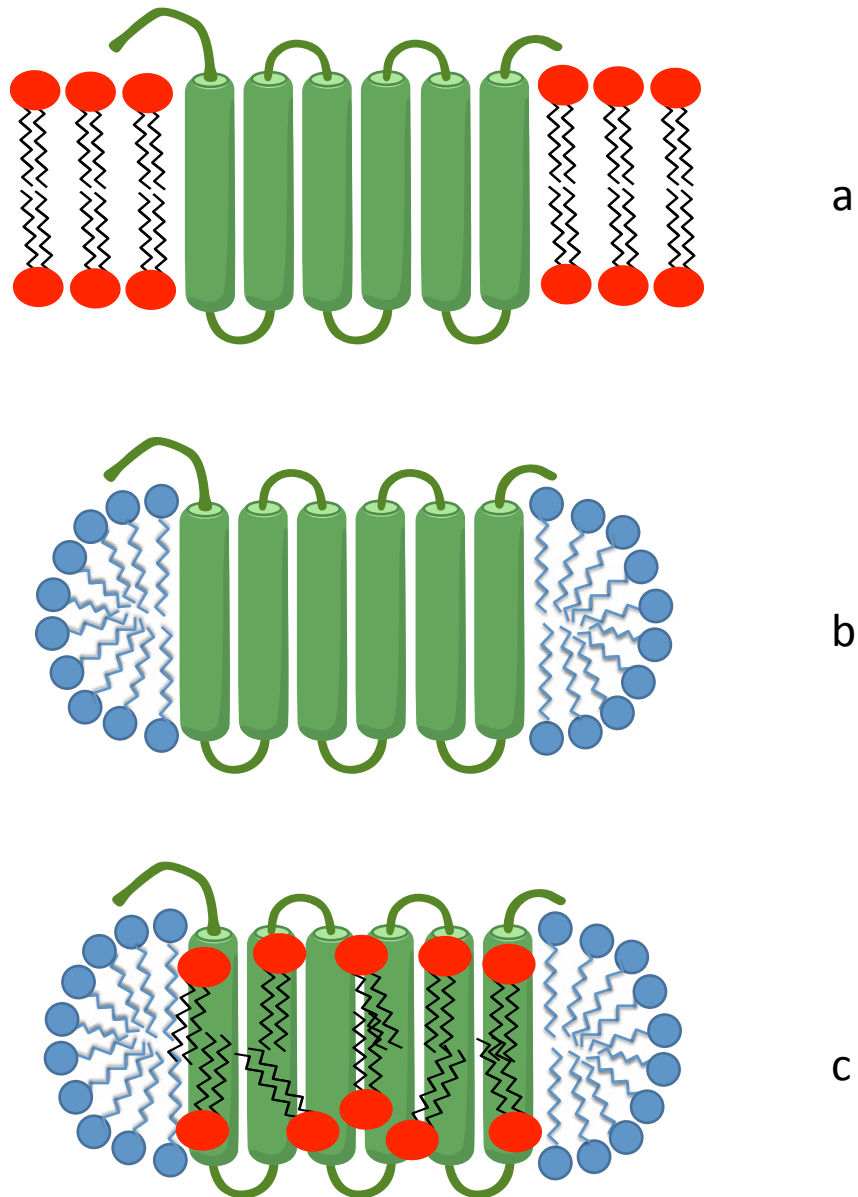


Figure 1. Cartoon of an α -helical membrane protein molecule. (a) The molecule is embedded in cell membrane. (b) The molecule is surrounded by detergent micelle. (c) The molecule is surrounded by detergent-lipid mixture.

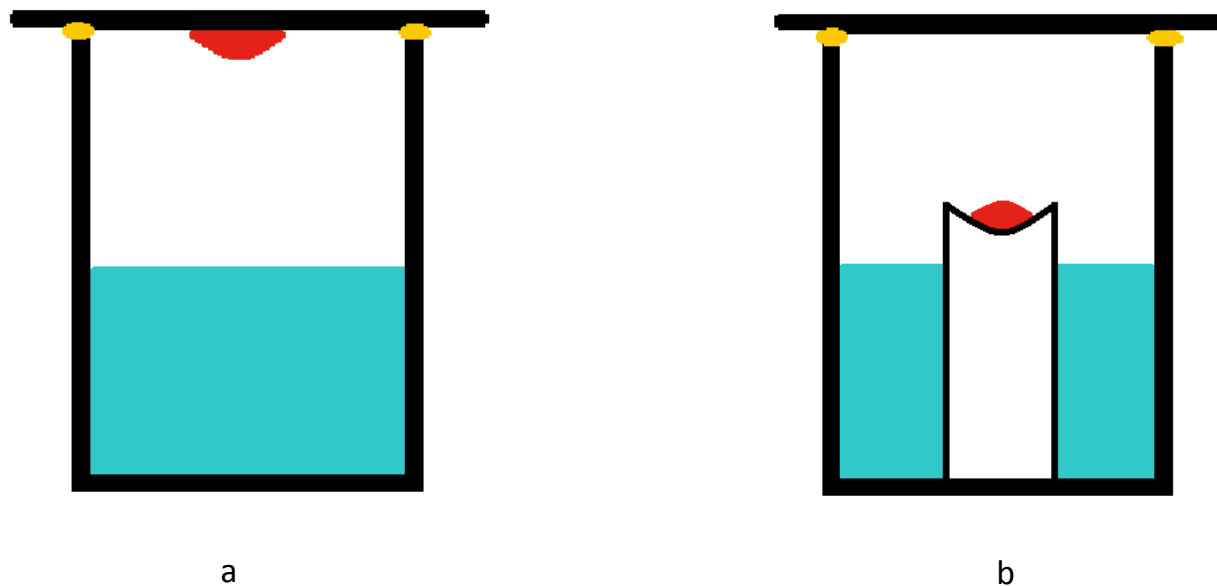


Figure 2. Vapor diffusion methods. (a) Hanging-drop vapor diffusion. (b) Sitting-drop vapor diffusion. In both (a) and (b), the drop composed of a mixture of protein sample and precipitating agents is in red. The hygroscopic reservoir solution containing two times higher in concentration of these precipitating agents is colored green. A cover slip is placed on the top of the vessel, which is sealed with a small amount of vaseline (yellow).

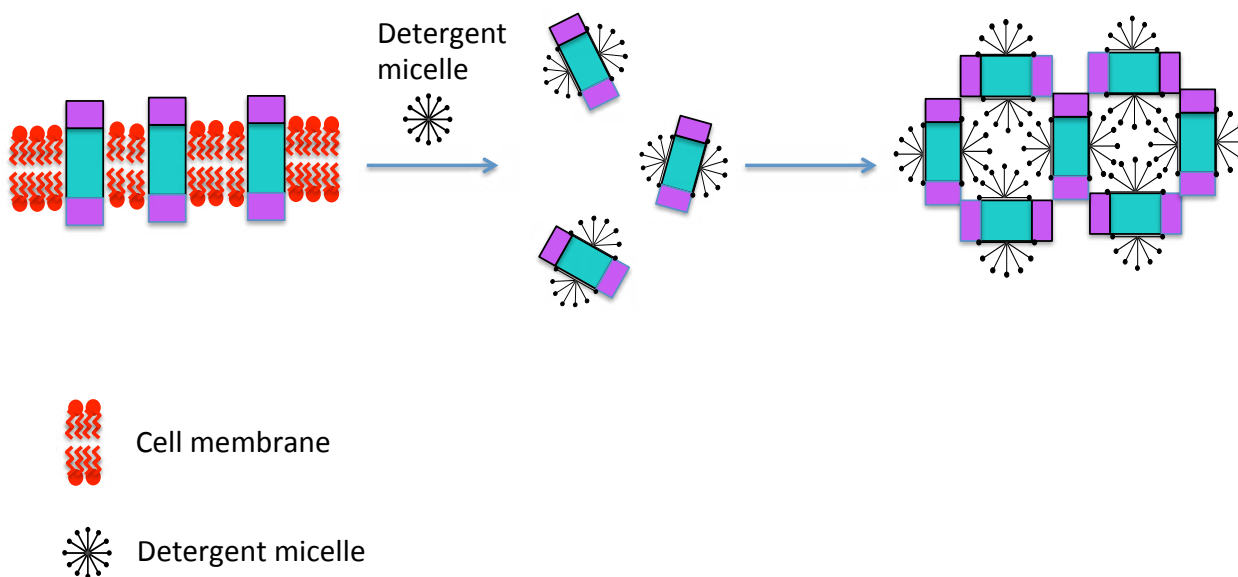
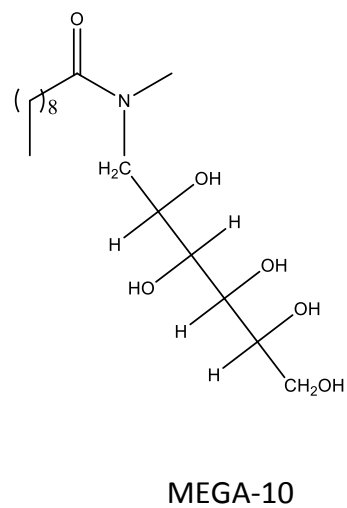
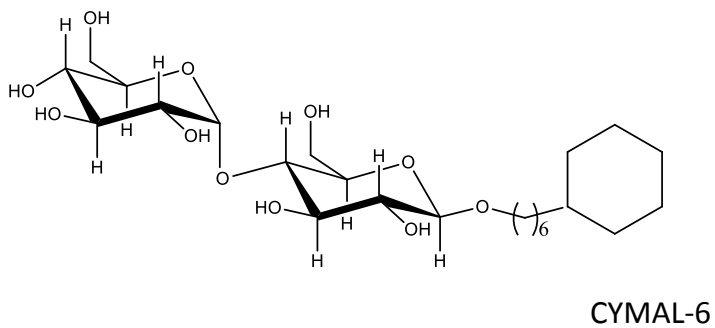
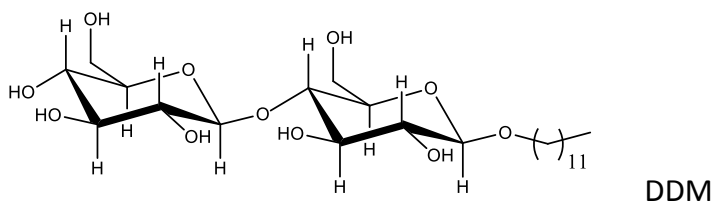
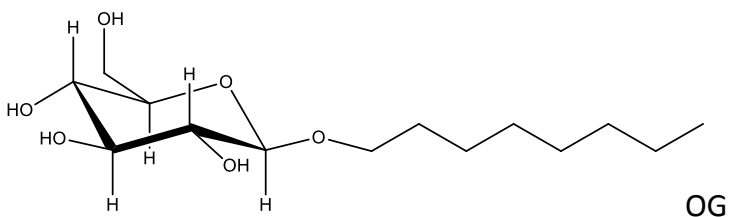


Figure 3. Schematic of detergent-based crystallization of membrane proteins. The membrane

protein is removed from native cell membrane using detergent micelle. The purified protein is then crystallized in detergent micelles. The hydrophobic and hydrophilic domains of the membrane protein molecule are in green and pink colors. The cell membrane is colored red.

(a)

Nonionic Detergents



(b)

Zwitterionic Detergents

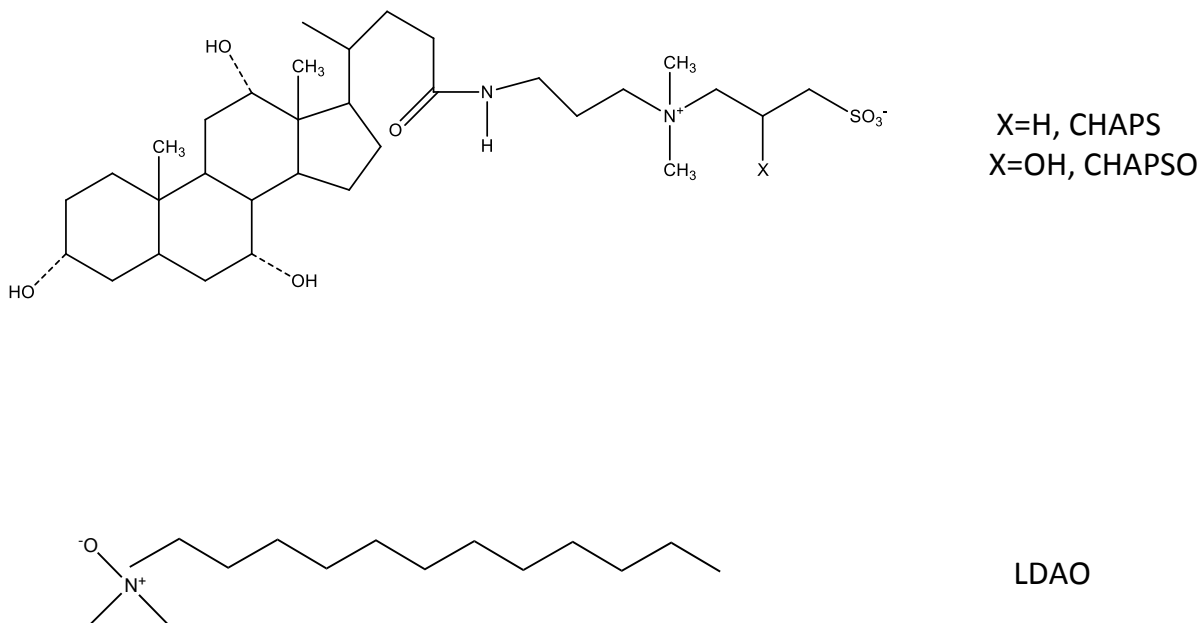


Figure 4. Chemical structures of represented detergent molecules. (a) Nonionic detergents (OG, *n*-octyl- β -D-glucopyranoside; DDM, *n*-dodecyl- β -D-maltopyranoside; CYMAL-6, 6-cyclohexyl-1-pentyl- β -D-maltoside; MEGA-10, Decanoyl-*N*-methylglucamide). (b) Zwitterionic detergents (CHAPS, 3-[(3-cholamidopropyl)dimethylammonio]-1-propanesulfonate; CHAPSO, 3-[(3-Cholamidopropyl)dimethylammonio]-2-hydroxy-1-propanesulfonate; LDAO, *n*-dodecyl-*N,N*-dimethylamine-*N*-oxide).

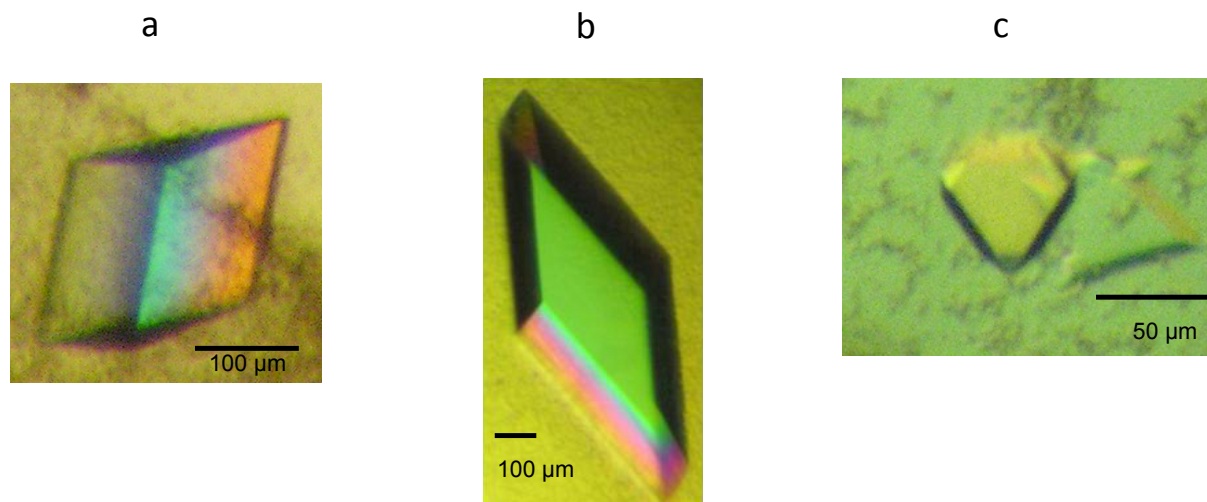


Figure 5. Crystals of the *E. coli* Cus efflux proteins. (a) A crystal of the CusA heavy-metal transporter. (b) A crystal of the CusB adaptor protein. (c) A crystal of the CusBA adaptor-transporter efflux complex.

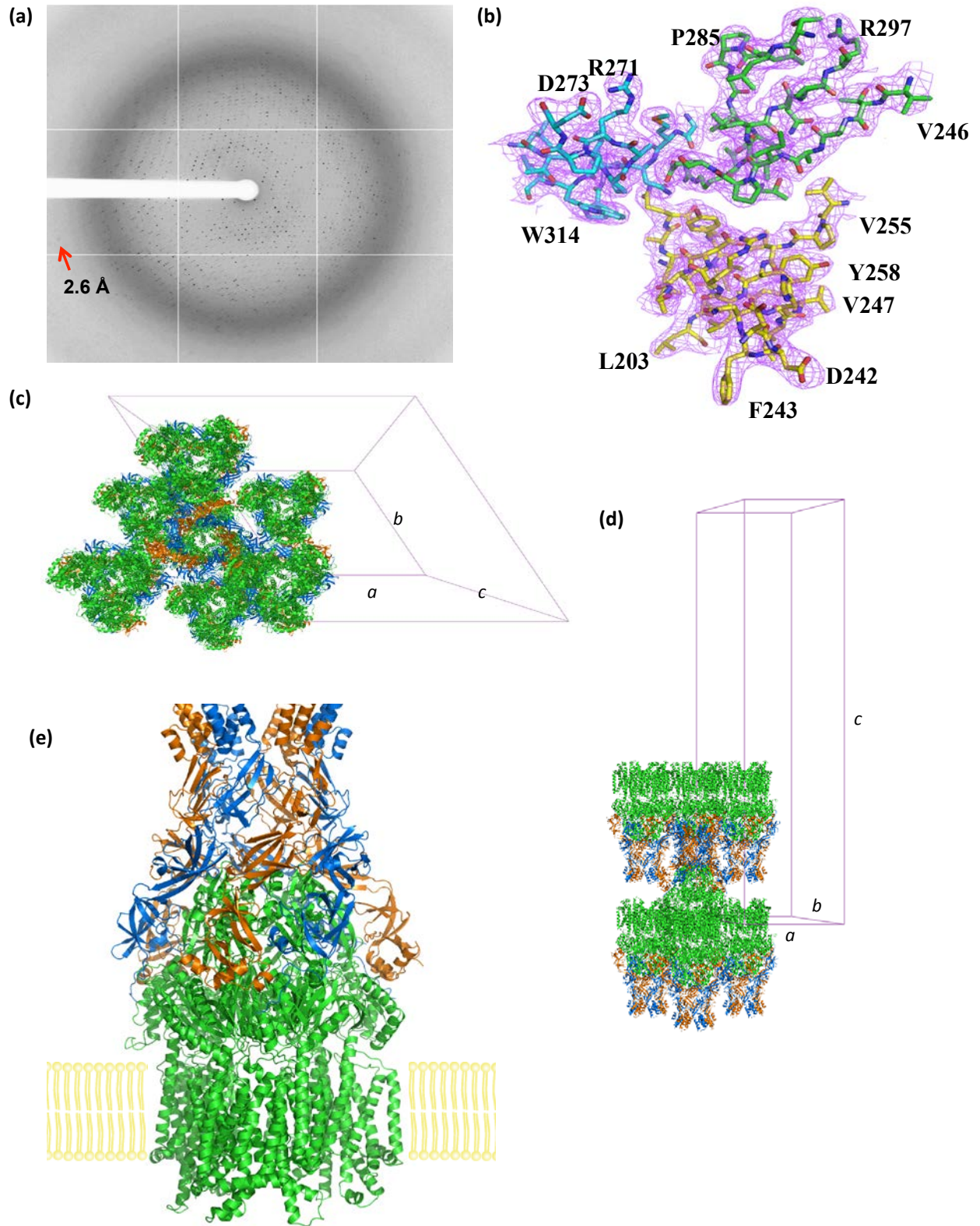


Figure 6. Crystal structure of the CusBA adaptor-transporter complex. (a) X-ray diffraction pattern of the CusBA crystal. The crystal took a trigonal space group $R32$ with unit cell parameters $a = b = 160.2 \text{ \AA}$, $c = 682.7 \text{ \AA}$. (b) Electron density map at a resolution of 2.9 \AA . The CusA and two CusB molecules are colored yellow, green and blue, respectively. (c) Packing diagram of the CusBA crystal complex viewed along the c axis (green, CusA; blue, CusB; orange, CusB). (d) Packing diagram of the CusBA crystal complex viewed orthogonal to (c). (e) Structure of the CusBA efflux complex viewed in the membrane plane (green, CusA; blue, CusB; orange, CusB).

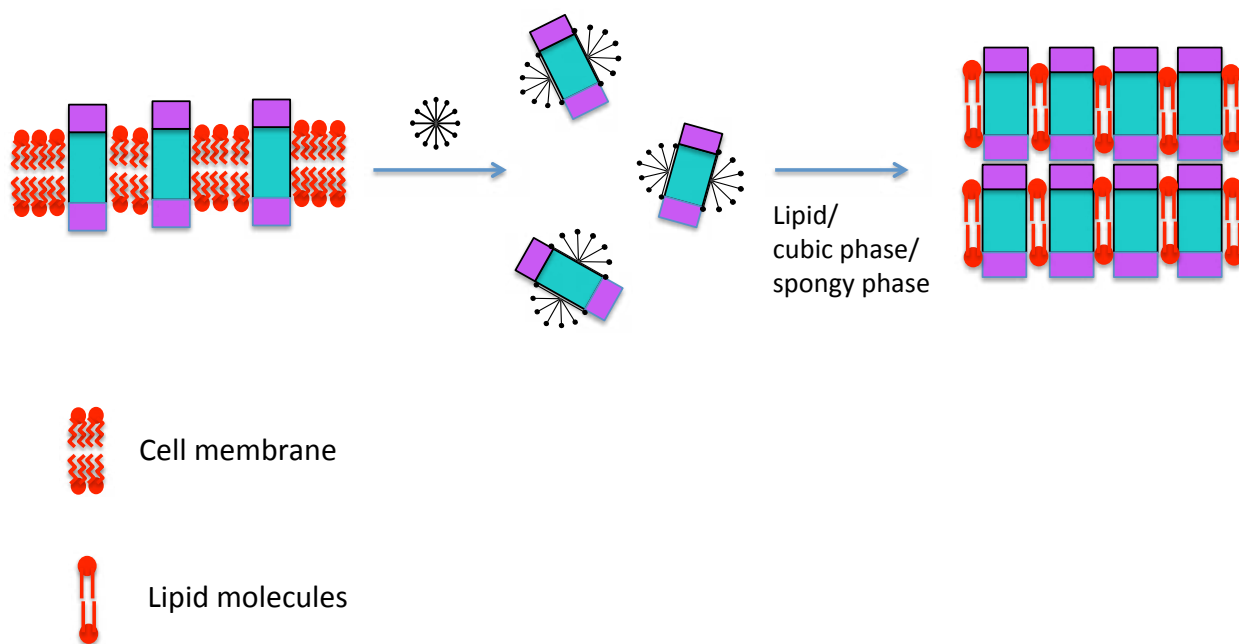


Figure 7. Schematic of lipid-based crystallization of membrane proteins. The purified protein is crystallized in the presence of lipid. The hydrophobic and hydrophilic domains of the membrane protein molecule are in green and pink colors. The cell membrane and lipid molecules are colored red.

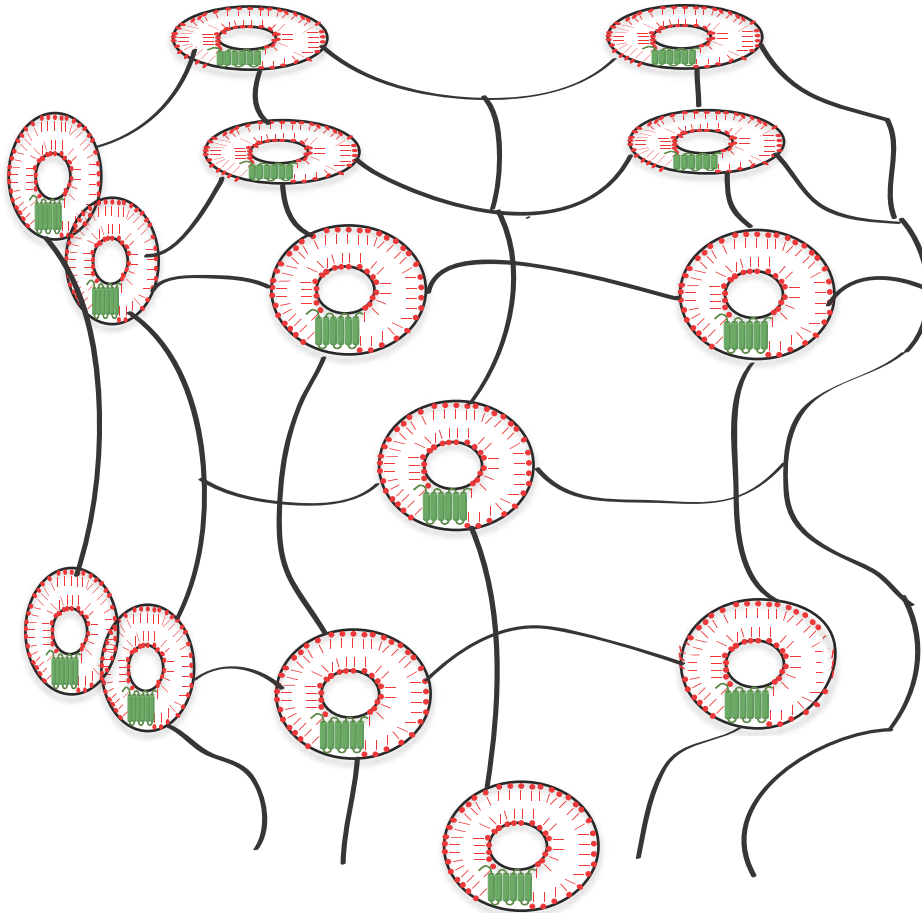


Figure 8. A cartoon representation of lipidic cubic phase. The membrane protein molecules embedded in the cubic phase are colored green.

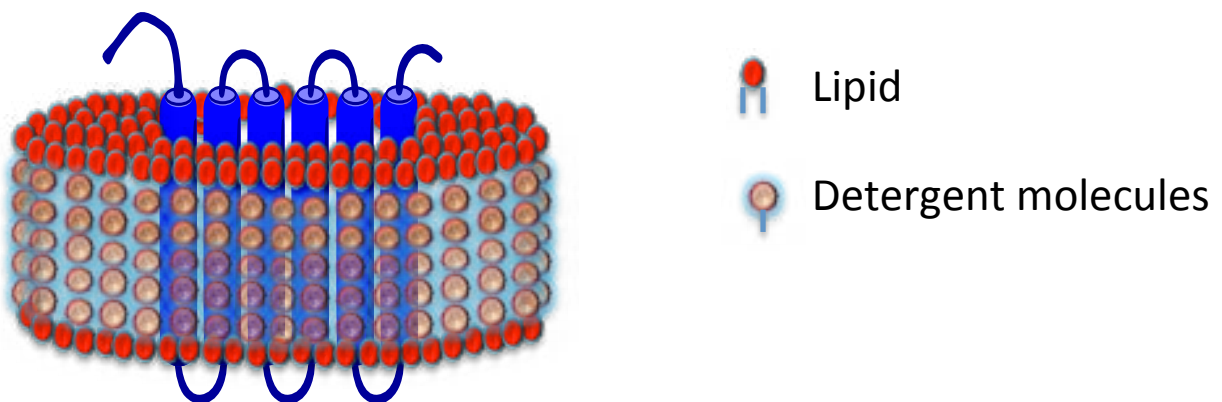


Figure 9. A cartoon representation of a disc-like bicelle. The membrane protein molecule embedded in the bicelle is colored blue.

Table 1. A list of commonly used detergents in membrane protein crystallization.

Detergent	Common Name	CMC ¹ (mM)
NONIONIC		
<i>n</i> -octyl- β -D-glucopyranoside	OG	18.00
<i>n</i> -nonyl- β -D-glucopyranoside	NG	6.50
<i>n</i> -dodecyl- β -D-glucopyranoside	DDG	0.19
<i>n</i> -octyl- β -D-maltopyranoside	OM	19.50
<i>n</i> -nonyl- β -D-maltopyranoside	NM	6.00
<i>n</i> -decyl- β -D-maltopyranoside	DM	1.80
<i>n</i> -undecyl- β -D-maltopyranoside	UDM	0.59
<i>n</i> -dodecyl- β -D-maltopyranoside	DDM	0.17
5-cyclohexyl-1-pentyl- β -D-maltoside	CYMAL-5	2.40
6-cyclohexyl-1-pentyl- β -D-maltoside	CYMAL-6	0.56
Tetraethylene glycol monoethyl ether	C ₈ E ₄	8.50
Pentaethylene glycol monoethyl ether	C ₈ E ₅	7.10
Polyoxyethylene(5)dodecyl ether	C ₁₀ E ₅	0.81
Polyoxyethylene(8)dodecyl ether	C ₁₂ E ₈	0.09
Polyoxyethylene(9)dodecyl ether	C ₁₂ E ₉	0.05
Decanoyl- <i>N</i> -methylglucamide	MEGA-10	6.00
ZWITTERIONIC		
<i>n</i> -decyl- <i>N,N</i> -dimethylamine- <i>N</i> -oxide	DDAO	10.48
<i>n</i> -undecyl- <i>N,N</i> -dimethylamine- <i>N</i> -oxide	UDAO	3.21
<i>n</i> -dodecyl- <i>N,N</i> -dimethylamine- <i>N</i> -oxide	LDAO	1.00
3-[(3-cholamidopropyl)dimethylammonio]- 1-propanesulfonate	CHAPS	8.00
3-[(3-Cholamidopropyl)dimethylammonio]- 2-hydroxy-1-propanesulfonate	CHAPSO	8.00

¹Critical Micelle Concentration (CMC)

CHAPTER 4

**CRYSTAL STRUCTURE OF THE *NEISSERIA GONORRHOEAE* MTRD INNER
MEMBRANE MULTIDRUG EFFLUX PUMP**

A paper published in PLoS One, 2014, 9:e97903

**Jani Reddy Bolla^{1,‡}, Chih-Chia Su^{2,‡}, Sylvia V. Do^{3,‡}, Abhijith Radhakrishnan¹, Nitin
Kumar¹, Feng Long², Tsung-Han Chou², Jared A. Delmar², Hsiang-Ting Lei¹,
Kanagalaghatta R. Rajashankar⁴, William M. Shafer^{5,6}, and Edward W. Yu^{1,2,3*}**

¹Department of Chemistry, Iowa State University, Ames, IA 50011, USA

²Department of Physics and Astronomy, Iowa State University, Ames, IA 50011, USA

³Bioinformatics and Computational Biology Interdepartmental Graduate Program, Iowa State
University, Ames, IA 50011, USA

⁴NE-CAT and Department of Chemistry and Chemical Biology, Cornell University, Bldg. 436E,
Argonne National Laboratory, 9700 S. Cass Avenue, Argonne, IL 60439, USA

⁵Department of Microbiology and Immunology, Emory University School of Medicine, Atlanta,
Georgia 30322, USA

⁶Laboratories of Microbial Pathogenesis, VA Medical Center, Decatur, Georgia 30033.

[‡]J.R.B., C.S. and S.V.D. contributed equally to this work.

* To whom correspondence should be addressed. E-mail: ewyu@iastate.edu

Abstract

Neisseria gonorrhoeae is an obligate human pathogen and the causative agent of the sexually-transmitted disease gonorrhea. The control of this disease has been compromised by the increasing proportion of infections due to antibiotic-resistant strains, which are growing at an alarming rate. The MtrCDE tripartite multidrug efflux pump, belonging to the hydrophobic and amphiphilic efflux resistance-nodulation-cell division (HAE-RND) family, spans both the inner and outer membranes of *N. gonorrhoeae* and confers resistance to a variety of antibiotics and toxic compounds. We here report the crystal structure of the inner membrane MtrD multidrug efflux pump, which reveals a novel structural feature that is not found in other RND efflux pumps.

Introduction

Neisseria gonorrhoeae is a Gram-negative obligate human pathogen. It is the causative agent of the sexually-transmitted disease gonorrhea and rare cases of disseminated disease. Although gonorrhea is one of the oldest described diseases, it remains a significant global problem with more than 100 million cases reported annually worldwide and antibiotic resistance is a major concern [1]. The gonococcus employs a number of strategies to evade host attack. It possesses an intricate mechanism of antigenic variability through differential expression of the genome and can easily acquire new genetic material to develop resistance to antimicrobial agents [1,2]. Gonococci utilize a number of resistance mechanisms, including antimicrobial inactivation, target modification and strategies that reduce antimicrobial concentration, such as reduced permeability of the cell envelope mediated through alteration of porin proteins and active export of multiple antimicrobial compounds from the cell by efflux pumps. Among these

different mechanisms, multidrug efflux is considered to be one of the major causes of failure of drug-based treatments of infectious diseases, which appears to be increasing in prevalence [3]. These bacterial multidrug efflux pumps have enormous clinical consequences. Simultaneously rendering the cell resistant to multiple structurally-unrelated compounds, their expression results in bacterial strains resistant to most clinically-relevant antibiotics [3].

The best characterized and most clinically important of these multidrug efflux systems in *N. gonorrhoeae* is the MtrCDE tripartite efflux pump [4-7]. It is composed of the MtrD inner membrane transporter, belonging to the HAE-RND protein family [8]; the MtrC periplasmic protein, a member of the membrane fusion protein family; and the MtrE integral outer membrane channel protein. This system provides resistance to a broad spectrum of antimicrobial agents, including bile salts, fatty acids, dyes, antibiotics and spermicides. The Mtr multidrug efflux system is also responsible for resistance to host-derived cationic antimicrobial peptides [7], which are important mediators of the innate host defense. Given that gonococci commonly infect mucosal sites bathed in fluids containing such peptides, the Mtr system indeed underscores the pathogenesis of gonococcal disease and its contribution to virulence. In addition, it has been shown that the MtrCDE tripartite efflux pump is capable of enhancing long-term colonization of the mouse vaginal mucosal layer and that gonococci lacking this efflux pump were highly attenuated [9].

At present, only two crystal structures of HAE-RND-type efflux pumps are available. These efflux pumps are the *Escherichia coli* AcrB [10-18] and *Pseudomonas aeruginosa* MexB [19] multidrug transporters. Their structures suggest that both AcrB and MexB span the entire width of the inner membrane and protrude approximately 70Å into the periplasm. Along with the models of these two HAE-RND transporters, the crystal structures of the other components

of these tripartite complex systems have also been determined. These include the outer membrane channels *E. coli* TolC [20] and *P. aeruginosa* OprM [21], as well as the periplasmic membrane fusion proteins *E. coli* AcrA [22] and *P. aeruginosa* MexA [23-25].

Currently, no structural information is available for any protein component of the MtrCDE tripartite complex system. To elucidate the mechanism used by this efflux system for multidrug recognition and extrusion, we here describe the crystal structure of the inner membrane MtrD multidrug efflux pump. The findings reveal a novel structural feature that is not found in other known RND efflux pumps.

Results and discussion

Overall structure of the *N. gonorrhoeae* MtrD multidrug efflux pump

We cloned, expressed and purified the full-length MtrD efflux pump containing a 6xHis tag at the C-terminus. We obtained crystals of this membrane protein following an extensive screening for crystallization conditions with different detergents. We then used molecular replacement, utilizing the structure of the “access” protomer of AcrB (pdb code: 2DHH) [12] to determine the three-dimensional structure. The diffraction data can be indexed to the space group *R*32. Data collection and refinement statistics are summarized in Table 1. The resulting electron density maps (Fig. 1) reveal that the asymmetric unit consists of one protomer. The crystal structure of the MtrD multidrug efflux pump has been determined to a resolution of 3.53 Å (Table 1). Currently, 97% of the amino acids (residues 2-493 and 508-1040) are included in the final model (Fig. 2a). The final structure is refined to R_{work} and R_{free} of 27.9% and 33.3%, respectively.

The structure of MtrD is closer to the conformation of the “access” protomer of AcrB. However, superimposition of these two structures results in a high RMSD of 7.6 Å over 1,000 C α atoms, suggesting that there are significant differences between these two transporters (Fig. S1).

MtrD assembles as a 125-Å long and 95-Å wide homotrimer (Fig. 2b). Each protomer comprises 12 transmembrane helices (TM1-TM12). Like other RND transporters, the N-terminal (TM1-TM6) and C-terminal (TM7-TM12) halves of MtrD are related by a pseudo-twofold symmetry. A large periplasmic domain is created by two extensive periplasmic loops connecting TM1 with TM2 and TM7 with TM8, respectively. As in AcrB [10-18] and MexB [19], this periplasmic domain can be divided into six sub-domains: PN1, PN2, PC1, PC2, DN and DC (Figs. 2 and 3). Sub-domains PN1, PN2, PC1 and PC2 form the pore domain, with PN1 making up the central pore and stabilizing the trimeric organization. However, sub-domains DN and DC contribute to form the docking domain, presumably interacting with the outer membrane channel MtrE. The trimeric MtrD structure suggests that sub-domains PN2, PC1 and PC2 are located at the outermost core of the periplasmic domain, facing the periplasm. Sub-domains PC1 and PC2 also form an external cleft, and this cleft is open in the MtrD structure (Fig. 2). Based on the co-crystal structure of CusBA [26,27] of the CusCBA tripartite efflux system [28-33], the upper regions of PN2, PC1, PC2 and sub-domains DN and DC should directly interact with the MtrC membrane fusion protein to form a functional adaptor-transporter complex.

The *N. gonorrhoeae* MtrCDE tripartite efflux system has the advantage that all these protein components are encoded by the same operon. Thus, the interactions between different proteins are likely to be specific, facilitating analyses of how different components function cooperatively.

Periplasmic multidrug binding site

Crystallization of AcrB with a variety of substrates [12,16-18] has identified that the periplasmic cleft of the pump forms several mini-binding pockets within the extensive, large periplasmic multidrug binding site. This site is supposed to play a predominant role in the selection of drugs for export. Protein sequence alignment reveals that many of the amino acids forming the large periplasmic binding site of AcrB are conserved among MexB and MtrD, indicating that these three multidrug efflux pumps may have a similar substrate binding profile for drug recognition. These conserved amino acids in MtrD include several charged and polar residues, such as S79, S134, R174, D272, E669 and R714, and aromatic residues, such as F136, F176, F610, F612 and F623 (Fig. 3).

A flexible loop is found inside the large periplasmic cleft (Fig. S1), which form the multidrug binding site of the pump. This flexible loop is located deep inside the cleft between subdomains PC1 and PC2, composed of residues 608-619, and should correspond to the Phe-617 loop [16] in AcrB. The loop is highly conserved among MtrD, AcrB and MexB. It is expected that this flexible loop is important for drug recognition and extrusion. There is a chance that this loop may shift positions during the course of the extrusion process to facilitate drug export.

Transmembrane helix TM9

Perhaps the most interesting secondary structural feature appears in TM9 of the MtrD pump. In contrast to other known structures of the RND transporters, MtrD contains an extended region that protrudes into the periplasm and contributes part of the periplasmic domain (Figs. 2 and 3). This region (residues 917-927) comprises an α -helix extending from the upper portion of TM9 and also to the loop connecting TM9 and TM10. Protein sequence alignment suggests that

these extra residues are only found in MtrD and not other homologous RND proteins. Therefore, this fragment should represent a unique feature of this pump that cannot be found in other RND pumps. TM9 is distinct in that it is not vertically oriented. Instead, it is inclined from the horizontal membrane plane by 54°. The spatial arrangement between the extra elongated helix and loop (upper portion of TM9) and the periplasmic cleft formed between PC1 and PC2 suggests that these extra structural features may help the pump to transport its substrates more effectively from the outer leaflet of the inner membrane to the multidrug binding site at the periplasmic domain (Fig. 4).

Proton-relay network

Drug export by RND transporters is proton motive force (PMF)-dependent. Based on the crystal structure of MtrD, it is expected that the charged residues D405 and D406 of TM4 and K948 of TM10 are important for forming the proton-relay network of the pump (Fig. 5). These residues are supposed to undergo protonation and deprotonation within the transport cycle. The involvement of these charged amino acids in proton translocation was supported by a previous study that showed mutations of these residues inhibits proton translocation [34]. In turn, the MtrE outer membrane channel protein is blocked and unable to dissociate from the MtrCDE tripartite efflux complex [34].

The MtrD multidrug efflux pump should operate through an alternating-access mechanism, similar to the AcrB transporter. Thus, the pump has to go through the transport cycle, which should involve different transient conformations, including the “access”, “binding” and “extrusion” states of this protein. In the MtrD trimer, the conformations of the three protomers are identical to each other, suggesting that these protomers represent the same

transient state. In comparison with the structures of AcrB, the conformation of MtrD is closer to that of the “access” protomer of AcrB (Fig. S1). Therefore, our MtrD structure should represent the “access” transient state of the pump. It is expected that this pump will change in conformation to go through the cycle. This conformational change should be coupled to the PMF initiated by the proton-relay network.

Methods

Cloning, expression and purification of the inner membrane MtrD efflux pump

Briefly, the full-length MtrD membrane protein containing a 6xHis tag at the C-terminus was overproduced in *E. coli* C43(DE3) Δ *acrB* cells, which harbor a deletion in the chromosomal *acrB* gene, possessing pET15b Ω *mtrD*. Cells were grown in 12 L of 2xYT medium with 100 μ g/ml ampicillin at 25°C. When the OD₆₀₀ reached 0.6, the culture was treated with 1 mM IPTG to induce *mtrD* expression, and cells were harvested within 15 h. The collected bacteria were resuspended in low salt buffer containing 100 mM sodium phosphate (pH 7.2), 10 % glycerol, 1 mM ethylenediaminetetraacetic acid (EDTA) and 1 mM phenylmethanesulfonyl fluoride (PMSF), and then disrupted with a French pressure cell. The membrane fraction was collected and washed twice with high salt buffer containing 20 mM sodium phosphate (pH 7.2), 2 M KCl, 10 % glycerol, 1 mM EDTA and 1 mM PMSF, and once with 20 mM HEPES-NaOH buffer (pH 7.5) containing 1 mM PMSF. The membrane protein was then solubilized in 2% (w/v) 6-cyclohexyl-1-hexyl- β -D-maltoside (Cymal-6). Insoluble material was removed by ultracentrifugation at 100,000 x g. The extracted protein was purified with a Ni²⁺-affinity column. The purity of the MtrD protein (>95%) was judged using 10% SDS-PAGE stained with

Coomassie Brilliant Blue. The purified protein was then dialyzed and concentrated to 20 mg/ml in a buffer containing 20 mM Na-HEPES (pH 7.5) and 0.05% Cymal-6.

Crystallization of MtrD

Crystals of the 6xHis MtrD were obtained using sitting-drop vapor diffusion. The MtrD crystals were grown at room temperature in 24-well plates with the following procedures. A 2 μ l protein solution containing 20 mg/ml MtrD protein in 20 mM Na-HEPES (pH 7.5) and 0.05% (w/v) Cymal-6 was mixed with a 2 μ l of reservoir solution containing 30% PEG 400, 0.1 M Na-Bicine (pH 8.5), 0.1 M NH_4Cl , 0.05 M BaCl_2 and 9% glycerol. The resultant mixture was equilibrated against 500 μ l of the reservoir solution. Crystals of MtrD grew to a full size in the drops within a week. Typically, the dimensions of the crystals were 0.2 mm x 0.2 mm x 0.2 mm. The crystals were flash-cooled, using solution containing 40% PEG 400, 0.1 M Na-Bicine (pH 8.5), 0.1 M NH_4Cl , 0.05 M BaCl_2 , 9% glycerol and 0.05% Cymal-6 as a cryoprotectant before data collection.

Data collection, structural determination and refinement

All diffraction data were collected at 100K at beamline 24ID-C located at the Advanced Photon Source, using an ADSC Quantum 315 CCD-based detector. Diffraction data were processed using DENZO and scaled using SCALEPACK [35].

Crystals of the MtrD efflux pump belong to the space group $R32$ (Table 1) and the best crystal diffracted x-ray to a resolution of 3.53 Å. Analysis of Matthew's coefficient indicated the presence of one MtrD protomer (113.69 kDa) per asymmetric unit, with a solvent content of 66.7%.

The structure of MtrD was phased using molecular replacement, utilizing the structure of the “access” protomer of AcrB (pdb id: 2DHH) [12] as a search model. After tracing the initial model manually using the program Coot [36], the model was refined against the native data at 3.53 Å-resolution using TLS refinement techniques adopting a single TLS body as implemented in PHENIX [37] leaving 5% of reflections in Free-R set. Iterations of refinement using PHENIX [37] and CNS [38] and model building in Coot [36] lead to the current model, which consists of 1,025 residues with excellent geometrical characteristics (Table 1).

Accession code

Atomic coordinates and structure factors have been deposited in the Protein Data Bank with accession code 4MT1.

Acknowledgements

This work was supported by NIH Grants R37AI021150 (W.M.S.) and R01GM086431 (E.W.Y.) and a VA Merit Award (W.M.S.) from the Medical Research Service of the Department of Veterans Affairs. W.M.S. is the recipient of a Senior Research Career Scientist from the Medical Research Service of the Department of Veterans Affairs. This work is based upon research conducted at the Northeastern Collaborative Access Team beamlines of the Advanced Photon Source, supported by an award GM103403 from the National Institutes of General Medical Sciences. Use of the Advanced Photon Source is supported by the U.S. Department of Energy, Office of Basic Energy Sciences, under Contract No. DE-AC02-06CH11357.

References

1. Tapsall J (2006) Antibiotic resistance in *Neisseria gonorrhoeae* is diminishing available treatment options for gonorrhea: some possible remedies. *Expert Review of Anti-infective Therapy* 4:619-628.
2. Stern A, Brown M, Nickel P, Meyer TF (1986) Opacity genes in *Neisseria gonorrhoeae*: Control of phase and antigenic variation. *Cell* 47:61-71.
3. Piddock LJ (2006) Multidrug-resistance efflux pumps? not just for resistance. *Clin Microbiol Rev* 19:382-402.
4. Warner DM, Shafer WM, Jerse AE (2008) Clinically relevant mutations that cause derepression of the *Neisseria gonorrhoeae* MtrC-MtrD-MtrE efflux pump system confer different levels of antimicrobial resistance and *in vivo* fitness. *Mol Microbiol* 70:462-478.
5. Hagman KE, Lucas CE, Balthazar JT, Snyder LA, Nilles M, Judd RC, Shafer WM (1997) The MtrD protein of *Neisseria gonorrhoeae* is a member of resistance/nodulation/division protein family constituting part of an efflux system. *Microbiology* 143:2117-2125.
6. Lucas CE, Hagman KE, Levin JC, Stein DC, Shafer WM (1995) Importance of lipooligosaccharide structure in determining gonococcal resistance to hydrophobic antimicrobial agents resulting from the *mtr* efflux system. *Mol Microbiol* 16:1001-1009.
7. Shafer WM, Qu XD, Waring AJ, Lehrer RI (1998) Modulation of *Neisseria gonorrhoeae* susceptibility to vertebrate antibacterial peptides due to a member of the resistance/nodulation/division efflux pump family. *Proc Natl Acad Sci USA* 95:1829-1833.
8. Tseng TT, Gratwick KS, Kollman J, Park D, Nies DH, Goffeau A, Saier MH, Jr. (1999) The RND permease superfamily: an ancient, ubiquitous and diverse family that includes human disease and development protein. *J Mol Microbiol Biotechnol* 1:107-125.
9. Jerse AE, Sharma ND, Simms AN, Crow ET, Snyder LA, Shafer WM (2003) A gonococcal efflux pump system enhances bacterial survival in a female mouse model of genital tract infection. *Infection and Immunity* 71:5576-5582.
10. Murakami S, Nakashima R, Yamashita E, Yamaguchi A (2002) Crystal structure of bacterial multidrug efflux transporter AcrB. *Nature* 419:587-593.
11. Yu EW, McDermott G, Zgurskaya HI, Nikaido H, Koshland DE, Jr. (2003) Structural basis of multiple drug binding capacity of the AcrB multidrug efflux pump. *Science* 300:976-980.
12. Murakami S, Nakashima R, Yamashita E, Matsumoto T, Yamaguchi A (2006) Crystal structures of a multidrug transporter reveal a functionally rotating mechanism. *Nature* 443:173-179.

13. Seeger MA, Schiefner A, Eicher T, Verrey F, Dietrichs K, Pos KM (2006) Structural asymmetry of AcrB trimer suggests a peristaltic pump mechanism. *Science* 313:1295-1298.
14. Sennhauser G, Amstutz P, Briand C, Storchenegger O, Grütter MG (2007) Drug export pathway of multidrug exporter AcrB revealed by DARPin inhibitors. *PLoS Biol* 5:e7.
15. Yu EW, Aires JR, McDermott G, Nikaido H (2005) A periplasmic-drug binding site of the AcrB multidrug efflux pump: a crystallographic and site-directed mutagenesis study. *J Bacteriol* 187:6804-6815.
16. Nakashima R, Sakurai K, Yamasaki S, Nishino K, Yamaguchi A (2011) Structures of the multidrug exporter AcrB reveal a proximal multisite drug-binding pocket. *Nature* 480:565-569.
17. Nakashima R, Sakurai K, Yamasaki S, Hayashi K, Nagata C, Hoshino K, Onodera Y, Nishino K, Yamaguchi A (2013). Structural basis for the inhibition of bacterial multidrug exporters. *Nature* 500:102-106.
18. Eicher T, Cha H, Seeger MA, Brandstätter L, El-Delik J, Bohnert JA, Jern WV, Verrey F, Grütter MG, Diederichs K, Pos KM (2012) Transport of drugs by the multidrug transporter AcrB involves an access and a deep binding pocket that are separated by a switch-loop. *Proc Natl Acad Sci USA* 109:5687-5692.
19. Sennhauser G, Bukowska MA, Briand C, Grütter MG (2009) Crystal structure of the multidrug exporter MexB from *Pseudomonas aeruginosa*. *J Mol Biol* 389:134-145.
20. Koronakis V, Sharff A, Koronakis E, Luisi B, Hughes C (2000) Crystal structure of the bacterial membrane protein TolC central to multidrug efflux and protein export. *Nature* 405:914-919.
21. Akama H, Kanemaki M, Yoshimura M, Tsukihara T, Kashiwaga T, Yoneyama H, Narita S, Nakagawa A, Nakae T (2004) Crystal structure of the drug discharge outer membrane protein, OprM, of *Pseudomonas aeruginosa*. *J Biol Chem* 279:52816-52819.
22. Mikolosko J, Bobyk K, Zgurskaya HI, Ghosh P (2006) Conformational flexibility in the multidrug efflux system protein AcrA. *Structure* 14:577-587.
23. Higgins MK, Bokma E, Koronakis E, Hughes C, Koronakis V (2004) Structure of the periplasmic component of a bacterial drug efflux pump. *Proc Natl Acad Sci USA* 101:9994-9999.
24. Akama H, Matsuura T, Kashiwaga S, Yoneyama H, Narita S, Tsukihara T, Nakagawa A, Nakae T (2004) Crystal structure of the membrane fusion protein, MexA, of the multidrug transporter in *Pseudomonas aeruginosa*. *J Biol Chem* 279:25939-25942.

25. Symmons M, Bokma E, Koronakis E, Hughes C, Koronakis V (2009) The assembled structure of a complete tripartite bacterial multidrug efflux pump. *Proc Natl Acad Sci USA* 106:7173-7178.
26. Su CC, Long F, Lei HT, Bolla JR, Do SV, Rajashankar KR, Yu EW (2012) Charged amino acids (R83, E567, D617, E625, R669, and K678) of CusA are required for metal ion transport in the Cus efflux system. *J Mol Biol* 422:429-441.
27. Su CC, Long F, Zimmermann MT, Rajashankar KR, Jernigan RL, Yu EW (2011) Crystal Structure of the CusBA Heavy-Metal Efflux Complex of *Escherichia coli*. *Nature* 470:558-562.
28. Long F, Su CC, Zimmermann MT, Boyken SE, Rajashankar KR, Jernigan RL, Yu EW (2010) Crystal structures of the CusA heavy-metal efflux pump suggest methionine-mediated metal transport mechanism. *Nature* 467:484-488.
29. Su CC, Yang F, Long F, Reyon D, Routh MD, Kuo DW, Mokhtari AK, Van Ornam JD, Rabe KL, Hoy JA, Lee YJ, Rajashankar KR, Yu EW (2009) Crystal structure of the membrane fusion protein CusB from *Escherichia coli*. *J Mol Biol* 393:342-355.
30. Kulathila R, Kulathila R, Indic M, van den Berg B (2011) Crystal structure of *Escherichia coli* CusC, the outer membrane component of a heavy-metal efflux pump. *PLoS One* 6:e15610.
31. Lei HT, Bolla JR, Bishop NR, Su CC, Yu EW (2014) Crystal structures of CusC reveal conformational changes accompanying folding and transmembrane channel formation. *J Mol Biol* 426:403-411.
32. Franke S, Grass G, Nies DH (2001) The product of the *ybdE* gene of the *Escherichia coli* chromosome is involved in detoxification of silver ions. *Microbiology* 147:965-972.
33. Franke S, Grass G, Rensing C, Nies DH (2003) Molecular analysis of the copper-transporting efflux system CusCFBA of *Escherichia coli*. *J Bacteriol* 185:3804-3812.
34. Janganan TK, Bavro VN, Zhang L, Borges-Walmsley MI, Walmsley AR (2013) Tripartite efflux pumps: energy is required for dissociation, but not assembly or opening of the outer membrane channel of the pump. *Mol Microbiol* 88:590-602.
35. Otwinowski Z, Minor M (1997) Processing of X-ray diffraction data collected in oscillation mode. *Methods Enzymol* 276:307-326.
36. Emsley P, Cowtan K (2004) Coot: model-building tools for molecular graphics. *Acta Crystallogr D* 60:2126.
37. Adams PD, Grosse-Kunstleve RW, Hung LW, Ioerger TR, McCroy AJ, Moriarty NW, Read RJ, Sacchettini JC, Sauter NK, Terwilliger TC (2002) PHENIX: building new software for automated crystallographic structure determination. *Acta Crystallogr D* 58:1948-1954.

38. Brünger AT, Adams PD, Clore GM, DeLano WL, Gros P, Grosse-Kunstleve RW, Jiang JS, Kuszewski J, Nilges M, Pannu NS, Read RJ, Rice LM, Simonson T, Warren GL (1998) Crystallography & NMR system: A new software suite for macromolecular structure determination. *Acta Crystallogr D* 54:905-921.

Legends of figures

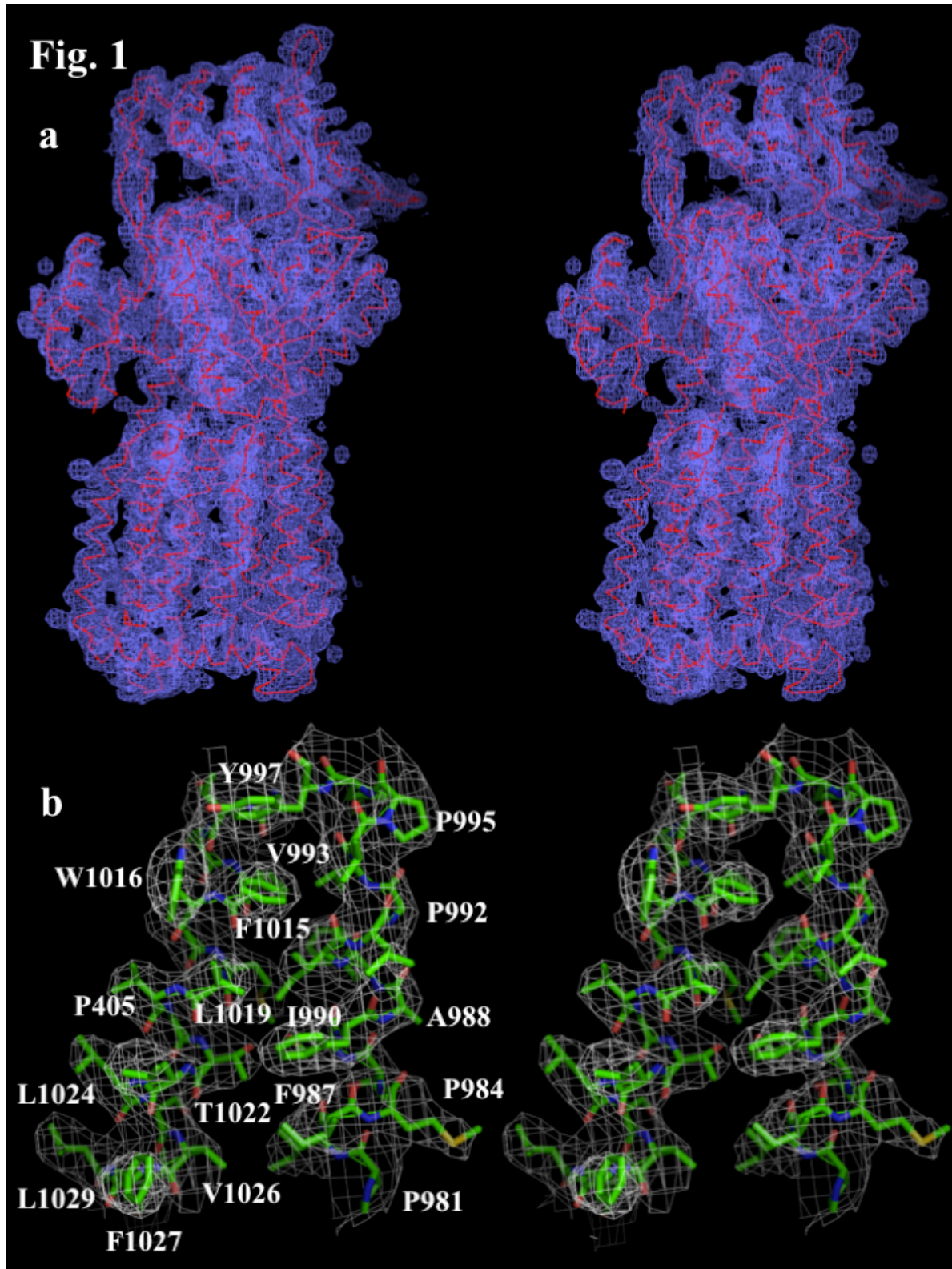


Fig. 1. Stereo view of the electron density map of the MtrD efflux pump at a resolution of 3.53 Å. (a) The electron density map contoured at 1.2σ is in blue. The C α traces of MtrD are in red. (b) Representative section of the electron density at the interface between TM11 and TM12 of MtrD. The electron density (colored white) is contoured at the 1.2σ level and superimposed with the final refined model (green, carbon; red, oxygen; blue, nitrogen).

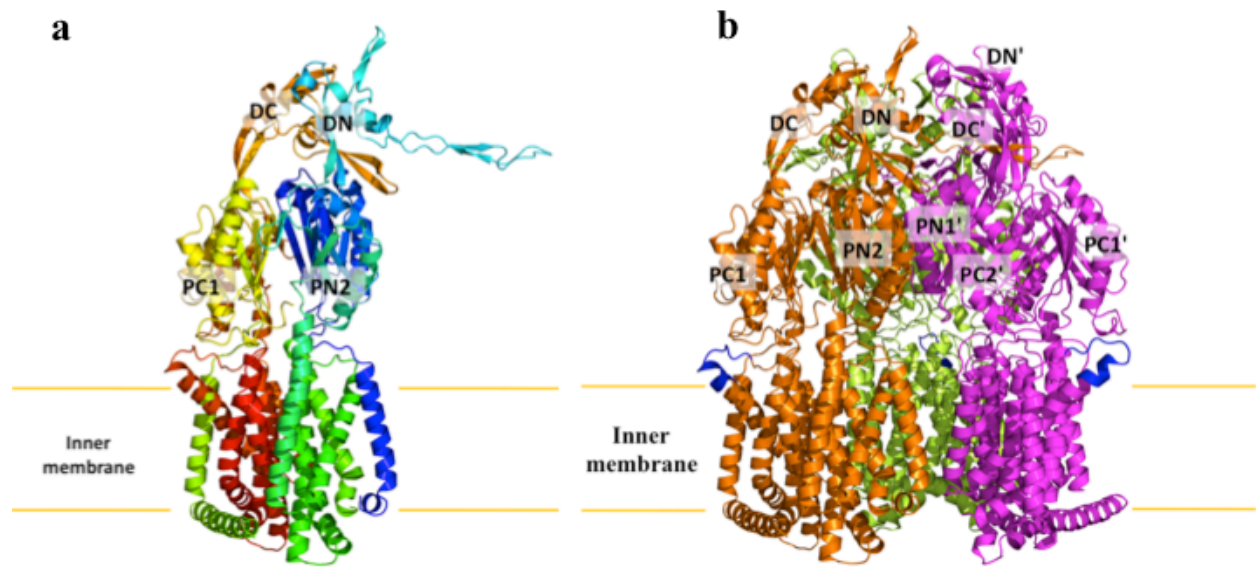


Fig. 2. Structure of the *N. gonorrhoeae* MtrD efflux pump. (a) Ribbon diagram of a protomer of MtrD viewed in the membrane plane. The molecule is colored using a rainbow gradient from the N-terminus (blue) to the C-terminus (red). Sub-domains DN, DC, PN2, PC1 and PC2 are labeled. The location of PN1 is behind PN2, PC1 and PC2. (b) Ribbon diagram of the MtrD trimer viewed in the membrane plane. Each subunit of MtrD is labeled with a different color. Residues 917-927 (only found in MtrD) forming the upper portion of TM9 and the loop connecting TM9 and TM10 are in blue color.

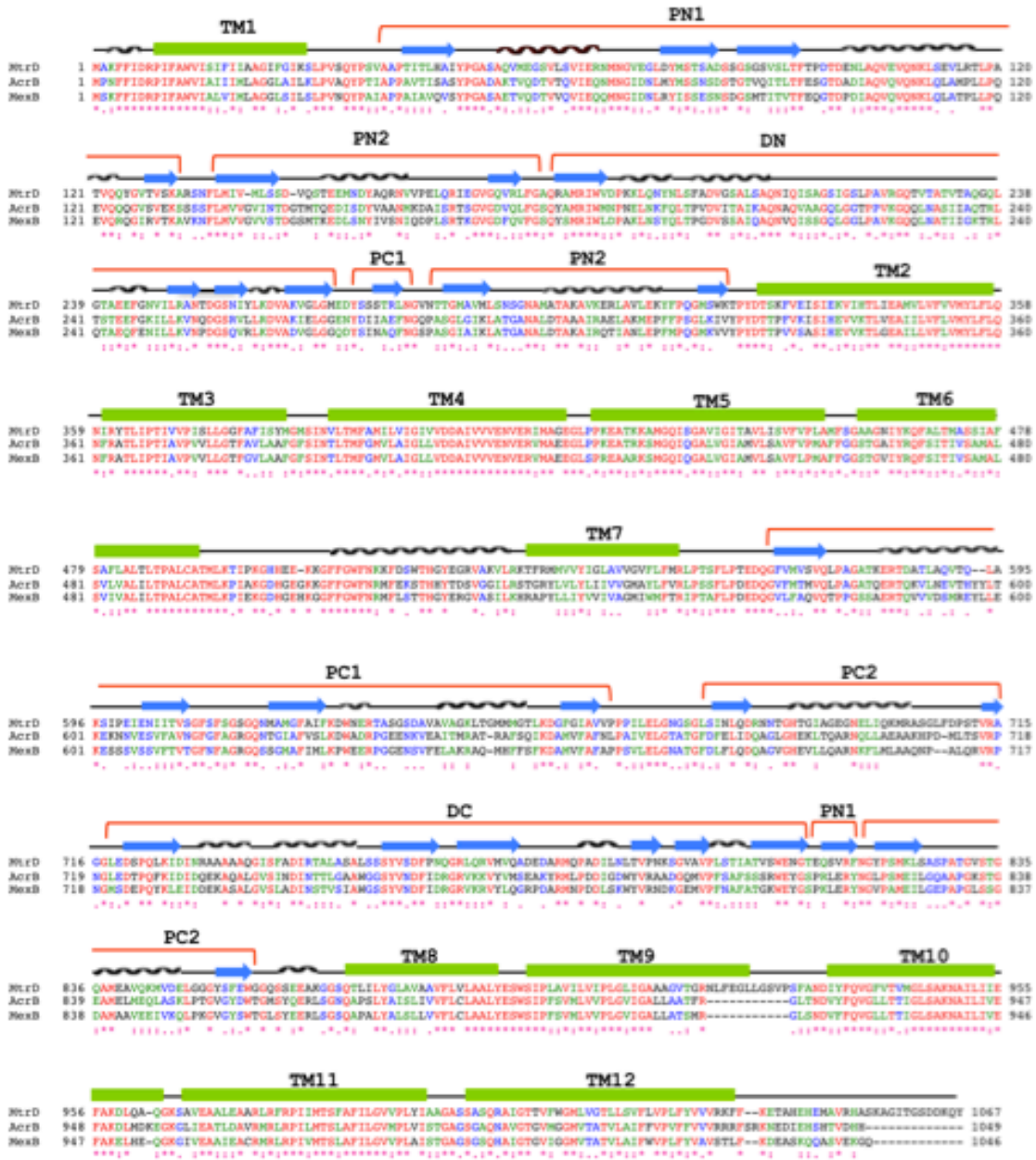


Fig. 3. Sequence and topology of MtrD, AcrB and MexB. Alignment of the amino acid sequences of MtrD, AcrB and MexB were done using CLUSTAL W (*, identical residues; ;, >60% homologous residues). Secondary structural elements are indicated: TM, transmembrane helix; N α and N β , helix and strand, respectively, in the N-terminal half; C α and C β , helix and strand, respectively, in the C-terminal half. The MtrE docking domain is divided into two sub-

domains, DN and DC; whereas the pore domain is divided into four sub-domains, PN1, PN2, PC1 and PC2. The sequence and topology of MtrD are shown at the top.

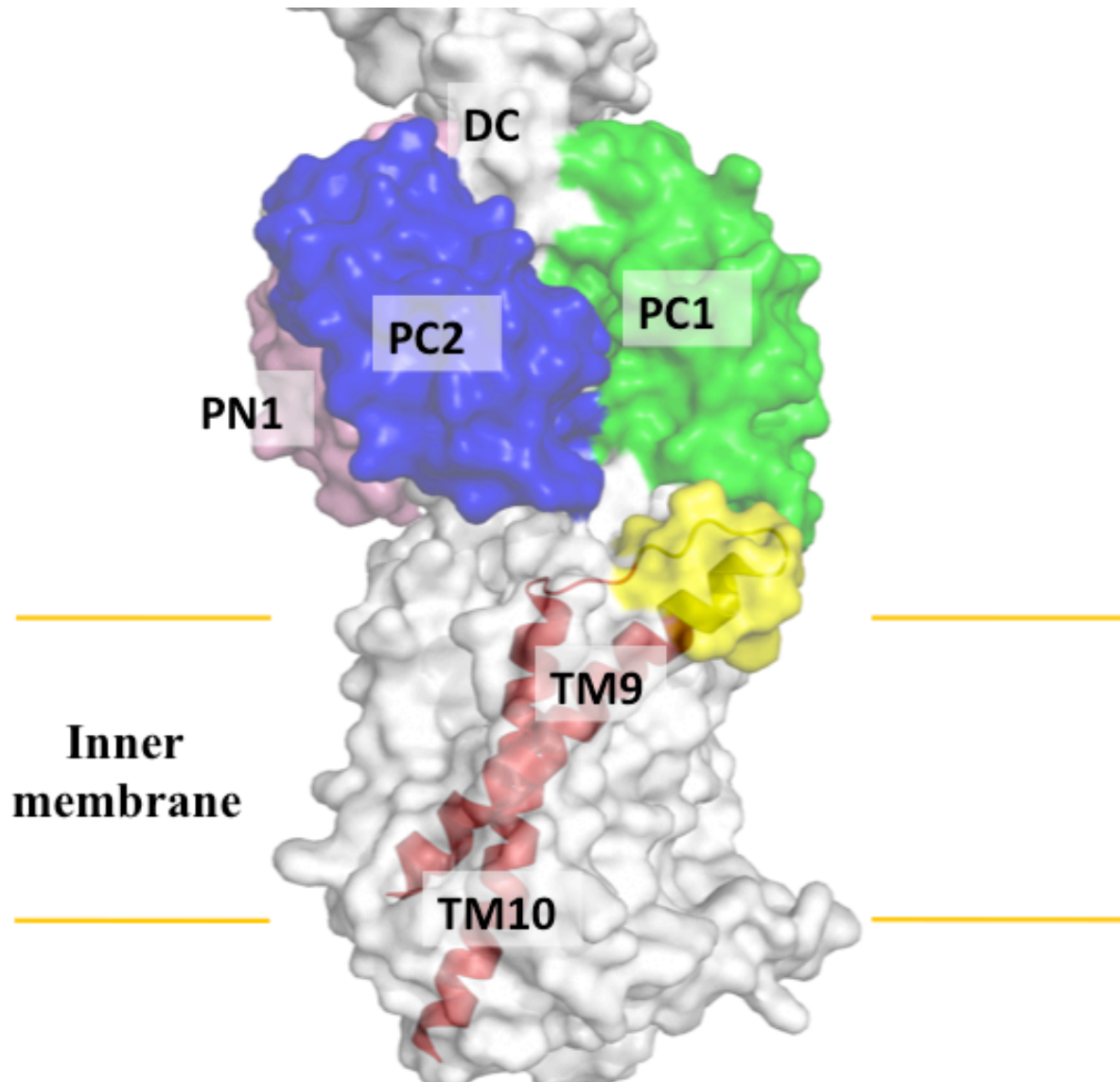


Fig. 4. Spatial arrangement between TM9 and the periplasmic cleft. TM9 is inclined from the horizontal membrane plane by 54° . The extra feature (yellow), which is only found in the MtrD pump within the family, is located right next the cleft formed by subdomains PC1 and PC2.

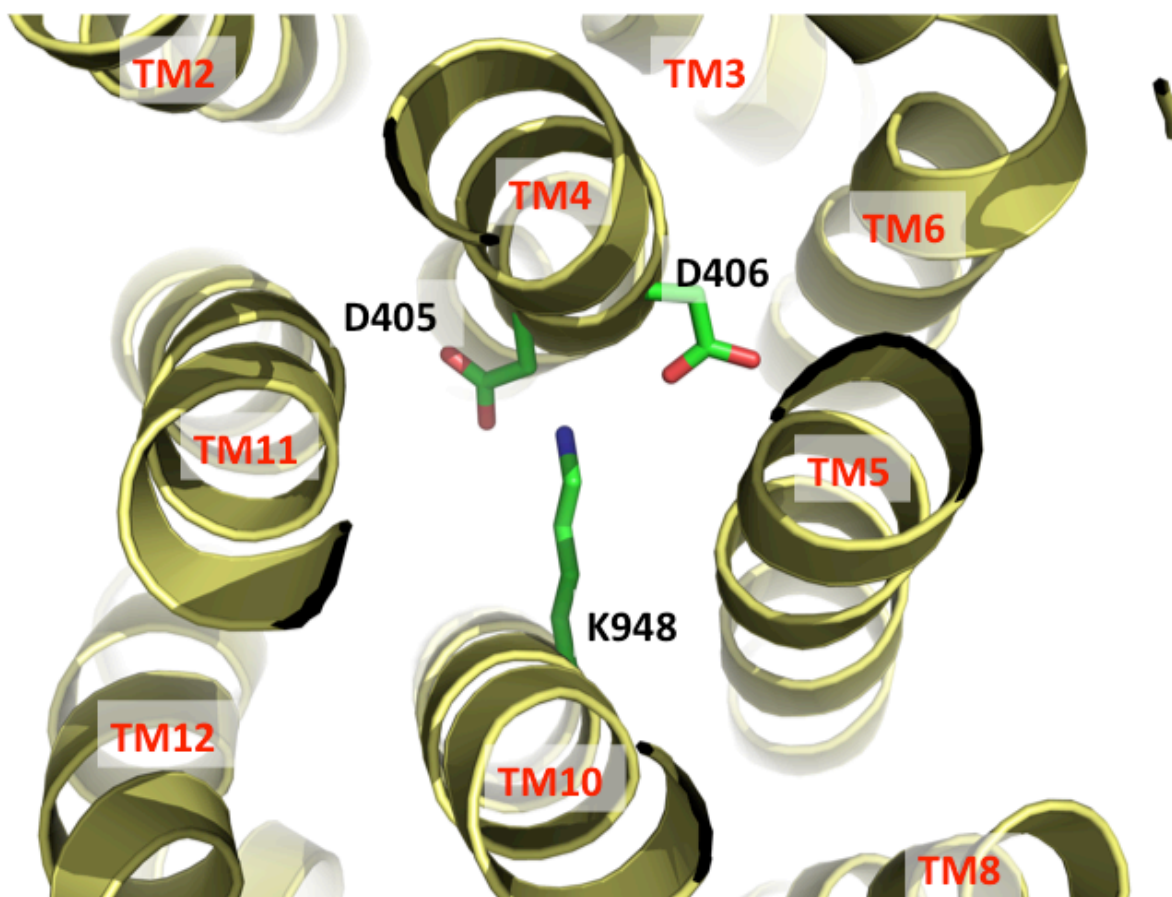


Fig. 5. Ion pairs in the transmembrane domain viewed from the cytoplasmic side. Residues D405 and D406 of TM4 and K948 of TM10 that form ion pairs, which may play an important role in proton translocation, are in green sticks.

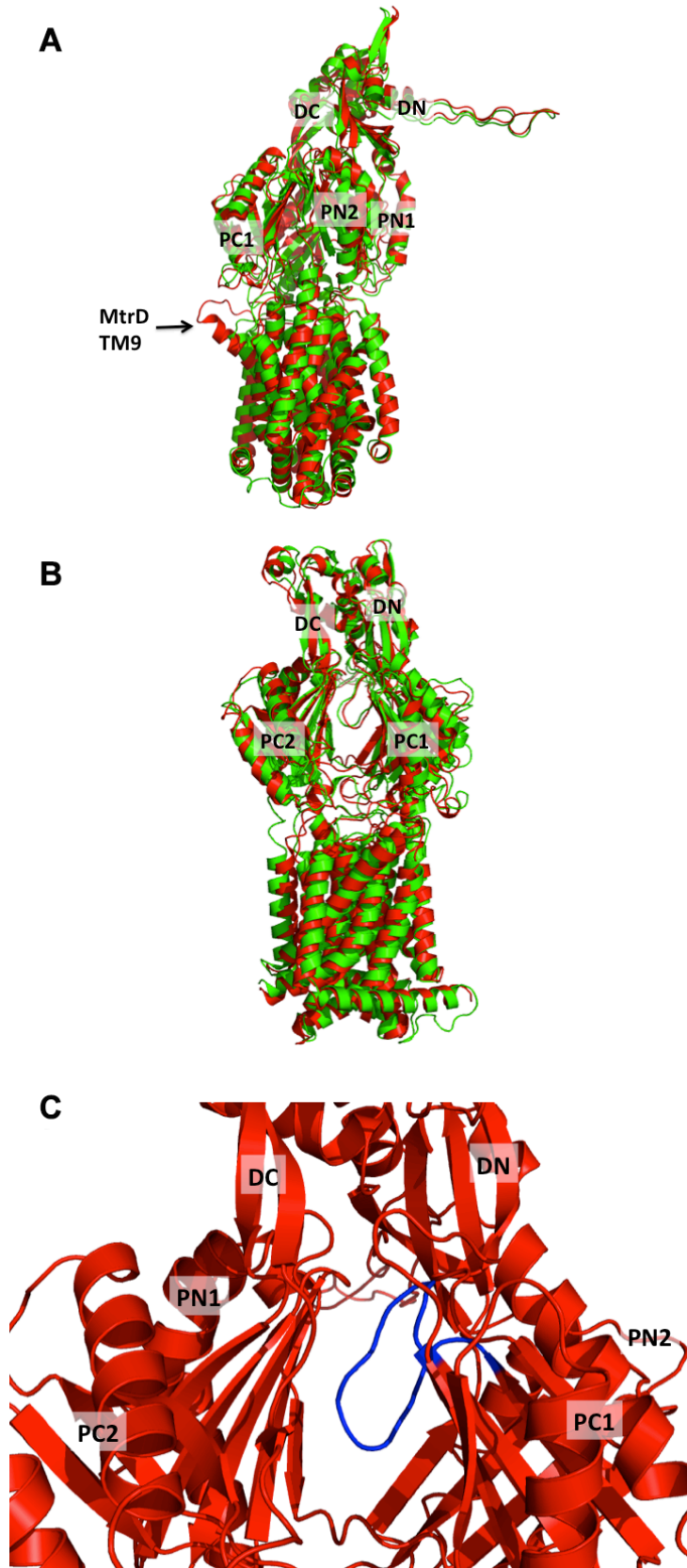


Figure S1: Comparison of the structures of the MtrD and AcrB efflux pumps. (a) Ribbon diagram of protomers of MtrD and AcrB viewed in the membrane plane. This is a superimposition of a subunit of MtrD (red) onto an “access” protomer of AcrB (pdb: 2DHH) (green), indicating that the structures of these two efflux pumps are quite distinct. Superimposition of these two structures result in a high RMSDs of 7.6 Å over 1,000 C^α atoms. (b) Front view of the periplasmic clefts, formed by subdomains PC1 and PC2, of MtrD and AcrB. The secondary structural elements of these two transporters are colored red (MtrD) and green (AcrB). (c) Potential multidrug binding within the periplasmic cleft of MtrD. The flexible loop created by residues 608–619 is colored blue. This loop should correspond to the Phe-617 loop in AcrB. It is suspected that this flexible loop may swing into this drug binding site to facilitate export during drug extrusion. The rest of the secondary structural elements of MtrD are colored red.

Table 1. Data collection and refinement statistics.

Data set	MtrD
Data Collection	
Wavelength (Å)	0.98
Space group	<i>R32</i>
Resolution (Å)	50 – 3.53 (3.68-3.53)
Cell constants (Å)	
a	152.99
b	152.95
c	360.74
α, β, γ (°)	90, 90, 120
Molecules in ASU	1
Redundancy	2.9 (2.9)
Total reflections	377,955
Unique reflections	20,296
Completeness (%)	97.7 (98.0)
R_{sym} (%)	7.7 (42.9)
$I / \sigma(I)$	17.16 (1.9)
Refinement	
Resolution (Å)	50 – 3.53
R_{work}	27.9
R_{free}	33.3
rms deviation from ideal	
bond lengths (Å)	0.003
bond angles (°)	0.794
Ramachandran	
most favoured (%)	89.6
additional allowed (%)	10.1
generously allowed (%)	0.3
disallowed (%)	0

CHAPTER 5

**STRUCTURE AND FUNCTION OF THE *NEISSERIA GONORRHOEAE* MTRF
ILLUMINATES A NOVEL CLASS OF ANTIMETABOLITE EFFLUX PUMPS**

Manuscript submitted to the journal Cell Reports

**Jani Reddy Bolla^{1,‡}, Chih-Chia Su^{2,‡}, Nitin Kumar¹, Abhijith Radhakrishnan¹, Jared A.
Delmar², Tsung-Han Chou², Kanagalaghatta R. Rajashankar³, William M. Shafer,^{4,5} and
Edward W. Yu^{1,2*}**

¹Department of Chemistry, Iowa State University, Ames, IA 50011.

²Department of Physics and Astronomy, Iowa State University, Ames, IA 50011.

³NE-CAT and Department of Chemistry and Chemical Biology, Cornell University, Bldg. 436E,
Argonne National Laboratory, 9700 S. Cass Avenue, Argonne, IL 60439.

⁴Department of Microbiology and Immunology, Emory University School of Medicine, Atlanta,
Georgia 30322.

⁵Laboratories of Microbial Pathogenesis, VA Medical Center, Decatur, Georgia 30033.

[‡]J.R.B. and C.S. contributed equally to this work.

* To whom correspondence should be addressed. E-mail: ewyu@iastate.edu

Summary

Neisseria gonorrhoeae is an obligate human pathogen and the causative agent of the sexually-transmitted disease gonorrhea. Although gonorrhea is one of the oldest described diseases, it remains a significant global problem with more than 100 million cases reported annually worldwide. The control of this disease has been compromised by the increasing proportion of infections due to antibiotic-resistant strains, which are growing at an alarming rate. *N. gonorrhoeae* MtrF is an integral membrane protein, which belongs to the AbgT family of transporters. Approximately 13,000 putative transporters of this family have been identified. However, no structural information is available and even existing functional data are fairly minimal for these membrane proteins. Here in we describe the crystal structure of *N. gonorrhoeae* MtrF, revealing a dimeric molecule with an architecture distinct from all other families of transporters. MtrF is a bowl-shaped dimer with a solvent-filled basin extending from the cytoplasm to halfway across the membrane bilayer. Each subunit of the transporter contains nine transmembrane helices and two hairpins. The structure directly suggests a plausible pathway for substrate transport. A combination of the crystal structure, genetic analysis and substrate accumulation assays indicates that MtrF is an exporter, capable of removing the metabolite *p*-aminobenzoic acid from bacterial cells. Further experimental data based on drug susceptibility and radioactive transport assays suggest that *N. gonorrhoeae* MtrF is an antibiotic efflux pump, which mediates bacterial resistance to sulfonamide antimetabolite drugs.

Introduction

Neisseria gonorrhoeae is a gram-negative diplococcus, which is found only in humans and causes the sexually transmitted disease gonorrhea. Since it is a strictly human pathogen and can colonize both male and female genital mucosal surfaces and other sites, it has developed mechanisms to overcome antimicrobial systems of the host's innate defense. One major mechanism that *N. gonorrhoeae* uses to resist antimicrobial agents is the expression of multidrug efflux pumps that recognize and actively export a variety of structurally unrelated toxic compounds from the bacterial cell, including antibacterial peptides, long-chain fatty acids, and several clinically important antibiotics (Lee and Shafer, 1999; Rouquette-Loughlin et al., 2003; Shafer et al., 1998; Shafer et al., 2001; Unemo and Shafer, 2014).

The best characterized efflux system in *N. gonorrhoeae* is the MtrC-MtrD-MtrE multidrug efflux system (Delahay et al., 1997; Lucas et al., 1995; Hagman et al., 1995; Hagman et al., 1997; Veal and Shafer, 2003; Warner et al., 2008). This system is similar to other efflux pumps of the resistance-nodulation-cell division (RND) superfamily (Tseng et al., 1999) possessed by many Gram-negative bacteria. MtrD (Bolla et al., 2014; Hagman et al., 1995; Hagman and Shafer, 1995; Hagman et al., 1997) is the inner membrane transporter component of the tripartite RND pump. The complex is formed by interactions between MtrD, the periplasmic membrane fusion protein MtrC (Hagman et al., 1995; Hagman et al., 1997; Veal et al., 2002; Janganan et al., 2013), and the outer membrane channel MtrE (Delahay et al., 1997; Lei et al., 2014; Janganan et al., 2011; Janganan et al., 2013). This powerful efflux complex mediates the export of several structurally diverse hydrophobic antimicrobial agents, such as antibiotics, nonionic detergents, antibacterial peptides, bile salts, and gonadal steroidal hormones (Delahay et al., 1997; Hagman et al., 1995; Hagman et al., 1997; Shafer et al., 1998). In addition, the Mtr

efflux system includes another inner membrane protein MtrF (Veal and Shafer, 2003; Folster and Shafer, 2005), which belongs to the AbgT family of transporters (Prakash et al., 2003). It has been proposed that MtrF cooperates with the MtrC-MtrD-MtrE complex to export certain antimicrobials by a yet unknown mechanism (Veal and Shafer, 2003).

To date, approximately 13,000 putative transporters of the AbgT family have been identified. AbgT-type proteins are commonly found in Gram-negative bacteria such as *Salmonella enterica*, Gram-positive bacteria such as *Staphylococcus aureus*, as well as yeasts such as *Saccharomyces arboricola*. Surprisingly, among proteins in this diverse AbgT family, only *Escherichia coli* AbgT (Hussein et al., 1998; Carter et al., 2007) and *N. gonorrhoeae* MtrF (Folster and Shafer, 2005; Veal and Shafer, 2003) have been partially characterized. Thus far, there is no structural information available for this family of membrane proteins, obscuring the details of their function and mechanism.

The products of the *E. coli* *abg* genes have been shown to catalyze the uptake and cleavage of the folate catabolite *p*-aminobenzoyl-glutamate (Carter et al., 2007). Particularly, *E. coli* AbgT has been demonstrated to import the catabolite *p*-aminobenzoyl-glutamate for *de novo* folic acid synthesis (Carter et al., 2007). As *E. coli* AbgT and *N. gonorrhoeae* MtrF belong to the same family of membrane transporters, it is expected that the MtrF protein may act as an importer to uptake *p*-aminobenzoyl-glutamate and related small molecules for the synthesis of the essential folate vitamin. However, since MtrF is needed for the high-level resistance of gonococci to hydrophobic antimicrobials, including erythromycin and TX-100 (Folster and Shafer, 2005), it seems more likely to participate in drug efflux. To understand the transport functions of members of the AbgT family, we present herein the crystal structure of the *N. gonorrhoeae* MtrF transporter. Importantly, we show that *N. gonorrhoeae* MtrF is capable of

exporting the folate metabolite *p*-aminobenzoic acid (PABA) from cells. A combination of the three-dimensional structure and genetic analysis allows us to identify key MtrF residues that are important for the function of this membrane protein. Finally, we demonstrate that MtrF does behave as an antibiotic efflux pump, which is responsible for removing sulfonamides from the cell and mediating bacterial resistance to this class of antimetabolites.

Results and discussion

Overall structure of *N. gonorrhoeae* MtrF

The *N. gonorrhoeae* MtrF transporter is composed of 522 amino acids, sharing 38% identity with *E. coli* AbgT (Fig. S1). The crystal structure of this membrane protein was determined to a resolution of 3.95 Å using single isomorphous replacement with anomalous scattering (SIRAS) (Table 1). Two molecules of MtrF, which assemble as a dimer, are found in the asymmetric unit (Fig. S2 and Fig. 1). Superimposition of these two MtrF molecules gives an RMSD of 0.5 Å over 506 C α atoms, indicating that their conformations are nearly identical to each other.

The fold of MtrF is unique and composed of a number of unusual structural elements. Each subunit of MtrF comprises nine α -helical transmembrane segments and two helical hairpins: TM1 (a (12-22) and b (26-47)), TM2 (a (78-92), b (94-112) and c (114-125)), HP1 (a (128-145) and b (147-164)), TM3 (a (168-182) and b (191-205)), TM4 (218-240), TM5 (269-292), TM6 (310-334), TM7 (a (341-353), b (356-374) and c (376-391)), HP2 (a (396-413) and b (417-434)), TM8 (a (438-451) and b (462-471)) and TM9 (480-506). It should be noted that five of these TMs (TM1, TM2, TM3, TM7 and TM8) are broken into segments within the membrane. In addition, HP1 and HP2 are formed by relatively short helices, which are only long enough to

span half of the membrane (Fig. 1a and b). Interestingly, the intramembrane loops of several of these TMs and HPs are right next to each other, allowing the transporter to form an internal cavity within the membrane (Fig. 1c and d).

Each protomer of MtrF contains a relatively small periplasmic domain. This domain is made up of two long loops formed between TMs 1 and 2, and TMs 5 and 6, respectively. Below the inner leaflet of the membrane, a small cytoplasmic domain links TMs 4 and 5 together. This domain is comprised by a relatively long random loop and helix ($\alpha 1$) (Fig. 1a).

Viewed in parallel to the membrane, the MtrF dimer is bowl-shaped with a concave aqueous basin facing the intracellular solution (Fig. 1b). The dimer is about 75 Å tall, 80 Å wide and 50 Å thick, with the transmembrane portion of the transporter lying approximately in the middle. The rim of the basin is as large as 45 Å. The bowl-shaped structure is 25 Å in depth and deeply penetrates into the inner leaflet of the cytoplasmic membrane (Fig. 1c). This basin probably allows aqueous solution to reach the midpoint of the membrane bilayer.

The structure of each MtrF protomer can be roughly divided into the inner and outer cores (Fig. 2). The outer core contains TMs 1, 2, 5, 6, and 7, creating a frame-like structure to house the inner core of the protein (Fig. 2a). A portion of this outer core is responsible for forming a dimerization domain of the transporter. Viewed along the membrane normal, TMs 1b, 2a, 2b, 6, 7a, and 7b, as well as their counter parts from the next subunit, contribute to this distinct dimerization domain.

Noticeably, the inner core of the MtrF protomer, comprising TMs 3, 4, 8, and 9, as well as HPs 1 and 2, folds into a cylindrical structural feature (Fig. 2a). It is most likely that this inner core cylinder forms a substrate-binding site and transport pathway. Based on the crystal structure, it was found that the inner core cylinder contributes to form a tunnel spanning

approximately from the middle of the inner membrane up to the periplasmic space (Fig. 2b). This tunnel is surrounded with HPs 1 and 2, as well as TMs 3 and 8. Interestingly, this tunnel is connected to the cytoplasmic space through an opening located at the basin of the bowl-shaped structure. The loop regions of HP1, HP2, TM3, and TM8 form this opening. Several conserved residues, including D193, S417, W420, P438, R446, D449, and P457, are found to line the wall of the channel (Fig. 2b). These residues may play an important role for the function of this transporter.

MtrF is capable of exporting *p*-aminobenzoic acid from the cell

As *E. coli* AbgT has been shown to enable uptake of the folate catabolite *p*-aminobenzoyl-glutamate (Carter et al., 2007), we investigated if *E. coli* cells expressing *N. gonorrhoeae* MtrF can grow in liquid minimal medium (containing 90.4 mM Na₂HPO₄, 22.0 mM KH₂PO₄, 8.5 mM NaCl, 0.1 mM CaCl₂, 1.0 mM MgSO₄, 20.0 mM NH₄Cl, and 22.2 mM glucose) supplemented with *p*-aminobenzoyl-glutamate. To facilitate this work, we made an *E. coli* knockout strain BL21(DE3) Δ *abgT* Δ *pabA* that lacks both the *abgT* (Hussein et al., 1998; Carter et al., 2007) and *pabA* (Kaplan and Nichols, 1986) genes. We then transformed these double knockout cells with pET15b Ω *mtrF*, expressing *N. gonorrhoeae* *mtrF*, or the empty vector pET15b. Surprisingly, the double knockout *E. coli* BL21(DE3) Δ *abgT* Δ *pabA* cells, transformed with either pET15b Ω *mtrF* or pET15b, could not grow in this liquid medium supplemented with *p*-aminobenzoyl-glutamate up to 1 mM. However, these cells were capable of growing in liquid minimal medium when supplemented with 30 nM *p*-aminobenzoic acid (PABA). Within the *E. coli* *abg* operon, there are two additional genes, *abgA* and *abgB*, located upstream of *abgT*. The products of these two genes are the AbgA and AbgB aminoacyl aminohydrolases, which cleave

the catabolite *p*-aminobenzoyl-glutamate imported by the AbgT transporter to form PABA for folic acid synthesis (Carter et al., 2007). In contrast, the *mtr* operon of *N. gonorrhoeae* does not possess *abgA* or *abgB* related genes (www.genome.ou.edu). Thus, our data suggest that MtrF and AbgT may function differently even though these two membrane proteins belong to the same family.

As PABA is an important precursor for folic acid synthesis, we thought that *N. gonorrhoeae* MtrF might enable uptake of PABA. It should be noted that PABA is capable of diffusing into bacterial cells through the membrane, participating as an intermediate in *de novo* synthesis of the essential vitamin folic acid. Nonetheless, we decided to compare the radioactive PABA content over time in cells transformed with either pET15b Ω *mtrF* or the empty vector pET15b. Surprisingly, as demonstrated in Fig. 3a, *E. coli* cells producing *N. gonorrhoeae* MtrF showed a significant decrease in the level of [³H]-PABA, in contrast to cells transformed with the empty pET15b vector. Instead of an importer, the data strongly suggested to us that MtrF may act as an exporter, capable of expelling the intracellular PABA metabolite from the cell.

In order to determine whether the conserved MtrF residues, D193, S417, W420, P438, R446, D449, and P457, lining the inner wall of the tunnel formed by each protomer are important for the function of the transporter, we mutated each residue to alanine, individually (Table S2). We expressed these mutant transporters in BL21(DE3) Δ *abgT* Δ *pabA*. Western analysis suggested that the expression levels of these mutant transporters are comparable with that of the wild-type MtrF protein (Fig. S3). We then measured the accumulation of [³H]-PABA in cells harboring the mutant transporters, D193A, S417A, W420A, P438A, R446A, D449A, and P457A. The results showed a significant increase in the levels of [³H]-PABA accumulation in cells possessing the mutant transporter D193A, W420A, P438A, D449A, or P457A, when

compared with cells expressing wild-type *N. gonorrhoeae* MtrF (Fig. 3b). However, cells expressing S417A and R426A only indicated a modest change in the [³H]-PABA concentration when compared with cells carrying wild-type MtrF (Fig. 3b). On the contrary, the levels of [³H]-PABA accumulation in cells expressing the mutants W420A and D449A were nearly the same as those transformed with the empty vector, indicating that these mutant transporters are not functional and cannot export PABA from cells. The data suggest that MtrF acts as an efflux pump, and these amino acids are important for its function.

Expression of the MtrF transporter decreases intracellular folic acid concentration

We hypothesized that *N. gonorrhoeae* MtrF is capable of catalyzing the efflux of the folate metabolite PABA. If this is the case, then cells expressing MtrF should show a lower level of intracellular folic acid concentration. Therefore, we decided to measure the intracellular folic acid content of these cells microbiologically using *Lactobacillus casei* (Wilson and Horne, 1982). Cells were grown in liquid minimal medium supplemented with 30 nM PABA. These cells were harvested when the optical density (OD_{600 nm}) reached 0.5 and then assayed to obtain their folic acid concentrations. Consistent with the results from PABA accumulation, the folic acid concentration in cells producing MtrF were markedly reduced in comparison with cells transformed with the empty vector (Fig. 4). These data further support our hypothesis that MtrF acts as an efflux pump and participates in exporting PABA from the cell.

We next investigated how residues D193, S417, W420, P438, R446, D449, and P457 affect the intracellular folic acid concentration. When transformed with plasmids expressing the mutant transporter W420A, folic acid production was nearly restored in these cells and the level of intracellular folic acid concentration was similar to that of the double knockout strain

transformed with the empty vector (Fig. 4). In addition, cells carrying the mutants, D193A, S417A, P438A, D449A, and P457A, indicated a significant increase in the level of folic acid concentration when compared with cells expressing wild-type MtrF (Fig. 4). Again, the data indicate that these residues are important for the function of the MtrF efflux pump. However, for cells expressing R446A, the intracellular folic acid content was similar to that of cells carrying the wild-type MtrF transporter.

MtrF is an antibiotic efflux pump

As PABA is an important metabolite for producing the essential folic acid in bacteria, we questioned why the function of MtrF appears to be decreasing the intracellular PABA concentration. We postulated that the answer may lie in the ability of MtrF to protect bacterial cells by extruding antimetabolites that are structurally similar to PABA, specifically sulfonamides. Sulfonamides are antimicrobial agents, sometimes referred to as antimetabolites or growth factor analogs, which are designed to specifically inhibit the essential metabolic pathway for folic acid synthesis in bacterial pathogens. At the chemical level, sulfonamides are structurally similar to the metabolite PABA, making them ideal competitive inhibitors. Sulfonamides were used in the late 1930s and early 1940s to treat gonorrhoea, but the rapid emergence of strains resistant to this class of drug resulted in its removal once penicillin became available (Unemo & Shafer, 2014); resistant strains were later found to contain mutations in *folP* that encodes the target for sulfonamides. We therefore suspect that MtrF may be a drug efflux pump, which is capable of recognizing and extruding sulfonamide antimetabolites. In fact, we found that the minimum inhibitory concentration (MIC) of sulfanilamide for the *N. gonorrhoeae*

strain WV16 (an *mtrF* knockout strain) differed from that of the *N. gonorrhoeae* parental strain FA140 by twofold (Table S3).

To determine if MtrF behaves like a sulfonamide efflux pump, we used *E. coli* as a surrogate host. We transformed BL21(DE3) Δ *abgT* Δ *pabA* with pET15b Ω *mtrF* or pET15b and tested for the susceptibility of these transformants to two different sulfonamide antimetabolites, sulfamethazine and sulfanilamide (Table S3). We found that the BL21(DE3) Δ *abgT* Δ *pabA* cells producing MtrF were 32-fold less sensitive to sulfamethazine when compared with BL21(DE3) Δ *abgT* Δ *pabA* cells containing the empty pET15b vector. In addition, this BL21(DE3) Δ *abgT* Δ *pabA*/pET15b Ω *mtrF* transformant was found to be eight times more resistant to sulfanilamide in comparison to the double knockout cells transformed with pET15b. These data indeed indicate that MtrF functions as a drug efflux pump and reduced bacterial susceptibility to sulfonamides.

In order to further test the drug efflux capability of MtrF, we expressed the mutant transporters D193A, S417A, W420A, P438A, R446A, D449A, and P457A in BL21(DE3) Δ *abgT* Δ *pabA* and evaluated for their ability to confer sulfamethazine and sulfanilamide resistance *in vivo*. In most cases, we found that strain BL21(DE3) Δ *abgT* Δ *pabA* carrying these MtrF mutants are more sensitive to these two sulfonamides in comparison with cells expressing wild-type MtrF (Table S3), thus agreeing with the idea that these residues are essential for the function of MtrF.

To confirm these drug susceptibility testing results, we measured the accumulation of radioactive sulfonamide in BL21(DE3) Δ *abgT* Δ *pabA* cells carrying pET15b Ω *mtrF* or pET15b. For these experiments, we compared the accumulation of [³H]-sulfamethazine over time in these cells. As shown in Fig. 5, the results indicate a much lower level of [³H]-sulfamethazine

accumulation in BL21(DE3) $\Delta abgT\Delta pabA$ cells producing MtrF, compared to controlled cells harboring the empty pET15b vector, suggesting that MtrF is capable of exporting sulfamethazine from the cell.

When transformed with plasmids expressing the mutant transporters, D193A, S417A, W420A, P438A, R446A, D449A, and P457A, the level of intracellular sulfamethazine accumulation were much higher than that of cells expressing wild-type MtrF (Fig. 5). Again, these data indicate that residues D193, S417, W420, P438, R446, D449, and P457 are critical for the function of the MtrF efflux pump.

MtrF behaves as a PMF-dependent drug efflux pump

It has been suggested that members of the AbgT family use the proton-motive-force (PMF) to transport substrates across the membrane (Prakash et al., 2003). To elucidate if *N. gonorrhoeae* MtrF is a PMF-dependent transporter, we measured the level of intracellular sulfamethazine accumulation in the presence of carbonyl cyanide *m*-chlorophenylhydrazone (CCCP), a de-coupler of the membrane proton gradient. After the addition of CCCP into the assay solution, the accumulation of [³H]-sulfamethazine increased drastically in the MtrF-expressing cells (Fig. 6a), suggesting the possibility that MtrF is PMF-dependent.

We then investigated the accumulation level of radioactive sulfamethazine in strain BL21(DE3) $\Delta abgT\Delta pabA/pET15b\Omega mtrF$ in the presence of NaCl or KCl. The concentrations of these metal ions were either 5 or 100 mM. In all cases, the levels of accumulation of [³H]-sulfamethazine were similar to that in the MtrF-producing strain without the addition of any metal ions (Figs. 5 and 6a), indicating that the function of MtrF is metal ion independent.

The drug accumulation data strongly suggest that MtrF is a PMF-dependent efflux pump. To test this possibility, we next measured the efflux of [³H]-sulfamethazine that had accumulated in strain BL21(DE3) Δ *abgT* Δ *pabA*/pET15b Ω *mtrF* over time, both in the absence and presence of Na⁺. Cells were first loaded with [³H]-sulfamethazine and CCCP was added to inhibit the pump. Cells were then re-energized by removing CCCP and adding glucose; thereafter, radioactive measurements were performed both in the absence and presence of 5 mM NaCl. As shown in Fig. 6b, the addition of Na⁺ has essentially no effect on sulfamethazine efflux in BL21(DE3) Δ *abgT* Δ *pabA*/pET15b Ω *mtrF*. These data suggest that MtrF is a PMF-dependent efflux pump.

Conclusions

In this paper, we report the crystal structure of the *N. gonorrhoeae* MtrF transporter, which reveals a dimeric molecule with a fold very distinct from all other families of transporters. Our experimental data strongly suggest that *N. gonorrhoeae* MtrF is a drug efflux pump, capable of removing sulfonamide antimetabolites and mediating resistance to this class of drugs in bacterial cells. It is likely that many members of the AbgT family of transporters may serve as antimetabolite efflux pumps to protect cells against these noxious agents.

Experimental procedures

Cloning, expression and purification of *N. gonorrhoeae* MtrF

Briefly, the full-length MtrF membrane protein containing a 6xHis tag at the N-terminus was overproduced in *E. coli* BL21(DE3) Δ *acrB* cells, which harbor a deletion in the chromosomal *acrB* gene, possessing pET15b Ω *mtrF*. Cells were grown in 12 L of Luria-Bertani

(LB) medium with 100 $\mu\text{g}/\text{mL}$ ampicillin at 25°C. When the $\text{OD}_{600 \text{ nm}}$ reached 0.5, the culture was treated with 0.2 mM isopropyl- β -D-thiogalactopyranoside (IPTG) to induce *mtrF* expression, and cells were harvested within 15 h. The collected bacteria were resuspended in low salt buffer containing 100 mM sodium phosphate (pH 7.2), 10% glycerol, 1 mM ethylenediaminetetraacetic acid (EDTA) and 1 mM phenylmethanesulfonyl fluoride (PMSF), and then disrupted with a French pressure cell. The membrane fraction was collected and washed twice with high salt buffer containing 20 mM sodium phosphate (pH 7.2), 2 M KCl, 10% glycerol, 1 mM EDTA and 1 mM PMSF, and once with 20 mM HEPES-NaOH buffer (pH 7.5) containing 1 mM PMSF as described previously (Long et al., 2010). The membrane protein was then solubilized in 2 % (w/v) n-dodecyl- β -D-maltoside (DDM). Insoluble material was removed by ultracentrifugation at 100,000 x g. The extracted protein was purified with a Ni^{2+} -affinity column. The purified protein was dialyzed and concentrated to 20 mg/ml in a buffer containing 20 mM Na-HEPES (pH 7.5) and 0.05% DDM. The 6xHis tag at the N-terminus was then cleaved by adding 5 units of thrombin (GE Healthcare Bio-Sciences, Pittsburgh, PA) per mg of purified MtrF at room temperature for 20 h. The protein was subsequently passed through a Ni^{2+} -affinity column to remove the free 6xHis tag. A final purification step was performed using a G200 size exclusion column loaded with buffer solution containing 20 mM Na-HEPES (pH 7.5) and 0.05% DDM. The purity of the MtrF protein (>95%) was judged using 10% SDS-PAGE stained with Coomassie Brilliant Blue. The purified protein was then concentrated to 20 mg/ml in a buffer containing 20 mM Na-HEPES (pH 7.5) and 0.05% DDM.

Crystallization of MtrF

Crystals of the MtrF transporter were obtained using sitting-drop vapor diffusion. The MtrF crystals were grown at room temperature in 24-well plates with the following procedures. A 2 μ L protein solution containing 20 mg/mL MtrF protein in 20 mM Na-HEPES (pH 7.5) and 0.05% (w/v) DDM was mixed with a 2 μ L of reservoir solution containing 30% PEG 400, 0.1 M sodium acetate (pH 5.0), 0.1 M magnesium acetate, 3% glycerol and 1% (w/v) Sucrose monododecanoate. The resultant mixture was equilibrated against 500 μ l of the reservoir solution. Crystals of MtrF grew to a full size in the drops within a month. Typically, the dimensions of the crystals were 0.2 mm x 0.2 mm x 0.2 mm. Cryoprotection was achieved by raising the PEG 400 concentration to 32%.

Crystals of the Ta₆Br₁₂²⁺ cluster derivative were prepared by incubating the crystals of MtrF in solution containing 32% PEG 400, 0.1 M sodium acetate (pH 4.6), 0.05 M magnesium acetate, 5% glycerol, 1% (w/v) Sucrose monododecanoate, 0.05% (w/v) DDM and 0.5 mM Ta₆Br₁₂·2Br (Jena Bioscience GmbH, Jena, Germany) for 4 hours at 25°C.

Data collection, structural determination and refinement

All diffraction data were collected at 100 K at beamline 24ID-C located at the Advanced Photon Source, using an ADSC Quantum 315 CCD-based detector. Diffraction data were processed using DENZO and scaled using SCALEPACK (Otwinowski and Minor, 1997). Crystals of MtrF belong to space group *P*6₁ (Table S1). Based on the molecular weight of MtrF (56.3 kDa), two molecules per asymmetric unit with a solvent content of 71.9% were expected. The heavy-atom derivative (Ta₆Br₁₂²⁺ cluster) (Jena Bioscience GmbH, Jena, Germany) was isomorphous with the native crystal (Table S1). Four tantalum cluster sites were identified using

SHELXC and SHELXD (Schneider and Sheldrick, 2002) as implemented in the HKL2MAP package (Pape and Schneider, 2004). Single isomorphous replacement with anomalous scattering (SIRAS) was employed to obtain experimental phases using the program MLPHARE (Otwinowski, 1991). These heavy-atom sites were refined by MLPHARE (Otwinowski, 1991) as well. The resulting phases were subjected to density modification and NCS averaging using the program RESOLVE (Terwilliger, 2001). Density modified phases were good enough to allow us to visualize the secondary structural features of the molecule. The resulting phases were of excellent quality and allowed for tracing of most of the molecule. After tracing the initial model manually using the program Coot (Emsley and Cowtan, 2004), the model was refined against the native data at 3.95 Å-resolution using PHENIX (Adams et al., 2002), leaving 5% of reflections in Free-R set. Iterations of refinement using PHENIX (Adams et al., 2002) and CNS (Brünger et al., 1998) and model building in Coot (Emsley and Cowtan, 2004) lead to the structural model of the MtrF transporter (Table S1).

Construction of the double knockout strain

The double knockout *E. coli* strain BL21(DE3) $\Delta abgT\Delta pabA$ was produced from the BL21(DE3) strain using an RED disruption system as described by Datsenko and Wanner (Datsenko and Wanner, 2000). The $\Delta abgT::kan$ cassette, which was used to replace the chromosomal *abgT* gene, was produced by PCR, and then introduced into pKD46/BL21(DE3) by electroporation. The knockout BL21(DE3) $\Delta abgT::kan$ strain was selected on LB plate containing 30 µg/ml kanamycin, and verified by PCR. The kanamycin resistant gene was then released to generate the BL21(DE3) $\Delta abgT$ knockout strain. The deletion of *pabA* from

BL21(DE3) $\Delta abgT$ was done using similar procedures as described above to generate the final BL21(DE3) $\Delta abgT\Delta pabA$ double knockout strain.

Site-directed mutagenesis

Site-directed point mutations on residues D193, S417, W420, P438, R446, D449, and P457, which are expected to be critical for the function of the MtrF efflux pump, were performed to generate the single point mutants D193A, S417A, W420A, P438A, R446A, D449A, and P457A. The primers used for these mutations are listed in Table S2. All oligonucleotides were purchased from Integrated DNA Technologies, Inc. (Coralville, IA) in a salt-free grade.

Accumulation assays of *p*-aminobenzoic acid

In brief, *E. coli* BL21(DE3) $\Delta abgT\Delta pabA$ carrying pET15b $\Omega mtrF$ or pET15b were grown in LB broth with 100 $\mu\text{g}/\text{mL}$ ampicillin at 37 °C. When the $\text{OD}_{600 \text{ nm}}$ reached 0.5, the culture was treated with 0.2 mM IPTG to induce *mtrF* expression, and cells were harvested within 2 h. Cells were washed twice with buffer containing 50 mM potassium phosphate (pH 7.5), twice with buffer containing 100 mM Tris-HCl (pH 7.5), and then suspended in the same buffer to $\text{OD}_{600 \text{ nm}}$ of 15. [^3H]-PABA (Moravek Biochemicals, Brea, CA) was then added to a final concentration of 0.3 μM . Samples of 100 μl were taken at intervals, applied directly to prewetted glass-fiber filters, and washed twice with 5-ml aliquots of the same buffer; 0.5- μm glass-fiber filters (MFS, Dubbin, CA) were used with a filter apparatus. Filters were then incubated for 30 min in scintillation fluid (ScintiVerse™ BD) and counted with a Packard Tri-Carb 1600TR liquid scintillation counter (Perkin Elmer, Waltham, MA).

For [³H]-PABA accumulations in cells expressing the MtrF mutants, the procedures for sample preparation were the same as above. Cells were incubated with 0.3 μM [³H]-PABA for 15 min, applied directly to prewetted glass-fiber filters, and washed immediately twice with 5-mL aliquots of the same buffer. Filters were then incubated for 30 min in scintillation fluid (ScintiVerse™ BD) and counted with a Packard Tri-Carb 1600TR liquid scintillation counter (Perkin Elmer, Waltham, MA).

Assays of folic acid

The concentration of folic acid in the double knockout BL21(DE3)Δ*abgT*Δ*pabA* strain transformed with pET15bΩ*mtrF* or pET15b was measured using *Lactobacillus casei* based on the microbiological procedure of Wilson and Horne (1982). The concentrations of folic acid in BL21(DE3)Δ*abgT*Δ*pabA* expressing the mutant transporters were measured using the same procedures.

Drug susceptibility assays

The susceptibilities to sulfamethazine and sulfanilamide of *E. coli* BL21(DE3)Δ*abgT*Δ*pabA* harboring pET15bΩ*mtrF* expressing the wild-type or mutant transporters, or the pET15b empty vector were tested on agar plates. Cells were grown in Luria Broth (LB) medium with 100 μg/mL ampicillin at 37 °C. When the OD_{600 nm} reached 0.5, the cultures were induced with 0.2 mM IPTG and harvested in two hours after induction. The minimum growth inhibitory concentrations (MICs) to sulfamethazine and sulfanilamide of *E. coli* BL21(DE3)Δ*abgT*Δ*pabA* (inoculum, 500 cells/mL) harboring these vectors were then

determined using LB agar containing 50 µg/mL ampicillin, 0.1 mM IPTG and different concentrations of sulfamethazine and sulfanilamide, respectively.

For the MIC studies with *N. gonorrhoeae* cells, we used strains FA140 and WV16 (as FA140 but *mtrF::kan*) described by Veal and Shafer (2003). These strains were grown on GCB agar plates. The susceptibilities to sulfanilamide were performed using the agar dilution assay described by Hagman et al. (1995).

Accumulation assays of sulfamethazine

The procedures for [³H]-sulfamethazine accumulation were the same as those for [³H]-PABA accumulation. Cells were incubated with 75 nM [³H]-sulfamethazine (Moravek Biochemicals, Brea, CA) for 15 min, applied directly to prewetted glass-fiber filters, and washed immediately twice with 5-ml aliquots of the same buffer. Filters were then incubated for 30 min in scintillation fluid (ScintiVerse™ BD) and counted with a Packard Tri-Carb 1600TR liquid scintillation counter (Perkin Elmer, Waltham, MA). For metal ion dependent experiments, cells were incubated with 75 nM [³H]-sulfamethazine in the presence of NaCl or KCl (5 or 100 mM) for 15 min, then applied directly to prewetted glass-fiber filters, and washed immediately twice with 5-ml aliquots of buffer containing 100 mM Tris-HCl (pH 7.5) and 5 or 100 mM salt (NaCl or KCl).

Efflux assays of sulfamethazine

E. coli BL21(DE3)Δ*abgT*Δ*pabA* carrying pET15bΩ*mtrF* or pET15b were grown in LB broth with 100 µg/ml ampicillin at 37°C. When the OD₆₀₀ reached 0.5, the culture was induced with 0.2 mM IPTG, and cells were harvested within 2 h. Cells were washed twice with buffer

containing 50 mM potassium phosphate (pH 7.5), twice with buffer containing 100 mM Tris-HCl (pH 7.5), and then suspended in the same buffer to OD_{600 nm} of 15. CCCP was added to the cell suspension at a final concentration of 100 μ M. Cells were then incubated for 10 min, pelleted, washed twice and resuspended in the same buffer to OD_{600 nm} of 10. [³H]-sulfamethazine was then added to a final concentration of 37 nM. Cells were incubated for 15 min, and a final concentration of 0.2% glucose was then added to the cell suspension. When needed, a final concentration of 5 mM NaCl was also added at the same time. At various time points, samples of 100 μ l were applied directly to prewetted glass-fiber filters, and washed twice with 5-ml aliquots of buffer containing 100 mM Tris-HCl (pH 7.5). Filters were then incubated for 30 min in scintillation fluid (ScintiVerse™ BD) and counted with a Packard Tri-Carb 1600TR liquid scintillation counter (Perkin Elmer, Waltham, MA).

Accession code

Atomic coordinates and structure factors for the structure of MtrF have been deposited at the RCSB Protein Data Bank with an accession code 4R1I.

Acknowledgements

This work was supported by NIH Grants R37AI021150 (W.M.S.) and R01GM086431 (E.W.Y.) and a VA Merit Award (W.M.S.) from the Medical Research Service of the Department of Veterans Affairs. W.M.S. is the recipient of a Senior Research Career Scientist from the Medical Research Service of the Department of Veterans Affairs. This work is based upon research conducted at the Northeastern Collaborative Access Team beamlines of the Advanced Photon Source, supported by an award GM103403 from the National Institutes of

General Medical Sciences. Use of the Advanced Photon Source is supported by the U.S. Department of Energy, Office of Basic Energy Sciences, under Contract No. DE-AC02-06CH11357.

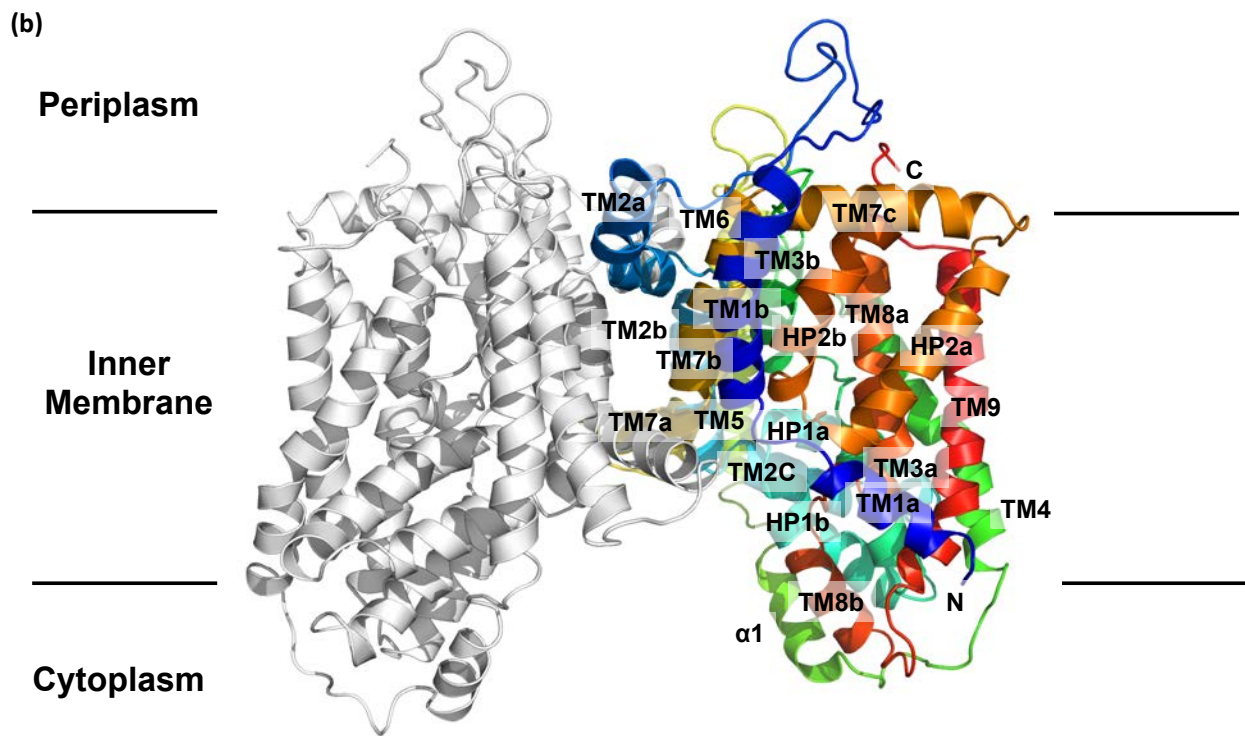
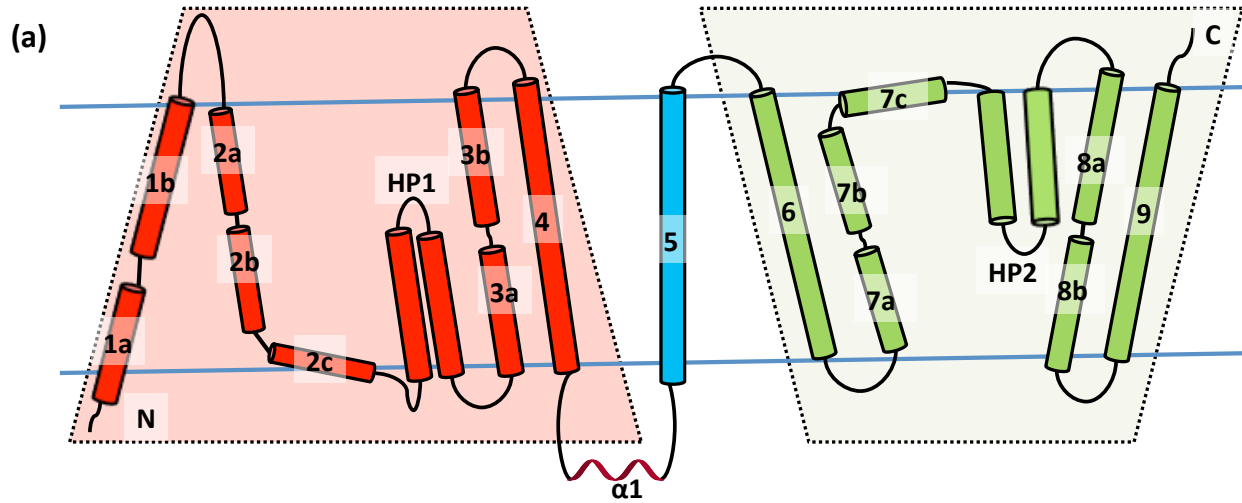
References

- Adams, P.D., Grosse-Kunstleve, R.W., Hung, L.W., Ioerger, T.R., McCroy, A.J., Moriarty, N.W. et al. (2002). PHENIX: building new software for automated crystallographic structure determination. *Acta Crystallogr.* *58*, 1948-1954.
- Brünger, A.T., Adams, P.D., Clore, G.M., DeLano, W.L., Gros, P., Grosse-Kunstleve, R.W., Jiang, J.S., Kuszewski, J., Nilges, M., Pannu, N.S., Read, R.J., Rice, L.M., Simonson, T., and Warren, G.L. (1998). Crystallography & NMR system: A new software suite for macromolecular structure determination. *Acta Crystallogr.* *D54*, 905-921.
- Bolla, J.R., Su, C.C., Do, S.V., Radhakrishnan, A., Kumar, N., Long, F., Chou, T.H., Delmar, J.A., Lei, H.T., Rajashankar, K.R., Shafer, W.M., and Yu, E.W. (2014). Crystal structure of the *Neisseria gonorrhoeae* MtrD inner membrane multidrug efflux pump. *PLoS One* *9*, e97903.
- Carter, E.L., Jager, L., Gardner, L., Hall, C.C., Willis, S., and Green, J.M. (2007). *Escherichia coli* *abg* genes enable uptake and cleavage of the folate catabolite *p*-aminobenzoyl-glutamate. *J. Bacteriol.* *189*, 3329-3334.
- Datsenko, K.A., and Wanner, B.L. (2000). One-step inactivation of chromosomal genes in *Escherichia coli* K-12 using PCR products. *Proc. Nat. Acad. Sci.* *97*, 6640-6645.
- Delahay, R.M., Robertson, B.D., Balthazar, J.T., and Ison, C.A. (1997). Involvement of the gonococcal MtrE protein in the resistance of *Neisseria gonorrhoeae* to toxic hydrophobic agents. *Microbiology* *143*, 2127-2133.
- Emsley, P., and Cowtan, K. (2004). Coot: model-building tools for molecular graphics. *Acta Crystallogr.* *D60*, 2126.
- Folster, J.P., and Shafer, W.M. (2005). Regulation of *mtrF* expression in *Neisseria gonorrhoeae* and its role in high-level antimicrobial resistance. *J. Bacteriol.* *187*, 3713-3720.
- Hagman, K.E., Pan, W., Spratt, B.G., Balthazar, J.T., Judd, R.C., and Shafer, W.M. (1995). Resistance of *Neisseria gonorrhoeae* to antimicrobial hydrophobic agents is modulated by the *mtrRCDE* efflux system. *Microbiology* *141*, 611-622.

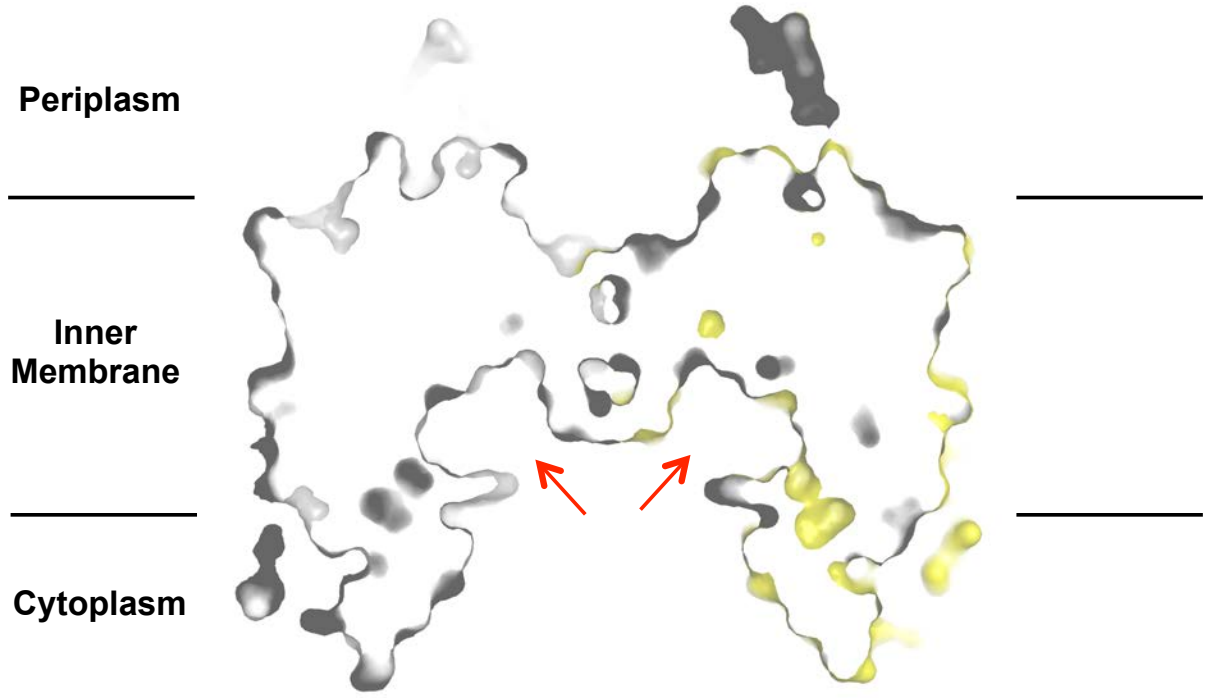
- Hagman, K.E., and Shafer, W.M. (1995). Transcriptional control of the *mtr* efflux system of *Neisseria gonorrhoeae*. *J. Bacteriol.* *177*, 4162-4165.
- Hagman, K.E., Lucas, C.E., Balthazar, J.T., Snyder, L.A., Nilles, M., Judd, R.C., and Shafer, W.M. (1997). The MtrD protein of *Neisseria gonorrhoeae* is a member of resistance/nodulation/division protein family constituting part of an efflux system. *Microbiology* *143*, 2117-2125.
- Hussein, M.J., Green, J.M., and Nichols, B.P. (1998). Characterization of mutations that allow p-aminobenzoate utilization by *Escherichia coli*. *J. Bacteriol.* *180*, 6260-6268.
- Janganan, T.K., Zhang, L., Bavro, V.N., Matak-Vinkovic, D., Barrera, N.P., Burton, M.F., Steel, P.G., Robinson, C.V., Borges-Walmsley, M.I., and Walmsley, A.R. (2011). Opening of the outer membrane protein channel in tripartite efflux pumps is induced by interaction with the membrane fusion partner. *J. Biol. Chem.* *286*, 5484-5493.
- Janganan, T.K., Bavro, V.N., Zhang, L., Borges-Walmsley, M.I., and Walmsley, A.R. (2013). Tripartite efflux pumps: energy is required for dissociation, but not assembly or opening of the outer membrane channel of the pump. *Mol. Microbiol.* *88*, 590-602.
- Kaplan, J. B., and Nichols, B. P. (1986). Nucleotide sequence of *Escherichia coli pabA* and its evolutionary relationship to trp(G)D. *J. Mol. Biol.* *168*, 451-468.
- Lee, E.H., and Shafer, W.M. (1999). The *farAB*-encoded efflux pump mediates resistance of gonococci to long-chained antibacterial fatty acids. *Mol. Microbiol.* *33*, 7753-7758.
- Lei, H.T., Chou, T.H., Su, C.C., Bolla, J.R., Kumar, N., Radhakrishnan, A., Long, F., Delmar, J.A., Do, S.V., Rajashankar, K.R., Shafer, W.M., and Yu, E.W. (2014). Crystal structure of the open state of the *Neisseria gonorrhoeae* MtrE outer membrane channel. *PLoS One* *9*, e97475.
- Long, F., Su, C.-C., Zimmermann, M.T., Boyken, S.E., Rajashankar, K.R., Jernigan, R.L., and Yu, E.W. (2010). Crystal structures of the CusA heavy-metal efflux pump suggest methionine-mediated metal transport mechanism. *Nature* *467*, 484-488.
- Lucas, C.E., Hagman, K.E., Levin, J.C., Stein, D.C., and Shafer, W.M. (1995). Importance of lipooligosaccharide structure in determining gonococcal resistance to hydrophobic antimicrobial agents resulting from the *mtr* efflux system. *Mol. Microbiol.* *16*, 1001-1009.
- Otwinowski, Z. (1991). ML-PHARE, CCP4 Proc. 80-88 (Daresbury Laboratory, Warrington, UK).
- Otwinowski, Z., and Minor, M. (1997). Processing of X-ray diffraction data collected in oscillation mode. *Methods Enzymol.* *276*, 307-326.
- Pape, T., and Schneider, T.R. (2004). HKL2MAP: a graphical user interface for macromolecular phasing with SHELX programs. *J. Appl. Crystallogr.* *37*, 843-844.

- Prakash, S., Cooper, G., Singhi, S., and Saier, M.H. Jr. (2003). The ion transporter superfamily. *Biochim. Biophys. Acta* *1618*, 79-92.
- Rouquette-Loughlin, C., Dunham, S.A., Kuhn, M., Balthazar, J.T., and Shafer, W.M. (2003). The NorM efflux pump of *Neisseria gonorrhoeae* and *Neisseria meningitidis* recognizes antimicrobial cationic compounds. *J. Bacteriol.* *185*, 1101-1106.
- Schneider, T.R., and Sheldrick, G.M. (2002). Substructure solution with SHELXD. *Acta Crystallogr. D* *58*, 1772-1779.
- Shafer, W.M., Qu, X.-D., Waring, A.J., and Lehrer, R.I. (1998). Modulation of *Neisseria gonorrhoeae* susceptibility to vertebrate antibacterial peptides due to a member of the resistance/nodulation/division efflux pump family. *Proc. Natl. Acad. Sci. USA* *95*, 1829-1833.
- Shafer, W.M., Veal, W.L., Lee, E.H., Zarentonelli, L., Balthazar, J.T., and Rouquette, C. (2001). Genetic organization and regulation of antimicrobial efflux systems possessed by *Neisseria gonorrhoeae* and *Neisseria meningitidis*. *J. Mol. Microbiol. Biotechnol.* *3*, 219-225.
- Terwilliger, T. C. (2001). Maximum-likelihood density modification using pattern recognition of structural motifs. *Acta Crystallogr. D* *57*, 1755-1762.
- Tseng, T.T., Gratwick, K.S., Kollman, J., Park, D., Nies, D.H., Goffeau, A., and Saier, M.H. Jr. (1999). The RND permease superfamily: an ancient, ubiquitous and diverse family that includes human disease and development protein. *J. Mol. Microbiol. Biotechnol.* *1*, 107-125.
- Unemo, M., and Shafer, W.M. (2014). Antimicrobial resistance in *Neisseria gonorrhoeae* in the 21st Century: Past, Evolution, and Future. *Clin. Microbiol. Rev.* *27*, 587-613.
- Veal, W.L., Nicholas, R.A., and Shafer, W.M. (2002). Overexpression of the MtrC-MtrD-MtrE efflux pump due to an *mtrR* mutation is required for chromosomally mediated penicillin resistance in *Neisseria gonorrhoeae*. *J. Bacteriol.* *184*, 5619-24.
- Veal, W.L., and Shafer, W.M. (2003). Identification of a cell envelope protein (MtrF) involved in hydrophobic antimicrobial resistance in *Neisseria gonorrhoeae*. *J. Antimicrob. Chemother.* *51*, 27-37.
- Warner, D.M., Shafer, W.M., and Jerse, A.E. (2008). Clinically relevant mutations that cause derepression of the *Neisseria gonorrhoeae* MtrC-MtrD-MtrE efflux pump system confer different levels of antimicrobial resistance and *in vivo* fitness. *Mol. Microbiol.* *70*, 462-478.
- Wilson, S.D., and Horne, W.D. (1982). Use of glycerol-cryoprotected *Lactobacillus casei* for microbiological assay of folic acid. *Clin. Chem.* *28*, 1198-1200.

Legends of figures



(c)



(d)

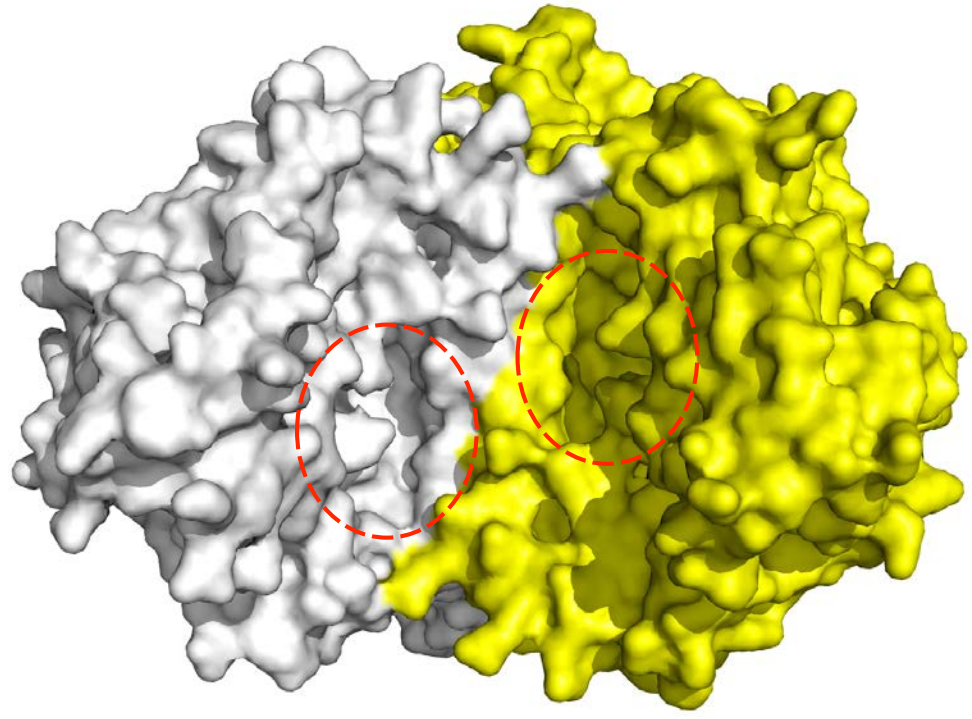
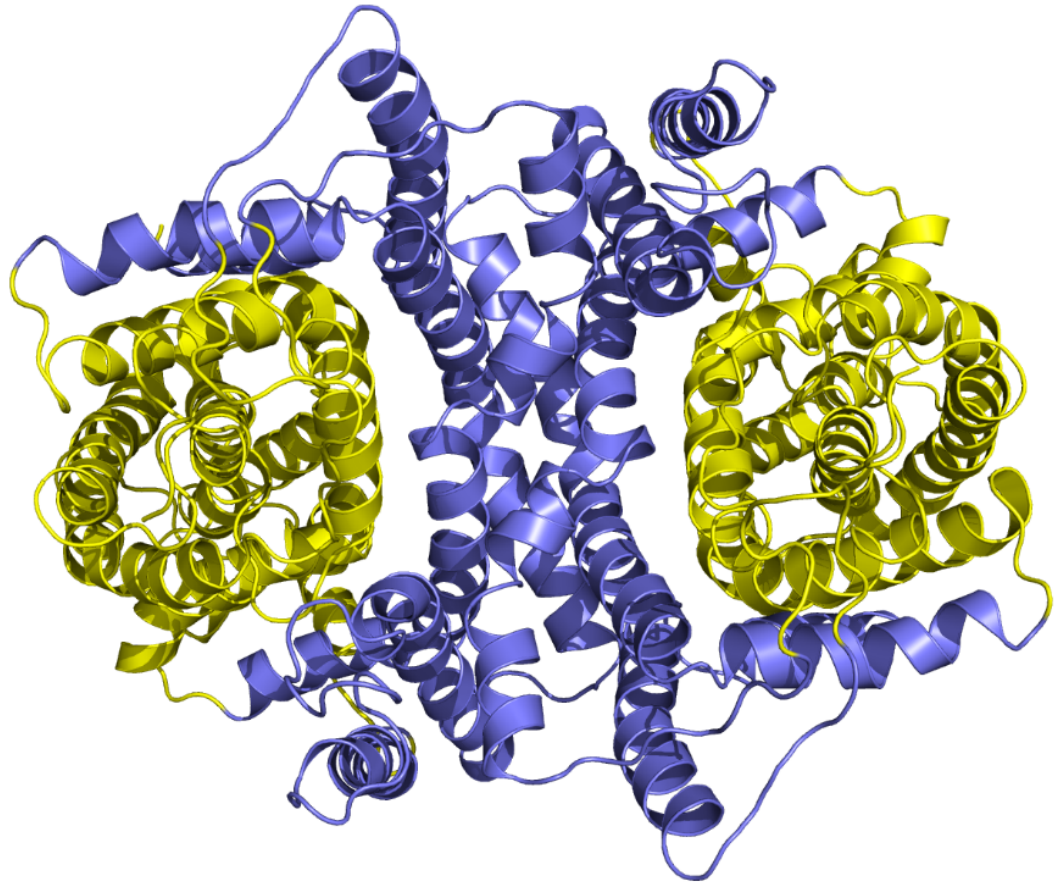


Fig. 1. Structure of the *N. gonorrhoeae* MtrF transporter. (a) Transmembrane topology of *N. gonorrhoeae* MtrF. The transporter contains nine transmembrane helices (TMs) and two hairpins (HPs). (b) Ribbon diagram of a dimer of MtrF viewed in the membrane plane. The right subunit of the dimer is colored using a rainbow gradient from the N-terminus (blue) to the C-terminus (red), whereas the left subunit is colored gray. The MtrF dimer forms a bowl-shaped structure with a concave aqueous basin facing the intracellular solution. (c) Surface representation of a cross section of the MtrF dimer sliced through the middle of the protein. Each protomer forms an internal cavity (red arrow), which is accessible to the cytoplasm. (d) Bottom view of a surface representation of the MtrF dimer, indicating a solvent accessible cavity (red circle) from each protomer of the protein. The two protomers are colored gray and yellow.

(a)



(b)

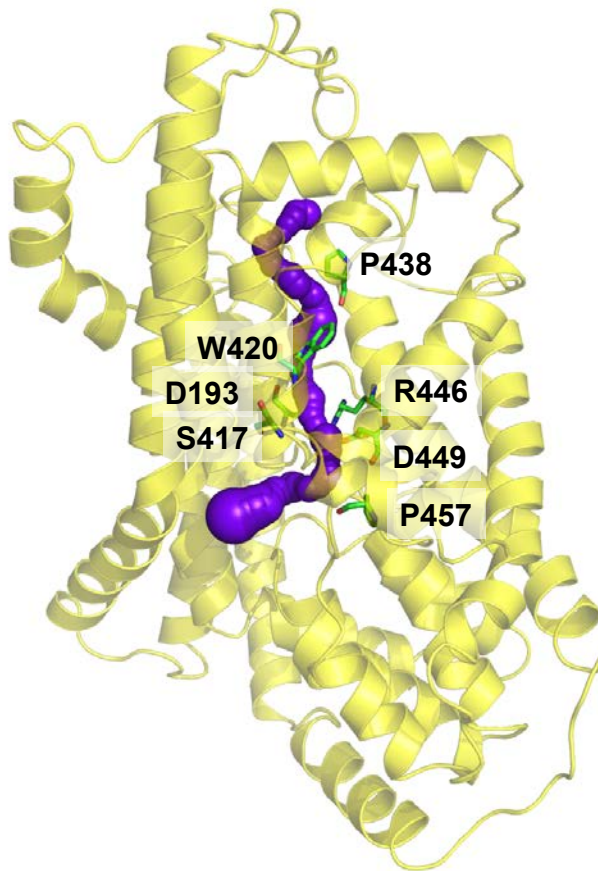
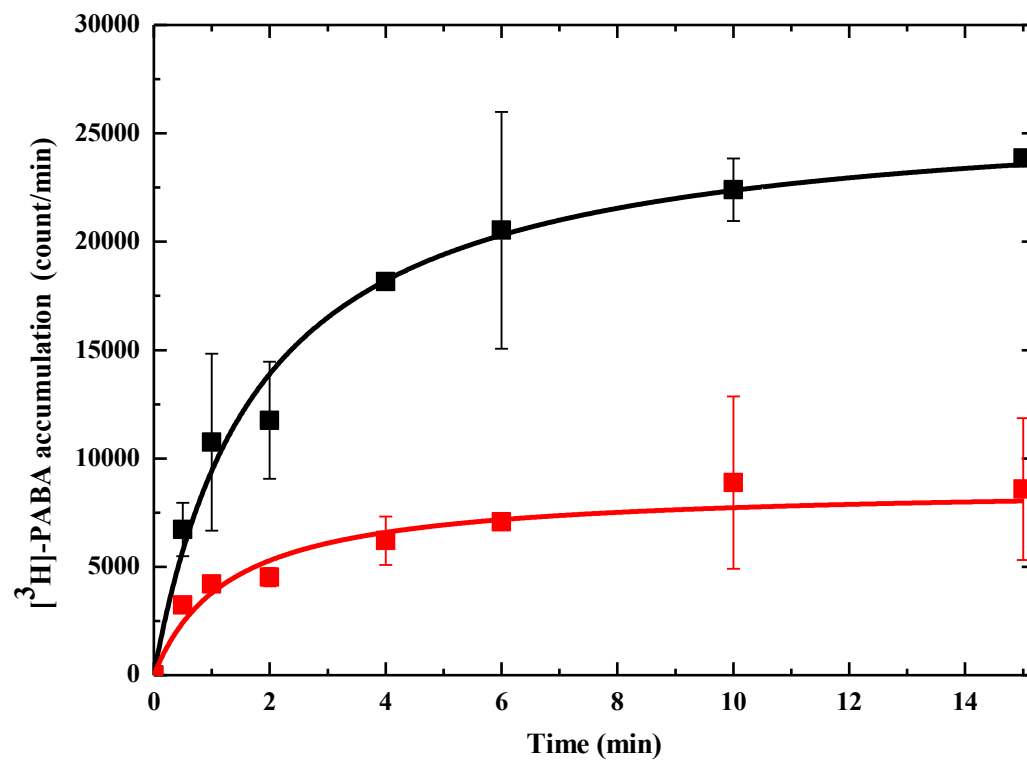


Fig. 2. Outer and inner cores of MtrF. (a) The outer core of MtrF, comprising TMs 1, 2, 5, 6 and 7 (colored slate), contributes to dimerization as well as formation of a frame-like structure housing the inner core of the protomer. The inner core of MtrF is composed of TMs 3, 4, 8, 9 as well as HPs 1 and 2 (colored yellow). (b) The inner core of MtrF forms a channel (colored purple) spanning approximately from the middle of the inner membrane up to the periplasmic space. This channel was calculated using the program CAVER (<http://loschmidt.chemi.muni.cz/caver>). The secondary structural elements of the MtrF protomer are in yellow. Residues D193, S417, W420, P438, R446, D449, and P457 are in green sticks.

(a)



(b)

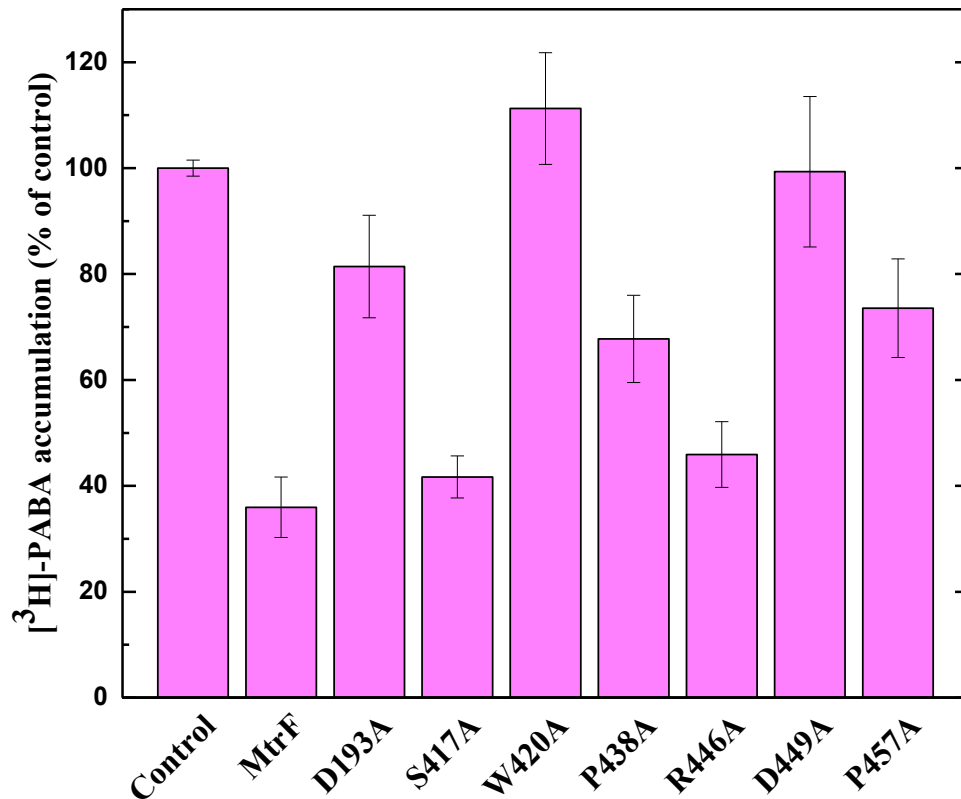


Fig. 3. Accumulation of radioactive *p*-aminobenzoic acid. (a) Time course of [³H]-PABA accumulation by *E. coli* BL21(DE3) Δ *abgT* Δ *pabA* double knockout cells transformed with pET15b Ω *mtrF* or pET15b. Cells expressing *mtrF* (red curve) show a significant decrease in [³H]-PABA accumulation when compared with cells carrying the empty vector (black curve). (b) Mutants of the MtrF transporter. Cells possessing the mutant transporter D193A, W420A, P438A, D449A and P457A show a significant increase in the level of [³H]-PABA accumulations compared with cells expressing wild-type MtrF. However, cells expressing S417A and R446A only show a modest change on the [³H]-PABA concentration when compared with cells carrying wild-type MtrF. The data showed in (a) and (b) are the cumulative average of three successive recordings.

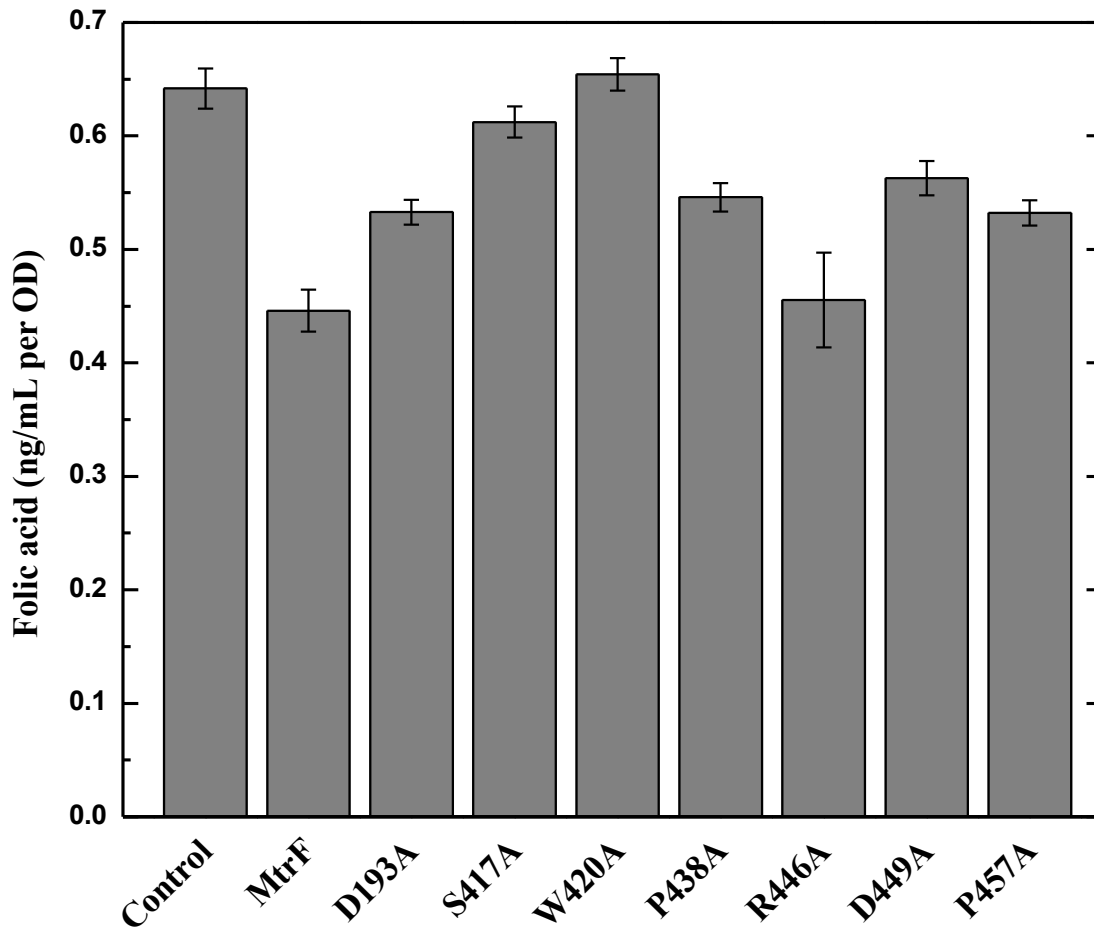


Fig. 4. Intracellular folic acid concentration. Folic acid concentration in *E. coli*

BL21(DE3) $\Delta abgT\Delta pabA$ double knockout cells expressing MtrF were markedly reduced in comparison with cells transformed with the empty vector. When transformed with plasmid expressing the mutant transporter, D193A, S417A, W420A, P438A, D449A, and P457A, folic acid production was significantly increased in these cells. However, the level of intracellular folic acid concentration in BL21(DE3) $\Delta abgT\Delta pabA$ cells expressing R446A was nearly identical to that of the double knockout strain carrying wild-type MtrF. Each bar represents the mean of three separate cultures.

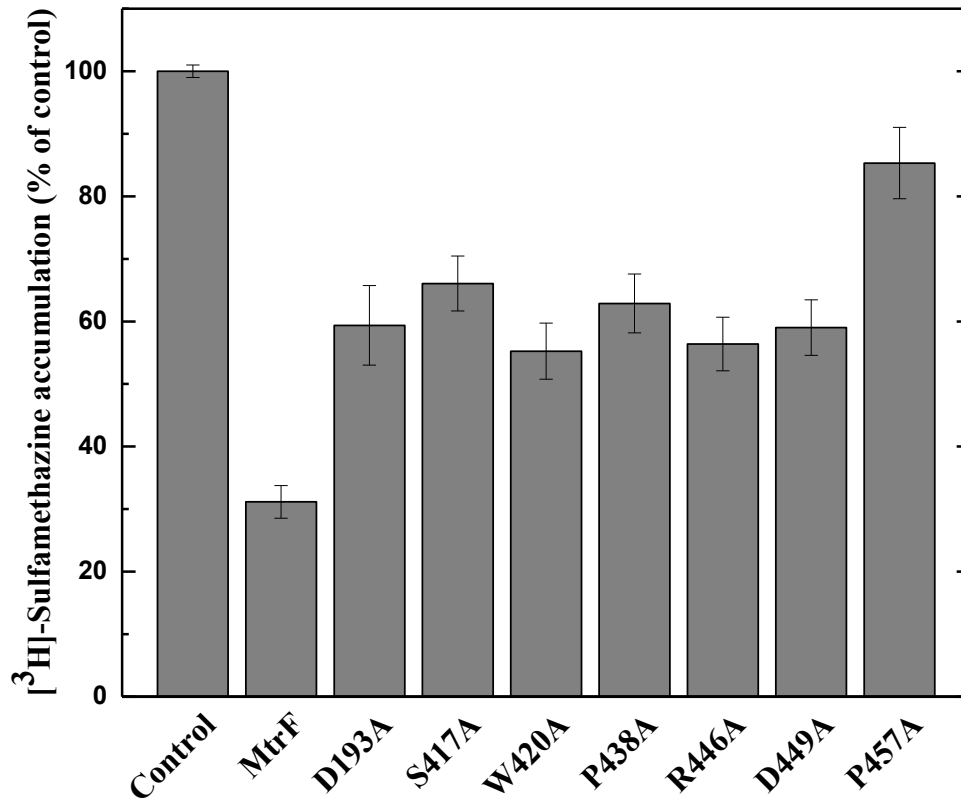
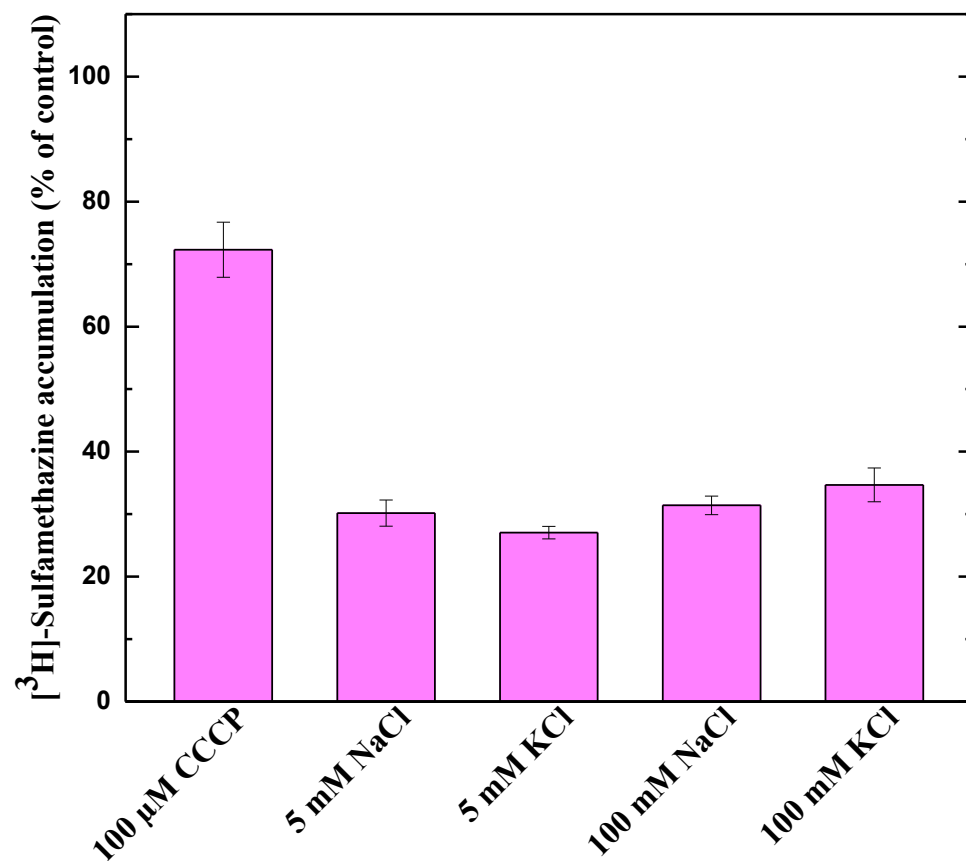


Fig. 5. Accumulation of radioactive sulfamethazine. *E. coli* BL21(DE3) Δ *abgT* Δ *pabA* cells expressing MtrF show a significant decrease in [³H]-sulfamethazine accumulation when compared with cells carrying the empty vector. When transformed with plasmids expressing the mutant transporters, D193A, S417A, W420A, P438A, R446A, D449A, and P457A, the levels of intracellular [³H]-sulfamethazine accumulation were much higher than that of cells expressing wild-type MtrF. Each bar represents the mean of three different cultures.

(a)



(b)

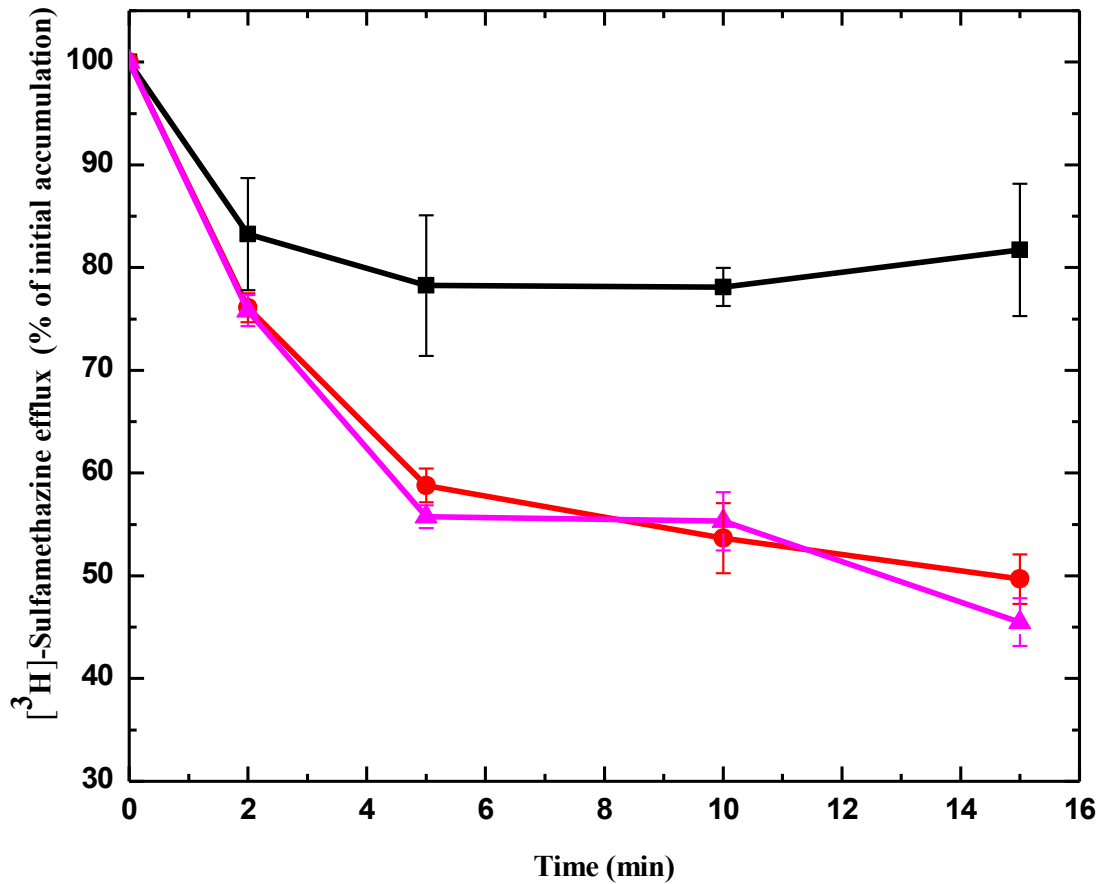


Fig. 6. Transport of sulfamethazine via MtrF. (a) Accumulation of radioactive sulfamethazine in BL21(DE3) Δ *abgT* Δ *pabA*/pET15b Ω *mtrF* cells with different sodium or potassium ion concentrations. (b) Efflux of radioactive sulfamethazine in BL21(DE3) Δ *abgT* Δ *pabA*/pET15b Ω *mtrF* cells in the absence and presence of sodium ions. The presence of Na⁺ does not affect [³H]-sulfamethazine efflux in BL21(DE3) Δ *abgT* Δ *pabA*/pET15b Ω *mtrF* cells (black, controlled cells transformed with empty vector; red, 0 mM NaCl; magenta, 5 mM NaCl). The data showed in (a) and (b) are the cumulative average of three successive recordings.

Supplemental Figures

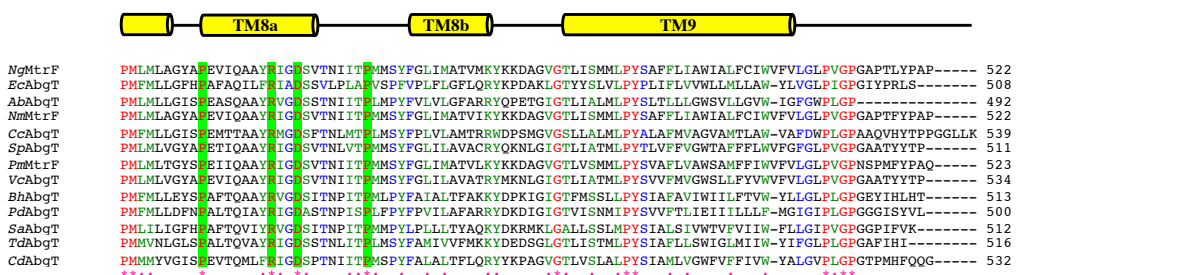
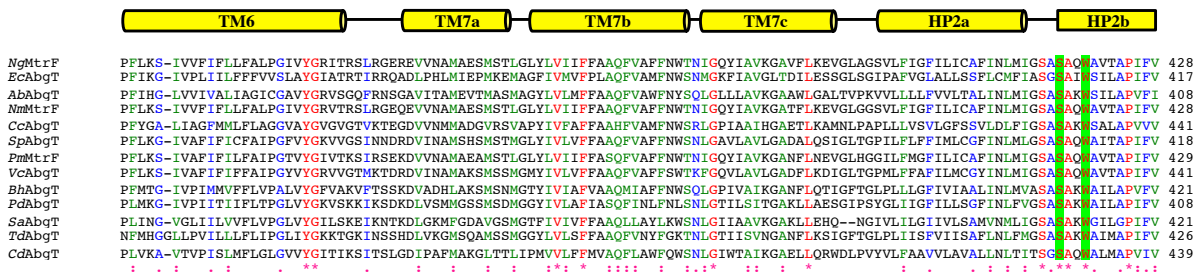
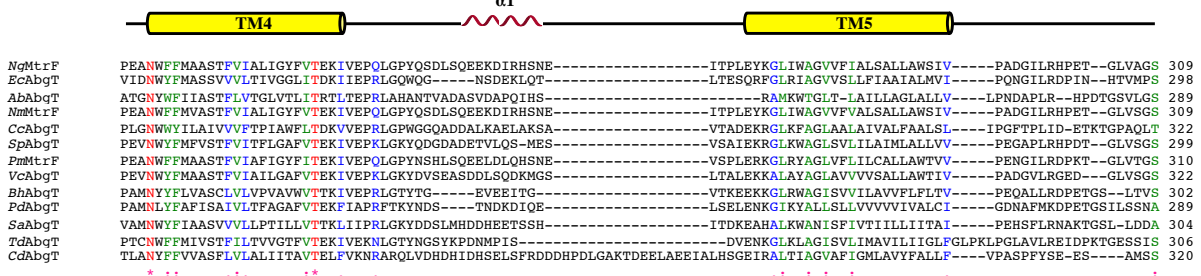
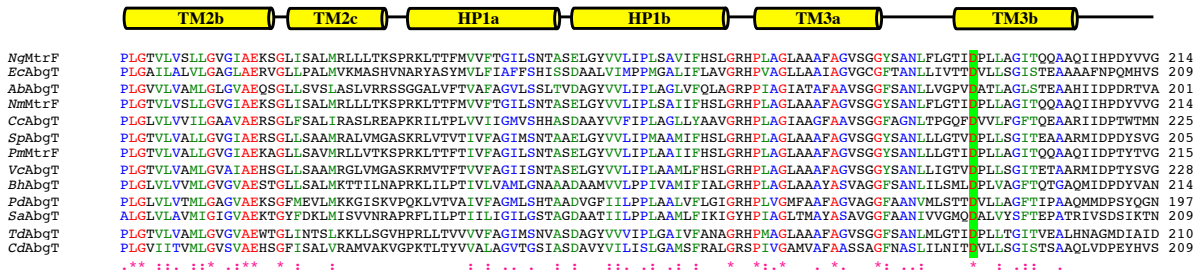
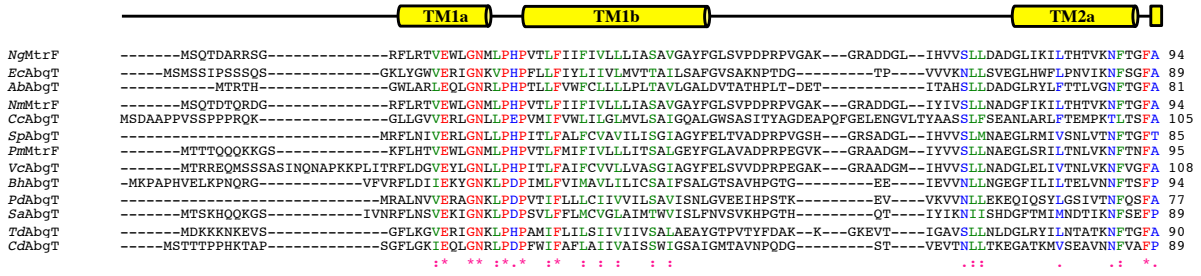
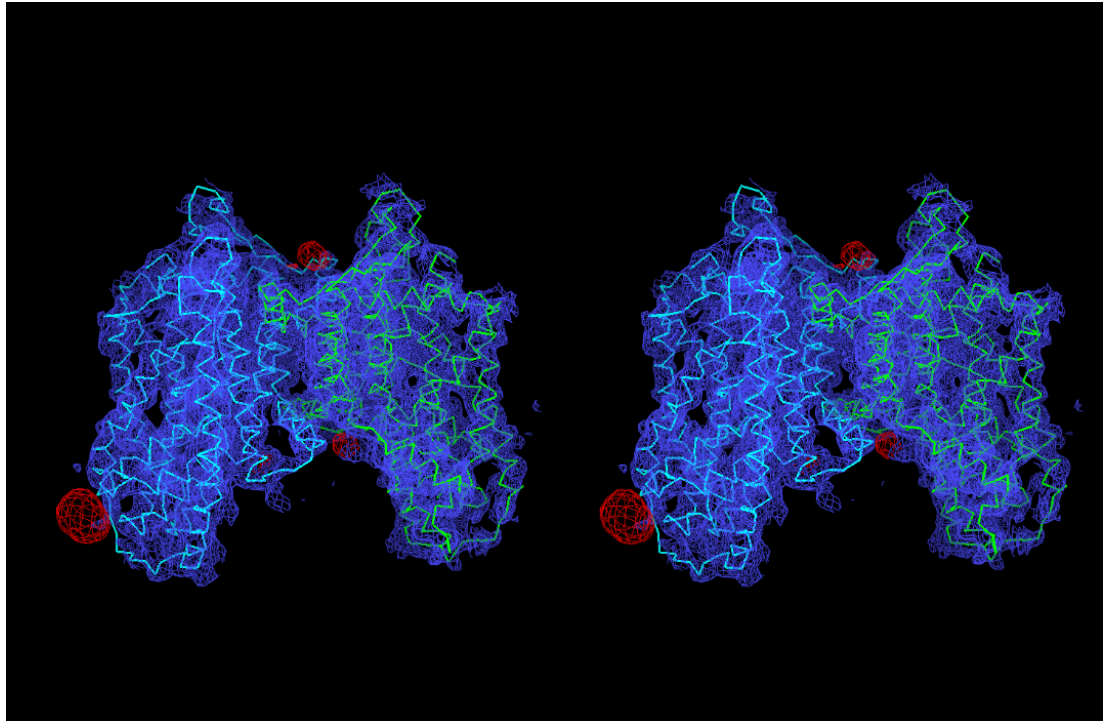


Fig. S1. Sequence and topology of *N.gonorrhoeae* MtrF. Alignment of the amino acid sequences of the AbgT family of transporters was done using CLUSTAL W. *, identical residues; :, >60% homologous residues. Secondary structural elements are indicated: TM, transmembrane helix; α , helix. The sequence and topology of *N. gonorrhoeae* MtrF are shown at the top. Conserved residues involved in lining the channel of the inner core of the protein are highlight with green bars.

(a)



(b)

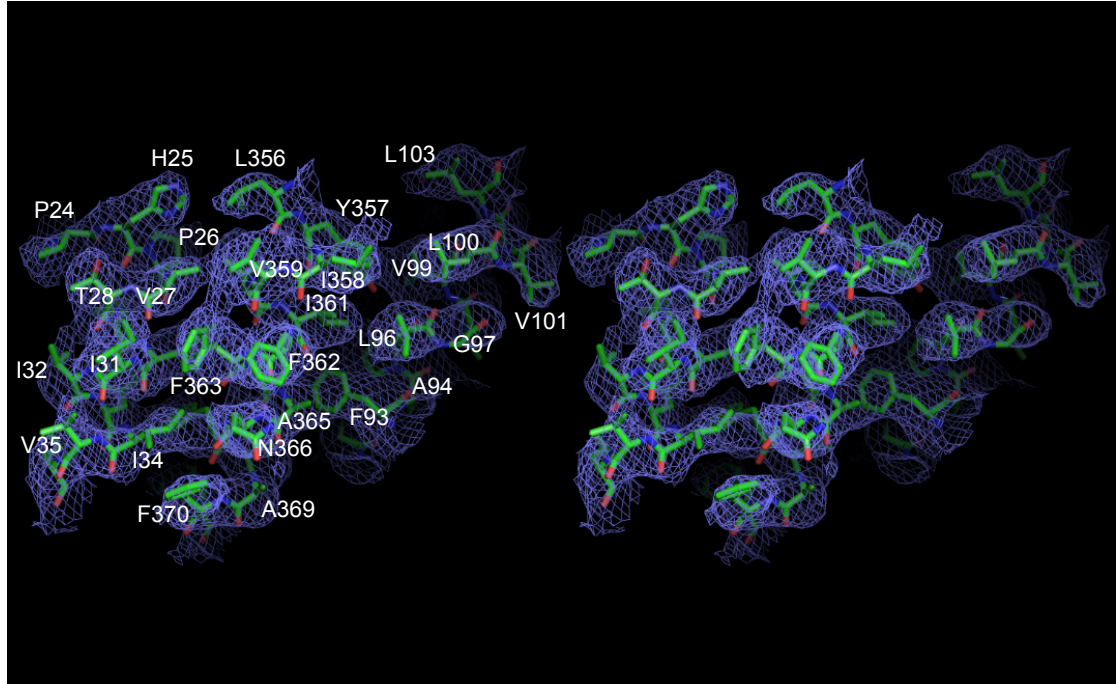


Fig. S2. Stereo view of the electron density maps of MtrF at a resolution of 3.95 Å. (a) The electron density maps are contoured at 1.2 σ . The C α traces of the MtrF dimer in the asymmetric unit are included. Anomalous signals of the four Ta₆Br₁₂²⁺ cluster sites (contoured at 4 σ) found in the asymmetric unit are colored red. (b) Representative section of the electron density at the interface of TM1 and TM7 of MtrF. The electron density (colored slate) is contoured at the 1.2 σ level and superimposed with the final refined model (green, carbon; red, oxygen; blue, nitrogen).



Fig. S3. Expression level of the MtrF pumps. An immunoblot against MtrF of crude extracts from 50 μ g dry cells of strain BL21(DE3) Δ *abgT* Δ *pabA* expressing the MtrF wild-type and mutant (D193A, S417A, W420A, P438A, R446A, D449A, and P457A) pumps are shown.

Table S1. Data collection, phasing and structural refinement statistics of MtrF.

Data set	MtrF	Ta ₆ Br ₁₂ ²⁺ derivative
Data Collection		
Wavelength (Å)	0.98	1.25
Space group	<i>P6₅</i>	<i>P6₅</i>
Resolution (Å)	50 – 3.95 (4.11 – 3.95)	50 – 6.53 (6.74 – 6.53)
Cell constants (Å)		
a	120.77	120.57
b	120.77	120.57
c	233.90	231.33
α, β, γ (°)	90, 90, 120	90, 90, 120
Molecules in ASU	2	2
Redundancy	4.7 (4.0)	5.7 (5.8)
Total reflections	868,348	28,1275
Unique reflections	16,832	3814
Completeness (%)	98.2 (92.8)	99.9 (99.9)
R _{merge} (%)	5.8 (46.8)	5.3 (49.5)
I / σ	29.65 (0.88)	45.42 (2.6)
Phasing		
Number of sites		4
Phasing power (acentric/centric)		1.31/0.67
Figure of merit		0.52 (0.40)
Refinement		
Resolution (Å)	50 – 3.95	
R _{work} (%)	29.9	
R _{free} (%)	33.5	
RMSD bond lengths (Å)	0.009	
RMSD bond angles (°)	1.52	
Ramachandran plot		
most favoured (%)	88.2	
additional allowed (%)	10.8	
generously allowed (%)	1.0	
disallowed (%)	0.0	

Table S2. Primers for site-directed mutagenesis.

Primer	Sequence
D193A-forward	5'-CTGTTCTGGGCACCATTTGCTCCGCTGCTGGCCGGTATC-3'
D193A-reverse	5'-GATACCGGCCAGCAGCGGAGCAATGGTGCCAGGAACAG-3'
S417A-forward	5'-GGTAGTGCTGCCGCACAATGGGCAGTGACCGCACCGATCT-3'
S417A-reverse	5'-CCATTGTGCGGCAGCACTACCGATCATCAGGTTAATAAA-3'
W420A-forward	5'-CGCACAAGCGGCAGTGACCGCACCGATCTTCGTTCCG-3'
W420A-reverse	5'-GGTCACTGCCGCTTGTGCGGAAGCACTACCGATCATCAG-3'
P438A-forward	5'-GGCTATGCTGCGGAAGTCATTCAGGCCGCATACCGC-3'
P438A-reverse	5'-GACTTCCGCAGCATAGCCTGCCAGCATCAGCATCGG-3'
R446A-forward	5'-GTCATTCAGGCCGCATACGCCATCGGTGATTCAGTTACC-3'
R446A-reverse	5'-GGTAACTGAATCACCGATGGCGTATGCGGCCTGAATGAC-3'
D449A-forward	5'-GCCGCATACCGCATCGGTGCTTCAGTTACCAATATTATC-3'
D449A-reverse	5'-GATAATATTGGTAACTGAAGCACCGATGCGGTATGCGGC-3'
P457A-forward	5'-ATCACGGCGATGATGTCGTATTTTGGTCTGATTATG-3'
P457A-reverse	5'-CGACATCATCGCCGTGATAATATTGGTAACTGAATC-3'

Table S3. MICs of sulfamethazine and sulfanilamide for different MtrF variants expressed in *E. coli* BL21(DE3) Δ *abgT* Δ *pabA*.

Gene in BL21(DE3) Δ <i>abgT</i> Δ <i>pabA</i>	Sulfamethazine (μ g/mL)	Sulfanilamide (μ g/mL)
Empty vector	62.5	500
<i>mtrF</i> (wild-type)	2000	4000
<i>mtrF</i> (D193A)	1000	2000
<i>mtrF</i> (S417A)	125	2000
<i>mtrF</i> (W420A)	125	2000
<i>mtrF</i> (P438A)	62.5	1000
<i>mtrF</i> (R446A)	1000	2000
<i>mtrF</i> (D449A)	62.5	1000
<i>mtrF</i> (P457A)	62.5	1000

CHAPTER 6

**YDAH IS AN EFFLUX PUMP THAT MEDIATES RESISTANCE TO SULFONAMIDE
ANTIMETABOLITES**

Manuscript submitted to the journal Nature Communications

**Jani Reddy Bolla^{1,¶}, Chih-Chia Su^{2,¶}, Jared A. Delmar², Abhijith Radhakrishnan¹, Nitin
Kumar¹, Tsung-Han Chou², Kanagalaghatta R. Rajashankar³, and Edward W. Yu^{1,2*}**

¹Department of Chemistry, Iowa State University, Ames, IA 50011.

²Department of Physics and Astronomy, Iowa State University, Ames, IA 50011.

³NE-CAT and Department of Chemistry and Chemical Biology, Cornell University, Bldg. 436E,
Argonne National Laboratory, 9700 S. Cass Avenue, Argonne. IL 60439.

¶J.R.B. and C.S. contributed equally to this work.

* To whom correspondence should be addressed. E-mail: ewyu@iastate.edu

The potential of the folic acid biosynthesis pathway as a target for the development of antibiotics has been corroborated by the clinical use of several drugs. However, many pathogens have developed resistance to these antibiotics, prompting a reevaluation of potential drug targets in the pathway. The gene *ydaH* of *Alcanivorax borkumensis* encodes an integral membrane protein of the AbgT family of transporters. Approximately 13,000 putative transporters of the family have been identified. However, no structural information has been made available and even functional data are fairly minimal for this family of membrane proteins. Here, we report the crystal structure of *A. borkumensis* YdaH at a resolution of 2.96 Å, revealing a dimeric molecule with architecture distinct from all other families of transporters. YdaH is a bowl-shaped dimer with a solvent-filled basin extending from the cytoplasm to halfway across the membrane bilayer. Each subunit of the transporter contains nine transmembrane helices and two hairpins. The structure directly suggests a plausible pathway for substrate transport. A combination of the crystal structure, genetic analysis and substrate accumulation assay indicates that YdaH is an exporter, capable of removing the folate metabolite *p*-aminobenzoic acid from bacterial cells. Further experimental data based on drug susceptibility and radioactive transport assay suggest that YdaH is an antibiotic efflux pump, which mediates bacterial resistance to sulfonamide antimetabolite drugs. The AbgT-family transporters may be important targets for the rational design of novel antibiotics to combat bacterial infections.

All cells, both prokaryotic and eukaryotic, require folic acid for the biosynthesis of a diverse range of cellular components. Folic acid is of particular importance in aiding cell growth

and division. While the cellular requirement for folates is universal, methods to acquire them vary between prokaryotes and eukaryotes. For example, mammals cannot make folates themselves. Instead, they rely on active transport systems, utilizing membrane-associated folate transport proteins to import this essential vitamin¹. In plants and most microorganisms, folates must be synthesized *de novo* through the folate biosynthetic pathway². Because of the presence of this pathway in pathogenic bacteria and, most importantly, its absence in mammals, the folate biosynthetic pathway has been an attractive target for the design of novel antimicrobial drugs.

The process of *de novo* synthesis of folates in bacteria can be simply interpreted as chemically linking pterin, *p*-aminobenzoic acid (PABA) and glutamic acid together. In *Escherichia coli*, mutations or deletions of enzymes in the folate pathway are known to generate non-viable phenotypes³. The possibility of targeting the folate biosynthesis system for antimicrobial therapeutics was proposed several decades ago based on the observation that sulfonamides prevented bacteria from using the metabolite PABA for folate biosynthesis⁴. Indeed, as early as the 1930s, sulfonamides were widely used as synthetic antibiotics to treat infections caused by a variety of pathogenic bacteria, including *Neisseria meningitidis* and *Pneumococcal pneumonia*^{5,6}.

Because of the rapid adaption of bacterial pathogens to antimicrobials, drug resistance to currently administered antibiotics is a serious problem that is rising at an alarming rate. For instance, it only took two years for *N. meningitidis* to develop resistant strains following the introduction of sulfonamides⁷. The problem is of particular severity in treating the parasitic malaria disease. A strong correlation has been found between mutations in *Plasmodium falciparum* and resistance to sulfonamides⁸⁻¹⁰.

The initial identification of enzymes involved in folate biosynthesis was largely carried out in the 1960-70s, leading to the detailed description of this enzymatic pathway¹¹⁻¹⁶. However, recent work demonstrated that *E. coli* AbgT^{17,18} is capable of catalyzing the uptake of the catabolite *p*-aminobenzoyl-glutamate for *de novo* folic acid synthesis¹⁸. Because of this finding, it is hypothesized that AbgT-family transporters¹⁹ contribute to the bacterial folate synthesis pathway by importing *p*-aminobenzoyl-glutamate for producing this essential vitamin. On the other hand, it has been observed that *N. gonorrhoeae* MtrF^{20,21}, also belonging to the AbgT family, functions as an antimicrobial resistant protein. It is needed for the high-level resistance of gonococci to hydrophobic antimicrobials^{20,21}. To date, approximately 13,000 putative transporters of the AbgT family have been identified. However, among proteins in this diverse family, only *E. coli* AbgT^{17,18} and *N. gonorrhoeae* MtrF^{20,21} have been partially characterized. Thus far, there is no structural information available for this family of membrane proteins.

In *A. borkumensis*, the gene *ydaH*²² encodes a membrane protein YdaH of previously unknown structure and function. Alignment of protein sequences suggests that this protein belongs to the AbgT family of transporters¹⁹. To understand how members of the AbgT family work, we here present the crystal structure of YdaH, revealing a novel topology distinct from other families of transporters.

In this paper, we also show that YdaH is capable of exporting the folate metabolite PABA from the bacterial cell. A combination of the three-dimensional structure and genetic analysis allows us to identify important residues for the function of this membrane protein. Our data demonstrate that *A. borkumensis* YdaH is an antibiotic efflux pump, which is able to remove sulfonamides from the cell and mediate bacterial resistance to this class of antimetabolites.

A. borkumensis YdaH consists of 492 amino acids, sharing 34% sequence identity with *E. coli* AbgT (Fig. S1). The crystal structure of YdaH was determined to a resolution of 2.96 Å (Fig. 1 and Table S1). Four molecules of YdaH were found in the asymmetric unit, forming two independent assembled dimers (Fig. S2). Superimposition of these two dimers gives an RMSD of 0.8 Å (942 C α atoms), suggesting that their conformations are nearly identical to each other. The topology of YdaH is unique among all known transporters (Fig. 1a). The YdaH dimer is bowl-shaped with a concave aqueous basin facing the intracellular solution. Viewed in parallel to the membrane, the dimer is about 60 Å tall, 80 Å wide and 60 Å thick, with the transmembrane portion of the transporter lying approximately in the middle (Fig. 1b). Thus, the transporter protrudes about 10 Å from each side of the membrane. The rim of the basin is as large as 50 Å. The bowl-shaped structure is 20 Å in depth and deeply penetrates into the inner leaflet of the cytoplasmic membrane. This basin probably allows aqueous solution to reach the midpoint of the membrane bilayer.

Each protomer of YdaH in the dimer contains nine transmembrane helices (TMs 1-9 and TMs 1'-9', respectively) and two helical hairpins (HPs 1-2 and HPs 1'-2', respectively) (Figs. 1a and S1). The TMs and HPs are designated numerically from the N- to C-termini: TM1 (21-42), TM2 (a (63-79), b (83-99) and c (101-112)), HP1 (a (115-131) and b (135-151)), TM3 (a (155-168) and b (178-194)), TM4 (204-228), TM5 (250-272), TM6 (290-314), TM7 (a (320-334), b (336-354) and c (356-371)), HP2 (a (375-392) and b (396-414)), TM8 (a (418-432) and b (441-452)) and TM9 (458-486). Of the nine TMs, four (TM2, TM3, TM7 and TM8) are broken into segments within the membrane. In addition, the helices making up HPs 1 and 2 are relatively short and can only span a portion of the inner membrane. Interestingly, the intramembrane loops

of several of these TMs and HPs are right next to one another, allowing the protein to form an internal cavity within the membrane (Fig. 1c and d).

The YdaH protomer also possesses a relatively small periplasmic domain formed by two loops, between TM1 and TM2 and between TM5 and TM6, respectively. The loop between TM1 and TM2 is found to form two β -strands (S1 and S2), which appears to run anti-parallel against one another. In the cytoplasmic region, there is a relatively long loop of 22 residues. This loop connects TM4 and TM5, forming a small cytoplasmic domain of the protomer.

The structure of the YdaH protomer can be roughly divided into two cores (Fig. 2a). The outer core contains TMs 1, 2, 5, 6 and 7, whereas the inner core comprises TMs 3, 4, 8, 9 as well as HPs 1 and 2. Viewed along the membrane normal, TMs 2a, 2b, 7a and 7b as well as the N-terminal ends of TMs 1 and 6 form a distinct dimerization domain of the transporter. In particular, TM2a (as well as TM2a') crosses over to the next subunit, securing the formation of this dimer. Each YdaH protomer shares a substantial intersubunit interface, with a volume of $\sim 10,000 \text{ \AA}^3$ per protomer. The residues lining the dimerization motif are predominantly hydrophobic in nature.

While the outer core of YdaH creates a frame-like architecture, the inner core of each protomer forms a cylindrical structure (Fig. 2a). It is most likely that this inner core cylinder forms a substrate-binding site and transport pathway. Interestingly, we found that the inner core cylinder indeed forms a channel spanning approximately from the middle of the inner membrane up to the periplasmic space (Fig. 2b). The entrance of this channel is formed by the internal cavity located at the basin of the bowl-shaped structure (Fig. 1c and d). This cavity constitutes the loop regions of HP1, HP2, TM3 and TM8 and is accessible to the cytoplasm. Based on its

location, this internal cavity may form a substrate-binding site of YdaH. Several conserved residues, including D180, W400, P418 and R426, line the wall of the channel (Fig. 2b). These residues are expected to play an important role in the function of this transporter.

In each protomer of YdaH, a strong spherical electron density sits in the flexible loops between HP2 and TM8. Because Na⁺ ions were used at all stages of purification and crystallization, it is possible that the extra electron density originates from a Na⁺ ion. We then used valence calculations²³ to predict if this location can form a metal ion-binding site. The results indicated that this site is most likely Na⁺-specific. Coordinating with this bound Na⁺ ion are the side chains of N390, D429, N433 and the backbone carbonyl oxygens of G394 and D429 (Fig. 2c). A water molecule also participates in the interaction, forming another coordinate bond with the Na⁺ ion.

As *E. coli* AbgT has been shown to enable uptake of the folate catabolite *p*-aminobenzoyl-glutamate, we investigated if cells expressing YdaH are able to grow on *p*-aminobenzoyl-glutamate. We made an *E. coli* knockout strain BL21(DE3) Δ *abgT* Δ *pabA* that lacked both the *E. coli* *abgT*^{17,18} and *pabA*²⁴ genes. We then expressed the YdaH transporter in this double knockout strain using the plasmid pET15b Ω *ydaH*. Surprisingly, the double knockout BL21(DE3) Δ *abgT* Δ *pabA* cells, either transformed with pET15b Ω *ydaH* or the empty vector pET15b, could not grow in liquid minimal medium (containing 90.4 mM Na₂HPO₄, 22.0 mM KH₂PO₄, 8.5 mM NaCl, 0.1 mM CaCl₂, 1.0 mM MgSO₄, 20.0 mM NH₄Cl, and 22.2 glucose) supplemented with *p*-aminobenzoyl-glutamate up to 1 μ M. Instead, these cells were able to grow in liquid minimal medium when supplemented with 30 nM of the folate metabolite PABA. It should be noted that PABA is capable of diffusing into bacterial cells and participating as an intermediate in the synthesis of the essential folic acid.

We thought that YdaH probably could not import *p*-aminobenzoyl-glutamate as a nutrient for growth. However, this membrane protein may facilitate the transport of PABA across the membrane. Thus, we directly measured the accumulation of PABA in BL21(DE3) Δ *abgT* Δ *pabA* expressing YdaH. We compared the radioactive PABA content over time in cells transformed with either pET15b Ω *ydaH*, encoding *A. borkumensis ydaH*, or the empty vector pET15b. Surprisingly, cells expressing YdaH show a significant decrease in the level of [³H]-PABA when compared with cells transformed with the empty pET15b vector (Fig. 3a) suggesting that YdaH may act as an efflux pump to export PABA from the cell.

To determine whether the conserved YdaH residues D180, W400, P418 and R426 (lining the inner wall of the tunnel formed by each protomer) are important for the function of the transporter, we mutated these residues into alanines, individually (Table S2). Based on the crystal structure, we found that residues N390, D429, N433 are involved in coordinating the bound Na⁺ ion. Therefore, these three residues were also replaced by alanines, respectively (Table S2). We then expressed these mutant transporters in BL21(DE3) Δ *abgT* Δ *pabA*. Western analysis indicated that the expression levels of these mutant transporters were comparable with that of wild-type YdaH (Fig. S3). We then measured the accumulation of [³H]-PABA in cells expressing these mutant transporters. The results showed a significant increase in the levels of [³H]-PABA accumulation in cells possessing the mutant transporter D180A, N390A, W400A, P418A, D429A or N433A, when compared with cells expressing wild-type YdaH (Fig. 3b). However, cells expressing R426A indicated a significant decrease in the [³H]-PABA concentration when compared with cells carrying wild-type YdaH (Fig. 3b). The data strongly suggest that YdaH is an efflux pump and these amino acids are important for the function of the pump.

We hypothesized that YdaH is capable of catalyzing the efflux of PABA and related compounds. If this is the case, then cells expressing YdaH may contain a lower level of folic acid content. Therefore, we decided to measure the intracellular folic acid concentration microbiologically using *Lactobacillus casei*²⁵. Cells transformed with pET15b Ω ydaH or pET15b were grown in liquid minimal medium supplemented with 30 nM PABA and harvested when the optical density (OD_{600 nm}) reached 0.5. Cells were then assayed to obtain their folic acid concentrations. Consistent with the results from PABA accumulation, the folic acid concentration in cells expressing YdaH was markedly reduced in comparison with cells transformed with the empty vector (Fig. 4). The data strongly support the idea that YdaH acts as an efflux pump and participates in exporting PABA from the cell.

When transformed with plasmids expressing the mutant transporters D180A, N390A, W400A, P418A, D429A and N433A, folic acid production was significantly increased in these cells. However, the level of intracellular folic acid concentration in cells expressing R426A was nearly identical to that of the double knockout strain carrying wild-type YdaH (Fig. 4).

As PABA is an important precursor for producing essential folic acid in bacteria, we did not understand why the function of YdaH appeared to lower the intracellular PABA concentration. Clearly, there was a significant reduction in PABA content, which led to the decrease in intracellular folic acid concentration in cells expressing the YdaH transporter. We hypothesized that this efflux pump may protect bacterial cells by extruding antimetabolites, such as sulfonamides. Sulfonamides are antimicrobial agents, antimetabolites or growth factor analogs, which specifically inhibit the essential folic acid metabolic pathway in bacterial pathogens. At the chemical level, sulfonamides are structurally similar to PABA, making them

ideal competitive inhibitors. Therefore, *A. borkumensis* YdaH may act as a drug efflux pump, capable of extruding sulfonamide antimetabolites.

To determine if *A. borkumensis* YdaH behaves as a sulfonamide efflux pump, we transformed BL21(DE3) $\Delta abgT\Delta pabA$ with pET15b $\Omega ydaH$ or pET15b and tested the susceptibility of these transformants to two different sulfonamide drugs (Table S3). Specifically, sulfamethazine was chosen because of the availability of its radioactive analog. We found that the BL21(DE3) $\Delta abgT\Delta pabA$ cells expressing *A. borkumensis* YdaH were 32-fold less sensitive to sulfamethazine when compared with BL21(DE3) $\Delta abgT\Delta pabA$ cells containing the empty pET15b vector. In addition, these BL21(DE3) $\Delta abgT\Delta pabA$ /pET15b $\Omega ydaH$ cells were eight times more resistant to sulfanilamide when compared with the double knockout cells transformed with the empty pET15b vector. These data indeed show that YdaH functions as a drug efflux pump, which confers resistance to sulfonamides.

Mutant transporters D180A, N390, W400A, P418A, R426A, D429A and N433A expressed in BL21(DE3) $\Delta abgT\Delta pabA$ were then tested for their ability to confer sulfamethazine and sulfanilamide resistance. We found that strain BL21(DE3) $\Delta abgT\Delta pabA$ carrying these YdaH mutants were more sensitive to sulfamethazine and sulfanilamide in comparison with cells expressing wild-type YdaH (Table S3), thus agreeing well with the idea that these residues are essential for the function of *A. borkumensis* YdaH.

To support the drug susceptibility testing results, we measured the accumulation of radioactive sulfamethazine in BL21(DE3) $\Delta abgT\Delta pabA$ cells that carried pET15b $\Omega ydaH$ or pET15b. For these experiments, we compared the accumulation of sulfamethazine over time in these cells. As shown in Fig. 5, the results indicated a lower level of [^3H]-sulfamethazine accumulation in BL21(DE3) $\Delta abgT\Delta pabA$ cells producing *A. borkumensis* YdaH compared to

controlled cells harboring the empty pET15b vector, suggesting that *A. borkumensis* YdaH is capable of exporting sulfamethazine from the cell.

When transformed with plasmids expressing the mutant transporters D180A, N390A, W400A, P418A, R426A, D429A and N433A, the levels of intracellular sulfamethazine accumulation were much higher than that of cells expressing wild-type YdaH (Fig. 5). Again, these data indicate that residues D180, N390, W400, P418, R426, D429 and N433 are critical for the function of the *A. borkumensis* YdaH efflux pump.

It has been suggested that members of the AbgT family use the proton-motive-force (PMF) to transport substrates across the membrane¹⁹. To determine which source of energy *A. borkumensis* YdaH utilizes to export substrates, we measured the level of intracellular sulfamethazine accumulation in the presence of carbonyl cyanide *m*-chlorophenylhydrazone (CCCP), an uncoupler of the membrane proton gradient. After the addition of CCCP into the assay solution, the accumulation of [³H]-sulfamethazine increased drastically in the YdaH-expressing cells (Fig. 6a), suggesting that the uncoupler CCCP was able to inhibit the function of this pump. As the crystal structure suggests that a Na⁺ ion is bound within each subunit of the YdaH transporter, we then investigated the accumulation level of radioactive sulfamethazine in strain BL21(DE3) Δ *abgT* Δ *pabA*/pET15b Ω *ydaH* in the presence of 5 or 100 mM NaCl. In both cases, the levels of accumulation of [³H]-sulfamethazine were significantly lower compared with that in the YdaH-producing strain without the addition of Na⁺ ions (Fig. 6a). The results strongly indicate that the function of *A. borkumensis* YdaH is Na⁺-ion dependent.

To confirm that YdaH is a Na⁺-ion dependent efflux pump, we next measured the efflux of radioactive sulfamethazine that had accumulated in strain BL21(DE3) Δ *abgT* Δ *pabA*/pET15b Ω *ydaH*, both in the absence and presence of Na⁺ or K⁺.

Cells were first loaded with [^3H]-sulfamethazine and CCCP was added to inhibit the pump. Thereafter, CCCP was removed and glucose was added to re-energize these cells. Cellular [^3H]-sulfamethazine levels were measured over time both in the absence and presence of 5 mM NaCl or KCl. As shown in Fig. 6b, the addition of Na^+ , but not K^+ , has a strong effect on sulfamethazine efflux in BL21(DE3) $\Delta abgT\Delta pabA$ /pET15b $\Omega ydaH$, confirming that *A. borkumensis* YdaH is a Na^+ -dependent efflux pump.

In this paper, we reported the crystal structure of the *A. borkumensis* YdaH transporter, which reveals a dimeric molecule with a fold very distinct from other families of transporters. Based on our experimental data, we propose that YdaH is a drug efflux pump, capable of removing sulfonamide antimetabolites and mediating resistance to this class of drugs in bacterial cells. It is likely that many members of the AbgT family of transporters may serve as antimetabolite efflux pumps to protect cells against these noxious agents. Our data also suggest a novel mechanism for sulfonamide antimetabolite resistance in bacteria.

Accession code

Atomic coordinates and structure factors for the structure of YdaH have been deposited at the RCSB Protein Data Bank with an accession code 4R0C.

Acknowledgements

This work was supported by an NIH Grant R01GM086431 (E.W.Y.). This work is based upon research conducted at the Northeastern Collaborative Access Team beamlines of the Advanced Photon Source, supported by an award GM103403 from the National Institutes of General Medical Sciences. Use of the Advanced Photon Source is supported by the U.S.

Department of Energy, Office of Basic Energy Sciences, under Contract No. DE-AC02-06CH11357. We are grateful to Dr. XiKui Fang at the Ames Laboratory for providing us the $\text{Na}_9[\beta\text{-SiW}_9\text{O}_{34}\text{H}]\cdot 23\text{H}_2\text{O}$ complex used in this study.

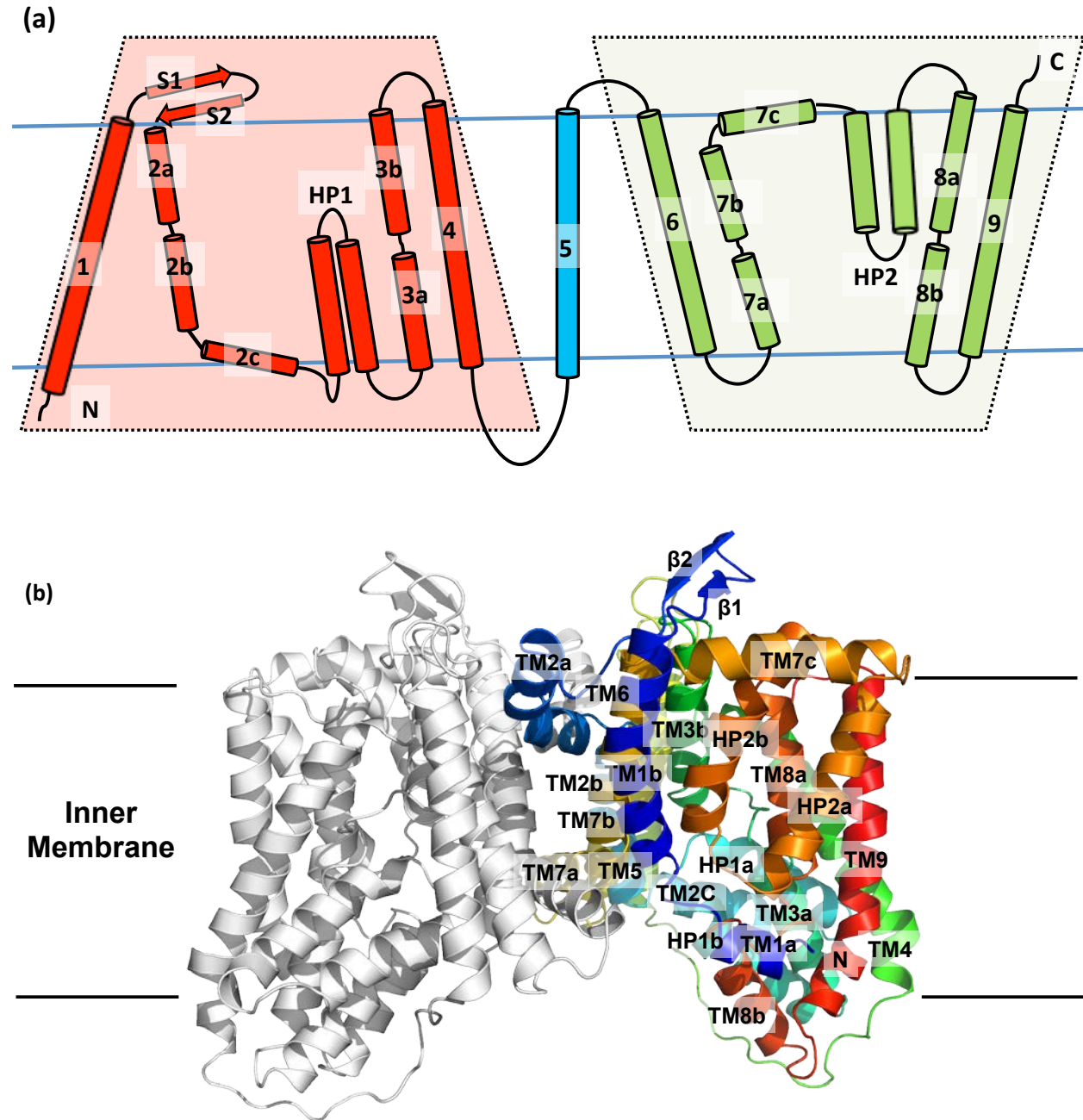
References

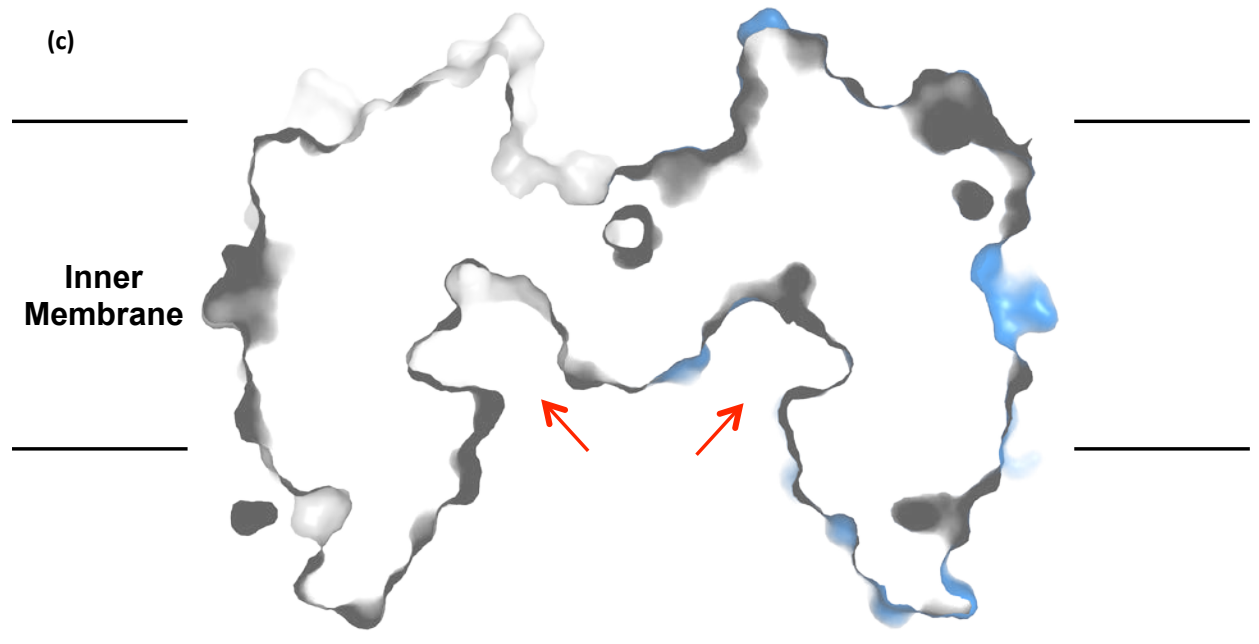
1. G. B. Henderson, G.B. & Huennekens, F.M. Membrane-associated folate transport proteins. *Methods Enzymol.* **122**, 260-269 (1986).
2. Hyde, J.E., Dittrich, S., Wang, P., Sims, P.F.G., de Crécy-Lagard, V. & Hanson, A.D. *Plasmodium falciparum*: a paradigm for alternative folate biosynthesis in diverse microorganisms? *Trends Parasit.* **24**, 502-508 (2008).
3. Pyne, C. & Bognar, A.L. Replacement of the *folC* gene, encoding folylpolyglutamate synthetase-dihydrofolate synthetase in *Escherichia coli*, with genes mutagenized in vitro. *J. Bacteriol.* **174**, 1750-1759 (1992).
4. Woods, D.D. The relationship of *p*-aminobenzoic acid to the mechanism of the action of sulphanilamide. *Br. J. Exp. Pathol.* **21**, 74-90 (1940).
5. Bermingham, A. & Derrick, J.P. The folic acid biosynthesis pathway in bacteria: evaluation of potential for antibacterial drug discovery. *Bioassays* **24**, 637-648 (2002).
6. Singer, M., Nambiar, S., Valappil, T., Higgins, K. & Gitterman, S. Historical and regulatory perspectives on the treatment effect of antibacterial drugs for community-acquired pneumonia. *Clin. Infect. Dis.* **47**, S216-S224 (2008).
7. Cartwright, K.A.V. (ed.) *Meningococcal disease*. (John Wiley & Sons, Chichester, 1995).
8. Wang, P., Read, M., Sims, P.F.G. & Hyde, J.E. Sulfadoxine resistance in the human malaria parasite *Plasmodium falciparum* is determined by mutations in dihydropteroate synthetase and an additional factor associated with folate utilization. *Mol. Microbiol.* **23**, 979-986 (1997).
9. Triglia, T. & Cowman, A.F. Primary structure and expression of the dihydropteroate synthetase gene of *Plasmodium falciparum*. *Proc. Natl. Acad. Sci. USA* **91**, 7149-7153 (1994).
10. Triglia, T., Menting, J.G., Wilson, C. & Cowman, A.F. Mutations in dihydropteroate synthase are responsible for sulfonamide resistance in *Plasmodium falciparum*. *Proc. Natl. Acad. Sci. USA* **94**, 13944-13949 (1997).

11. Brown, G.M., Weisman, R.A. & Molnar, D.A. The biosynthesis of folic acid: I. Substrate and cofactor requirements for enzymatic synthesis by cell-free extracts of *Escherichia coli*. *J. Biol. Chem.* **236**, 2534-2543 (1961).
12. Brown, G.M. The biosynthesis of folic acid: II. Inhibition by sulfonamides. *J. Biol. Chem.* **237**, 536-540 (1962).
13. Reynolds, J.J. & Brown, G.M. The biosynthesis of folic acid. IV. Enzymatic synthesis of dihydrofolic acid from guanine and ribose compounds. *J. Biol. Chem.* **239**, 317-325 (1964).
14. Burg, A.W. & Brown, G.M. The biosynthesis of folic acid VI. Enzymatic conversion of carbon atom 8 of guanosine triphosphate to formic acid. *Biochim. Biophys. Acta* **117**, 275-278 (1966).
15. Richey, D.P. & Brown, G.M. The biosynthesis of folic acid. IX. Purification and properties of the enzymes required for the formation of dihydropterotic acid. *J. Biol. Chem.* **244**, 1582-1592 (1969).
16. Mathis, J.B. & Brown, G.M. The biosynthesis of folic acid. XI. Purification and properties of dihydroneopterin aldolase. *J. Biol. Chem.* **245**, 3015-3025 (1970).
17. Hussein, M.J., Green, J.M. & Nichols, B.P. Characterization of mutations that allow *p*-aminobenzoyl-glutamate utilization by *Escherichia coli*. *J. Bacteriol.* **180**, 6260-6268 (1998).
18. Carter, E.L., Jager, L., Gardner, L., Hall, C.C., Willis, S. & Green, J.M. *Escherichia coli* *abg* genes enable uptake and cleavage of the folate catabolite *p*-aminobenzoyl-glutamate. *J. Bacteriol.* **189**, 3329-3334 (2007).
19. Prakash, S., Cooper, G., Singhi, S. & Saier, M.H., Jr. The ion transporter superfamily. *Biochim. Biophys. Acta* **1618**, 79-92 (2003).
20. Veal, W.L. & Shafer, W.M. Identification of a cell envelope protein (MtrF) involved in hydrophobic antimicrobial resistance in *Neisseria gonorrhoeae*. *J. Antimicrob. Chemother.* **51**, 27-37 (2003).
21. Folster, J.P. & Shafer, W.M. Regulation of *mtrF* expression in *Neisseria gonorrhoeae* and its role in high-level antimicrobial resistance. *J. Bacteriol.* **187**, 3713-3720 (2005).
22. Schneiker, S. et al. Genome sequence of the ubiquitous hydrocarbon degrading marine bacterium *Alcanivorax borkumensis*. *Nature Biotech.* **24**, 997-1004 (2006).
23. Nayal, M. & Di Cera, E. Valence screening of water in protein crystals reveals potential Na⁺ binding sites. *J. Mol. Biol.* **256**, 228-234 (1996).
24. Kaplan, J.B. & Nichols, B.P. Nucleotide sequence of *Escherichia coli* *pabA* and its evolutionary relationship to *trp(G)D*. *J. Mol. Biol.* **168**, 451-468 (1986).

25. Wilson, S.D. & Horne, W.D. Use of glycerol-cryoprotected *Lactobacillus casei* for microbiological assay of folic acid. *Clin. Chem.* **28**, 1198-1200 (1982).

Legends of figures





(d)

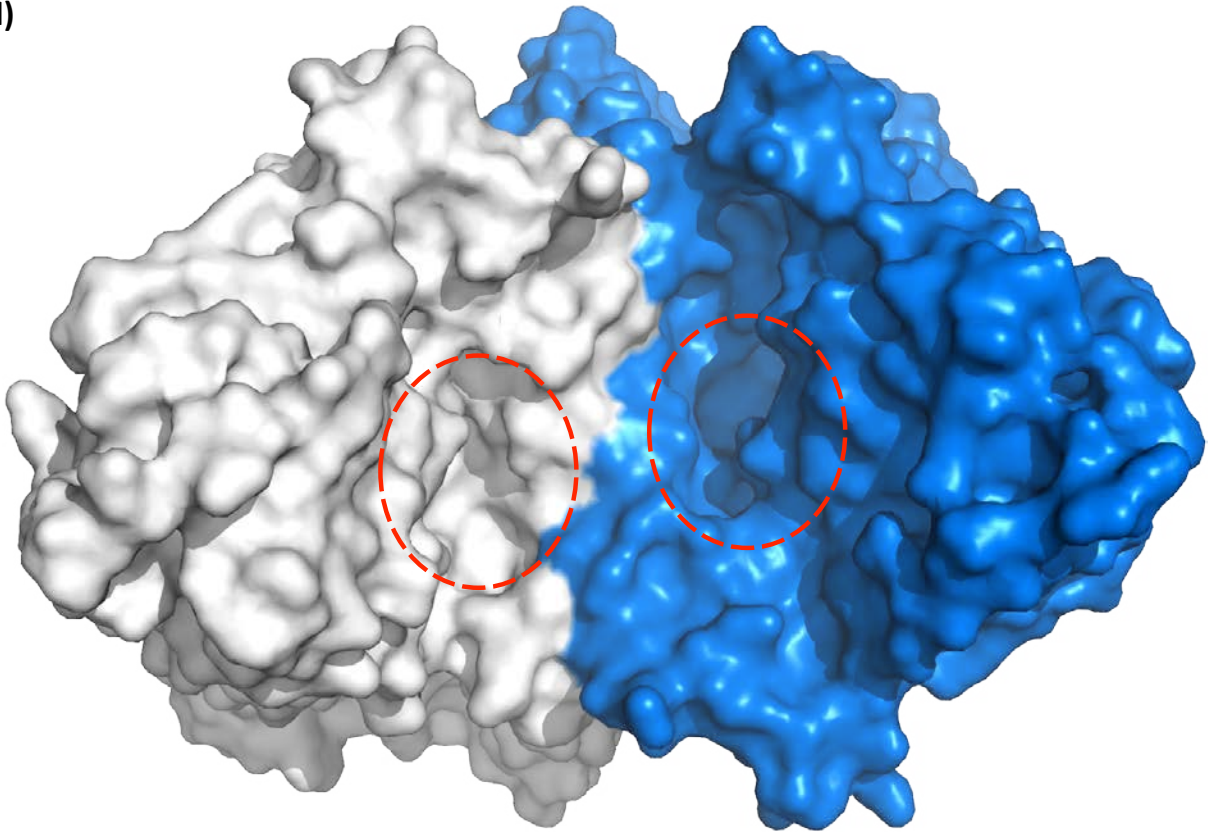
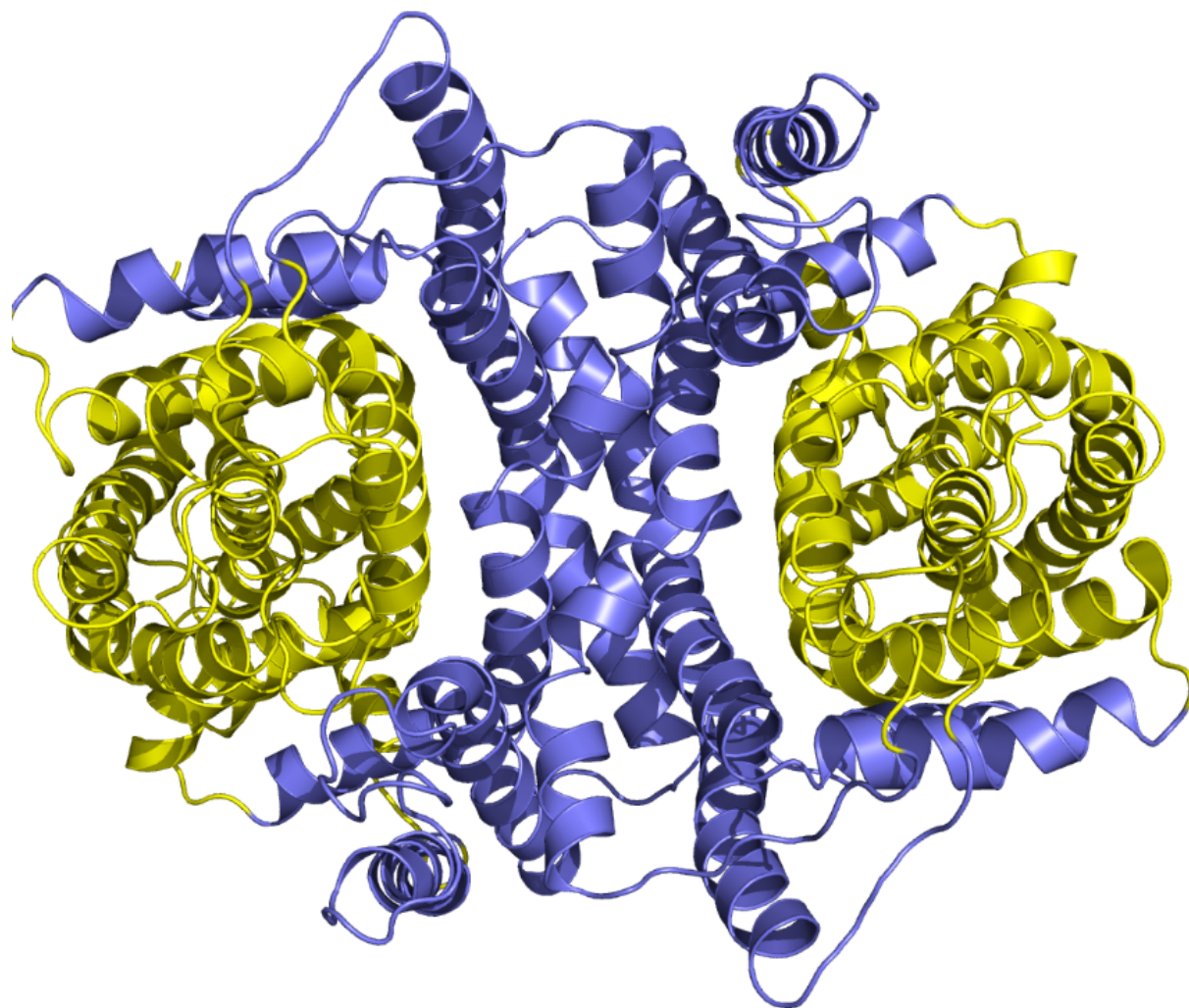


Fig. 1. Structure of the *A. borkumensis* YdaH transporter. (a) Transmembrane topology of *A. borkumensis* YdaH. The transporter contains nine transmembrane helices (TMs) and two hairpins (HPs). (b) Ribbon diagram of a dimer of YdaH viewed in the membrane plane. The right subunit of the dimer is colored using a rainbow gradient from the N-terminus (blue) to the C-terminus (red), whereas the left subunit is colored gray. The YdaH dimer forms a bowl-shaped structure with a concave aqueous basin facing the intracellular solution. (c) Surface representation of the YdaH dimer sliced through the middle of the protein. Each protomer forms an internal cavity (red arrow), which is accessible to the cytoplasm. (d) Bottom view of a surface representation of the YdaH dimer, indicating a solvent accessible cavity (red circle) from each protomer of the protein. The two protomers are colored gray and blue.

(a)

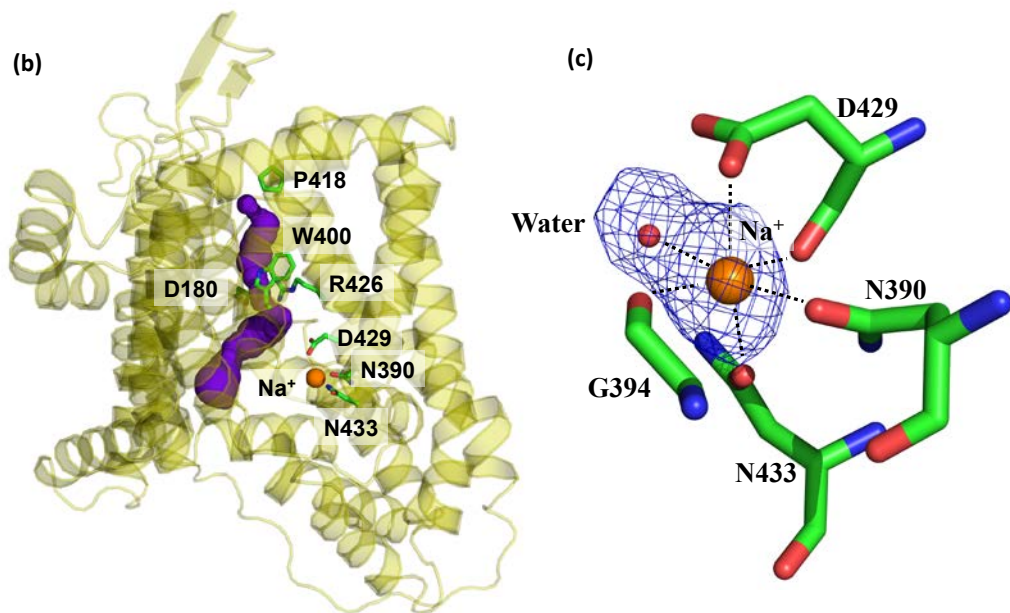
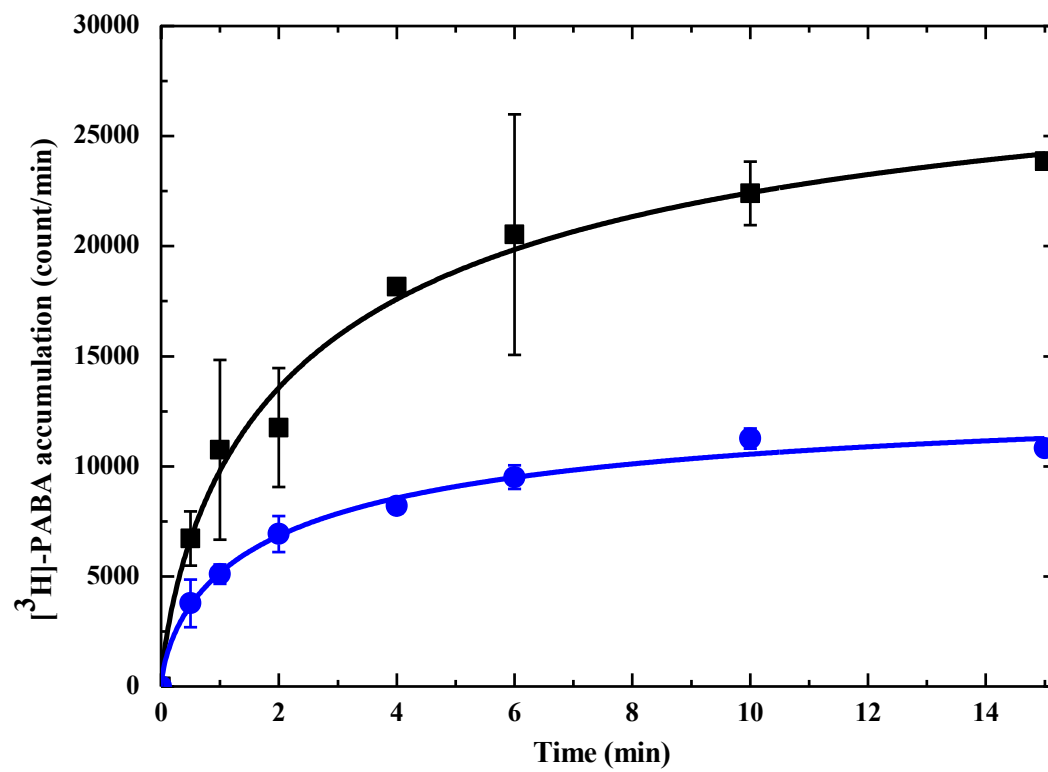


Fig. 2. Outer and inner cores of YdaH. (a) The outer core of YdaH, comprising TMs 1, 2, 5, 6 and 7 (colored slate), contributes to dimerization as well as formation of a frame-like structure housing the inner core of the protomer. The inner core of YdaH is composed of TMs 3, 4, 8, 9 as well as HPs 1 and 2 (colored yellow). (b) The inner core of YdaH forms a channel (colored purple) spanning approximately from the middle of the inner membrane up to the periplasmic space. This channel was calculated using the program CAVER (<http://loschmidt.chemi.muni.cz/caver>). The secondary structural elements of the YdaH protomer are in yellow. Residues D180, N390, W400, P418, R426, D429 and N433 are in green sticks. The bound sodium ion is shown as an orange sphere. (c) The bound Na^+ (orange sphere) is found to coordinate with N390, G394, D429, N433 and a water molecule (red sphere). The F_o-F_c map, showing the bound Na^+ and H_2O , is contoured at 3.0σ (blue mesh).

(a)



(b)

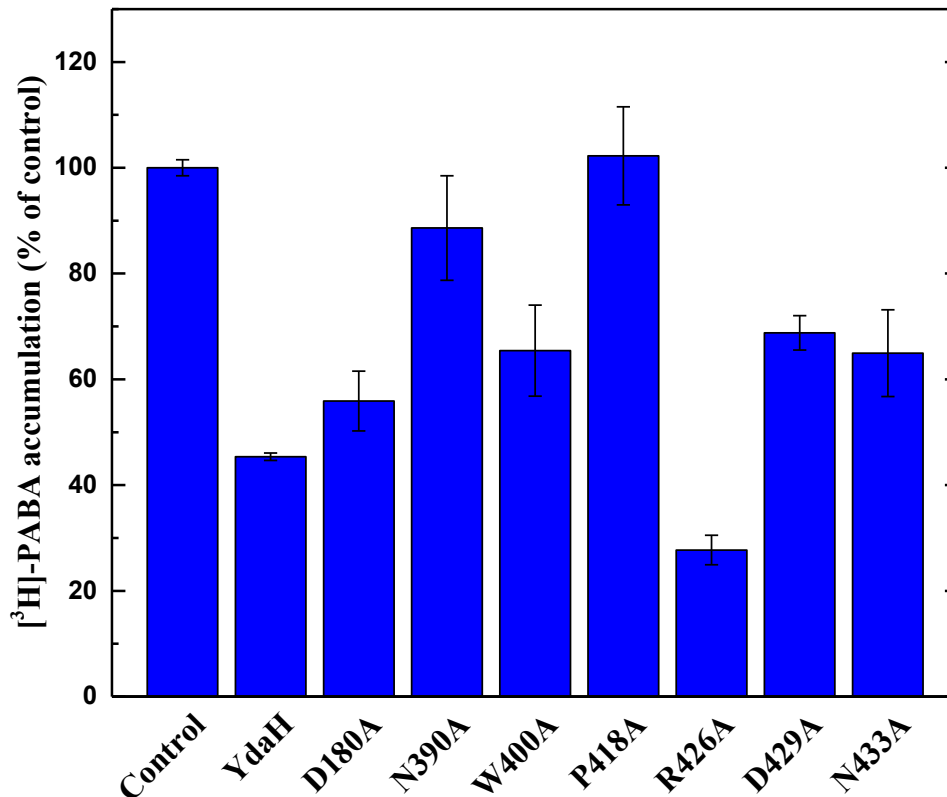


Fig. 3. Accumulation of radioactive *p*-aminobenzoic acid. (a) Time course of [³H]-PABA accumulation by *E. coli* BL21(DE3) Δ *abgT* Δ *pabA* double knockout cells transformed with pET15b Ω *ydaH* or pET15b. Cells expressing *ydaH* (blue curve) show a significant decrease in [³H]-PABA accumulation when compared with cells carrying the empty vector (black curve). (b) Mutants of the YdaH transporter. Cells possessing the mutant transporter D180A, N390, W400A, P418A, D429A and N433A show a significant increase in the level of [³H]-PABA accumulations compared with cells expressing wild-type YdaH. However, cells expressing R426A are able to decrease the [³H]-PABA concentration when compared with cells carrying wild-type YdaH. The data showed in (a) and (b) are the cumulative average of three successive recordings.

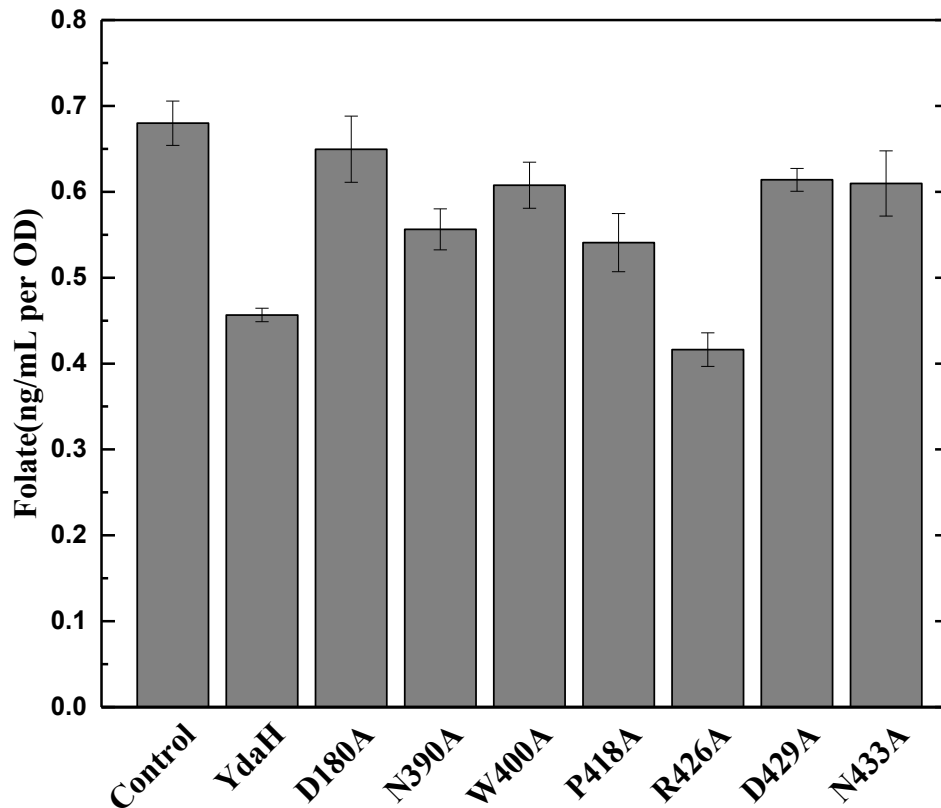


Fig. 4. Intracellular folic acid concentration. Folic acid concentration in *E. coli* BL21(DE3) $\Delta abgT\Delta pabA$ double knockout cells expressing YdaH were markedly reduced in comparison with cells transformed with the empty vector. When transformed with plasmid expressing the mutant transporter, D180A, N390, W400A, P418A, D429A and N433A, folic acid production was significantly increased in these cells. However, the level of intracellular folic acid concentration in BL21(DE3) $\Delta abgT\Delta pabA$ cells expressing R426A was nearly identical to that of the double knockout strain carrying wild-type YdaH. Each bar represents the mean of three separate cultures.

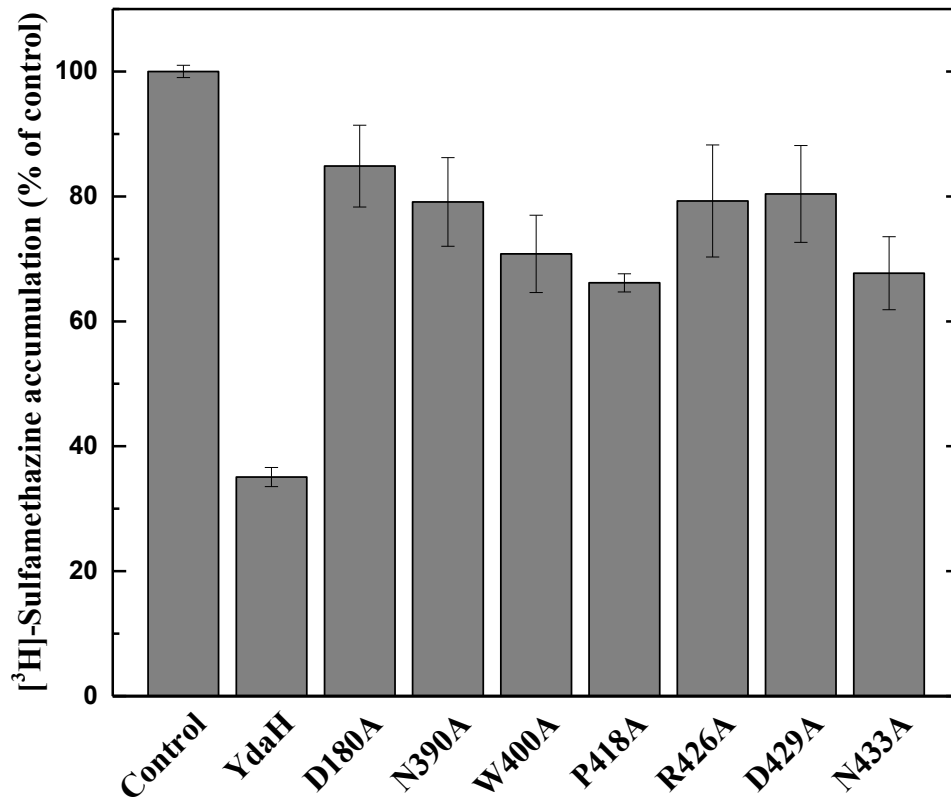
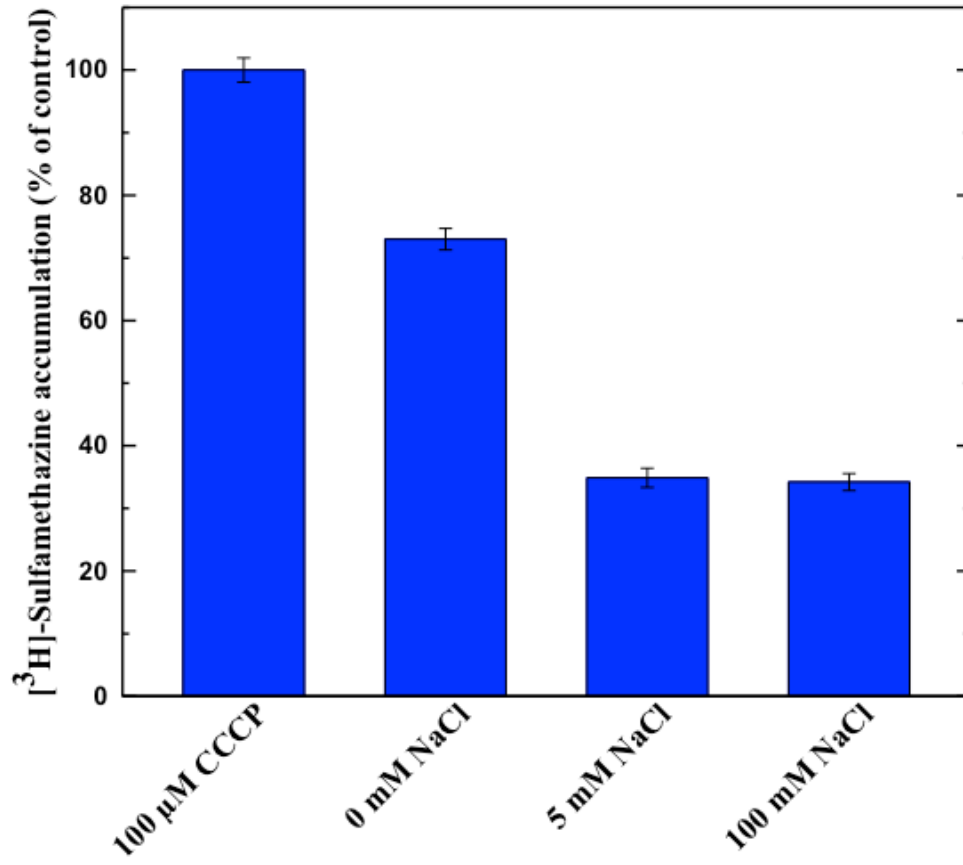


Fig. 5. Accumulation of radioactive sulfamethazine. *E. coli* BL21(DE3) Δ abgT Δ pabA cells expressing YdaH show a significant decrease in [³H]-sulfamethazine accumulation when compared with cells carrying the empty vector. When transformed with plasmids expressing the mutant transporters, D180A, N390, W400A, P418A, R426A, D429A and N433A, the levels of intracellular [³H]-sulfamethazine accumulation were much higher than that of cells expressing wild-type YdaH. Each bar represents the mean of three different cultures.

(a)



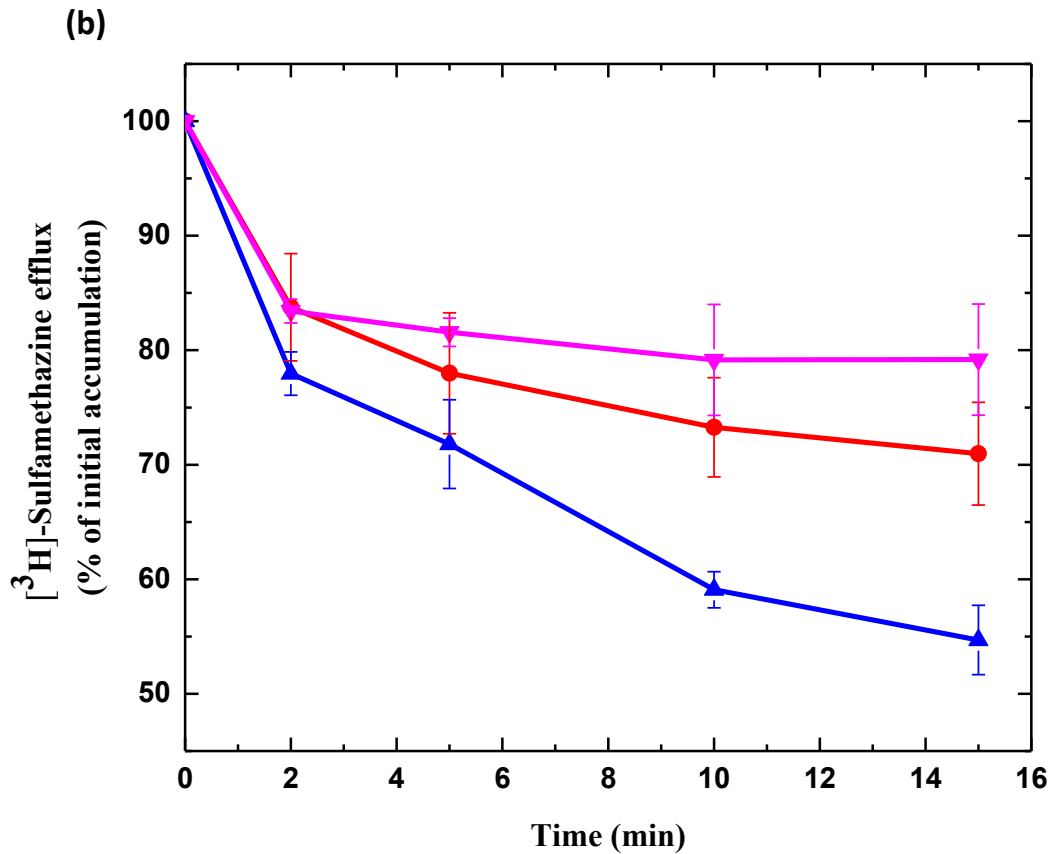


Fig. 6. Sodium ion enhances sulfamethazine efflux via YdaH. (a) Accumulation of radioactive sulfamethazine in BL21(DE3) Δ *abgT* Δ *pabA*/pET15b Ω *ydaH* cells with difference sodium ion concentrations. Cells showed a significant decrease in [3 H]-sulfamethazine accumulation in the presence of Na $^+$. (b) Efflux of radioactive sulfamethazine in BL21(DE3) Δ *abgT* Δ *pabA*/pET15b Ω *ydaH* cells in the presence of sodium or potassium ions. The presence of Na $^+$ significantly enhances [3 H]-sulfamethazine efflux in BL21(DE3) Δ *abgT* Δ *pabA*/pET15b Ω *ydaH* cells (red, 0 mM NaCl; magenta, 5 mM KCl; blue, 5 mM NaCl). The data showed in (a) and (b) are the cumulative average of three successive recordings.

Methods

Cloning, expression and purification of *A. borkumensis* YdaH

Briefly, the full-length YdaH membrane protein containing a 6xHis tag at the N-terminus was overproduced in *E. coli* BL21(DE3) Δ *acrB* cells, which harbors a deletion in the chromosomal *acrB* gene, possessing pET15b Ω *ydaH*. Cells were grown in 12 L of LB medium with 100 μ g/ml ampicillin at 25°C. When the OD₆₀₀ reached 0.5, the culture was treated with 0.2 mM isopropyl- β -D-thiogalactopyranoside (IPTG) to induce *ydaH* expression, and cells were harvested within 15 h. The collected bacteria were resuspended in low salt buffer containing 100 mM sodium phosphate (pH 7.2), 10 % glycerol, 1 mM ethylenediaminetetraacetic acid (EDTA) and 1 mM phenylmethanesulfonyl fluoride (PMSF), and then disrupted with a French pressure cell. The membrane fraction was collected and washed twice with high salt buffer containing 20 mM sodium phosphate (pH 7.2), 2 M KCl, 10 % glycerol, 1 mM EDTA and 1 mM PMSF, and once with 20 mM HEPES-NaOH buffer (pH 7.5) containing 1 mM PMSF as described previously²⁶. The membrane protein was then solubilized in 2% (w/v) n-dodecyl- β -D-maltoside (DDM). Insoluble material was removed by ultracentrifugation at 100,000 x g. The extracted protein was purified with a Ni²⁺-affinity column. The purified protein was dialyzed and concentrated to 20 mg/ml in a buffer containing 20 mM Na-HEPES (pH 7.5) and 0.05% DDM. The 6xHis tag at the N-terminus was then cleaved by adding 5 units of thrombin (GE Healthcare Bio-Sciences, Pittsburgh, PA) per mg of purified YdaH at room temperature for 20 h. The protein was subsequently passed through a Ni²⁺-affinity column to remove the free 6xHis tag. A final purification step was performed using a G200 size exclusion column loaded with buffer solution containing 20 mM Na-HEPES (pH 7.5) and 0.05% DDM. The purity of the YdaH protein (>95%) was judged using 10% SDS-PAGE stained with Coomassie Brilliant Blue. The

purified protein was then concentrated to 20 mg/ml in a buffer containing 20 mM Na-HEPES (pH 7.5) and 0.05% DDM.

For 6xHis selenomethionyl-substituted (SeMet)-YdaH protein expression, a 10 ml LB broth overnight culture containing *E. coli* BL21(DE3) Δ *acrB*/pET15b Ω *ydaH* cells was transferred into 120 ml of LB broth containing 100 μ g/ml ampicillin and grown at 37°C. When the OD₆₀₀ value reached 1.2, cells were harvested by centrifugation at 6000 rev/min for 10 min, and then washed two times with 20 ml of M9 minimal salts solution. The cells were re-suspended in 120 ml of M9 media and then transferred into a 12 L pre-warmed M9 solution containing 100 μ g/ml ampicillin. The cell culture was incubated at 25°C with shaking. When the OD₆₀₀ reached 0.4, 100 mg/l of lysine, phenylalanine and threonine, 50 mg/l isoleucine, leucine and valine, and 60 mg/l of L-selenomethionine were added. The culture was induced with 0.2 mM IPTG after 15 min. Cells were then harvested within 15 h after induction. The procedures for purifying SeMet-YdaH were identical to those of the native protein.

Crystallization of YdaH

Crystals of the YdaH protein were obtained using sitting-drop vapor diffusion. The YdaH crystals were grown at room temperature in 24-well plates with the following procedures. A 2 μ l protein solution containing 20 mg/ml YdaH in 20 mM Na-HEPES (pH 7.5) and 0.05% (w/v) DDM was mixed with a 2 μ l of reservoir solution containing 28% PEG 400, 0.1 M sodium acetate (pH 5.0), 0.05 M magnesium acetate, 3% glycerol and 2% (w/v) n-octyl- β -D-glucoside (OG). The resultant mixture was equilibrated against 500 μ l of the reservoir solution at 25°C. The crystallization conditions for SeMet-YdaH were the same as those for the native YdaH

protein. Crystals of both YdaH and SeMet-YdaH grew to a full size in the drops within a month. Typically, the dimensions of the crystals were 0.2 mm x 0.2 mm x 0.2 mm. Cryoprotection was achieved by raising the PEG 400 concentration to 32% in a single step. Crystals of the tungsten cluster derivative were prepared by incubating the crystals of YdaH in solution containing 32% PEG 400, 0.1 M sodium acetate (pH 5.0), 0.05 M magnesium acetate, 3% glycerol and 2% (w/v) OG, 0.05% (w/v) DDM and 0.5 mM $\text{Na}_9[\beta\text{-SiW}_9\text{O}_{34}\text{H}]\cdot 23\text{H}_2\text{O}$ for 4 hours at 25°C.

Data collection, structural determination and refinement

All diffraction data were collected at 100K at beamline 24ID-C located at the Advanced Photon Source, using a Platus 6M detector. Diffraction data were processed using DENZO and scaled using SCALEPACK²⁷. Crystals of YdaH belonged to space group $P2_1$ (Table S1). Based on the molecular weight of YdaH (51.6 kDa), four molecules per asymmetric unit with a solvent content of 73.4% were expected. The heavy-atom derivative ($[\beta\text{-SiW}_9\text{O}_{34}\text{H}]^{9-}$ cluster)²⁸ was isomorphous with the native crystal (Table S1). Six heavy-atom sites for the tungsten derivative were identified using SHELXC and SHELXD²⁹ as implemented in the HKL2MAP package³⁰. These heavy-atom sites were refined using the program MLPHARE^{31,32}. The resulting phases were subjected to density modification and fourfold NCS averaging by RESOLVE³³ using the native structure factor amplitudes. Density modified phases allowed us to visualize the helical structural features of the molecule. The initial model was built manually using Coot³⁴. The SeMet data was then used to help determine the 4.10 Å-resolution structure of YdaH by molecular replacement with single-wavelength anomalous diffraction using the program Phaser³⁵. The manually built model was used as initial search model. The full-length YdaH protein consists of 11 methionine residues and all of these 11 selenium sites were identified in

each protomer of the protein (44 total selenium sites in the asymmetric unit). These phases were then improved by NCS averaging with density modification using the program RESOLVE³³. The resulting phases were of excellent quality, which enabled us to trace of most of the molecule. After tracing the initial model manually using the program Coot³⁴, the model was refined using PHENIX³⁶ leaving 5% of reflections in Free-R set. Iterations of refinement using PHENIX³⁶ and CNS³⁷ and model building in Coot³⁴ lead to the 4.10 Å-resolution structural model of the YdaH transporter. This structure was then used to refine against the 2.96 Å-resolution data using PHENIX³⁶ as described above. Iterations of refinement using PHENIX³⁶ and CNS³⁷ and model building in Coot³⁴ lead to the current 2.96 Å-resolution model with excellent geometrical characteristics (Table S1).

Construction of the double knockout strain

The double knockout *E. coli* strain BL21(DE3) Δ *abgT* Δ *pabA* was produced from the BL21(DE3) strain using an RED disruption system as described by Datsenko and Wanner³⁸. The Δ *abgT::kan* cassette, which was used to replace the chromosomal *abgT* gene, was produced by PCR, and then introduced into pKD46/BL21(DE3) by electroporation. The knockout BL21(DE3) Δ *abgT::kan* strain was selected on LB plate containing 30 µg/ml kanamycin, and verified by PCR. The kanamycin resistant gene was then released to generate the BL21(DE3) Δ *abgT* knockout strain. The deletion of *pabA* from BL21(DE3) Δ *abgT* was done using similar procedures as described above to generate the final BL21(DE3) Δ *abgT* Δ *pabA* double knockout strain.

Site-directed mutagenesis

Site-directed point mutations on residues D180, N390, W400, P418, R426, D429 and N433, which are expected to be critical for the function of the YdaH efflux pump, were performed to generate the single point mutants D180A, N390A, W400A, P418A, R426A, D429A and N433A. The primers used for these mutations are listed in Table S2. All oligonucleotides were purchased from (Integrated DNA Technologies, Inc., Coralville, IA) in a salt-free grade.

Accumulation assays of *p*-aminobenzoic acid

In brief, *E. coli* BL21(DE3) Δ *abgT* Δ *pabA* carrying pET15b Ω *ydaH* or pET15b were grown in LB broth with 100 μ g/ml ampicillin at 37°C. When the OD₆₀₀ reached 0.5, the culture was treated with 0.2 mM IPTG to induce *ydaH* expression, and cells were harvested within 2 h. Cells were washed twice with buffer containing 50 mM potassium phosphate (pH 7.5), twice with buffer containing 100 mM Tris-HCl (pH 7.5) and 5 mM NaCl, and then suspended in the same buffer to OD₆₀₀ of 15. [³H]-PABA (Moravек Biochemicals, Brea, CA) was then added to a final concentration of 0.3 μ M. Samples of 100 μ l were taken at intervals, applied directly to prewetted glass-fiber filters, and washed twice with 5-ml aliquots of the same buffer; 0.5- μ m glass-fiber filters (MFS, Dubbin, CA) were used with a filter apparatus. Filters were then incubated for 30 min in scintillation fluid (ScintiVerse™ BD) and counted with a Packard Tri-Carb 1600TR liquid scintillation counter (Perkin Elmer, Waltham, MA).

For [³H]-PABA accumulations in cells expressing the YdaH mutants, the procedures for sample preparation were the same as above. Cells were incubated with 0.3 μ M [³H]-PABA for 15 min, applied directly to prewetted glass-fiber filters, and washed immediately twice with 5-ml

aliquots of the same buffer. Filters were then incubated for 30 min in scintillation fluid (ScintiVerse™ BD) and counted with a Packard Tri-Carb 1600TR liquid scintillation counter (Perkin Elmer, Waltham, MA).

Assays of folic acid

The concentration of folic acid in the double knockout BL21(DE3) Δ *abgT* Δ *pabA* strain transformed with pET15b Ω *ydaH* or pET15b was measured using *Lactobacillus casei* based on the microbiological procedure of Wilson and Horne²⁵. The concentrations of folic acid in BL21(DE3) Δ *abgT* Δ *pabA* expressing the mutant transporters were measured using the same procedures.

Drug susceptibility assays

The susceptibilities to sulfamethazine and sulfanilamide of *E. coli* BL21(DE3) Δ *abgT* Δ *pabA* harboring pET15b Ω *ydaH* expressing the wild-type or mutant transporters, or the pET15b empty vector were tested on agar plates. Cells were grown in Luria Broth (LB) medium with 100 μ g/ml ampicillin at 37 °C. When the OD₆₀₀ reached 0.5, the cultures were induced with 0.2 mM IPTG and harvested in two hours after induction. The minimum growth inhibitory concentrations (MICs) of sulfamethazine and sulfanilamide for *E. coli* BL21(DE3) Δ *abgT* Δ *pabA* (inoculum, 500 cells/ml) harboring these vectors were then determined using LB agar containing 50 μ g/ml ampicillin, 0.1 mM IPTG and different concentrations of sulfamethazine and sulfanilamide, respectively.

Accumulation assays of sulfamethazine

The procedures for [^3H]-sulfamethazine accumulation were the same as those for [^3H]-PABA accumulation. Cells were incubated with 75 nM [^3H]-sulfamethazine (Moravsek Biochemicals, Brea, CA) for 15 min, applied directly to prewetted glass-fiber filters, and washed immediately twice with 5-ml aliquots of the same buffer. Filters were then incubated for 30 min in scintillation fluid (ScintiVerseTM BD) and counted with a Packard Tri-Carb 1600TR liquid scintillation counter (Perkin Elmer, Waltham, MA). For the Na^+ -dependent experiments, cells were incubated with 75 nM [^3H]-sulfamethazine in the presence of NaCl (0, 5 or 100 mM) for 15 min, then applied directly to prewetted glass-fiber filters, and washed immediately twice with 5-ml aliquots of buffer containing 100 mM Tris-HCl (pH 7.5) and 0, 5 or 100 mM NaCl.

Efflux assays of sulfamethazine

E. coli BL21(DE3) $\Delta abgT\Delta pabA$ carrying pET15b $\Omega ydaH$ or pET15b were grown in LB broth with 100 $\mu\text{g}/\text{ml}$ ampicillin at 37°C. When the OD_{600} reached 0.5, the culture was induced with 0.2 mM IPTG, and cells were harvested within 2 h. Cells were washed twice with buffer containing 50 mM potassium phosphate (pH 7.5), twice with buffer containing 100 mM Tris-HCl (pH 7.5), and then suspended in the same buffer to OD_{600} of 15. CCCP was added to the cell suspension at a final concentration of 100 μM . Cells were then incubated for 10 min, pelleted, washed twice and resuspended in the same buffer to OD_{600} of 10. [^3H]-sulfamethazine was then added to a final concentration of 37 nM. Cells were incubated for 15 min, and a final concentration of 0.2% glucose was then added to the cell suspension. When needed, a final concentration of 5 mM NaCl or KCl was also added at the same time. At various time points, samples of 100 μl were applied directly to prewetted glass-fiber filters, and washed twice with 5-

ml aliquots of buffer containing 100 mM Tris-HCl (pH 7.5). Filters were then incubated for 30 min in scintillation fluid (ScintiVerse™ BD) and counted with a Packard Tri-Carb 1600TR liquid scintillation counter (Perkin Elmer, Waltham, MA).

References

26. Long, F., Su, C.-C., Zimmermann, M.T., Boyken, S.E., Rajashankar, K.R., Jernigan, R.L. & Yu, E.W. Crystal structures of the CusA heavy-metal efflux pump suggest methionine-mediated metal transport mechanism. *Nature* **467**, 484-488 (2010).
27. Otwinowski, Z. & Minor, M. Processing of X-ray diffraction data collected in oscillation mode. *Methods Enzymol.* **276**, 307-326 (1997).
28. Tézé, A. & Hervé, G. α -, β -, and γ -dodecatungstosilicic acids: isomers and related lacunary compounds. *Inorganic Synthesis* **27**, 85-96 (1990).
29. Schneider, T.R. & Sheldrick, G.M. Substructure solution with SHELXD. *Acta Cryst.* **D58**, 1772-1779 (2002).
30. Pape, T. & Schneider, T.R. HKL2MAP: a graphical user interface for macromolecular phasing with SHELX programs. *J. Appl. Cryst.* **37**, 843-844 (2004).
31. Otwinowski, Z. MLPHARE, CCP4 Proc. 80 (Daresbury Laboratory, Warrington, UK, 1991).
32. Collaborative Computational Project No. 4. The CCP4 suite: programs for protein crystallography. *Acta Cryst.* **D50**, 760-763 (1994).
33. Terwilliger, T.C. Maximum-likelihood density modification using pattern recognition of structural motifs. *Acta Cryst.* **D57**, 1755-1762 (2001).
34. Emsley, P. & Cowtan, K. Coot: model-building tools for molecular graphics. *Acta Cryst.* **D60**, 2126 (2004).
35. McCoy, A.J., Grosse-Kunstleve, R.W., Adams, P.D., Winn, M.D., Storoni, L.C. & Read, R.J. Phaser crystallographic software. *J. Appl. Cryst.* **40**, 658-674.
36. Adams, P.D., Grosse-Kunstleve, R.W., Hung, L.W., Ioerger, T.R., McCroy, A.J., Moriarty, N.W. et al. PHENIX: building new software for automated crystallographic structure determination. *Acta Cryst.* **58**, 1948-1954 (2002).
37. Brünger, A.T., Adams, P.D., Clore, G.M., DeLano, W.L., Gros, P., Grosse-Kunstleve, R.W., Jiang, J.S., Kuszewski, J., Nilges, M., Pannu, N.S., Read, R.J., Rice, L.M., Simonson, T. &

- Warren, G.L. Crystallography & NMR system: A new software suite for macromolecular structure determination. *Acta Cryst.* **D54**, 905-921 (1998).
38. Datsenko, K.A. & Wanner, B.L. One-step inactivation of chromosomal genes in *Escherichia coli* K-12 using PCR products. *Proc. Nat. Acad. Sci. USA* **97**, 6640-6645 (2000).

Supplemental figures

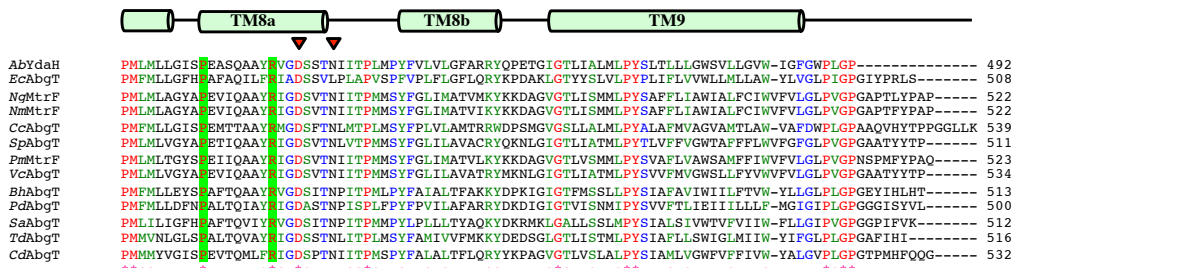
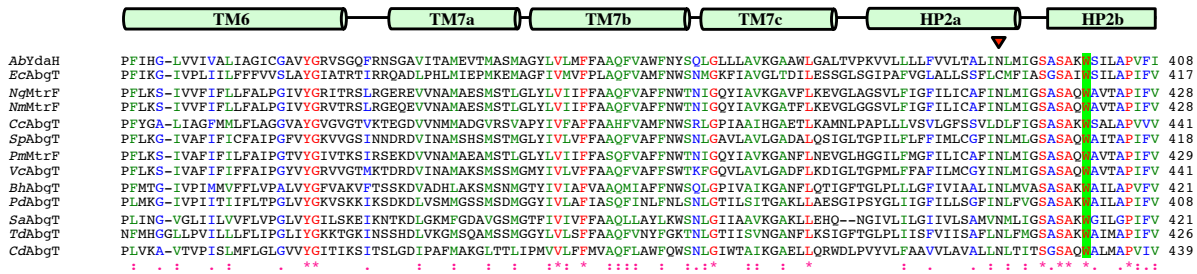
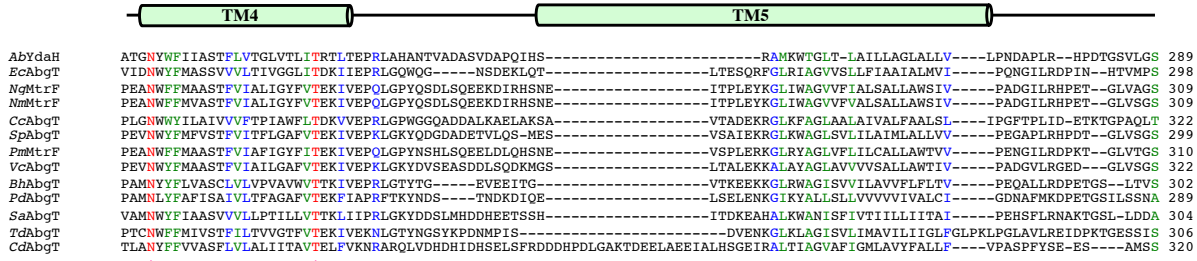
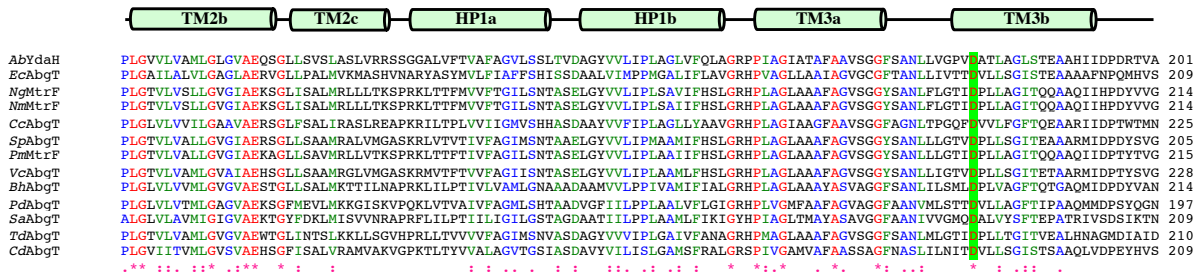
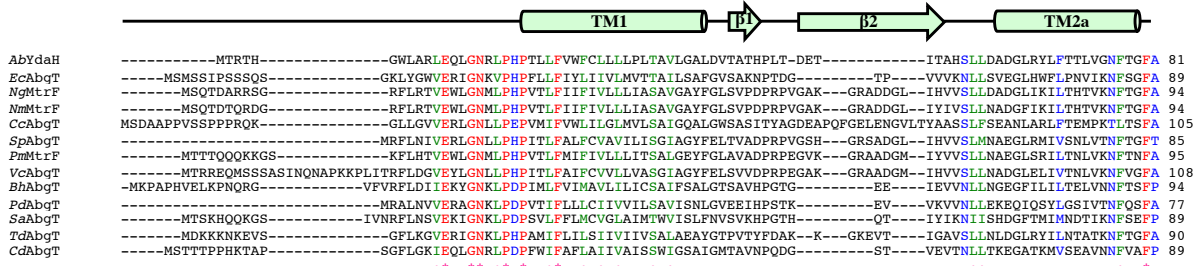
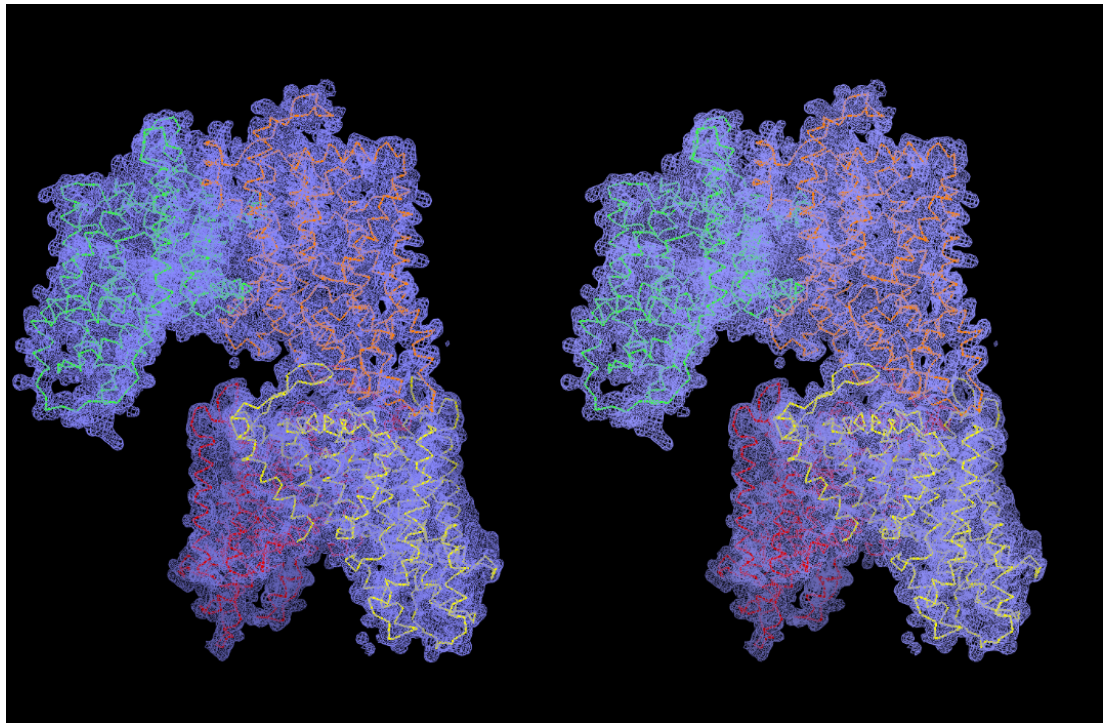
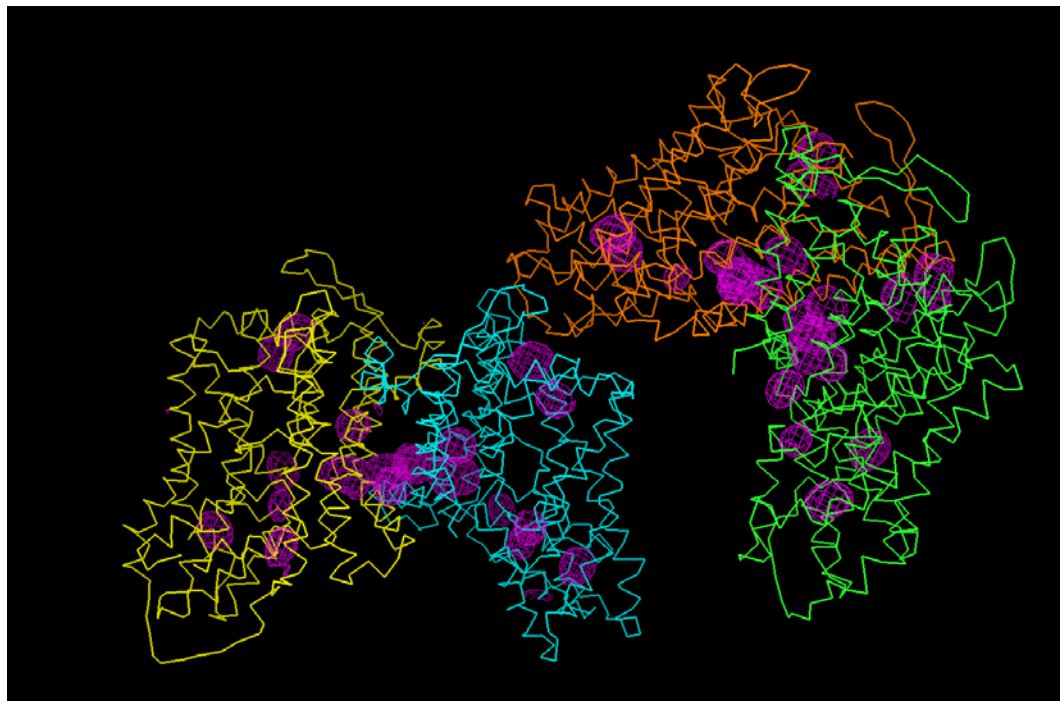


Fig. S1. Sequence and topology of *A. borkumensis* YdaH. Alignment of the amino acid sequences of the AbgT family of transporters were done using CLUSTAL W. *, identical residues; :, >60% homologous residues. Secondary structural elements are indicated: TM, transmembrane helix; β , strand. The sequence and topology of *A. borkumensis* YdaH are shown at the top. Conserved residues involved in lining the channel of the inner core of the protein are highlight with green bars. Residues coordinating with the bound Na^+ are indicated with red arrows.

(a)



(b)



(c)

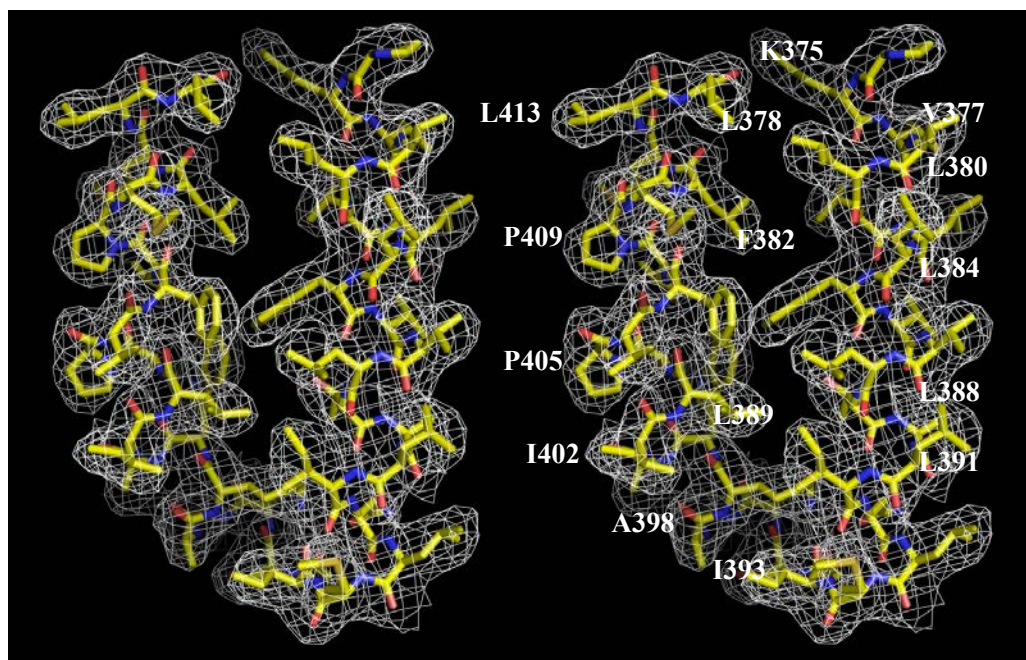


Fig. S2. Stereo view of the electron density maps of YdaH at a resolution of 2.96 Å. (a) The electron density maps are contoured at 1.2 σ . The C α traces of the two YdaH dimers in the asymmetric unit are included. (b) Anomalous maps of the 44 selenium sites (contoured at 4 σ).

Four protomers forming two dimers of YdaH are found in the asymmetric unit. Each protomer contributes 11 selenium sites corresponding to the 11 methionines (magenta). The C α traces of the four YdaH monomers are colored green, orange, cyan and yellow. (c) Representative section of the electron density within HP2 of YdaH. The electron density (colored white) is contoured at the 1.2 σ level and superimposed with the final refined model (yellow, carbon; red, oxygen; blue, nitrogen).

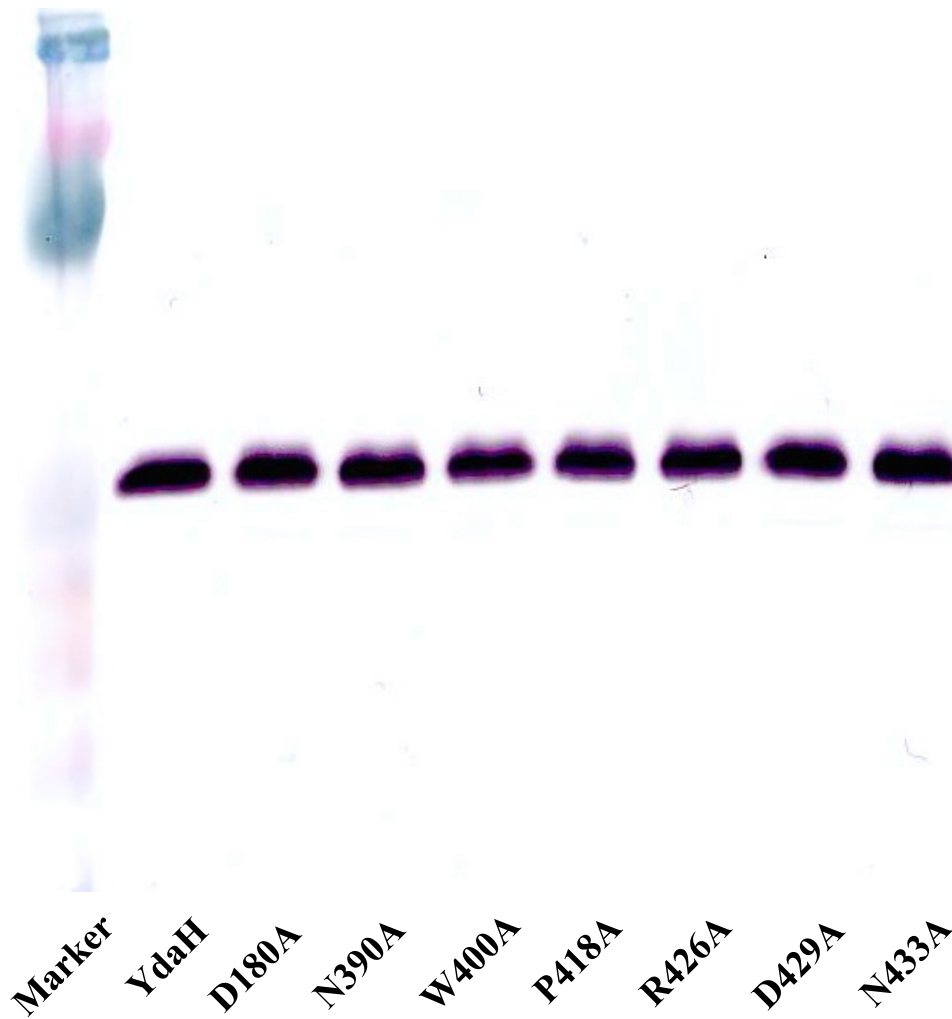


Fig. S3. Expression level of the YdaH pumps. An immunoblot against YdaH of crude extracts from 50 μ g dry cells of strain BL21(DE3) Δ *abgT* Δ *pabA* expressing the YdaH wild-type and mutant (D180A, N390, W400A, P418A, R426A, D429A and N433A) pumps are shown.

Table S1. Data collection, phasing and structural refinement statistics.

	Native YdaH	$[\beta\text{-SiW}_9\text{O}_{34}\text{H}]^{9-}$	Se (peak)
Data Collection			
Wavelength (\AA)	0.98	1.02	0.98
Space group	$P2_1$	$P2_1$	$P2_1$
Resolution (\AA)	50 – 2.96 (3.09 – 2.96)	50 – 7.70 (7.98 – 7.70)	50 – 4.10 (4.25 – 4.10)
Cell constants (\AA)			
a	94.15	94.31	98.26,
b	200.98	199.33	193.57,
c	101.49	102.95	102.83
α, β, γ ($^\circ$)	90, 92.82, 90	90, 93.46, 90	90, 94.72, 90
Molecules in ASU	4	4	4
Redundancy	3.7 (3.5)	1.9 (1.9)	1.8 (1.7)
Total reflections	2813,494	243,367	509,675
Unique reflections	83,133	12,402	19,264
Completeness (%)	99.3 (97.4)	96.2 (97.9)	97.1 (94.9)
R_{sym} (%)	5.4 (46.5)	4.4 (39.4)	6.1 (46.2)
I / σ	19.9 (2.2)	24.6 (2.0)	12.5 (1.5)
Phasing			
Number of sites		6	44
Phasing power (acentric/centric)		1.45 / 0.94	1.34/0.96
R_{cullis} (acentric/centric)		0.80/0.90	0.87/0.87
Figure of merit		0.285	0.486
Refinement			
Resolution (\AA)	YdaH		
Resolution (\AA)	50 – 2.96		
R_{work} (%)	20.05		
R_{free} (%)	24.37		
Average B-factor (\AA^2)	74.70		

RMSD bond lengths (Å)	0.009
RMSD bond angles (°)	1.392

Ramachandran plot

most favoured (%)	94.2
additional allowed (%)	5.6
generously allowed (%)	0.2
disallowed (%)	0

Table S2. Primers for site-directed mutagenesis.

Primer	Sequence
D180A-forward	5'-CCCGGTGGCTGCAACCCTGGCTGGTCTGTCAACGGA-3'
D180A-reverse	5'-CAGGGTTGCAGCCACCGGGCCGACCAGCAGATTCGCC-3'
N390A-forward	5'-GTGCTGACGGCCCTGATTGCCCTGATGATCGGTAGTGCG-3'
N390A-reverse	5'-CGCACTACCGATCATCAGGGCAATCAGGGCCGTCAGCAC-3'
W400A-forward	5'-CGCCAAGGCGAGTATTCTGGCCCCGGTGTTCATCCCC-3'
W400A-reverse	5'-CAGAATACTCGCCTTGCGGACGCACTACCGATCATCAG-3'
P418A-forward	5'-CATCAGTGCGGAAGCATCCCAGGCAGCTTATCGCGT-3'
P418A-reverse	5'-GATGCTTCCGCACTGATGCCCAGCAGCATCAGCATC-3'
R426A-forward	5'-GCATCCCAGGCAGCTTATGCCGTTGGTGATTCATCGACC-3'
R426A-reverse	5'-GGTCGATGAATCACCAACGGCATAAGCTGCCTGGGATGC-3'
D429A-forward	5'-GCAGCTTATCGCGTTGGTGCTTCATCGACCAATATTATC-3'
D429A-reverse	5'-GATAATATTGGTTCGATGAAGCACCAACGCGATAAGCTGC-3'
N433A-forward	5'-GTTGGTGATTCATCGACCGCTATTATCACGCCGCTGATG-3'
N433A-reverse	5'-CATCAGCGGCGTGATAATAGCGGTTCGATGAATCACCAAC-3'

Table S3. MICs of sulfamethazine and sulfanilamide for different YdaH variants expressed in *E. coli* BL21(DE3) Δ *abgT* Δ *pabA*.

Gene in BL21(DE3) Δ <i>abgT</i> Δ <i>pabA</i>	Sulfamethazine (μ g/mL)	Sulfanilamide (μ g/mL)
Empty vector	62.5	500
<i>ydaH</i> (wild-type)	2000	4000
<i>ydaH</i> (D180A)	1000	2000
<i>ydaH</i> (N390A)	62.5	2000
<i>ydaH</i> (W400A)	62.5	2000
<i>ydaH</i> (P418A)	250	2000
<i>ydaH</i> (R426A)	125	2000
<i>ydaH</i> (D429A)	62.5	2000
<i>ydaH</i> (N433A)	62.5	2000

CHAPTER 7

GENERAL CONCLUSIONS AND FUTURE DIRECTIONS

The continual emergence of multidrug resistance among pathogenic bacteria has kept up a great demand for developing or designing more new effective antibiotics and smarter treatment strategies. Bacterial multidrug efflux pumps constitute a major mechanism for conferring multidrug resistance and thus provide attractive therapeutic targets [1]. Understanding the action mechanisms of these efflux pumps and their transcriptional regulators is essential for the development of efflux pump inhibitors. This dissertation is focused on the study of bacterial multidrug efflux transporters, MtrD and MtrF of *N. gonorrhoeae* and YdaH of *A. borkumensis* and a transcriptional regulator, Rv3066 of *M. tuberculosis*.

The Mmr multidrug efflux pump (belongs to the SMR family) of *M. tuberculosis*, has been shown to mediate resistance to several toxic compounds, including acriflavine, ethidium bromide, erythromycin, pyronin Y, safranin O, tetraphenyl phosphonium and thioridazine [2-4]. Although, homolog structures of this family of proteins are available, knowledge of their gene regulation is fairly minimal.

In Chapter 2, we proposed that the expression of Mmr efflux pump is controlled by the transcriptional regulator Rv3066, whose open reading frame is located downstream of the *mmr* operon. To understand the structural basis of Rv3066 regulation, we have determined the crystal structures of Rv3066, both in the absence and presence of bound ethidium. Comparison of the apo-Rv3066 and Rv3066-ethidium crystal structures suggests that the conformational changes leading to drug-mediated derepression is primarily due to a rigid body rotational motion within the dimer interface of the regulator. The Rv3066 regulator creates a multidrug-binding pocket;

important residues for drug binding were identified using mutagenesis and fluorescence polarization. *In vitro* studies reveal that the dimeric Rv3066 regulator binds to a 14-bp palindromic inverted repeat sequence in the nanomolar range. Together with the experimental data from electrophoretic mobility shift, footprinting analysis, qRT-PCR, mutagenesis, gel filtration and fluorescence polarization, the crystal structures support the role of Rv3066 in regulating the expression level of the multidrug efflux pump Mmr in *M. tuberculosis*.

In Chapter 3, we outlined different methods for use in the crystallization of membrane proteins. All the known multidrug efflux transporters and targets of more than 50% of currently administrative pharmaceutical agents are integral membrane proteins. Unfortunately, the understanding of the structure and function of these membrane proteins hampered by difficulties associated with obtaining crystals that diffract to high resolution. This brief summary will provide a useful guide for researchers working in the field of membrane proteins.

In Chapter 4, the wild-type *N. gonorrhoeae* MtrD of MtrCDE tripartite complex has been cloned, expressed and crystallized. The findings reveal a novel structural feature that is not found in other known members of RND efflux pumps. MtrD contains an extended region that protrudes into the periplasm and contributes part of the periplasmic domain. Protein sequence alignment suggests that this region is only found in MtrD and not other homologous RND proteins. The spatial arrangement between the extra elongated helix and loop (upper portion of TM9) and the periplasmic cleft formed between PC1 and PC2 suggests that these extra structural features may help the pump to transport its substrates more effectively from the outer leaflet of the inner membrane to the multidrug binding site at the periplasmic domain. Protein sequence alignment reveals that many of the amino acids forming the large periplasmic binding site of AcrB are conserved between MexB and MtrD, indicating that these three multidrug efflux pumps may

have a similar substrate binding profile for drug recognition. The MtrD multidrug efflux pump should operate through an alternating-access mechanism, similar to the AcrB transporter. Thus, the pump has to go through the transport cycle, which should involve different transient conformations, including the “access”, “binding” and “extrusion” states of this protein. In comparison with the structures of AcrB; the conformation of MtrD is closer to that of the “access” protomer of AcrB [5].

In Chapter 5, the wild-type *N. gonorrhoeae* MtrF, which belongs to the AbgT family of transporters, has been cloned, expressed, crystallized. The findings from the structure of MtrF highlight a unique fold of dimeric molecule distinct from all other families of transporters. MtrF is a bowl shaped dimer with a solvent-filled basin extending from the cytoplasm to halfway across the membrane bilayer. The structure directly suggests a plausible pathway for substrate transport. A combination of the crystal structure, genetic analysis and substrate accumulation assay indicate that MtrF is an exporter, capable of removing the metabolite *p*-aminobenzoic acid from bacterial cells. Further experimental data based on drug susceptibility and radioactive transport assay suggest that *N. gonorrhoeae* is an antibiotic efflux pump, which mediates bacterial resistance to sulfonamide antimetabolite drugs. Our data also suggest that MtrF is proton motive force dependent efflux pump and important residues for the function of this protein were identified. Our data strongly agrees with the previous observation that MtrF is needed for high-level resistance of gonococci to hydrophobic agents.

In Chapter 6, the crystal structure of *A. borkumensis* YdaH, which is a distinct member of the AbgT family, has been determined to a resolution of 2.96 Å. The dimeric architecture of YdaH is distinct from all other transporters, but is similar to that of MtrF. The residues lining along the wall of the predicted channel for substrate pathway are well conserved between YdaH

and MtrF. Different from MtrF, we observed a bound Na^+ ion in each protomer of YdaH. Our initial attempts to see whether YdaH function to catalyze the uptake of *p*-aminobenzoyl-glutamate for *de novo* folic acid synthesis (similar to *E. coli* AbgT) or function as an antimicrobial resistant protein (similar to *N. gonorrhoeae*), reveal that YdaH behaves similar to MtrF. From our accumulation assays, drug susceptibility assays and radioactive transport assay, we demonstrated that *A. borkumensis* YdaH is an antibiotic efflux pump, which is able to remove sulfonamides from the cell and mediate resistance to this class of antimetabolites. In addition, we identified important residues for the function of this protein and our results strongly suggest that function of YdaH is Na^+ -ion dependent. It is likely that many members of the AbgT family transporters may serve as antimetabolite efflux pumps to protect cells against these noxious agents.

Towards understanding the molecular mechanism used by the MtrCDE efflux pump of *N. gonorrhoeae* to expel various classes of antibiotics, we have determined the crystal structure of the MtrD and the accessory protein MtrF. Much more structural and biochemical information will be necessary for a detailed understanding of how these two membrane proteins work together and transport mechanism of these multidrug efflux pumps. Such understanding may prompt the use of new approaches to manipulate the function of these proteins, thereby inhibiting their efflux activity. Approaches to prevent the overexpression of Mmr efflux pump by targeting the Rv3066 regulator provide an alternative strategy to combat drug resistant *M. tuberculosis* pathogenic bacteria. The inhibition of AbgT family proteins would aid in restoring the effectiveness of sulfonamide drugs. The use of small molecule efflux system blockers will be an expanding research discipline in the treatment of infectious diseases [6-8].

References

1. Kumar S, Varela MF. Biochemistry of bacterial multidrug efflux pumps. *Int J Mol Sci* 2012;13:4484-95.
2. De Rossi E, Branzoni M, Cantoni R, Milano A, Riccardi G, Ciferri O. 1998. *mmr*, a *Mycobacterium tuberculosis* gene conferring resistance to small cationic dyes and inhibitors. *J Bacteriol* 180:6068-6071
3. Tate CG, Kunji ER, Lebendiker M, Schudiner S. 2001. The projection structure of EmrE, a proton-linked multidrug transporter from *Escherichia coli*, at 7 Å resolution. *EMBO J* 20:77-81
4. Chen YJ, Pornillos O, Lieu S, Ma C, Chen AP, Chang G. 2007. X-ray structure of EmrE supports dual topology model. *Proc Natl Acad Sci USA* 104:18999-190004
5. Murakami S, Nakashima R, Yamashita E, Matsumoto T, Yamaguchi A. 2006. Crystal structures of a multidrug transporter reveal a functionally rotating mechanism. *Nature* 443: 173–179
6. Bhardwaj AK, Mohanty P. Bacterial Efflux Pumps Involved in Multidrug Resistance and their Inhibitors: Rejuvenating the Antimicrobial Chemotherapy. *Recent Pat Antiinfect Drug Discov* 2012
7. Pages JM, Sandrine AF, Mahamoud A, Bolla JM, Davin-Regli A, Chevalier J, Garnotel E. 2010. Efflux pumps of gram-negative bacteria, a new target for new molecules. *Current topics in medicinal chemistry* 10:1848-57
8. Kourtesi C, Ball AR, Huang YY, Jachak SM, Vera DM, Khondkar P, Gibbons S, Hamblin MR, Tegos GP. 2013. Microbial efflux systems and inhibitors: approaches to drug discovery and the challenge of clinical implementation. *Open Microbiol J* 7:34-52

ACKNOWLEDGEMENTS

I would like to thank my major advisor, Dr. Edward Yu for his valuable support, encouragement, and useful suggestions during the course of my graduate studies. His infectious enthusiasm, passion, guidance, and patience have been immeasurable in the development and progress of my research. I am especially grateful to Ed for his devotion to his students' success. Ed has been more than just a mentor to me at work; he has been a friend. I am truly fortunate to have been able to enjoy working with him over the past years.

I would like to thank my committee members: Dr. Robert Sam Houk, Dr. Keith Woo, Dr. Young Jin Lee and Dr. Drena Dobbs for their valuable advices and kind help.

I have had the great pleasure of working in close relationships with several colleagues in the lab. Namely, Dr. Chih-Chia Su, Dr. Feng Long, Dr. Hsiang-Ting Lei, Sylvia V. Do, Abhijith Kumar R.P.S., Nitin Kumar, Jared Delmar, Tsung-Han Chou, Rajiv Kaudal, and Fudan Zhang. These people have always been there to share exciting and precious moments as well as the frustrations of research. I thank them for their valuable suggestions and their time in experiencing great lunches and dinners together. I will always treasure the memories of our days together in some of the beautiful places in the world.

I would like to thank Dr. Kanagalaghatta R. Rajashankar and all the staff members of NE-CAT in Advanced Photon Source for their help during X-ray data collection and structure determination. I want to thank our great collaborators Dr. William Shafer, for the work related to the Mtr efflux system and Dr. Qijing Zhang, for the work related to Rv3066. I also want to thank the ISU facilities, including DNA facility, protein facility, hybridoma facility and chemical instrumentation facility.

I want to thank all my friends who made my stay in the past years at ISU an interesting and memorable experience. Their names are too numerous to mention, but the time spent with them was unforgettable. Also, I want to thank all coffee shop baristas in Ames for keeping me awake everyday.

Last, but certainly not least, I would like to thank my family members and friends. I would not have made it to ISU without the support and inspiration of my parents and family members, who have always encouraged me to pursue my interests. Being so far away was tough, and I am fortunate to have great friends to encourage me all the time. I would like to dedicate this dissertation work to my grandmother Thirapamma, and my family for their endless love and support, whose life lessons made my accomplishments possible.

VITA

NAME OF AUTHOR: Jani Reddy Bolla

DATE AND PLACE OF BIRTH: May 2, 1988, Mukundapuram, India

DEGREES AWARDED:

- M.Sc. Chemical Sciences, Pondicherry University, 2008-2010
- B.Sc. Chemistry, Physics and Mathematics, Osmania University, 2005-2008

PROFESSIONAL EXPERIENCE:

- Graduate Student, Department of Chemistry, Iowa State University, 2011-2014
- Teaching Assistant, Department of Chemistry, Iowa State University, 2010-2014
- Masters Student, Department of Chemistry, Pondicherry University, 2008-2010

AWARDS, HONORS AND SCHOLARSHIPS:

- Science Highlight 2012, Advanced Photon Source, ANL, USA, 2012
- Science Highlight 2012, National Institute of General Medical Sciences, USA, 2012
- Science Highlight 2012, Iowa State University, USA, 2012
- University Gold Medal, Pondicherry University, India, 2010
- Merit Scholarship, AstraZeneca, Bangalore, India, 2010
- Qualified Nationwide Graduate Aptitude Test in Engineering (GATE), Indian Institute of Technology and Indian Institute of Sciences, India, 2010

- Qualified National Eligibility Test (NET), Council of Scientific and Industrial Research, India, 2009
- Merit Scholarship, Pondicherry University, India, 2009
- Sitaram Jindal Scholarship, Sitaram Jindal Foundation, Bangalore, India, 2008-2010

PUBLICATIONS:

- **Bolla JR***, Su CC*, Delmar JA, Radhakrishnan A, Kumar N, Chou TH, Rajashankar KR, Yu EW (2014). YdaH is an efflux pump that mediates resistance to sulfonamide antimetabolites. Submitted.
- Su CC*, **Bolla JR***, Kumar N, Radhakrishnan A, Delmar JA, Chou TH, Rajashankar KR, Shafer WM, Yu EW (2014). Structure and function of *Neisseria gonorrhoeae* MtrF illuminates a novel class of antimetabolite efflux pumps. Submitted.
- Delmar JA, Su CC, **Bolla JR**, Yu EW (2014). Crystallization of membrane proteins *via* vapor diffusion. Methods Enzymol. In press
- **Bolla JR***, Su CC*, Do SV*, Radhakrishnan A, Kumar N, Long F, Chou TH, Delmar JA, Lei HT, Rajashankar KR, Shafer WM, Yu EW (2014). Crystal structure of the *Neisseria gonorrhoeae* MtrD inner membrane multidrug efflux pump. PLoS One 9:e97903.
- Lei HT, Chou TH, Su CC, **Bolla JR**, Kumar N, Radhakrishnan A, Long F, Delmar JA, Do SV, Rajashankar KR, Shafer WM, Yu EW (2014). Crystal structure of the open state of the *Neisseria gonorrhoeae* MtrE outer membrane channel. PLoS One 9:e97475.
- Su CC, Radhakrishnan A, Kumar N, Long F, **Bolla JR**, Lei HT, Delmar JA, Do SV, Chou TH, Rajashankar KR, Zhang Q, Yu EW (2014). Crystal structure of the

Campylobacter jejuni CmeC outer membrane channel. Protein Sci 23:954-961. (Cover page)

- Radhakrishnan A, Kumar N, Wright CC, Chou TH, Tringides ML, **Bolla JR**, Lei HT, Rajashankar KR, Su CC, Purdy GE, Yu EW (2014). Crystal structure of the transcriptional regulator Rv0678 of *Mycobacterium tuberculosis*. J Biol Chem 289:16526-16540.
- Kumar N, Radhakrishnan A, Wright CC, Chou TH, Lei HT, **Bolla JR**, Tringides ML, Rajashankar KR, Su CC, Purdy GE, Yu EW (2014). Crystal structure of the transcriptional regulator Rv1219c of *Mycobacterium tuberculosis*. Protein Sci 23:423-432.
- Lei HT*, **Bolla JR***, Bishop NR, Su CC, Yu EW (2014). Crystal structures of CusC reveal conformational changes accompanying folding and transmembrane channel formation. J Mol Biol 426:403-411.
- **Bolla JR**, Su CC, Yu EW (2012). Biomolecular membrane protein crystallization. Philos Mag 92:2648-2661.
- **Bolla JR***, Do SV*, Long F, Dai L, Su CC, Lei HT, Chen X, Gerkey JE, Murphy DC, Rajashankar KR, Zhang Q, Yu EW (2012). Structural and functional analysis of the transcriptional regulator Rv3066 of *Mycobacterium tuberculosis*. Nucleic Acids Res 40:9340-9355.
- Su CC, Long F, Lei HT, **Bolla JR**, Do SV, Rajashankar KR, Yu EW (2012). Charged amino acids (R83, E567, D617, E625, R669, and K678) of CusA are required for metal ion transport in the Cus efflux system. J Mol Biol 422:429-441.

- Long F, Su CC, Lei HT, **Bolla JR**, Do SV, Yu EW (2012). Structure and mechanism of the tripartite CusCBA heavy-metal efflux complex. *Philos Trans R Soc Lond B Biol Sci* 367:1047-1058.

**Authors contributed equally*

Book Chapters

- Do SV, Su CC, Long F, Lei HT, **Bolla JR**, Yu EW (2012). Structure, mechanism and assembly of the tripartite CusCBA heavy-metal efflux complex. *Microbial efflux pumps: current research*. Horizon scientific press Ltd., UK.

PRESENTATIONS:

- “Structural and functional analysis of the transcriptional regulator Rv3066 of *Mycobacterium tuberculosis*” at the 2013 Midwest Regional Meeting (MWRM-2013), Springfield, MO, October 18, 2013.
- “Crystal structure of the CusBA heavy-metal complex of the *Escherichia coli*” poster presentation at the Department of Chemistry open house, Iowa State University, IA, February 24, 2012.